Sedimentological characterisation of continental sabkhas: an example from the cedar mesa sandstone of the Paradox Basin, Utah, USA

Ross Peter Pettigrew

Doctor of Philosophy

October 2019

Keele University

Abstract

Continental sabkhas are present within many arid sedimentary basins, however they are often overlooked compared to coeval aeolian and fluvial deposits, despite their potential to record and preserve sedimentary signatures relating to basin formation and fill.

The relationships between evaporitic sabkha deposits and genetically-related coeval clastic sediments are strongly influenced by complex processes between autocyclic and allocyclic controls, including climate, however within arid continental settings these signatures are often difficult to detect within the preserved sediments.

This thesis presents results from the margin of the Cedar Mesa erg of the Paradox Basin, Utah, USA, which preserves complex interactions of clastic and evaporitic sediments. Studies are based upon extensive regional fieldwork examining the sedimentology, geometries, and interactions, complemented with outcrop gamma ray data and microfacies analysis. The sedimentology shows large variations spatially and temporally which grade through aeolian, sabkha and lacustrine settings with complex interactions occurring where these sediments transition.

This work details the facies present in a continental sabkha allowing for identification and interpretation of these complex interbedded relationships over a regional scale. The results have been developed into idealised models and recognisable log signatures which characterise and assess their impact on reservoir quality. Cyclic climatic trends, on various orders of magnitude, have been identified in relation to distinct spatial facies changes. Identification of these allows for basin-wide correlation and prediction of where facies will occur in space and time.

These results are applied to evolutionary models applicable to subsurface data from the arid Permian basins of the North Sea, in order to better characterise basin-scale migration and reservoir quality in terms of the evolving basin fill.

Acknowledgments

Firstly I extend my gratitude to my supervisor Dr Stuart Clarke, for his continued academic help and invaluable feedback. Secondly I wish to thank all the members of the BDRG at Keele for their friendship and spell checks, special thanks to Charlotte for putting up with me. Finally I wish to thank my family for their unwavering support.

Contents

List of Figures and Tables

CD Rom

Chapter One: Thesis Introduction and Organisation

This chapter outlines the research aims and objectives of this thesis and provides a literature synthesis of the geology of the Colorado Plateau, USA, to contextualise the following chapters.

1.1 Introduction

This research provides the first detailed study of the sedimentology and cyclicity of the distal portion of the early Permian Cedar Mesa Sandstone Formation, with outcrops throughout parts of south-eastern Utah and northern Arizona (Fig. 1.1). The Cedar Mesa Sandstone Formation has been interpreted to be a large aeolian erg, which at its distant margin grades to sabkha, or sabkha-influenced sediments comprising the deposits of aeolian, fluvial, lacustrine and evaporitic settings (e.g. Condon, 1997). The Cedar Mesa Sandstone provides world class outcrop examples of arid continental sediments and, while the aeolian erg has been studied in great detail (see Loope, 1984; Langford & Chan, 1989; Mountney & Jagger, 2004), the transition to these sabkha influenced sediments has been relatively overlooked. Furthermore, the depositional setting of the sabkha sediments (continental vs marine) remains equivocal (Langford & Massad, 2015; Stanesco & Campbell, 1989). This is despite excellent outcrops and available examples of unique and interesting sedimentology that can be used to test depositional models proposed by previous workers.

Arid continental settings deposit and preserve complex interactions between aeolian, alluvial, lacustrine, fluvial and sabkha sediments. While the distribution and preservation of different facies associations within any one of these environments are reasonably well constrained, the relationships between deposits of coeval environments and their temporal evolution have, received comparatively little

attention despite their potential to affect both basin-scale fluid migration and reservoir quality.

These interactions are strongly influenced by complex processes between autocyclic and allocyclic controls, including climate, however within arid continental settings these signatures are often difficult to detect within the sediments preserved.

This research investigates the deposits of sabkhas within arid, dominantly siliciclastic, continental settings and describes and interprets the relationships between evaporitic and clastic sediments deposited within sabkhas and those deposited in neighbouring arid continental settings. Generic depositional models depicting the sedimentology, architecture and interactions at a range of scales have been developed. Models of the interplay between evaporitic and clastic sediment supply, accommodation space and climate are discussed to provide insight into probable distributions of, and relationships between, evaporitic and clastic strata in similar subsurface settings.

The work presents a high-resolution dataset that allows three-dimensional demonstration of the sedimentary responses of a continental sabkha system to changes in climate, and of the preserved sedimentary relationships between evaporites and associated clastic deposits that these responses create. The work builds upon previous models of sabkha systems (e.g. Warren, 2016; Handford, 1981), refines them for arid continental settings, and sets the models in the context of the evolving arid climate.

1.2 Research Aims and Objectives

This project sets out to address three key aims:

- Aim 1: Identify and fully describe the sedimentology of an arid continental sabkha and the influence of competing coeval settings on the sedimentary sequence.
- Aim 2: Identify regional-scale variations imposed by climatic cyclicity within the depositional system, both sedimentologically and petrophysically.
- Aim 3: Apply these findings to downhole data from the Silverpit Formation and Leman Sandstone of the southern North Sea to better characterise potential reservoir units.

1.2.1 Aim 1: Sedimentology

This research will describe how the evaporitic sabkha sediments influence and affect contemporaneous arid continental aeolian and lacustrine deposits using the distal portions of the Cedar Mesa Sandstone Formation, and provides geological models that test previously-published models of these settings.

Detailed sedimentary logging across the extent of the preserved sabkha deposits of the Cedar Mesa Sandstone, utilising thorough sedimentological investigation of grain size, shape, sorting and minerology is used to characterise the deposits. From these data, facies can be determined, allowing for identification and interpretation of small-scale interactions between the competing environments. Facies are grouped into facies associations, allowing the identification of larger scale environmental interactions and the reconstruction of past depositional settings and the changing spatial relationships between the primary depositional settings.

Sedimentological interpretations will be independently verified with results from outcrop gamma ray spectroscopy and carbonate petrography to further constrain and place the depositional interpretations in context.

Work to fulfil the first aim of this research can be summarised by the following objectives:

- Acquisition and utilisation of a detailed field data set, including ten sedimentary logs covering a combined total of 7.5 km of vertical sediment thickness.
- Detailed microfacies analysis of 65 carbonate samples to identify microfacies which better constrain depositional environments.
- Acquisition of five high-resolution spectral gamma ray logs at 20 cm spacing at key localities.

1.2.2 Aim 2: Climatic Cyclicity

The second aim of this project is to identify and quantify cyclicity observed within the Cedar Mesa Sandstone.

Analysis of the data derived from sedimentary logging, outcrop gamma ray logging and a petrographic study of the Cedar Mesa Sandstone will be used to identify regional scale alternating cyclic changes. Drying-upwards cyclic trends in the observed sedimentology can be correlated across the extent of the Cedar Mesa Sandstone can be and quantified using spectral gamma ray datasets. Large-scale autocyclic processes can be identified using this combined approach.

Work to fulfil the second aim of this research can be summarised by the following objectives:

- Identify cyclic changes within sedimentary deposits.
- Develop depositional models depicting the cyclic changes in sedimentary deposits and controls upon them.
- Correlate on the basis of cyclic models.
- Quantify the cyclicity using gamma ray data to link to autocyclic processes.

1.2.3 Aim 3: Application

Outcrop data will be complemented with the study of downhole gamma ray data from the Silverpit Formation and Leman Sandstone of the Southern North Sea; a similar basin setting.

Models and idealised gamma ray trends from the outcrop study of the Cedar Mesa Sandstone will be used to correlate within the Silverpit Formation and the Leman Sandston on the basis of cyclic trends, to identify potential reservoir units within heterogeneous sabkha sediments.

Work to fulfil the third aim of this research can be summarised by the following objectives:

- Application of idealised gamma ray trends from the Cedar Mesa Sandstone to key sections of the Leman Sandstone/Silverpit Formation.
- Correlation of trends within the Silverpit Formation and Leman Sandstone based on climatic cycles.
- Develop a climatic-based depositional model that can be used to identify potential reservoir units.

This chapter provides a summary of literature relating to the geology of south-eastern Utah, and more specifically, the Colorado plateau and Paradox Basin in which the deposits of the Cutler Group – the focus of this study- accumulated. This review will focus on the structural development and paleogeographic setting of the Paradox Basin during Pennsylvanian and early Permian times, and the stratigraphy and sedimentology of the Paradox-basin fill, in particular the Cutler-Group of which the Cedar Mesa Sandstone Formation is a constituent part. Additional emphasis will be placed on the sedimentology of the Cedar Mesa Sandstone and previous studies of the formation.

1.3 Geological Evolution of the Western United States

The Cedar Mesa Sandstone belongs to part of the sedimentary succession of the Colorado Plateau (Fig 1.2), which is a relatively undeformed, high-standing geological province in the south-western United States, bordered by the Basin and Range province to the west and the Rio Grande Rift to the east. The Uinta Mountains of Utah and Rocky Mountains of Colorado define the Plateau's northern and north-easterly boundaries respectively (Foos, 1999; Liu & Gurnis, 2010). The collision of Gondwana and Laurussia created a compressional tectonic regime resulting in numerous thrust-bound structural uplifts collectively known as the Ancestral Rocky Mountains (Barbeau, 2003). Up to twenty flexural-controlled foreland basins were created, with the Cedar Mesa Sandstone deposited within one of these, the Paradox Basin (Fig 1.3).

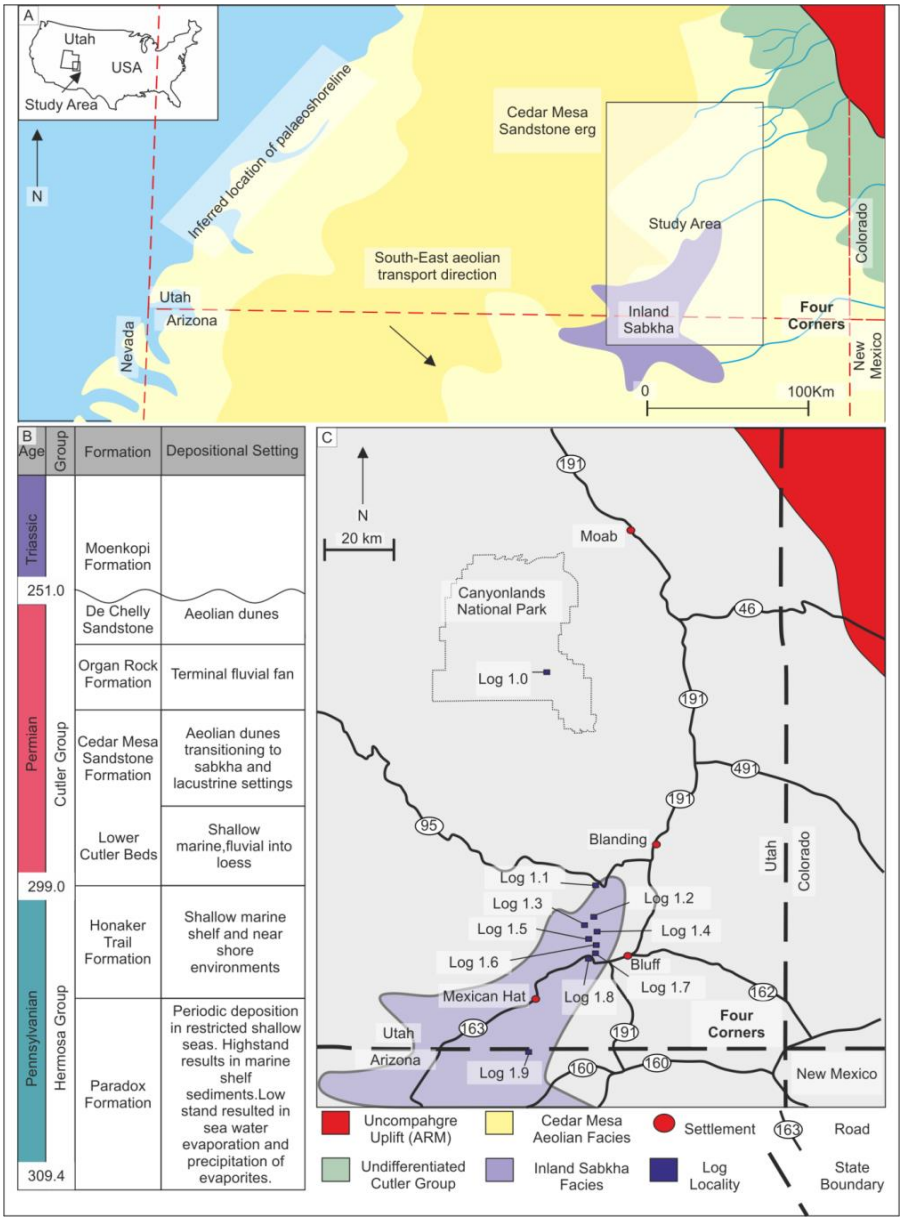

Figure 1.1 Summary figure detailing the study area, paleogeography and stratigraphy A) Reconstructed paleogeography of the Cedar Mesa Sandstone Formation during the early Permian Period (after Blakey et al., 1988). Location of the dune field is marked in dark yellow, with the location of sabkha sediments shown in purple against an inferred land surface (light yellow). Present day state boundaries are superimposed along with highlighted study area. B) Stratigraphy of the study area from Pennsylvanian to Triassic. Unconformities are marked with an undulating line (after Barbeau, 2003). C) Study area and log localities pictured with roads, national parks and state boundaries. Paleogeographical location of the sabkha facies (purple) and Uncompahgre Uplift (red) are also shown (after Blakey et al., 1988).

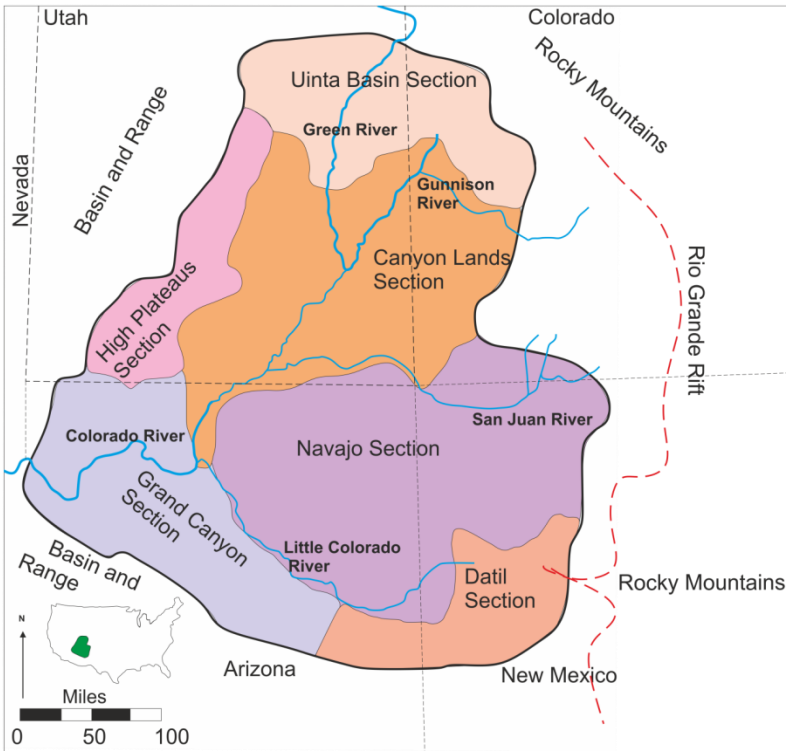

Figure 1.2 The location of the Colorado Plateau, its major rivers and subdivisions (after Foos 1999)

The few Precambrian exposures within the Colorado Plateau reveal basal metamorphosed gneiss and schist overlain by younger sedimentary rocks (Gilluly, 1963).

During the Precambrian eon, north-south compression resulted in large-scale southwest-northeast trending wrench faults. These faults have been reactivated numerous times over the geological history of the plateau, and are responsible for the orientation of the later major structures, including the main basins (Foos, 1999).

Tectonic stability throughout the early Palaeozoic era resulted in low rates of sedimentation within shallow seas, however, Middle to Upper Ordovician and Silurian rocks were eroded by falling sea level resulting in major unconformities (Gilluly, 1963; Stokes, 1952; Foos, 1999).

Reactivation of basement faults during the Pennsylvanian epoch through to the Triassic period resulted in the uplift of the Ancestral Rocky Mountains forming a series of northwest trending uplifts, which shed sediment into the adjacent basins (Fig 1.3) (Mallory, 1960).

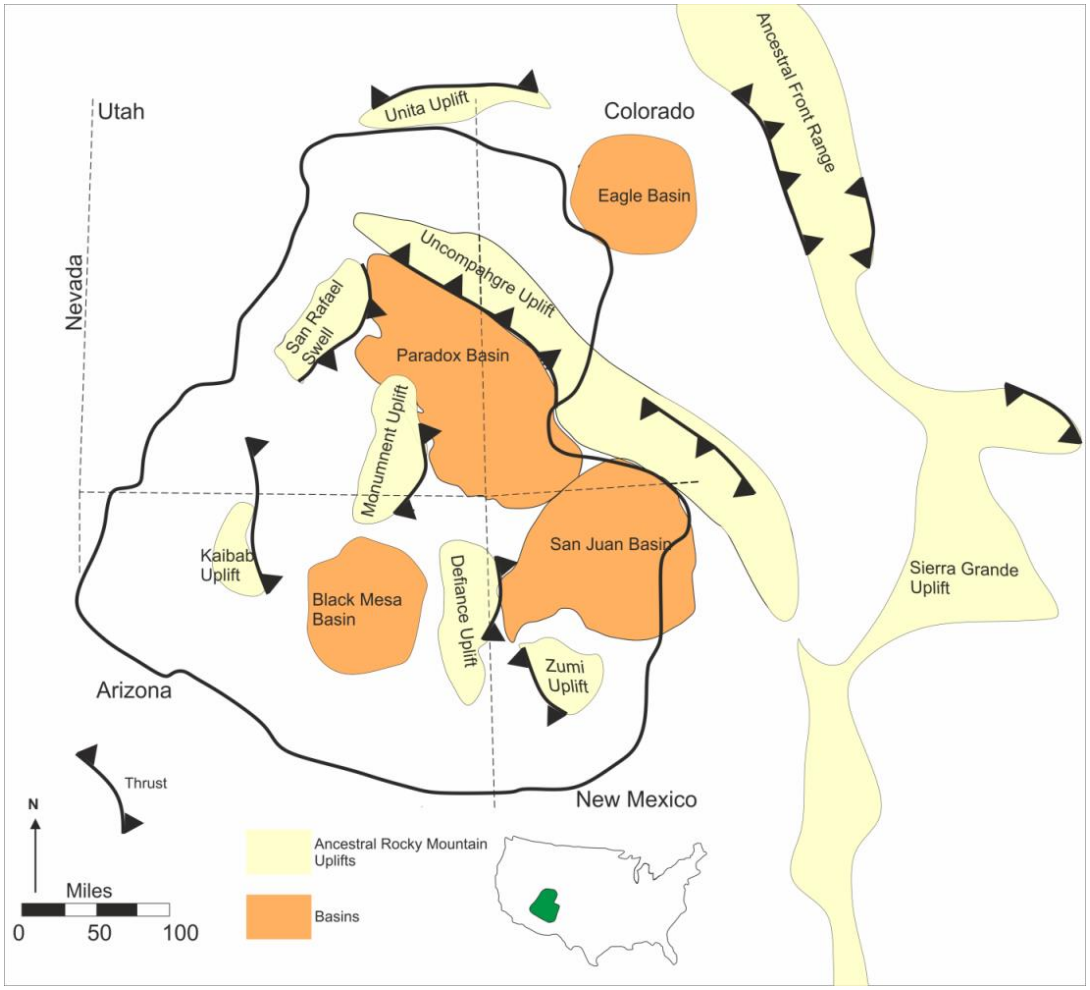

Figure 1.3 The location of the major basins and uplifts associated with the Colorado plateau (after Foos 1999: Baars 2000: Baars & Stevenson, 1981)

The Nevadan and Sevier orogenies, during the Jurassic and Cretaceous periods respectively, created highlands on the west coast, supplying sediment including volcanic bentonites onto the Colorado Plateau (Foos, 1999).

The end Cretaceous to early Paleogene Laramide Orogeny formed the present day Rocky Mountains, however Laramide deformation of the Colorado Plateau was mild resulting in monoclines and normal faulting. Most Laramide structures on the plateau have been subsequently buried by sediments sourced from eroded Eocene mountains (Foos, 1999).

The current elevation of the plateau is around two thousand metres, yet the timing and mechanisms for its uplift remain uncertain (Liu & Gurnis, 2010). Paleobotanical studies show the surrounding Central Rocky Mountain region reached present elevation in the Eocene (Wolfe *et al.,* 1998,) but basalt vesicularity interpretations from Cenozoic volcanics around the plateau margins suggest a Miocene origin for the uplift (Sahagian *et al,* 2002). However, apatite thermochronology research shows a latest Cretaceous origin for a one thousand metre scale elevation in the south-western part of the plateau (Flowers *et al.,* 2008). Late Cretaceous shallow-marine deposits curtail any evidence for earlier uplift (Bond, 1976). Whether the uplift was a single event or occurred in multiple stages is debated by Burchfiel, *et al.,* (1992), Wolfe *et al.,* (1998) and Flowers *et al.,* (2008).

The causes of the uplift are multiple, including crustal thickening (Bird, 1988; McQuarrie & Chase, 2000), mantle lithosphere removal (England *et al.,*1988; Spencer, 1996), chemical alteration of the lithosphere (Humphreys *et al.,* 2003; Roy *et al*., 2004), or mantle upwelling (Parsons *et al.*,1994; Moucha *et al.* 2009).

1.4 Paradox Basin

Formation of the Paradox Basin (Fig. 1.4) was initiated during the Pennsylvanian series when Utah occupied a palaeolatitude just north of the equator on the western margin of Pangea (Barbeau, 2003; Blakey, 1996; Condon, 1997). The collision of Gondwana and Laurussia created a compressional tectonic regime resulting in

numerous thrust-bound structural uplifts. These are collectively known as the Ancestral Rocky Mountains, and are composed of crystalline igneous and metamorphic basement (Barbeau, 2003). Up to twenty flexural-controlled foreland basins were created, with the Paradox Basin considered the largest, covering an area of fifty thousand square kilometres across southeast Utah and western Colorado (Barbeau, 2003; Condon, 1997).

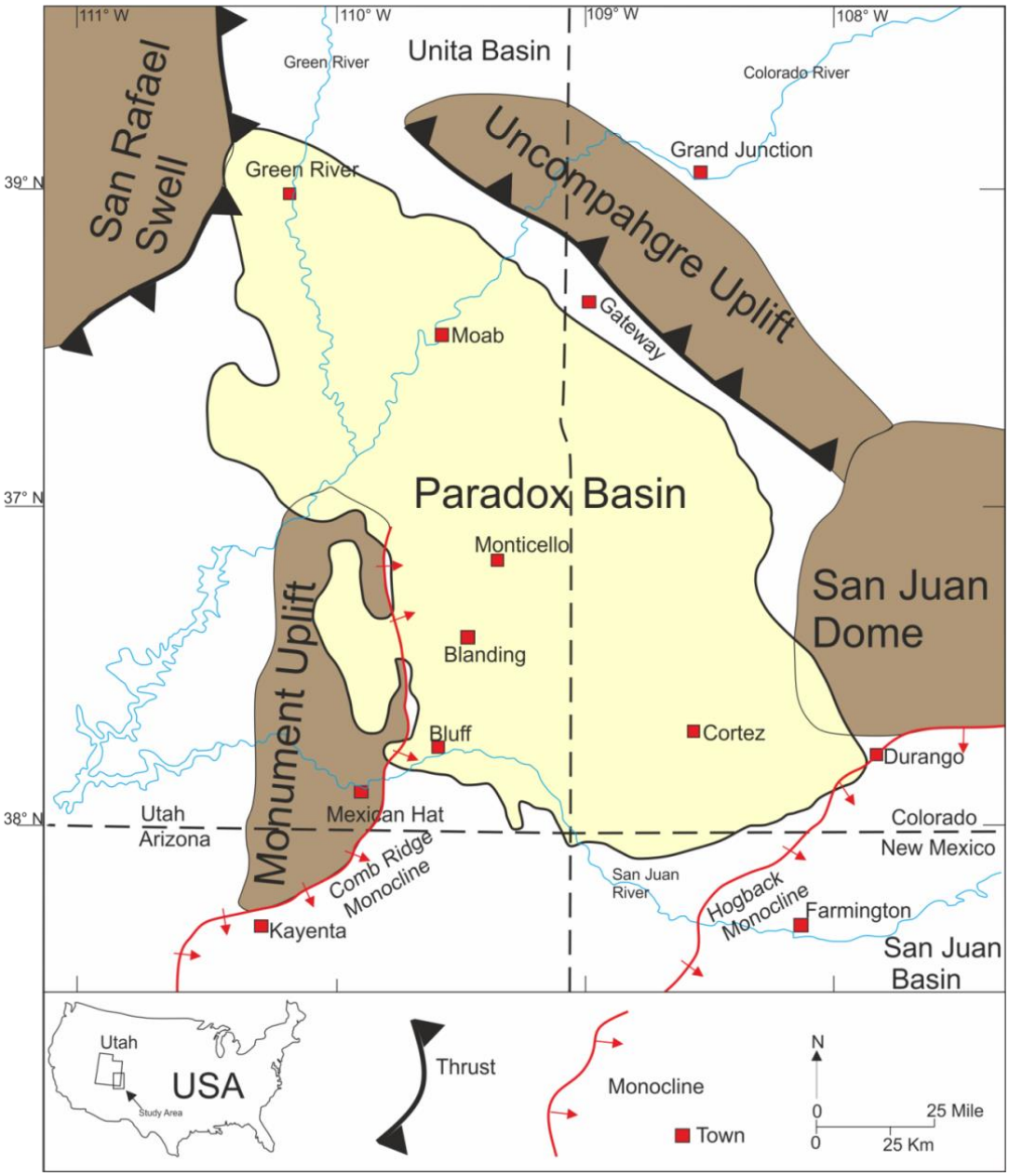

Figure 1.4 Location of the Paradox Basin and geographical features within the Four Corners region of the western USA. (After Lawton & Buck 2006: Kelley, 1958)

1.4.1 Structural Evolution

The broadly oval shaped Paradox Basin developed as an intercontinental flexural basin (Barbeau, 2003), in response to the rapid uplift and ensuing crustal loading of the Uncompahgre Uplift during the development of the Ancestral Rocky Mountains. Initial subsidence during the Middle Pennsylvanian was rapid, resulting in an asymmetric transverse basin profile, with the foredeep region lying to the immediate southwest of the Uncompahgre Uplift (Nuccio & Condon, 1996; Barbeau, 2003).

The stratigraphical limits of the basin are defined as the maximum extent of the salt deposits of the Paradox Formation (Condon, 1997). Salt remobilisation and dissolution form many of the topographical and structural features present within the basin (Condon, 1997; Barbeau, 2003).

Structural limits of the basin consist of the Uncompahgre Uplift which runs along the north-eastern margin of the basin. The San Rafael Swell forms the boundary to the north-west, with the northern margin merging with the southern end of the Unita Basin (Condon 1997). The south-eastern margin is defined by the Hogback Monocline, which separates the Paradox Basin from the San Juan Basin by an area of topographic relief known as the Four Corners Plateau (Condon, 1997). The south and southwestern boundaries are poorly-defined, but are considered to trend northwest from the Four Corners Plateau across Monument Upwarp (Condon, 1997).

1.4.2 Stratigraphy and Paleogeography

A stratigraphic summary of the Paradox Basin is presented in Fig. 1.5. The units within the basin itself are divided into the Hermosa Group (Pennsylvanian) and the Cutler Group (Permian) in which four thousand metres of sediment accumulated sourced primarily from the erosion of the Uncompahgre Plateau, forming a large

alluvial clastic wedge in the proximal basin (Mack & Rasmussen 1984; Nuccio & Condon, 1996; Barneau, 2003).

Hermosa Group

The Pennsylvanian Hermosa Group is divided into the Paradox and Honaker Trail Formations (Barbeau, 2003; Nuccio & Condon, 1996). Transgressive-regressive events and cyclic glacio-eustatic sea level changes are the dominant controls on observed sedimentology (Goldhammer *et al.,* 1991; Blakey & Ranney, 2008; Williams, 2009).

Paradox Formation

Deposited during the maximum phase of subsidence, the formation comprises black marine siltstones and mudstones, evaporites and dolostone formed by cyclic marine transgression, and subsequent desiccation of a restricted inland sea (Barbeau, 2003; Nuccio & Condon, 1996). The basin forebulge became exposed during periods of sea level fall, isolating the basin waters and resulting in brines. The salts within this formation are responsible for multiple structural and topographic features due to dissolution and post depositional halokinesis (Barbeau, 2003; Nuccio & Condon, 1996).

Honaker Trail Formation

The Honaker Trail Formation lies conformably over the Paradox Formation and is a mix of cyclic marine limestones, sandstones and mudstones to the south and west of the basin, with terrestrial deltaic, fluvial and aeolian deposits present in the north-east of the basin. This represents a north-easterly transition from a shallow marine to a continental environment (Barbeau, 2003; Condon, 1997; Nuccio & Condon, 1996).

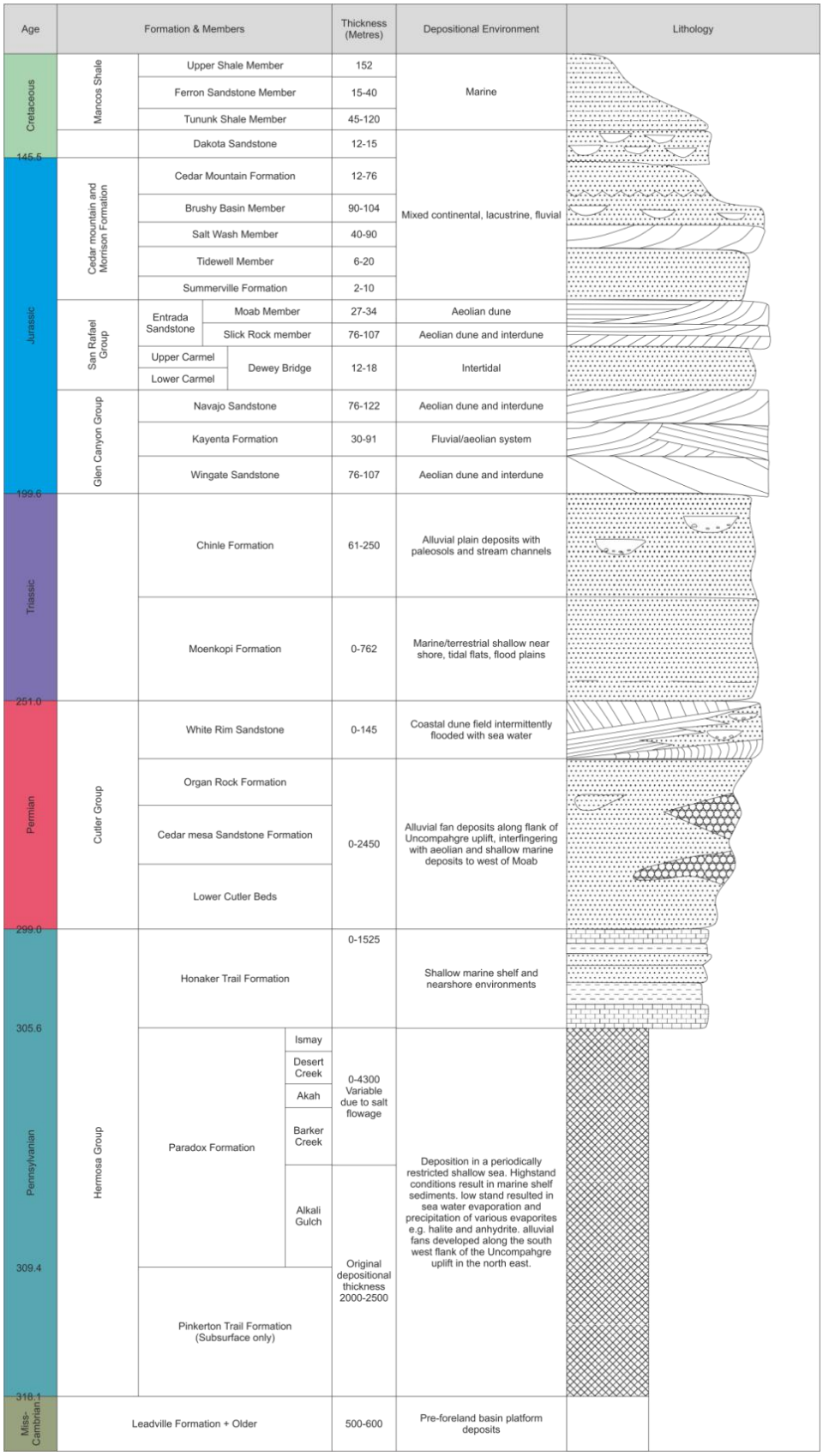

Figure 1.5 Stratigraphy of the Paradox Basin (After Trudgill 2011)

The Cutler Group

The Cutler Group lies within the central part of the Paradox Basin and forms a near-complete geological record of the basin from the latest Pennsylvanian until the mid-Permian (Blakey *et al.* 1988; Peterson, 1988). It is subdivided into: the Lower Cutler beds; the Cedar Mesa Sandstone; the Organ Rock Formation; the De Chelly Sandstone; the White Rim Sandstone; the Kaibab Limestone, and a laterally equivalent undivided unit of the Cutler Group (Fig 1.6). This undifferentiated unit occurs to the east of the basin, proximal to the sediment source shed from the Uncompahgre Uplift (Condon, 1997).

The Cutler Group shows great thickness variations over the span of the Paradox Basin, with thicknesses around 1800 m present in the proximal foredeep regions (Condon, 1997), to thicknesses of 530 m in the distal part of the basin (Barbeau, 2003). The thickness variations are an outcome of structural damming as a result of halokinetic deformation of the Paradox Formation evaporite deposits (Condon, 1997). Structural damming and concurrent subsidence of the proximal foredeep region confined clastic sediment shed from the Uncompahgre Uplift, limiting the expansion of the Cutler Group westerly, to the proximal regions of the basin until all available accommodation space filled (Barbeau, 2003).

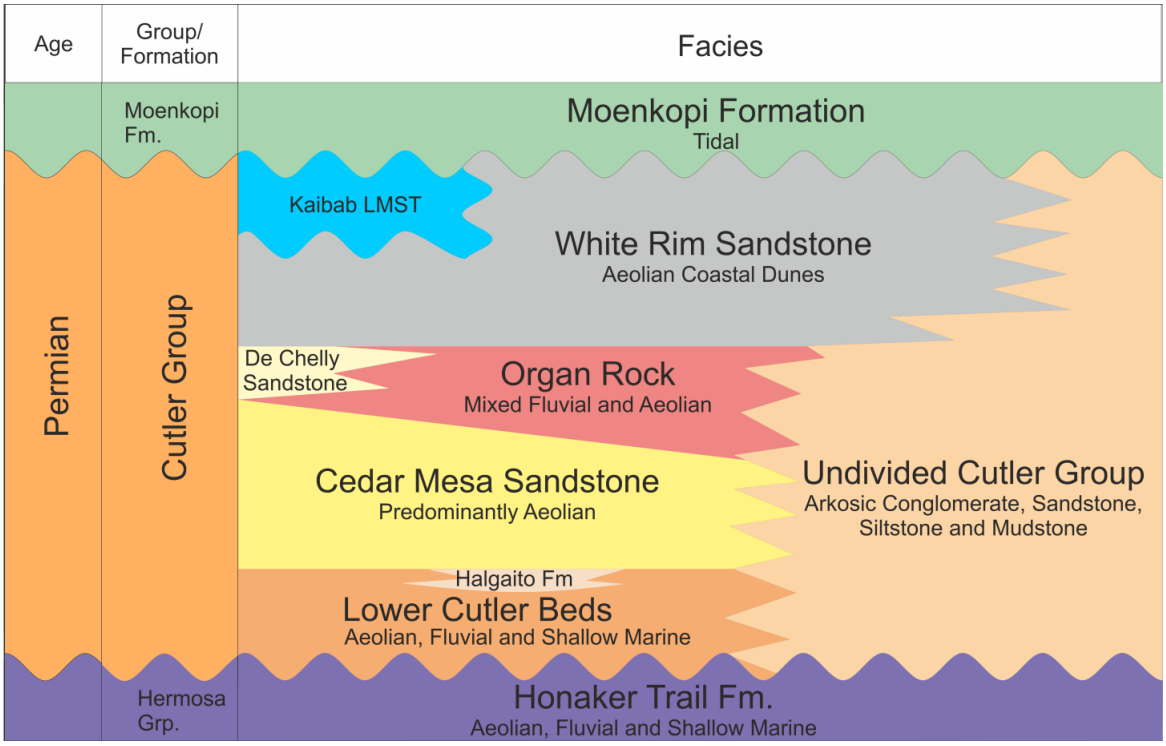

Figure 1.6 Stratigraphy and facies found in South East Utah (after Condon 1997)

The lower Cutler beds

The lower Cutler beds (Fig. 1.7A) deposited in during the late Pennsylvanian to early Permian, form the oldest strata of the Cutler Group, and conformably overly deposits of the Hermosa Group (Loope *et al.,* 1990). In places, the lower Cutler beds are intercalated with the Cedar Mesa Sandstone, and interdigitate with the fluvial deposits of the undifferentiated Cutler Group to the north-east of the basin close to the Uncompahgre Uplift (Nuccio & Condon, 1996; Condon, 1997).

The lower Cutler beds were previously known as the Rico Formation (McKnight, 1940) and was described as a transitional unit between the underlying marine units of the Hermosa Group and the continental units of the overlying Cutler Group. Baars (1962) argued for a shallow marine origin of the formation's cross-bedded sandstone and claimed an unconformable relationship between the Hermosa and Cutler groups, suggesting that they formed in two separate basins. This resulted in the renaming of the lower Cutler beds to the Elephant Canyon Formation and an

assignment to the lowermost part of the Cutler Group (due to interfingering with the Cedar Mesa Sandstone, and appearing disparate to the Hermosa Group) (Baars, 1979). Loope (1984) and Loope *et al.* (1990) questioned the existence of the unconformity based on faunal evidence, recommending it be once again related to the underlying Hermosa Group, and proposed the adoption of the now widely-accepted informal term 'lower Cutler beds' (e.g. Condon, 1997; Rankey, 1997; Soreghan & Elmore 2002; Jordan & Mountney, 2010 Jordan & Mountney 2012).

The formation consists of three main facies associations: aeolian; fluvial and shallow marine (Jordan & Mountney 2010). Sediment was supplied to the basin from the uplift of the Uncomphagre Uplift via alluvial fans and braided rivers which flowed to the south-west (Mack, 1977; Campbell, 1980; Mack & Rasmussen, 1984). The distal parts of the basin were composed of south-easterly migrating aeolian dune fields (Loope, 1981; 1985). Shallow seas, that periodically transgressed eastward across low-relief parts of the basin, bordered the western edge of the dune fields (Loope, 1984). This has led to a complex relationship of facies architectures, with periodic marine transgressions from the west mixed with a paleowind transport direction to the south-east and paleofluvial flow direction to the south-west (Jordan & Mountney, 2010).

Previous work by Terrell (1972) describes these features as a delta plain and shoreline setting, influenced by fluctuations between an arid to humid climate. This resulted in fluvial channels, sourced from the Uncompahgre Uplift, flowing south-west through an aeolian dune field before reaching a shallow sea lying to the west. Condon (1997) suggests a similar deltaic depositional environment with shifting depocentres to account for continental deposits grading into marine sequences in the north-west of the basin. However, recent work has contextualised the deposits within a sequence stratigraphic framework (Jordan & Mountney 2012), and show

the deposits as part of a cyclic succession recording repeated oscillations between episodes of sea level lowstand occurring concurrently with an arid climate generating aeolian deposits and highstand occurring with a change to more seasonal humid conditions in which fluvial systems dominate. Rising sea levels result in fluvial encroachment into former dune fields and deflation of dunes not preserved below base level. Episodes of transgression and marine flooding resulted in the deposition of carbonate and mixed clastic-carbonate sediments across large parts of a low relief coastal plane. Twelve separate parasequences record these oscillating conditions, with the maximum final transgression forming a maximum flooding surface which represents the end of the lower Cutler beds sedimentation (Jordan & Mountney, 2012).

The Halgaito Formation

The Halgaito Formation, also referred to as the Halgaito Tongue, outcrops in a small area of south-eastern Utah and is described as dominantly aeolian by Condon (1997). The formation grades northwards into the Cedar Mesa Sandstone, and is equivalent to a portion of the lower Cutler Beds in the Canyonlands area (Fig 1.1), which grade laterally into the Cedar Mesa Sandstone (Baars, 1987). Chaney *et al.,* (2013) has associated *Arthropleurid* trackways in cyclic aeolian, fluvial and marine bands to the Halgaito Formation sandwiched between the underlying Honaker Trail Formation and overlying Cedar Mesa Formation. The Halgaito Formation is absent through much of the modern literature with Jordan & Mountney (2012) describing this succession as the lower Cutler beds, therefore the Halgaito Formation may not be classified as a distinct Formation, as it is coeval with the lower Cutler beds and shows similar facies.

Cedar Mesa Sandstone

The Cedar Mesa Sandstone, (Fig. 1.7B) deposited during the early Permian (Cisuralian), conformably overlies the lower Cutler beds. The boundary is defined either as the last marine limestone bed of regional extent (Shafer Limestone) at the top of the lower Cutler beds, or where absent, the boundary is gradational with a complex interfingering relationship. In the north of the basin (Moab (Fig 1.1) the two units are time equivalent (Loope, 1984, 1985; Jagger & Mountney, 2004; Jordan & Mountney, 2010).

The formation is predominantly aeolian, outcropping extensively in the south western Paradox Basin (Condon 1997, Baars, 1987). It grades into interbedded sandstones, limestones, siltstones and evaporites to the southeast of Monument Uplift near Bluff into the San Juan Basin (Huffman & Condon, 1993, Condon, 1997).

Organ Rock Formation

The Organ Rock Formation (Fig. 1.7C) was deposited during the Permian Artinskian stage and conformably overlies the Cedar Mesa Sandstone with a gradational boundary (Baars, 1975; Blakey, 1996; Condon, 1997; Stanesco *et al.*, 2000). The Organ Rock Formation is overlain conformably by the White Rim or De Chelly sandstones to the west of the Colorado River, near Bluff (Blakey, 1996; Dubiel *et al.,* 1996; Condon, 1997; Stanesco *et al.,* 2000). However, in the Canyonlands area and across the Monument Uplift these units are not present and it is overlain unconformably by either the Triassic Moenkopi or Chinle Formations (Condon, 1997).

The formation is described as either a terminal fluvial fan system (Cain & Mountney 2009) or a distributive fluvial system (Owen *et al.,* 2015) and has been divided into several different fluvial and aeolian facies associations.

De Chelly Sandstone

The De Chelly Sandstone (Fig 1.7D), deposited during the Artinskian has an uncertain relationship with the underlying Organ Rock Formation (Condon, 1997; Stanesco *et al.,* 2000), however local interfingering relationships in the Monument Valley area suggest a conformable and gradual transition (Stanesco *et al.,* 2000).

Initially considered contemporaneous with the White Rim Sandstone (Baars, 1962), subsequent work (Blakey; 1990) has correlated the White Rim Sandstone to the older Kaibab Limestone, and the De Chelly with the older Coconino Sandstone (an aeolian erg deposited in northern Arizona). This shows an age difference between the White Rim Sandstone and the De Chelly sandstone, either due to an unrecognised unconformity within the Organ Rock Formation (as this is considered to conformably underlie either the De Chelly or White Rim Sandstone) or that there is an unconformable boundary between the Organ Rock Formation and the White Rim Sandstone (Blakey; 1996; Condon, 1997). The De Chelly Sandstone is unconformably overlain by either the Triassic Moenkopi Formation or the Chinle Formation (Condon, 1997).

The formation is divided into three subunits (Condon, 1997; Stanesco, 1991) two cross-bedded aeolian sandstone units, one representing migration to the southeast, the second with a migration direction to the south-west. A final unit of aeolian sandsheet, sabkha and mudflat deposits is present in northern Arizona (Stanesco, 1991).

White Rim Sandstone

The White Rim Sandstone (Fig. 1.7E), also deposited during the Artinskian is conformably underlain by either the Organ Rock Formation, or where the Organ Rock Formation is absent, the lower Cutler beds or the Cedar Mesa Sandstone. In the northwest the White Rim Sandstone is underlain by carbonates belonging to the

lower Cutler Beds (Baars, 1987, Condon, 1997) and is either overlain conformably by the Kaibab Limestone or unconformably by the Moenkopi Formation (Condon, 1997).

The White Rim Sandstone is primarily a distinct aeolian cross-bedded sandstone unit which in outcrop forms a prominent white coloured horizon, with overlying strata weathering back to form benches above it (Condon, 1997). The deposits represent brachanoid dunes migrating to the southeast within a large erg (Huntoon & Chan, 1987; Steele-Mallory, 1982). A younger thin drape of marine facies has been recognised (Chan & Huntoon, 1984; Huntoon & Chang, 1987; Stanesco *et al.,* 2000), composed of wave-ripples, escape structures and rip-up clasts derived from the underlying lower unit (Stanesco *et al.,* 2000).

Kaibab Limestone

The Kaibab Limestone (Fig 1.7F) consists of limestone and dolomite and only exists in the western part of the Paradox Basin, though no outcrop is present and is only recognised from borehole data. The formation onlaps the underlying White Rim Sandstone and has an erosive contact with the pre-Triassic unconformity above (Condon, 1997).

Triassic Succession

The top of the Cutler Group is represented by the Permo-Triassic unconformity which cuts down into the underlying succession. The Kaibab Limestone and White Rim Sandstone are truncated by this unconformity and, where absent, the Permo-Triassic unconformity cuts down to the The De Chelly Sandstone and Organ Rock Formations (Condon, 1997; Stanesco *et al.,* 2000). In south-eastern Utah the Permian succession is overlain by the basal-Triassic Moenkopi Formation, whereas in the Colorado portion of the basin, the underlying Cutler Group is unconformably overlain by the Chinle or correlative Dolores Formation (Condon, 1997).

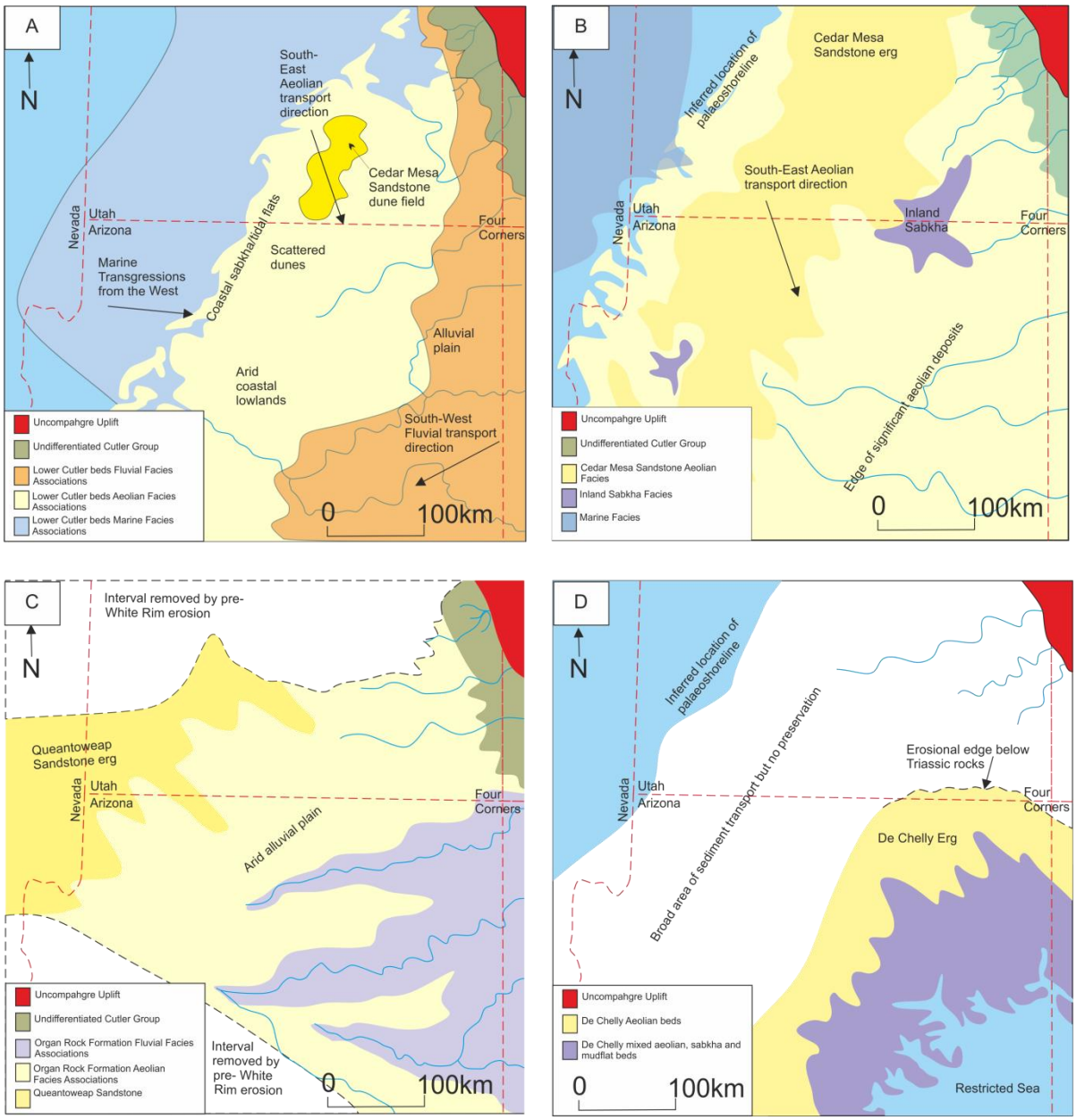

Figure 1.7 Paleogeography and facies found in the (A) lower Cutler beds, (B) Cedar Mesa Sandstone, (C) Organ Rock Formation, (D) De Chelly Sandstone, (E) White Rim Sandstone and (F) Kaibab Limestone (after Blakey 1996) See facies key shown in lower left side of each diagram for more information.

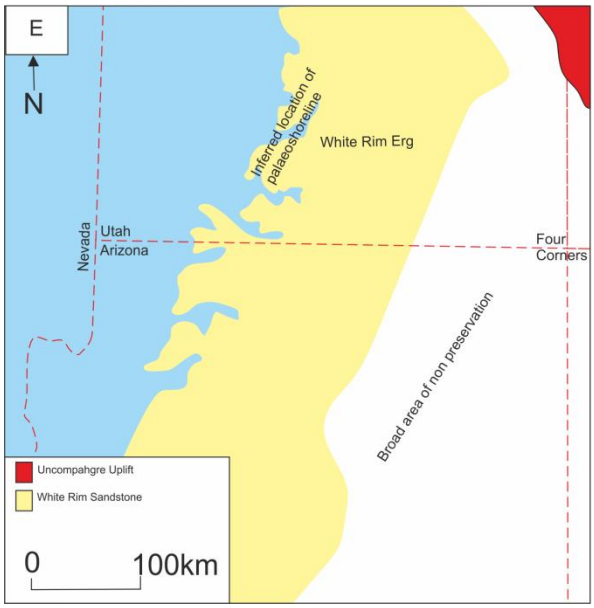

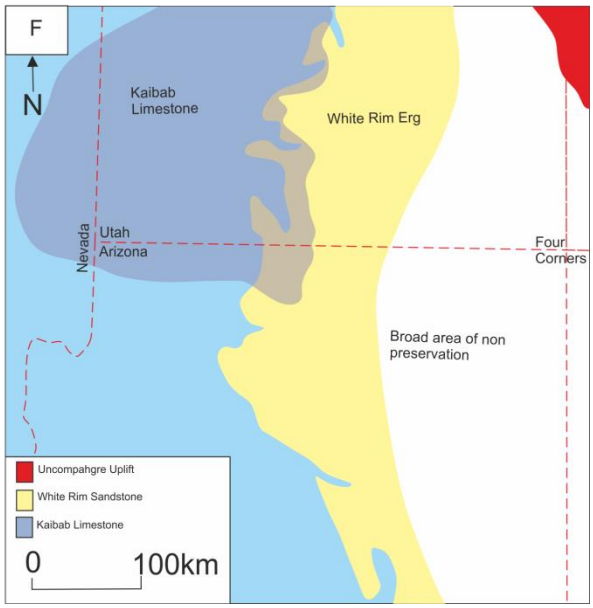

The Moenkopi Formation

The Moenkopi Formation features mixed marine and terrestrial strata deposited along shallow, near-shore tidal flats, and fluvial flood plains (Stewart *et al*., 1972; Doelling, 1988). The Formation shows thickness variations ranging from 700 m at the subsurface to being locally absent over salt highs (Doelling & Morgan, 2000; Trudgill *et al*., 2004).

The Chinle Formation

The Chinle Formation shows a variety of depositional environment and thicknesses, with processes and facies being strongly controlled by localised salt movement. Several local angular unconformities form adjacent to salt wall structures (Trudgill, 2011), with depositional environments ranging from lacustrine, perennial-fluvial, semi-arid fluvial to aeolian (Doelling, 1988; Hazel, 1994).

1.5 Sedimentology & Geological Background of the Cedar Mesa Sandstone

The Cedar Mesa Sandstone is a predominantly aeolian succession of early Permian (Cisuralian) age (Baars, 1962). Originally described as aeolian (McKnight, 1940;

Baker, 1946), Baars (1962, 1979) and Mack (1977, 1979) claimed the deposits were shallow marine in origin. However, the presence of aeolian stratification in the form of reverse-graded forsets (Loope, 1984) and other non-marine indicators such as rhizoliths (Stanesco & Campbell, 1989) reaffirmed an aeolian origin. Exposed across the Canyonlands, Indian Creek and Needles area of southern Utah (Fig. 1.1) the Cedar Mesa Sandstone has a complex interfingering relationship with the fluvial dominated strata of the distal Cutler Group in the Indian Creek and Needles district. Whereas, north-west of Canyonlands, the Cedar Mesa Sandstone interacts with shallow marine limestones. The fluvial strata shed south westerly from the Uncompaghre Uplift - an uplifted block of the Ancestral Rockies - into the Paradox Basin (Mack, 1977; Mountney & Jagger, 2004).

Shallow marine limestones and paleocurrent data indicate the location of a palaeoshoreline towards the northwest (Fig. 1.7b) and a predominant northwest-southeast transport direction with sediment sourced from marine shelf sand blown inland (Loope, 1984). The aeolian deposits represent a northeast-southwest trending coastal erg system parallel to the palaeoshoreline (Blakey, 1988; Blakey *et al.,* 1988). The erg extends one hundred kilometres southwards, with the centre of the erg located 80 miles west of Blanding near Hite (Fig. 1.1), Utah (Langford & Chan, 1993; Mountney, 2006). Major flooding surfaces, present in the southeast, subdivide the erg (Langford & Chan, 1989), which eventually grades into sabkha deposits near Bluff (Fig 1.1) (Blakey, 1988; Blakey *et al.,* 1988; Peterson, 1988; Huntoon *et al.,* 2000; Mountney & Jagger, 2004).

1.5.1 Facies Associations

Nine distinct facies associations have previously been observed in the Cedar Mesa Sandstone and are described below.

Aeolian Dune Facies Association

The aeolian dune facies of the Cedar Mesa Sandstone is primarily composed of fine-grained quartzose sandstone with occasional layers or lenses of medium-to coarse-grained sand (Stanesco & Campbell, 1989). Three facies types are described by Mountney & Jagger (2004), these being: moderate-angle cross-laminated translatent wind ripple facies; moderate-to high-angle cross-stratified grainflow facies; and grainfall facies.

The cross-laminated wind ripple facies are characterised by fine-grained, moderate to well sorted sandstones, with one to four millimetres thick, sharp-based tabular-planar laminae arranged into 0.1-15 m thick sets averaging at 1.4 m (Mountney & Jagger, 2004; Stanesco & Campbell, 1989). Foreset dip direction is dominantly southeast suggesting transverse or barchanoid ridge dunes migrating to the southeast (Stanesco & Campbell, 1989; Blakey & Middleton, 1983). Inverse grading, though rare, where present, is repetitive and in sequences several millimetres thick (Mountney & Jagger, 2004; Stanesco & Campbell, 1989). Pinstripe lamination, as described by Fryberger & Schenk (1988), is also widely reported (Mountney & Jagger, 2004; Ahlbrandt & Fryberger, 1982; Stanesco & Campbell, 1989).

Grainflow facies show fine- to medium-grained, well-sorted sandstone several centimetres thick (1.5cm) (Mountney & Jagger, 2004) with grainflow toes interfingering and pinching out against wind ripple strata along the base of foreset beds (Mountney & Jagger, 2004; Stanesco & Campbell, 1989).

Contorted and convolute bedding is common amongst the foreset layers of the aeolian dune facies within the Cedar Mesa Sandstone (up to 3m) (Stanesco & Campbell, 1989). This soft sediment deformation has been attributed to storms wetting sand, which subsequently slumped down the slip face (Thompson, 1969) or post depositional earthquake-induced liquefaction (Doe & Dott, 1980; Horowitz,

1982). Loope (1981) and Horowitz (1982) infer the high porosity created in grainflow strata is what primarily limits the deformation of foreset layers.

Interdune Facies Association

The Interdunal Facies Associations reflect the environment in which deposition occurred. Dry interdune associations found in the Cedar Mesa Sandstone show horizontally to low-angle laminated wind rippled strata (Mountney & Jagger, 2004; Stanesco & Campbell, 1989).

Damp interdune associations show wavey laminated sandstones, adhesion features, small-scale contorted bedded (<0.2m) and calcrete-baring palaeosols (Kocurek, 1981; Kocurek & Fielder, 1982 Mountney & Jagger, 2004). Bioturbated burrows and surface traces, rhizoliths and evaporite replacement pseudomorphs are also common (Loope, 1984, 1988).

The wet interdune associations of the Cedar Mesa show thin bands of micritic freshwater limestone, pinching out into planar laminate siltstones and fine grained sandstones (Stanesco & Campbell, 1989; Mountney & Jagger, 2004). Nodular and laminar chertsilcretes are present as well as reworked aeolian sandstone. Surfaces show wave ripples, desiccation cracks and polygons, gypsum casts, burrows, and root casts (Stanesco & Campbell, 1989; Mountney & Jagger, 2004).

Sandsheet Facies Association

Sandsheet associations have been identified in the Cedar Mesa Sandstone by Stanesco & Campbell (1989), Mountney (2006) and Cecil (2015). The facies is described as low-angle to horizontally stratified wind-rippled fine grained sandstone. Medium to coarse sand grains coating finer grained bedding is described as aeolian deflationary lag (Stanesco & Campbell, 1989). These units are 1 -3 m thick with a large lateral extent often several hundred metres (Mountney, 2006). Facies

also show small-scale root casts, trace fossils and calcified rhizoliths (Mountney & Jagger, 2004; Stanesco & Campbell 1989).

Cecil (2015) describes red chert (jasper) in sandsheet associations, linking its continentally-derived parentage and silica source to aeolion deposition of siliceous sediments or 'dust'.

Paleosols Association

Paleosols are widespread within the Cedar Mesa Sandstone, typically fine grained sandstone exhibiting mottled colouring, massive textures and lenses of claystone and discontinuous nodular limestones (Stanesco & Campbell, 1989). The paleosols are commonly bioturbated with large infilled burrows. Dzenowski *et al.* (2013) have identified large-diameter burrows of probable amphibian or reptile origin (Hasiotis & Rasmussen, 2010) within the paleosol deposits at Comb Ridge, and within fluvial and interdune associations at Moki Dugway. The subhorizontal elliptical burrows are up to 50 cm in length and 15 cm in diameter. The paleosols lack the distinct soil horizon shown in mature pedogenic systems, however, they do represent stabilization due to soil development within a dune field (Stanesco & Campbell, 1989).

The multicoloured sandstones are interbedded with fluvial and interdune facies. Upper and lower contacts, though occasionally gradational, are most commonly distinct, resulting in horizontal bedding planes that have great lateral extent and can be traced for the length of the outcrop up to 200 km (Loope, 1985; Stanesco & Campbell, 1989).

Initially, the origin of these bedding planes was proposed as a climbing bedform migration surface (Kocurek, 1981; Rubin & Hunter, 1982). However Loope (1984) argues that these planes are Stokes surfaces (Stokes, 1968) in which erosional surfaces are caused by a marine transgression or change in wind direction, which

leads to deflation down to the water table (Loope, 1984, 1985; Kocurek, 1984). Stanesco & Campbell, (1989) have shown their correlation of palaesols to climb stratigraphically downwind, using Rubin & Hunter's (1984) model: which shows paleosols and evaporite bounding surfaces can be formed by climbing dunes; they conclude that these bounding surfaces are related to adjacent migrating aeolian facies and are climbing bedforms.

Fluvial Facies Association

Channels, braided, sheet flood and ponded fluvial systems are common around erg margins (Landford & Chan, 1988, 1989). Mountney & Jagger (2004) divide fluvial facies found within the Cedar Mesa Sandstone into: arkosic sandstone facies forming the majority of fluvial strata (80% within their study area), mudstone and siltstone facies (15%) and fluvial conglomerate facies (5%).

The arkosic sandstone facies is feldspar, clay and mica rich, forming massive parallel-laminated and trough cross bedded, purple and brown, moderate- to poorly-sorted sandstones, which are texturally immature, with a large grainsize variation ranging from very fine to very coarse (Mountney & Jagger, 2004). Features within the facies include angular to subround quartz and feldspar pebbles, rip-up clasts and mudballs up to cobble grade (Mountney & Jagger, 2004). The sandstone facies has been described as up to 10 m thick with individual trough cross sets ranging between 0.25-2.0 m thick and 8 m wide (Stanesco & Campbell, 1989).

The mudstone and siltstone facies exhibit massive, blocky and low-angle to horizontal laminations, with root traces, rhizoliths and calcrete nodules (Loope, 1988; Mountney & Jagger, 2004).

The fluvial conglomerate facies shows extraformational quartz, feldspar and lithic clasts, with intraformational sandstone and mudstone rip-up clasts (Mountney & Jagger, 2004).

All three fluvial facies interfinger with each other and the aeolian facies. The fluvial facies are interpreted as channel and overbank deposits from streams draining the ancestral Uncompahgre Uplift primarily in a northeast southeast direction (Stanesco & Campbell, 1989).

Several reptile bones and plant stems and leaves have been observed within the fluvial facies, plant impressions are fragmental suggesting transportation into the sediments rather than insitu deposition (Stanesco & Campbell, 1989).

Lacustrine Facies Association

A semi-perennial lake association is described by Massad (2013) as thin sandy limestone deposits found in the Comb Ridge area. The limestones are thin (0.25-0.90 m) horizontally bedded, with occasional chert nodules, and sandstone and silt interbeds (Massad, 2013). The limestones pinch out laterally into aeolian facies and have sharp upper and lower contacts with mudstone units and stabilised vegetated aeolian dunes. A complete lack of any body fossils is also noted (Massad, 2013).

Interdunal pond deposits have been previously described by Stanesco & Campbell (1989), Duncan (2006), and Langford *et al.,* (2008); however, Massad (2013) rejects this interpretation due to the lateral extent (up to 4 km) of the lacustrine facies. The lack of microfossils and fossil fragments, a smooth upper and lower surface compared to the rough surface seen in pond deposits, and the lack of confinement to interdune areas form the basis of this facies interpretation (Massad, 2013).

Freshwater to brackish interdunal pond deposits fed by streams entering the dune field have been described by Stanesco & Campbell (1989), Duncan (2006), and Langford *et al.,* (2008). These deposits occur as randomly-distributed lenses of limestone, chert and sandstone, with a thin thickness (0.30–0.60 m).They have irregular upper and lower contacts and a distinct rough and bumpy appearance

(Massad, 2013), also showing ostracod microfacies, dolomite cementation and intense rooting at the margins.

Sabkha/Evaporitic Facies Association

Southeast of Monument Uplift, near Bluff and Comb Ridge, at the edge of the Cedar Mesa Sandstone, there is an abrupt facies change into thin aeolian sandstone, massive gypsum or anhydrite, light pink to grey siltstone, and thin limestone beds (Stanesco & Campbell, 1989; Sears, 1956; O' Sullivan, 1965; Condon, 1997). This facies was initially considered as part of the undifferentiated Cutler (Baars, 1962), but this evaporite facies was correlated to the Cedar Mesa Sandstone and can be traced south-eastward into the San Juan basin as a distinct lithological unit on the basis of geophysical logs (Huffman & Condon, 1993; Condon & Huffman, 1994).

The gypsum is massive to nodular, with localised chert nodules, forming thick layers up to 10 m which interfinger with thicker siltstone. Adjacent siltstone layers commonly show gypsum veins which cross cut bedding (Stanesco & Campbell 1989). Limestone beds are thin, bioturbated and show desiccation features and potential localised stromatalitc structures toward the top of the interval (Stanesco & Campbell 1989). Interfingering sandstones show indicative aeolian structures, such as grainflow and cross bedded wind ripples. Burrows and trails are observed, however, rhizoliths are absent (Stanesco & Campbell 1989). These features suggest that aeolian dunes encroached upon and interacted with an ephemeral evaporating body of water, for instance the lacustrine association reported by Massad (2013). Water level fluctuations often led to subaerial exposure of deposits as supported by the occurrence of desiccation and brecciation features (Stanesco & Campbell 1989).

Saline Pan Association

In the same locality as the sabkha facies, dark brown and pastel- purple fine grained silts and muds are found in association with the evaporitic beds described above.

These deposits typically are less than 2 mm thick, laminar, fissile, lacking any indication of vegetation and show evidence of soft sediment deformation and post-depositional compaction (Langford & Massad 2014).

Mudcracks infilled with aeolian sand are present and the beds are highly gypsiferous, with veins, nodules and thin gypsum beds. Underlying contacts are rough and irregular due to the dissolution of associated gypsum strata suggesting a syndeposition origin (Langford & Massad 2014).

These beds are interpreted as muds deposited on the edges of a saline sabkha or playa lake lying near to a dune field, and are termed a *saline pan.* The absence of any evidence of marine deposition suggests an origin far from the coast in a continental setting or as part of an extensive coastal sabkha (Langford & Massad 2014).

Inland vs. Coastal Sabkha

The geological features described previously can indicate either an inland sabkha associated with playas, or a coastal sabkha adjacent to marine tidal flats (Glennie, 1972). Lack of outcrop to properly define the environment led Stanesco & Campbell (1989) to carry out geochemical analysis. S^{34} isotope data of gypsum samples from the Comb Ridge area fell within the narrow marine indicator range for the Permian (Claypool *et al.,* 1980). However oxygen and carbon isotope were less than definitive, with only two out of four limestones tested falling within the common marine range for limestones (Hudson, 1977). This tentative isotopic result led Stanesco & Campbell (1989) to conclude that the Cedar Mesa Sandstone was in part fed by marine waters, with a mixing of fresh and marine waters under conditions of intense evaporation.

Work by Taberner *et al.* (2000) has shown that pure sulphate isotopic analysis as an environmental indicator can be problematic. Working with a known continentally-derived evaporite, isotopic composition analysis of sulphates suggested a fully

marine origin. Recycling of previous evaporites within a system may also throw up false isotopic results; marine evaporites may be fully recycled into continental evaporites but will maintain their marine isotopic signature. Ayora *et al.,* (1994) and Taberner *et al.,* (2000) suggest that any evaporites that show evidence of recycling should be avoided for isotopic analysis. Taberner *et al.,* (2000) suggest an integrated approach using numerical modelling of sulphate isotopic composition to quantify distinct water inflows aided with interpretations made from the formation, environmental markers, solutes and bromine content.

Massad (2013) claims an inland sabkha depositional environment for the gypsum facies based upon abundant evidence of fresh water vegetation in nearby sandsheet and fluvial facies, with the gypsum derived during a dry period resulting in evaporation of the semi permanent lacustrine facies described previously. Langford & Massad (2014) also suggest an environment isolated from marine waters by observing that the mudcracks found within the saline pan facies resemble mudcracks from the episodic drying of an inland evaporitic lake (*cf*. Clemmensen, 1978).

1.6 Thesis Overview

This section outlines the contents of each of the succeeding chapters within this thesis. Chapter Two gives an overview of the literature on arid continental basins focusing on aeolian and sabkha processes and their deposits. Chapter Three describes the sedimentary lithofacies, and deposits of the distal portion of the Cedar Mesa Sandstone, and develops depositional model. And provides a detailed microfacies description of carbonates found within the study area, and links them to the overall depositional setting interpreted previously. Chapter Four examines the facies gained from detailed gamma ray logging of outcrops, and places them in the

context of the interpreted sedimentary depots. Chapter Six details the cyclicity within the deposits and attempts to place the cyclic deposits within allocyclic processes. Chapter Seven applies the outcrop study of the Cedar Mesa Sandstone to a subsurface dataset on the Leman Sandstone and Silverpit Formation of the southern North Sea, UK. Finally conclusions and further work are discussed in Chapter Eight. Table 1.1 summarised the structure of the thesis and includes a brief description of each chapter and the data within.

Table 1.1 Summary Table of Thesis Organisation

Summary of Thesis Organisation

Chapter	Title	Description
1	Introduction	This chapter introduces the aim of the thesis and the study area. The chapter also summarises the current literature on the geological study of the western USA
2	Literature Review	This chapter presents a critical evaluation of current sedimentological research in arid continental basins. The main components of this chapter details the processes and deposits of aeolian and sabkha deposits
3	Facies, microfacies, facies associations and sedimentological interpretation of the Cedar Mesa Sandstone Formation	This chapter provides detailed description of each of the lithofacies identified within the Cedar Mesa Sandstone Formation. Facies associations based on dominant depositional processes are defined, which are then placed in context of their spatial distribution. Depositional models are then

		built which take into account these previous interpreted features.
4	Gamma Ray	This chapter describes the facies which have been identified from gamma ray logging of outcrop sections. The identified facies are then compared to sedimentological facies previously defined.
5	Cyclicity	This chapter examines the cyclic deposits identified. Models are built which describe the cyclic changes and these are placed in context of larger allocyclic processes. Correlations are made based on cyclicity, which is combined with gamma ray data to provide quantifiable interpretations of the cyclic mechanisms
6	Application to the Rotliegend of the southern North Sea	The analogue developed for the Cedar Mesa Sandstone is applied to downhole gamma ray data from the Rotliegend of the southern North Sea. Previously identified idealised trends are used to correlate and identify facies distributions. These are used to identify potential reservoir units and constraining the deposits within a climatic regime.
7	Conclusions and Wider Implications	The final chapter of this thesis presents the conclusions for the work, as well as

	outlining the future direction for understanding arid continental sedimentology, at both a depositional environment and basin-scale.

Chapter Two: Arid Continental Processes and Deposits- A Literature Review

This chapter will review the literature on arid continental settings, and will specifically focus upon the processes which act within aeolian and evaporites settings and the rocks deposited and preserved within them.

2.1 Introduction

Arid continental systems comprise many environments including: alluvial fans, aeolian, fluvial, sabkha, and lacustrine settings (Fig. 2.1). There is a wealth of study on each individual element, however the competing nature of each coeval setting is often overlooked.

Alluvial fans are conical-shaped coarse grained clastic deposits shed from elevated mountainous highs, common within the proximal regions of continental basins (e.g. Parsons & Abrahams, 2009; Harvey & Mathers, 2005; Blair & McPherson, 1994; Bull, 1977, Hooke, 1967; Blissenbach, 1954). These pass laterally and interact with the central basin deposits of aeolian or fluvial systems (Fig. 2.1).

Aeolian and fluvial deposits within continental basins commonly interact and are often dependant on climatic conditions. During arid periods aeolian deposits dominant and form large bedforms of multiple complex morphologies, whereas fluvial systems are restricted to ephemeral flash flood type deposits (e.g. North & Taylor, 1996). During humid periods dunes are much smaller and isolated whereas fluvial deposits dominate, restricting and reworking aeolian deposits (Fig. 2.1).

Deposits of the distal portion of arid continental basins often are composed of lacustrine or sabkha deposits, again often dependant upon climatic conditions. During humid periods desert lakes are pervasive, however during arid times these

lakes contract and often concentrate forming evaporites and vast saline pans (Fig 2.1).

This chapter specifically reviews the literature in relation to aeolian and evaporitic processes within arid continental settings in detail and describes the typical rocks deposited and preserved.

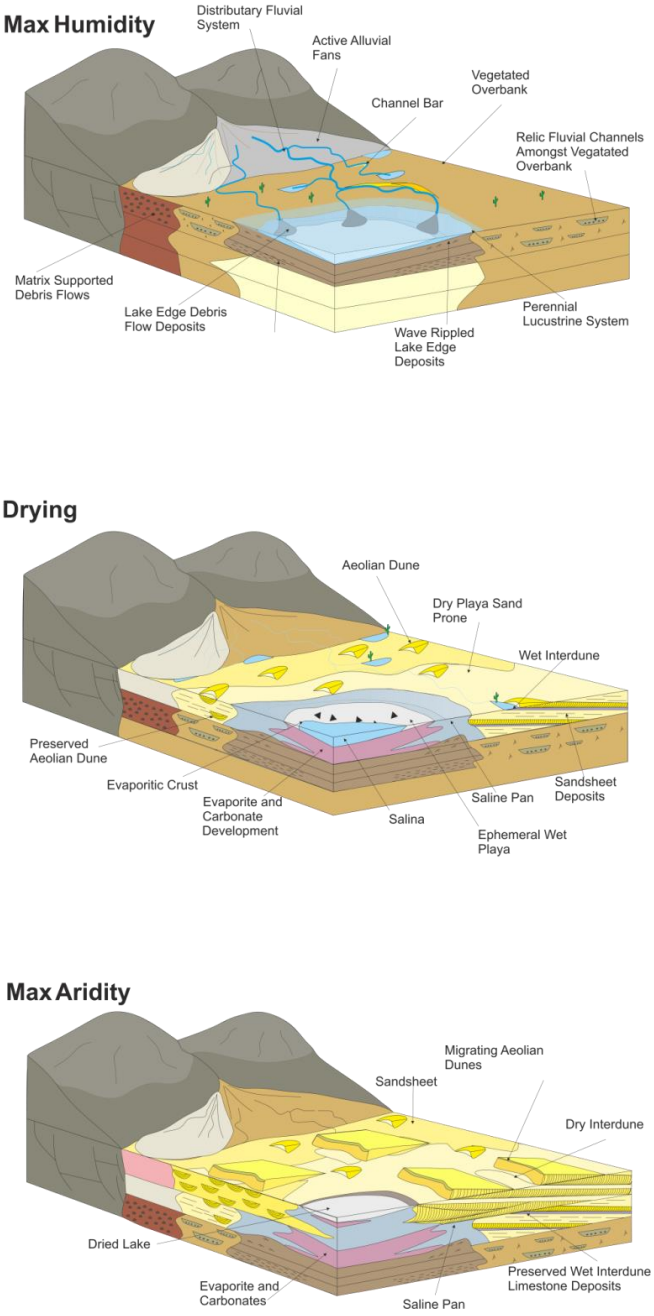

Figure 2.1 Summary diagram of arid continental basins and the environments they contain during arid or humid periods

2.2 Aeolian Processes

Aeolian processes occur wherever there is a supply of granular material and winds of sufficient strength to move them. Particles of ~ 110 μm diameter are the first to be transported by saltation, these grains collide with each other and further mobilise a wide range of other sized particles (Bagnold, 1941; Shao, 2008; Kok *et al.,* 2012). Particles over 500 μm generally do not saltate and are moved along the depositional surface when saltating grains knock into them, in a process known as reptation (Ungar & Haff, 1987).

Saltation is initiated when wind stress is sufficient to lift surface particles into the fluid stream, this occurs in loose sand at 0.05 N/m^2 (Greenley & Iversen, 1985). Wind accelerates the particles into ballistic trajectories with resulting impacts ejecting new particles giving an exponential increase in particle concentration (Duran *et al*., 2011), however this increased particle concentration results in a drag in the wind saltation layer (Bagnold, 1936). This impairment of the wind acts as a negative feedback, reducing the speed of the particles and decreasing the number of new particles which saltate. Ultimately limiting the number of saltating particles partially determines the characteristics of steady state saltation (Owen, 1964; Kok *et al.,* 2012).

The physics on aeolian saltation can be divided into four physical processes (Anderson & Haff, 1991; Kok & Renno, 2009):

1. The initiation of saltation by the aerodynamic lifting of surface particles.
2. Subsequent trajectories of saltating particles.
3. Splashing of surface particles in saltation by impacting saltators.
4. Modification of the wind profile caused by the drag of saltating particles.

These physical processes over an initially flat sand bed and cause instability and generates ripples with bedforms of a few centimetres to dunes with waveforms between 5–250 m (Collinson *et al.,* 2006; Kok *et al.,* 2012).

Dune formation is due to hydrodynamic instability (Kok *et al.,* 2012). Any change to an initial flat surfaces will results in a change in the wind dynamics. A small mound will force wind pressures to change and results in an increase in wind velocities as the streamlines are forced upwards and closer together, as the wind passes over this obstacle the streamlines spread out again as pressure changes are released (Fig. 2.2). Increased velocities towards the crest line results in erosion of previously deposited sediment whereas the subsequent decrease in air pressure and velocities deposits sediments on the lee side (Bagnold, 1941; Fourriere *et al.,* 2010; Kok *et al.,* 2012) (Fig. 2.2).

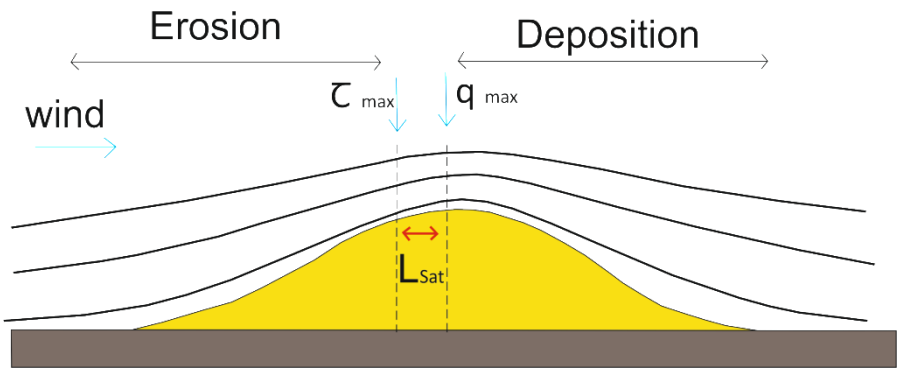

Figure 2.2 Physicals of wind-blown deposition (after Kok et al., 2012)

2.3 Aeolian Bedforms

Aeolian bedforms range in size from grain-scale ripples (less than 1 mm in height) to large scale draa (greater than 100 m in height), and primarily depend upon sediment supply (Willson, 1972).

2.3.1 Ripple Scale Bedforms

Ripples have a saturation length smaller than required by the hydrodynamic instability of wind to form dunes, and form due to the instability of the sand surface caused by impacting saltating particles (Bagnold, 1941; Anderson, 1987; Fourriere *et al.,* 2010; Kok *et al.,* 2012). Small depressions are formed on the surface of a sand bed from obliquely-colliding saltating grains creating chains of asymmetric undulations with a steeper profile on the lee side than the windward side (Kok *et al.,* 2012). Collisions of the grains may release more grains and cause forward movement. The upwind side of the ripples receive far more impacts than the downwind surface areas which is known as the shadow zone (Fig. 2.3). Ejected particles that reach this shadow zone are far less likely to be impacted and ejected again, leading to sand accumulation and growth (Kok *et al.,* 2012).

The instability leading to aeolian ripples is controlled by grain impact rather than hydrodynamics (as in the case of dune scale bedforms). Saltating particles provide the energy required for the low energy transport mechanism of grain movement by reptation (Kok *et al.,* 2012)

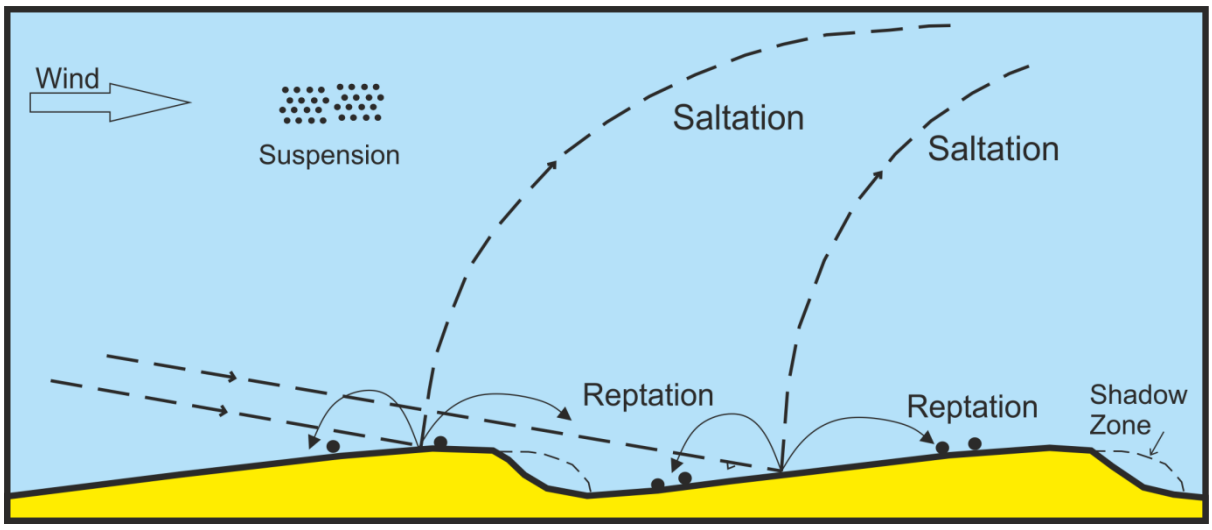

Figure 2.3 Saltation and reputation processes (after Duran et al., 2011)

Migration speeds and the morphology of ripples were initially documented by Bagnold (1941) and Sharp (1963) whilst wind tunnel studies showed an increase in ripple wavelength over time, up to a fully developed state existed (Seppälä & Lindé 1978). This was further developed by Andreotti *et al* (2006) concluding that the time scale for ripple formation is smaller than the one for dunes and transversely orientated ripples to wind direction on the surface of dunes provide an example of fully developed bedforms and can be used to reconstruct paeleowind directions (Kok *et al.,* 2012).

2.3.2 Dune Scale Bedforms

Dune scale bedforms with wavelengths 5-500 m primarily form by bedload transport from saltating grains (Parteli *et al.*, 2007) which accumulate as saltating grains bounce off the hard desert surface more effectively than off loose sand, creating a lower transport rate over the looser sand than the surroundings, leading to accretion (Bagnold, 1941). Dunes can coalesce to form mega dunes several hundred metres in height, limited only by the atmospheric layer within which sand transport occurs; mega dunes show complex morphology and superimposed bedforms of varying types (Kok *et al.,* 2012).

2.3.3 Draa Scale Bedforms

Draa are bedforms with wavelengths of 500–5000 m exceed 50 m in height and occur only in large ergs with very high sediment supply and transport rates (Wilson, 1971). Draa can be described as:

- *Simple*; which lack superimposed bedforms.
- *Compound*; show superimposed bedforms of the same morphological type.
- *Complex*; superimposed bedforms of different morphological type are shown (Mckee, 1979).

Complex draa bedforms preserved in the rock record have been attributed to the migration of superimposed dunes over slow moving larger draa (Mountney, 2006b).

2.3.4 Bedform Morphology

Wind direction and amount of sand available for transport are the dominant controlling factors of aeolian bedform shape (Wasson & Hyde 1983). Transverse bedforms (Fig. 2.4) form when the prevalent wind direction remains fairly constant and sand supply is high to form bedforms perpendicular to transport direction, with ripples on a dune providing an archetypal case (Kok *et al.,* 2012).

With scarce sediment supply and unidirectional wind, dual limbed crescent shaped Barchan dunes (Fig 2.4) form, arms pointing in the direction of migration (Kok *et al.,* 2012).

Wind trends can vary seasonally between two main directions, this variation results in longitudinal seif dunes (Fig 2.4) which show a meandering shape and align parallel to the sand transport direction. Multiple wind directions results in the dune becoming a depositional centre with star shaped (Fig 2.4) slip faces radiating out from the centre peak (Lancaster 1989).

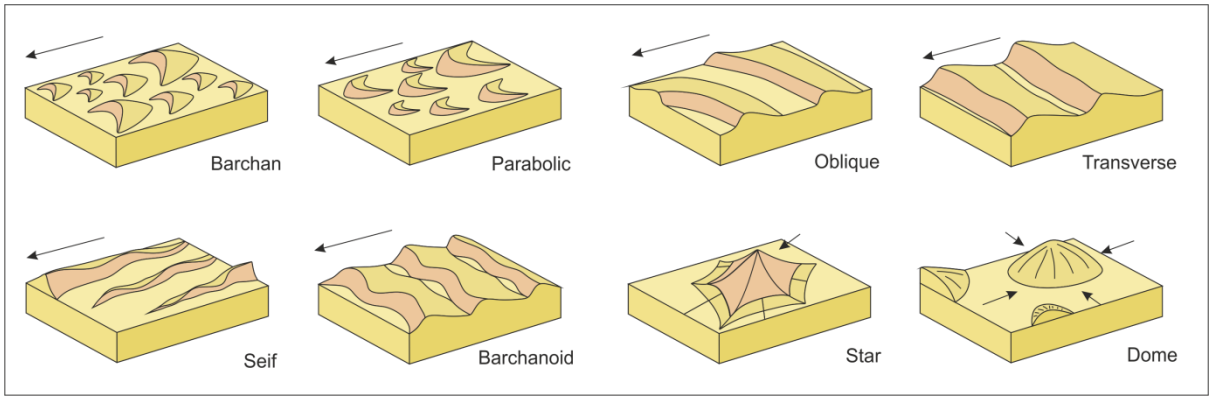

Figure 2.4 Varieties of aeolian bedform morphology (after Collinson et al., 2006)

2.4 Aeolian Sedimentary structures

2.4.1 Wind Ripples

Aeolian ripples form deposits in sandsheets, dry interdunes, and on low-relief dune and draa slopes often showing weak inverse grading due to a combination of finer material accumulating in sheltered ripple troughs and a relative lack of saltation related low-angle impacts or settling between coarser grains, resulting in a pour-in texture (Sharp, 1963; Fryberger *et al.,* 1992). Coarser grains accumulate on the upper part of the ripples due to high angle impacts of saltating grains on the stoss side promoting creep of the coarser grains towards the ripple crest (Mountney, 2006b) (Fig 2.5).

2.4.2 Grainflow

When angles of 34° are exceeded on the lee slope of aeolian dunes active slipfaces are generated resulting in numerous avalanche grainflow strata in which intergranular cohesion is lost and results in a cone-shaped deposit devoid of internal structure (Mountney, 2006b) (Fig 2.5).

Grainflows can show reverse grading due to coarse grains flowing further down-slope, in well-sorted sand hierarchical grainflows may not be distinctive, therefore the unit can only be categorised as an aggradation of flows (Howell & Mountney, 2001).

2.4.3 Grainfall

Reduction in wind transport capacity as wind carries saltating grains over the lee side of a dune results in the gravity driven deposition of these particles onto the upper lee slope (Nickling *et al.,* 2002). Repeated grainfall deposition on the upper lee slope is the dominant process and can lead to the critical angle being exceeded

resulting in avalanche processes reworking the grainfall strata into grainflow (Mountney, 2006b)(Fig 2.5).

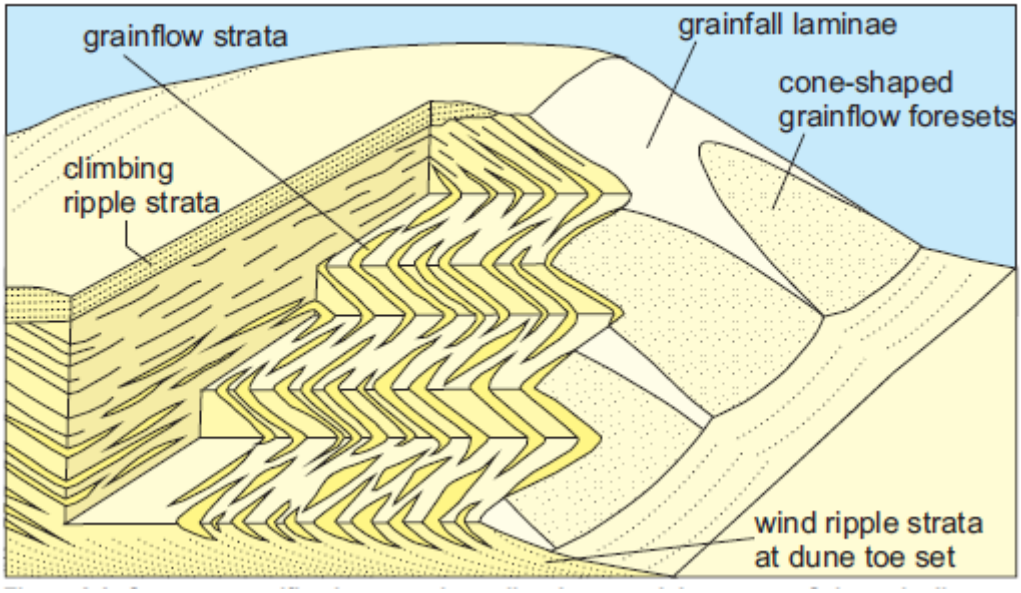

Figure 2.5 Schematic diagram showing the common small scale stratification types present in aeolian dunes and draa. (from Cain, 2009; Hunter 1977).

2.4.4 Adhesion

When the accumulation surface is damp, transported grains generate a range of adhesion structures, adhesion plane beds, adhesion ripples (Kocurek & Fielder, 1982) and adhesion warts (Olsen *et al.,* 1989). Adhesion plane beds stick to a damp surface devoid of previous adhesion ripple or warts features, resulting in a smooth bed with faint, crinkly laminations only a few millimetres thick which although hard to recognise are distinct from other laminated deposits by thickness, faintness and crinkly laminations (Kocurek & Fielder, 1982). Adhesion ripples form by trapping wind-blown sand with their crests lying transversely to wind direction. Adhesion warts form small domes or oval bumps (Fig 2.6) more randomly distributed than adhesion ripples. Warts and ripples can look like rain impact structures but are purely a surface feature (Kocurek & Fielder, 1982).

Figure 2.6 Adhesion warts forming small domes on an interdune surface within the Cedar Mesa Sandstone Formation

2.4.5 Cross Bedding

Cross bedding (Fig 2.7) is a process caused by continual and repetitive sedimentation on the lee slope of aeolian dunes due to grain fall, ripple and grainflow processes mentioned previously. Most aeolian bedforms show cross bedding and from this the former position of the lee slope and the process in which the sediment was deposited can be determined. Bedform migration leads to truncation of the cross bedding generating erosional bounding surfaces (Mountney, 2006b).

2.4.6 Soft Sediment Deformation

Small-scale deformation takes the form of either intradune folding caused by near-surface liquefaction, or slumping of moist lee slope sand triggered by surface precipitation (Doe and Dott, 1980).

Larger scale deformation is often the result of liquefaction below the water table caused due to loading of saturated sand by an advancing dune (Mckee *et al.,* 1971; Collinson, 1994; Horowitz, 1982; Mountney, 2006b) (Fig 2.7).

Figure 2.7 Large aeolian dune showing deformed cross beds in the lower half overlain by large planar cross bedded sets.

2.4.7 Non-Aeolian structures

Non-aeolian processes are common in aeolian systems, and can be the result of physical, chemical and biological process. Physical features include; desiccation cracks, raindrop imprints, current ripples, cross strata and wavy laminations formed from interactions with water, either from fluvial systems or elevated groundwater levels (Ahlbrandt *et al.*, 1978; Langford, 1989; Langford & Chan, 1989). Chemical features include: evaporitic crusts, tepee structures (Fig 2.8), pseudomorphs and fenestral porosity (Kocurek, 1981; Mountney, 2006b). Biogenic features include: trackways (Fig. 2.8), burrows, root structures and rhizoliths (Fig. 2.8) and algae growths (Ahlbrandt *et al.,* 1978; Hasiotis, 2007; Loope, 1988). Palaeosols are also common deposits within desert systems, formed from the modification of previous deposits (Kocurek *et al*,. 1991; Mountney 2006b).

Figure 2.8 Non aeolian structures. Top left shows tepee structure formed in a deformed evaporite crust, below a root structure is preserved in an aeolian interdune. Right hand side a possible vertebrate footprint on a damp interdune surface

2.5 Architectural Elements

Three main architectural elements are identified within aeolian systems; dunes, interdunes and sandsheets, interdunes are further subdivided into dry, damp and wet interdunes.

2.5.1 Dune

Aeolian dune (Fig 2.9) elements form from the accumulation and migration of ripple and dune scale aeolian bedforms, which can be a variety of shapes and sizes, moving at different rates and directions to one another. With positive sediment budget bedforms climb over each other at different angles preserving sets of cross bedding and bounding surfaces (Rubin & Hunter, 1982; Rubin, 1987; Mountney, 2006b). The sets and co-sets are composed of smaller scale structures; grainfall, grainflow, wind

ripple structures, each being bound and controlled by the process responsible for their generation. Therefore dune elements are large scale stratal units composed of a variety of arrangements of smaller scale bodies (Mountney, 2006).

2.5.2 Dry Interdune

Interdunes are considered dry when sedimentation shows no influence of moisture. Dry interdunes can range from small isolated hollows surrounded by dunes, up to long elongate corridors extending several kilometres between linear or transverse dunes (Fig. 2.9). The architectural elements of interdune corridors typically are largest at erg margins becoming smaller and less-connected towards the erg centre as dunes increase. Interdunal partitions are influenced by the degree of sinuosity of adjacent dune forms with straight-crested dunes resulting in straight interdune corridors, whereas sinuous-crested dunes result in separate isolated hollows (Mountney, 2006b).

Common features include wind rippled strata and much larger pebble lags if the interdune has undergone deflation (Hunter, 1977). Lack of near surface moisture restricts vegetation colonisation and animal trackways are limited (Mountney, 2006b).

2.5.3 Damp Interdune

In damp interdunes sedimentation is influenced by the presence of water due to contact of the depositional surface with the capillary fringe of the water table. This results in adhesion and salt precipitation structures (Ahlbrandt & Fryberger, 1981; Kocurek, 1981). Near surface water is congenial to life resulting in a range of roots, burrows and surface traces (Ahlbrandt *et al.,* 1978; Loope, 1988; Hasiotis, 2007). Moisture acts to stabilise damp interdunes restricting sediment for aeolian transport (Mountney, 2006b) (Fig 2.9).

2.5.4 Wet Interdune

Wet interdunes occur when the water table rises above or to the level of the depositional surface resulting in episodic or continuous periods in which the interdune is flooded (Mountney, 2006b). Mud, silt and sand are supplied to the interdune either through fluvial or aeolian processes, carbonates may also form in long livedlakes and ponds (Fig 2.9)(Driese, 1985).

Current and wave ripple laminations, desiccation cracks and mud curls are common sedimentary structures associated with wet interdunes (Kocurek, 1981; Doe & Dott, 1980; Fryberger, 1990). The presence of water enables plant colonisation and wet interdunes often show considerable biogenic structures especially if deposited on a damp muddy substrate (Ahlbrandt *et al.,* 1978; Mountney, 2006b). Flooding of interdunes may be due to intra-erg rainfall events, fluvial inundation, localised and temporary water table rise associated with rain fall, seasonal variations in regional ground-water table, and longer term variations reflecting larger scale interactions between the water table sedimentation, subsidence and regional climatic variations (Langford, 1989; Langford & Chang 1989; Kocurek & Havholm, 1993).

2.5.5 Sandsheet

Sandsheets are wind-blown sands characterised by low angle stratification, wind ripples and occasionally small domes termed *zibar* (Nielson & Kocurek, 1986). They form under conditions of periodic flooding by fluvial systems, where the presence of vegetation restricts dune movement and growth, or where significant coarse-grained sediment and/or lack of sediment supply restrict the availability for aeolian transport (Kocurek & Nielson, 1986) (Fig. 2.9).

Sandsheets are often the erosional remains of previously high-angle aeolian strata in a system with negative sediment supply which has led to widespread deflation.

Sheets covered in a pebble and granular lag represent the end point of the deflation process (Mountney, 2006b).

2.6 Bounding Surfaces

Bounding surfaces are erosional surfaces formed due to the migration of aeolian dunes. Migratory behaviour has been developed in to a system of first, second or third order surfaces (Mountney 2006b).

2.6.1 Reactivation Surfaces

Reactivation surfaces relate to episodic lee slope erosion followed by renewed sedimentation with a change of previous conditions, be it bedform migration, direction, speed, asymmetry or slope angle variation (Rubin 1987; Mountney 2006b) (Fig 2.9).

Reactivation surfaces occur within aeolian sets and have planar or scalloped shaped erosional surfaces dipping downwards at angles lower than the cross beds they truncate between 10-20° (Mountney 2006b). In sections running perpendicular to transport direction reactivation surfaces trend parallel to subparallel to the cross strata often present for tens of metres along strike. Sections running parallel to transport direction can extend up to the full height of a set or may only show an asymptotic base (Mountney, 2006b).

Reactivation surfaces can either be present randomly or in sets with regular spacing (i.e. Navajo Sandstone Utah (Chan & Archer, 1999; Loope *et al.,* 2012)). Overlying cross bedded strata either lie concordantly or show a downlapping relationship (Mountney, 2006b).

Lee slope airflow is seldom steady leading to the above modifications. The process can be regular due to seasonal wind flow changes which in turn can generate cyclic

reactivation surfaces (Hunter & Rubin, 1983; Loope *et al.,* 2001; Mountney 2006). Multiple cyclic forces operating at different frequencies can lead to multi-scale reactivation surfaces (Crabaugh & Kocurek, 1993).

2.6.2 Superimposition Surfaces

Superimposition surfaces form as a result of migration of superimposed dunes over a larger parent bedform or migration of scour troughs on the lee slope of a bedform. Oblique migration is the most common method of migration due to secondary airflow, caused from the high relief of dunes being directed along the lee slope of the parent bedform (Mountney, 2006).

Superimposition surfaces occur within cosets and show planar to highly scalloped erosional surfaces in a multitude of directions (Collinson *et al.,* 2006). In sections parallel to transport superimposition surfaces appear similar to reactivation surfaces, making identification problematic, however in sections perpendicular to transport, superimpositions surfaces are obliquely orientated to the cross strata they truncate. Where reactivation and superimposition surfaces are both present, reactivation surfaces will always be truncated by superimposition surfaces (Collinson *et al.,* 2006).

2.6.3 Interdune Migration Surfaces

Interdune migration surfaces form as a result of bedform migration separated by interdunes. Erosional scour movement defines the erosional trough between bedforms and the scour depth defines the erosion of previous bedforms (Mountney, 2006) (Fig. 2.9).

Interdune surfaces are low-angle inclined surfaces extending down-wind for up to several kilometres. They appear planar to slightly scalloped in sections parallel to transport and truncate sets or co-set. Perpendicular to transport direction interdune

bounding surfaces appear moderately to highly scalloped in cross-section (Kocurek, 1981; Mountney & Howell, 2000). Interdune surfaces are of higher magnitude and truncate superimposition surfaces and reactivation surfaces (Mountney, 2006).

2.6.4 Super Surfaces

Super surfaces are generated when accumulation ceases and is replaced by bypass or deflation, representing a change from positive sediment supply to negative or neutral sediment supply (Collinson *et al.,* 2006). Super surfaces are generally flat lying erosive surfaces that truncate all other aeolian bounding surfaces and can have large lateral extent. They often contain paleonenvironmental indicators such as; desiccation cracks, bioturbation and rhizoliths. Super surfaces can be used to correlate aeolian environments laterally to non-aeolian environments such as basin wide marine transgressions (Collinson *et al.,* 2006).

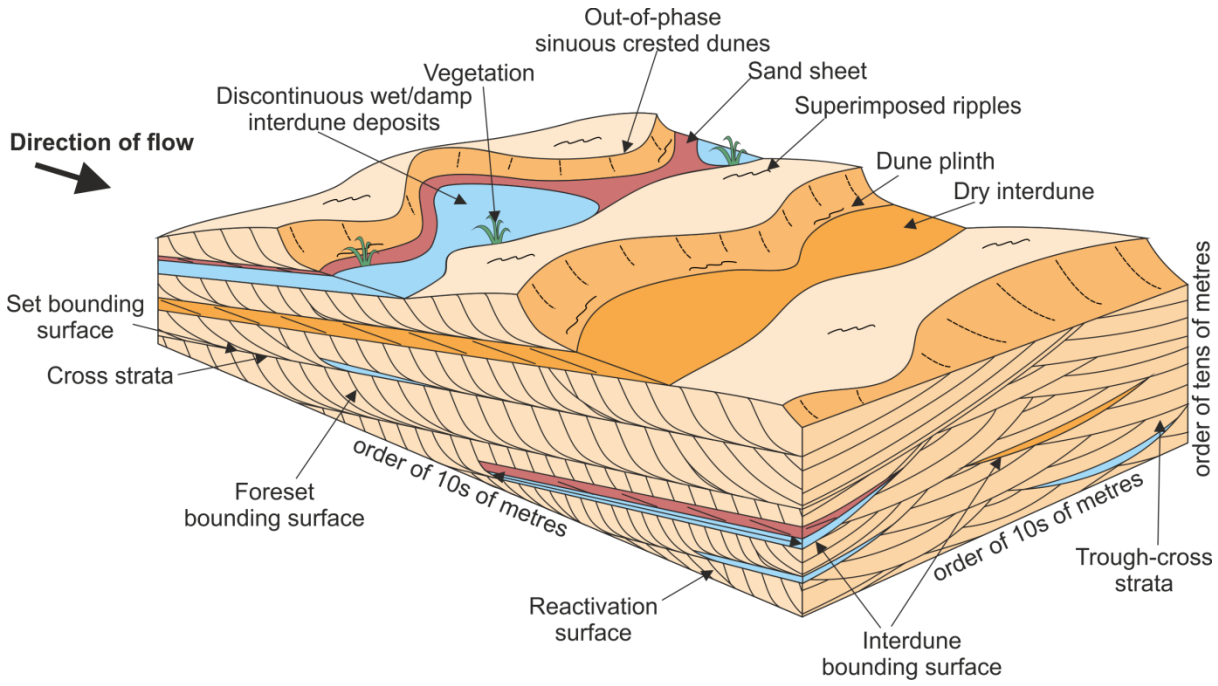

Figure 2.9 Schematic aeolian facies model showing typical depositional settings and preserved bounding surfaces (after Warrener 2016)

2.7 Controls on Aeolian Deposition

Preservation of an aeolian system is complex, reflecting multiple allogenic controls which control the construction, accumulation and preservation of deposits in the rock record.

2.7.1 Construction

Sediment supply, sediment availability and the transport capacity of wind are the main controls on erg construction (Kocurek & Lancaster, 1999). Sediment supply, which is defined as the volume of sediment of a grain size eligible for windblown transport per unit time, can form a contemporaneous or time lagged source of sediment for aeolian construction (Kocurek, 1999: Mountney, 2006b). This is derived from a range of sources both terrestrial and marine.

Sediment availability is the susceptibility of surface grains to be carried by the wind and is often controlled by stabilising factors such as, vegetation, mud drapes, coarse-grained lags, elevated water table and/or surface binding or cementing agents (Kocurek & Lancaster, 1999). The actual sediment transport rate is determined by the sediment available for a given wind (Mountney, 2006).

Transport capacity measures the potential for airflow to carry sediment, this increases with increased wind power. Lack of sediment supply results in an undersaturated windflow. Conversely, an airflow at maximum transport capacity which suffers a decrease in flow will become oversaturated and sheds a part of its load resulting in bedform growth (Mountney, 2006).

2.7.2 Accumulation

Aeolian deposits are either accumulating, in bypass or deflating. Accumulation is the generation of strata by sediment in which the accumulation surface level rises over time (Kocurek & Havholm, 1993). Bypass occurs when the level of the accumulation

surface remains constant, whereas, deflation occurs when the surface falls (Mountney, 2006).

Whether accumulation, bypass or deflation occurs depends on the net sediment budget of the system (Mainguet & Chemin, 1983). A positive sediment budget results from a higher sediment influx than that leaving the system, generating accumulation, whilst a neutral or negative results in bypass or deflation (Mountney, 2006).

For accumulation to occur a decrease in wind flow or concentration is needed, this is often achieved by airflow moving into a topographic basin, or a spatial decrease in pressure gradient. Accumulation of migrating bedforms related to the accumulation surface is dependent on the angle of climb. Typically in aeolian systems, migration rates are higher than accumulation rates which leads to low angled subcritical climb (Hunter, 1977) that truncates the tops of previous bedforms as migration occurs, this leads to only the lower parts being accumulated as cross strata sets (Mountney, 2006). Critical climb is where the angle of climb is the same as stoss slope of the bedforms, which results in preservation of the complete bedform (Hunter, 1977; Mountney, 2006). In supercritical climb the angle exceeds that of the stoss slope allowing for accumulation of the stoss and lee slope, preserving laminae which can be traced between successive sets. Critical and supercritical climbing is most commonly restricted to ripple scale bedforms (Mountney, 2006b).

In dry systems, a low water table means water has no influence on the sedimentation and deposition is solely reliant on airflow (Kocurek & Havholm, 1993) and are characterised by cross bedded dune strata with minimal interdune successions (Mountney, 2006b).Interdune flats within a dry system are areas of accelerating airflow, this results in erosion of interdune flats depositing sediment on lee slopes of nearby bedforms. Growth of dunes within a dry system is at the

expense of interdunes, with bedform climb only occurring after interdune areas are cannibalised.

In wet systems, the water table is in contact with the accumulation surface, influencing sedimentation, airflow and moisture, therefore affecting deposition (Kocurek & Havholm, 1993). Wet systems are characterised by downwind climbing dunes separated by damp interdune units (Mountney, 2006b). Damp sediment is more restricted to aeolian transport than dry, leading to lower transported volumes (Mountney, 2006b). Progressive water table rise is the dominant mechanism of accumulation in wet systems (Hummel & Kocurek, 1984; Pulvertaft, 1985) with the angle of climb determined by the ratio of water table rise versus downwind migration of the bedforms.

2.7.3 Preservation of aeolian sequences

Accumulation does not guarantee preservation. For preservation to occur, accumulation sequences need to be below a regional erosive baseline (Mountney, 2006b). Primarily, generation of accommodation space and infill time is a key factor in preservation of sediment (Howell & Mountney, 1997) and are controlled by multiple, for example, subsidence due to tectonics and/or compaction (Blakely, 1988; Blakey *et al.,* 1988), water table rise, sea level rise and surface stabilisation.

2.8 Sabkhas & Playa Lake Non-Marine Evaporites

Sabkhas are low-gradient, sub-aerially exposed saline environments that are typically contiguous with bodies of water. They are characterised by frequent and typically cyclic fluctuations in groundwater that concentrate solutes and precipitate evaporites within the sediment or upon the surface (Warren and Kendall, 1985; Warren 1989). Marginal-marine sabkhas (Fig. 2.10) are defined as those located in the upper intertidal to supratidal zone of arid coastlines and are strongly influenced

by marine waters (e.g. Alsharhan & Kendall, 2003; Lokier & Steuber, 2008). Continental sabkhas (Fig. 2.10) are defined variously as saline pans, mudflats, or interdunal sabkhas, and are present in arid, inland closed basins (e.g. Benison & Goldstein, 2001; Gunatilaka & Mwango, 1987; Handford 1982; Hardie & Lowenstein 1978; Lowenstein & Hardie, 1985).

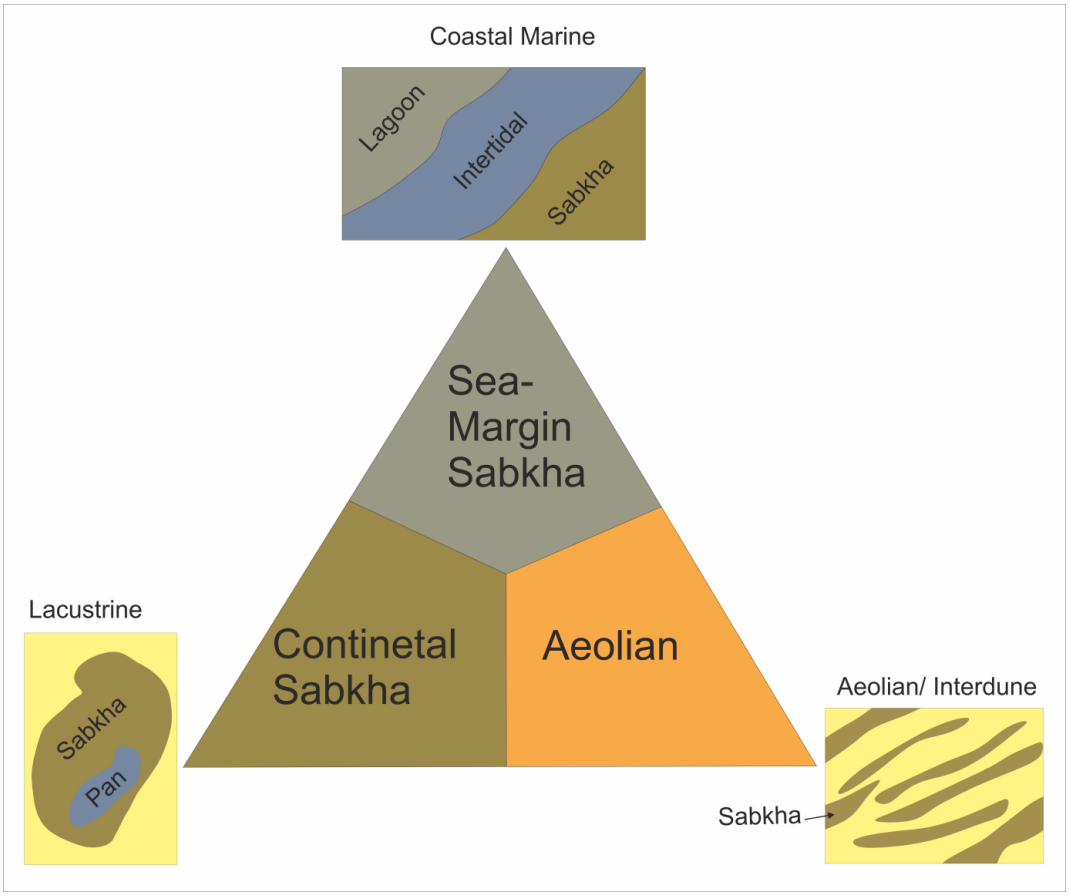

Figure 2.10 Different types of sabkhas (from Handford, 1981**)**

2.8.1 Continental Sabkhas

Continental sabkhas (Fig 2.10) are primarily deposited within saline lakes. These evaporites form over a wide range of settings, from deep stable lakes to centimetre scale lakes existing briefly over the course of days before drying completely for many years.

In dominantly-submerged settings, periodic expansion and contraction of a saline lake results in a salt pan of layered evaporites and clastics in which the sediments record a 'saline lake stage' and a 'desiccation stage' (Lowenstein & Hardie, 1985) as the lake dries (Fig. 2.11). During times of flood, lake waters usually inundate an area greater than that of the pan to form a wide shallow, brackish lake. Clastic sediments derived from lake-marginal environments are re-deposited from suspension through the lake waters as thin strata, typically with rippled and wavy bedding surfaces recording slight agitation of the water by wind shear (Eugster & Hardie, 1978) (Fig 2.11). With evaporation, salts are concentrated in the remaining water to form a smaller saline lake in which evaporite minerals precipitate (e.g. Last, 1984; Smoot & Lowenstein, 1991). The earliest precipitates nucleate at the water-air interface as thin rafts of connected platy euhedral cumulate crystals that are held by surface tension until they grow too large and sink (Hardie et al., 1985; Last, 1984; Smoot & Lowenstein, 1991; Lowenstein & Hardie, 1985; Schreiber & Kinsman, 1975; Castens-Seidell, 1984; Alderman, 1985). As lake waters evaporate further, bottom-nucleating vertically elongated crystals, with a radial texture, precipitate as crusts from the brine (Kendal, 1978). Wind shear on the surface of the saline lake periodically disarticulates rafts and crusts that are then reworked into slumps and debris flows characterised by sediments of euhedral evaporitic crystals dispersed in a clastic matrix (Weiler et al., 1974; Gwynn & Murphy, 1980; Last, 1984; Smoot & Lowenstein, 1991). Complete desiccation of the saline lake produces polygonal fractures in the lakebed that typically fill with detrital evaporitic or clastic sediment. They preserve as crack fills, or as so-called 'tepee structures' where the fill incorporates displacive evaporites (Lowenstein & Hardie, 1985; Lokier & Steuber, 2009; Warren, 1983) (Fig 2.11).

Lake-marginal saline mudflats form in dominantly-emergent settings and are characterised by fine-grained clastic sediments that are deposited by settlement

through the floodwater of the shallow brackish lake. With lake contraction, the mudflats are exposed. Variations in ground water levels and circulation promote subsurface phreatic evaporite growth resulting in random crystals or nodules, or as concentrated thick layers, displacing surrounding sediment (Warren, 2016; Smoot & Lowenstein, 1991). Efflorescent evaporites, forming either powdery undulating surfaces or hard crystalline crusts, precipitate from the evaporation of saline ground waters at the surface (Warren, 2016; Smoot & Lowenstein, 1991).

2.8.2 Perennial Saline Lakes

Perennial saline lakes (Fig.2.12) are standing brines, requiring large inflow usually from perennial streams and rivers, and a closed drainage system allowing solute concentration. Evaporation concentrates inflow water into a brine and eventually precipitating evaporites (Smoot & Lowenstein, 1991).

Perennial saline lakes are typically stratified with denser brines at the bottom. Wave action can destroy stratification, however, deep lakes remaining stratified for long periods of time can develop an anoxic lower brine layer (Kirklan, 2003, Sonnenfeld & Hudec, 1985, Smoot & Lowenstein, 1991).

Lakes or areas of lakes that are unable to mix freely with inflow waters form more soluble minerals such as trona and halite in shallow waters, whereas insoluble minerals (Aragonite and gypsum) form in deep water (Smoot & Lowenstein, 1991). More dilute perennial lakes, will precipitate more alkaline minerals i.e. Mg- Calcite, Aragonite, monohydrocalcite, or dolomite than their concentrated counterparts (Von der Borch, 1976, Stoffers & Hecky, 1978; Spencer, *et al.,* 1984).

Smoot & Lowenstein, (1991), have classified four features of perennial saline lake evaporites:

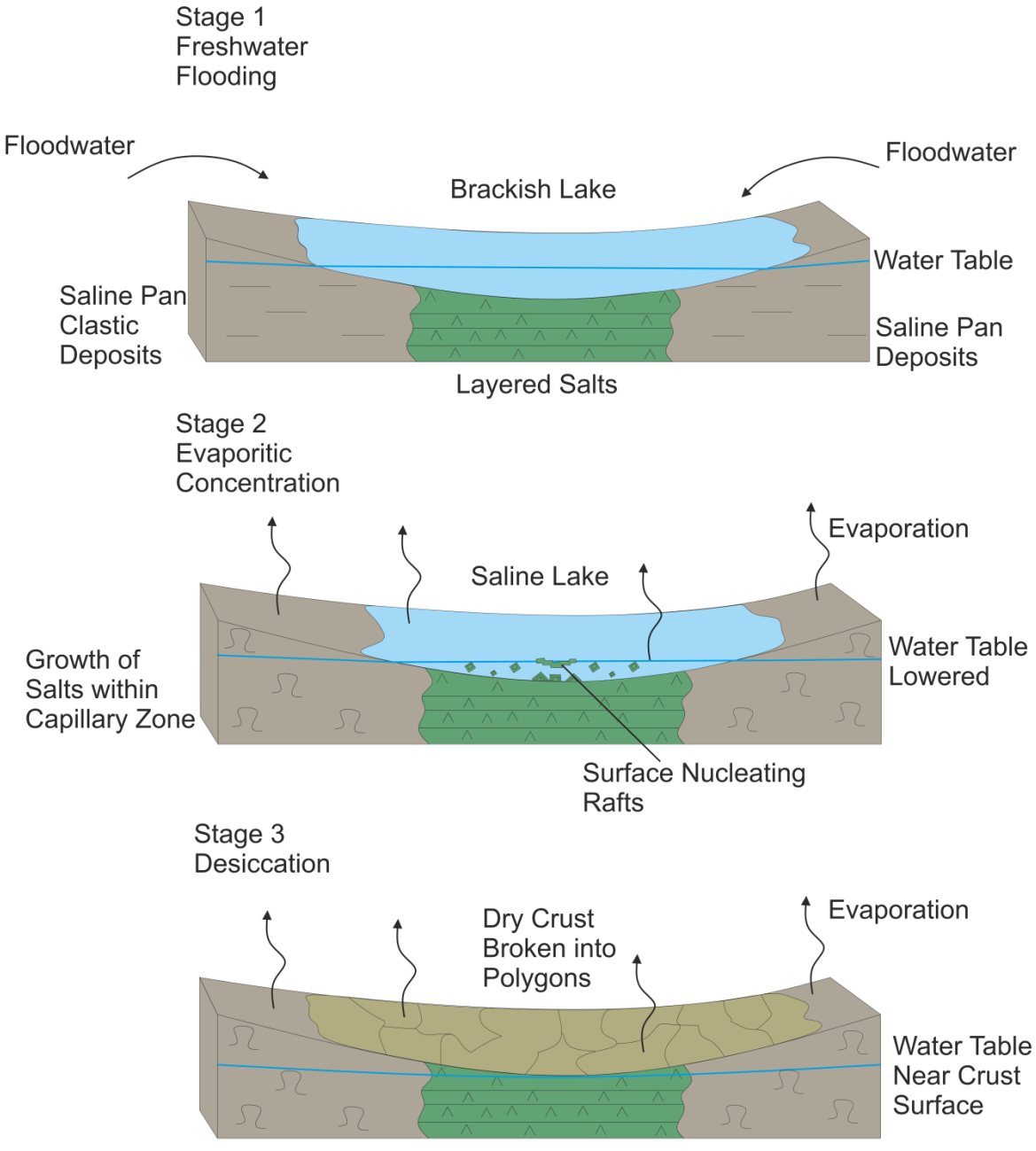

Figure 2.11 Evolution and depositional cycle in a continental sabkha (after Lowenstein & Hardie, 1985)

1. Cumulus crystals that precipitate at the air-water interface and sink to the bottom of the brine.
2. A crust that precipitates on the brine bottom.
3. Detrital evaporites.
4. Intrasediment crystal growths and cements.

Cumulus crystals

Cumulus crystals are thin, platy and euhedral and form into floating crusts held by surface tension until they grow too large and sink or wave action disrupts the surface tension (Hardie *et al* 1985; Last, 1984; Smoot & Lowenstein, 1991). Graded layering can be formed if large subhedral skeletal crystals form first and smaller euhedral crystals form later from supersaturated brines. Reverse grading occurs when crystals remain afloat longer as the surface brine becomes denser and more concentrated (Hardie *et al* 1985; Smoot & Lowenstein, 1991).

Evaporitic crystal precipitation follows a sequence of concentrated brines sinking when they reach sufficient densities, which then mix with deeper waters. Further evaporation increases both the salinity and density of the entire water column resulting in the surface brines having to be concentrated even more before reaching sufficient density to sink (Smoot & Lowenstein, 1991).

If the evaporation rate exceeds the inflow into the lake, saline mineral accumulation at the lake bottom will reflect an increase in brine salinity and show a sequence of minerals with increased solubility i.e. calcite-aragonite- gypsum-halite (Smoot & Lowenstein, 1991). With increased inflow, surface waters become more dilute leading to a dissolution of evaporites if the water column is mixed, or isolation of the bottom brine. A close down of influx water will lead to rapid water level drop and precipitation of a single layer of evaporites (Smoot & Lowenstein, 1991).

Crystal layering is generated from the precipitation of different saline minerals, or different abundances of minerals due to influx of fresher waters. Repetitive concentration of brines results in progressive layers of crystal laminations, showing a larger percentage of soluble mineral components as it develops. Layers may also form from intermixing of evaporites with flood derived detritus, or mixing with ongoing background detrital and biogenic sediments (Smooth & Lowenstein, 1991).

Evaporite Crusts

Crusts form on perennial lake floors from well-mixed supersaturated brines and develop best in shallow lakes or the shallow portion of deeper lakes. Crystals are typically vertically elongated with radial texture and competitive growth boundaries similar to crusts in saline pans (Goodall *et al.,* 2000; Warren 2016; Smoot & Lowenstein, 1991).

Lake marginal deposits may be dissolved by dilute surface brines resulting in fabrics indistinguishable from saline pans. The effects of salinity stratification in deeper portions of the lake can protect the crusts allowing for detrital and chemical layers to form. This absence of dissolution fabrics and presence of layered sediment drapes over crystal terminations is indicative of lake saline crusts over saline pan crusts (Smoot & Lowenstein, 1991).

Intrasediment crystal growth and cements

Intrasediment crystal growth and cements are composed of saline minerals that precipitate from lake bottom brines, interstitial brines or a mixture of the two. Saturated bottom brines can alter and cement evaporite beds into coarse crystalline mosaics. Later diffusion of this saturated bottom brine can occur, generating authigenic clays and silicates such as illite, stevensite, kerolite, nontronite and sepiolite, the presence of which can often be the only indication of evaporitic conditions (Smooth & Lowenstein, 1991).

Lake depth is a strong control on the deposits. Deep stratified lakes form flat laminations in central areas with lenticular and irregular layering at the lake margins. Cumulate crystal layers and gravity flow deposits form within the centre, with evaporite crusts and intrasediment evaporites found towards lake edges. Shallower lakes feature intrasedimentary growths and crusts across the entire

bottom, with desiccation cracks found commonly near the shallow lake margins (Smooth & Lowenstein, 1991).

2.8.3 Ephemeral Saline Lake

Ephemeral saline lakes (Fig 2.12) are shallow brine-concentrated bodies of water that will dry up and leave exposed layers of salts precipitated as the brine evaporates. This is process occurs regularly, with a time frame of at least once every few years (Hardie *et al.,* 1978). This environment has also been described as a salina, alkali lake or playa lake when wet and as a playa, dry lake, alkali flat, salt flat, salt pan, or inland sabkha when dry (Reeves, 2009; Cooke & Warren, 1973; Glennie, 1972)

Recharge occurs due to infrequent storms and spring waters. In the periods between flooding the newly expanded lake will contract by evaporation of brines until super saturation results in the formation of halite or trona before drying up completely (Hardie *et al.,* 1978). Catastrophic expansion and contraction results in a subdivision into: a salt pan, composed of layered salts in the lowest part of the lake, and a saline mudflat, formed of muddy clastic sediment with crystals of salt minerals, surrounding the salt pan (Hardie *et al.,* 1978).

Clastic sediment is mainly derived from suspension during calm periods, deposited in thin layers with ripple and wavy laminations representing storm events or wind ripples, interbedded with salt deposits of either saline pans or mudflats (Hardie *et al.,* 1978).

2.8.4 Saline Pans

Saline pans (Fig. 2.12) are dry areas underlain by layers of salt, found in both marine and non-marine environments (Benison & Goldstein, 2001; Lowenstein & Hardie, 1985). Non marine pans are commonly found in areas of closed drainage

surrounded by saline mudflats, with their outer edge having strong potential for geological preservation (Warren, 2016). They are stratified with evaporitic crusts separated either by solution surfaces or mud (Lowenstein & Hardie, 1985). Most commonly formed of halite, though they may also be composed of trona, mirabilite, epsomite or bloedite and thenardite (Lowenstein & Hardie, 1985; Eugster, 1970; Last, 1984).

Saline pans are formed under cyclic conditions composed of; a flooding stage, a saline lake stage, and a desiccation stage (Lowenstein & Hardie, 1985). Floodwaters inundate a saline pan, over an area usually greater than that of the pan, either seasonally or sporadically forming a shallow temporary brackish lake. Fine grain sediment introduced by flood waters is deposited thickest in areas near the source, whilst suspended clay minerals are rapidly deposited due to flocculation (Last, 1984; Sonnenfeld & Hudec, 1985).

The solutes in these ephemeral lakes are derived from the dissolution of the salts of efflorescent crusts by dilute surface run off and brackish lake water, and partial to full dissolution of previous saline pan crusts. Solutes in saline pans are primarily composed of the recycled salts of the most soluble salts from the previously mentioned processes (Smoot & Lowenstein, 1991).

During the saline lake stage water is concentrated by evaporation with the earliest precipitates from the brine being small crystals which nucleate at the water-air interface, either flat platy euhedral halite, gypsum lathes or radial crystallites of natron (Lowenstein & Hardie, 1985; Schreiber & Kinsman, 1975; Castens-Seidell, 1984; Alderman, 1985; Smoot & Lowenstein, 1991).

Crystals may sink and form loose packed cumulative layers. Crystals that remain afloat due to surface tension form fluid inclusion rich, hopper shaped crystals or floating rafts that eventually sink. Wave action may rework floating crystals into flat

layers, ripples or shoreline bars (Stoertz & Erickson, 1974; Carstens-Seidell, 1984; Last, 1984).

Monomineralic salt crusts develop when waters are dominated by solutes derived from earlier efflorescent crusts and saline pan layers; otherwise several minerals precipitate as crusts from the brine resulting in a bulls eye pattern as lake waters decrease and the most soluble minerals form at the centre (Hardie, 1968, 1984; Eugster, 1970; Smoot & Lowenstein, 1991).

The final stage is the complete desiccation of the ephemeral lake. Surface brines sink below the surface salt crust and continue to concentrate due to evaporative pumping (Smoot & Lowenstein, 1991). Surface brines may mix with groundwater creating a hybrid brine different in concentration from that produced from evaporative concentration of either water which can result in hybrid evaporate minerals or the recrystallisation of older minerals (Hardie, 1968; Smoot & Lowenstein, 1991).

A common feature of crystal growth during the desiccation stage of saline pans is polygonal fractures with overthrust edges ranging in size from metres to tens of metres in diameter; these are caused by the expansion of the crust. Most commonly found in halite crusts, but have been noted in gypsum crusts, trona crusts and thenardite-burkeite crusts (Lowenstein & Hardie, 1985; Stoertz & Ericksen 1974; Castens-Seidell, 1984; Eugster, 1980; Smoot & Lowenstein, 1991).

2.8.5 Saline mudflat

Saline mudflats (Fig. 2.12) are areas of fine grained sediment (wet plastic clay to sandy mud), where intrasediment evaporates and surface efflorescence salt crusts form from ground water brines. Saline mudflats lie on the margins of saline lakes

and saline pans aggrading due to a combination of fluvial, lacustrine and aeolian processes (Smoot & Lowenstein, 1991).

The evaporites which form in a saline mudflat are dependant upon the chemistry of the groundwater brine, sinking of the surface brine and the mixing of surface brines with groundwater brines. Saline mudflat groundwaters develop concordantly with the adjacent saline pan or saline lake. Immature groundwater systems will produce predominantly gypsum in the mudflats and thin halite crusts from saline pans (e.g. Bowler, 1986).

Saline mudflats display concentric zones of intrasedimentary growth evaporitic minerals, with the more soluble minerals occurring in central portions surrounded by progressively less soluble minerals. This is due to progressive evaporitic concentration of groundwater and mixing with saline surface brine (Smoot & Lowenstein, 1991). Mineral growth causes displacement pushing aside surrounding brine soaked sediment by the force of crystallisation and incorporative growth (Smoot & Lowenstein, 1991).

Evaporite minerals related to saline mudflat display a number of crystal habits. Gypsum occurs commonly as either discoidal hemipyramids or bladed hemipyramids (Eardley & Stringham, 1952; Gwynn & Murphy, 1980; Bowler & Teller, 1986), both may also form twinned rosettes (Smoot & Lowenstein, 1991). This discoidal morphology has been linked to confining pressures from surrounding mud, or organic material restricting growth of certain crystal faces (Cody, 1979; Shearman, 1978). Large gypsum crystals with banded sediment inclusions alternating with clear gypsum represent periods of solution and precipitation, similar bands have been observed in halite crystals (Draper & Jensen, 1976; Arakel, 1980; Gornitz & Schreiber, 1981). Anhydrite forms nodules of fine crystalline material within a sedimentary matrix from the dehydration of gypsum, this

intrasediment nodular habit is also common for ulexite and magadiite (Moiola & Glover, 1965; Castens-Seidell, 1984; Euguster, 1970).

Deep groundwater tables at saline mudflat margins results in the development of vadose zone evaporites; vadose zone evaporites are finely crystalline, subject to dehydration and restricted to porous layers or fenestrae. Minerals formed in brine saturated sediment are subject to modification with crystals showing dissolution features from periodic exposure to dilute water, such as rainfall. Dehydration leads to the formation of dry zones which increase away from the saline pan or lake as the depth to brine saturated sediment is increased (Smoot & Lowenstein, 1991).

Efflorescent Crusts

Saline mudflat surfaces are almost entirely covered by porous fine crystalline efflorescent crusts formed from the evaporation of groundwater brine when raised to the surface. Their mineralogy is reflective of the chemistry of the underlying brine. Efflorescent crusts are ephemeral features, and are easily dissolved. The thickest crusts are developed where groundwater is close to the surface and they lie outside the reach of saline pan and saline lake waters (Goodall *et al.,* 2000; Smoot & Lowenstein, 1991).

Efflorescent crusts range from powdery undulating surfaces to hard crystalline crusts. Thin crusts show polygonal patterns of mounds and trough grading into progressively narrower trough and irregular surface as crusts thicken basinwards. Dissolution surfaces are common including fluted pinnacles, solution pits and rubbly brecciations (Goodall *et al.,* 2000; Stoertz & Ericksen, 1974).

Powdery crusts have granular porosity whilst crystalline crusts show a 'popcorn' surface rich in clastic sediment (Goodall *et al.,* 2000; Smoot & Lowenstein, 1991). Crusts which overlie predominantly sand incorporate the upper surface of the sediment into their crust distorting the layers and displaying a non-distinct

boundary, whereas crusts overlying mud show a sharp contact with a mud rich bottom layer and no displacement of underlying layers (Goodall *et al.,* 2000; Smoot & Lowenstein, 1991).

Saline mudflats can be characterised by a lack of efflorescent crusts preserved in underlying sediment due to the size and minerology of the crystals making them readily soluble to unsaturated groundwater. Less soluble minerals such as gypsum can be partially preserved in the forms of irregular, humpy layer of sand sized crystal fragments (Smoot & Lowenstein, 1991).

2.8.6 Dry mudflat

Dry mudflats (Fig 2.12) are plains bordering saline mudflats, saline lakes or occupying the floor of closed basins termed *playa flats* or *clay pans*. Composed of fine-grained sediments, they produce predominantly desiccation and pedegenic features. Due to low groundwater level, formation and preservation of evaporites is uncommon, they are defined in contrast to saline mudflats due to lack of evaporites and plentiful desiccation features (Smoot & Lowenstein, 1991).

2.8.7 Aeolian Sabkhas

Sabkhas are defined by their matrix not their salts (marine sabkha host fossiliferous fine-grained sediments whereas continental sabkhas are evaporites within fine grained fluvial-lacustrine sediments). Aeolian sabkhas are characterised as capillary salts accumulating in any aeolian-derived matrix, sitting below a deflationary surface (Warren, 2016). Sediment supplied is either dune sediment blown in to areas of shallow water table, or material provided by fluvial processes cutting through sand seas. Aeolian sabkhas can form either in marginal marine or a continental lacustrine setting, (within interdunal depressions, in sandsheet deposits, or areas of desert loess, Warren, 2016). Close proximity to aeolian dunes will result

in aeolian dunes interfingering with aeolian sabkhas forming lateral discontinuities within potential aeolian reservoirs (Warren, 2016).

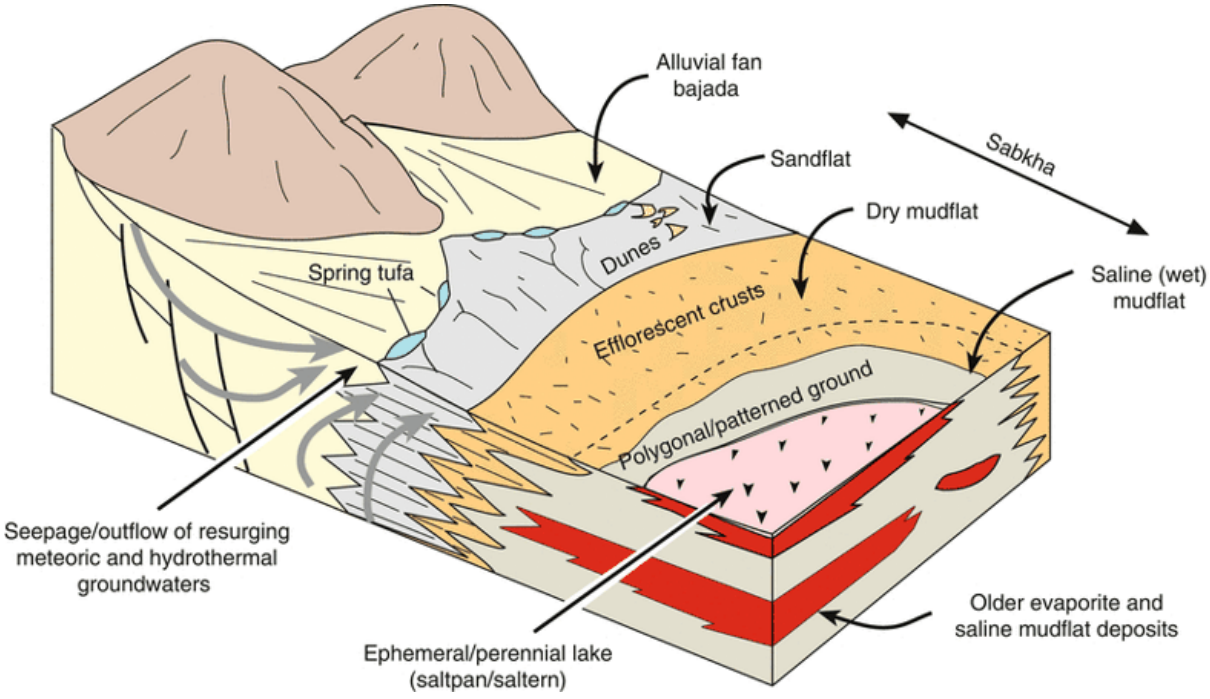

Figure 2.12 Depositional environements of a continental sabkha (from Warren, 2016; Kendall, 1992; Eugster & Hardie, 1978)

Within aeolian interdunes, sabkhas may form when a saline water table is in contact with, or above, the depositional surface (Warren, 2016). They are typically classified as 'wet aeolian sabkhas' if they display a capillary succession showing haloturbation but little to no preserved capillary salt, or as 'chemically-dominated saline aeolian sabkha' if abundant capillary salts are preserved (Warren, 2016). The sediments of wet aeolian sabkhas typically show some or all of the following: subaqueous current and wave ripples and associated cross-lamination; wavy laminae and contorted bedding; adhesion structures; bioturbated structures; desiccation cracks; megapolygons (Warren & Kendall, 1985); deflation surfaces; and wind-ripple lamination (Warren, 2016; Mountney & Thompson, 2002; Goodall et al., 2000; Martin & Evans, 1988). Similar structures are seen in chemically dominated saline aeolian sabkhas (Warren, 2016), although overprinting by extensive disruptive

evaporite crystal growth can modify or destroy primary depositional features (Ahlbrandt & Fryberger, 1981; Warren, 2016).

Evaporites form in interdune areas as saline crusts and intrasediment crystals. Euhedral crystals form from groundwater brines as poikilitic growths encasing sand grains. Efflorescent salt crusts coat sand grains and form polygonal ridge patterns which deform layering and trap sediment (Fryberger *et al.*, 1983; Smoot & Lowenstein, 1991). Adhesion ripples, a common feature in Aeolian environments may be hard to distinguish from efflorescent salt crusts; Glennie (1972, 1983, 1987) has described distorted fabrics within cores of the Permian Rotliegend from the north sea as adhesion ripples.

Sedimentary structures of wet aeolian sabkhas typically show ephemeral water and aeolian features, including; subaqueous current and wave ripples, wavy laminae and contorted bedding, adhesion structures, bioturbated structures, desiccation cracks, megapolygons and Stokes surfaces, and wind ripple lamination (Warren, 2016; Mountney & Thompson, 2002; Goodall *et al.,* 2000). Similar structures are seen in saline aeolian sabkhas, however overprinting by salts and subsequent haloturbation disrupts features (Warren, 2016).

The preservation potential of interdunal sabkhas depends greatly upon sediment supply, accommodation and movement of the water table. Accretion of the sediment surface is required for preservation and occurs most readily in settings with high sediment supply and developing accommodation. Deflationary systems have little preservation potential, often with only an evaporite-cemented deflationary surface preserved (Warren 2016).

2.9 Summary

This chapter has provided a detailed literature review on the processes which form aeolian and evaporitic environments within arid continental basins. The sedimentological deposits found within these settings have also been referenced in relation to these processes. The following chapters will relate primary data back to the published literature to contextualise depositional interpretations of the sediments encountered.

Chapter Three: Sedimentary Lithofacies of the Cedar Mesa Sandstone Formation and Spatial Distribution

This chapter details the nineteen facies, six microfacies, and eleven facies associations, observed within the Cedar Mesa Sandstone Formation. The facies are based principally on the lithological, sedimentary textures and structures present within them, and are grouped according to their depositional process, either: subaqueous, sub-aerial, or evaporitic processes. The facies associations contain multiple facies and are grouped by broad scale depositional setting: aeolian, fluvial, lacustrine or sabkha.

3.1 Lithofacies of the Cedar Mesa Sandstone

This chapter will examine the lithofacies, associations and spatial distribution of the distal sedimentary deposits of the Cedar Mesa Sandstone. Facies analysis is a well-established tool for the interpretation of preserved sedimentary deposits (e.g. Cant, 1978; Miall, 1985) and describes sediment in terms of their lithology, sedimentary textures and structures. A variety of facies schemes have been proposed for the deposits of the Cedar Mesa Sandstone (e.g Pettigrew et al., 2018; Mountney, 2006a; Mountney & Jagger, 2004; Loope, 1984; Langford & Chan, 1989). Most of these, however, have focused purely on the aeolian and fluvial deposits found within the central and marginal erg, these studies are summarised in Table 3.1. The first detailed lithofacies scheme for the distal sabkha deposits was by Langford & Massad (2014) who described an aeolian-sabkha transition zone. This work provides a more detailed and thorough description of the lithofacies present within this 'sabkha transition zone'. Nineteen facies and eleven facies associations are identified and described fully, these belong to a broad range of depositional settings including aeolian, fluvial, lacustrine and continental sabkha.

The schemes presented below build upon these published observations and provide additional detail where relevant. The descriptions and interpretations are the result of field observations conducted as part of this study, interpreted from the logged sections. A summary of the depositional environments, facies and facies associations is shown in Fig. 3.1

3.2 Methodology

Ten detailed sedimentary logs were recorded at ~3 km intervals from north to south through east-west orientated canyons which cut perpendicular to the general north-south strike orientation along a 15 km long north–south transect, and totalling approximately 7.5 km of recorded sediment. A further two logs (one 60 km to the south and one 100 km to the north of Bluff) were recorded to show the spatial variability in sediments preserved, and to provide regional context. The logs were correlated to one another using the base and top of the Cedar Mesa Sandstone Formation, and by tracing prominent units within continuous outcrop. The sedimentary logs range from 30–150 m thick, with the carbonates appearing sporadically throughout six of the logged sections (Logs 1.2, 1.3, 1.4, 1.5, 1.7, 1.8).

Facies and facies associations have been derived from log data, to examine relationships between the sediments of competing arid environments of the Cedar Mesa Sandstone Formation. Facies are based on differences in lithology, sedimentary textures and structures, whereas associations are groupings of genetically linked facies spatially and temporally.

Six microfacies have also been identified from the analysis of carbonate samples. Individual carbonate beds are generally 20–50 cm in thickness present as either isolated lenses (up to 3 m in width) or laterally continuous units (10s of metres in lateral width). The carbonates are interbedded between thick successions (up to

10m) of either aeolian, fluvial/lacustrine derived sandstones, or evaporites. Samples were collected from the middle of each available carbonate unit, or from the top and bottom of the bed where possible with thicker deposits (40-50 cm). This resulted in 65 samples (rock samples and thin sections) collected from the log localities. 30 μm thick, un-stained, thin sections were made and subsequently investigated using a Nikon Eclipse LV100N POL microscope, at Keele University, UK. The microfacies of the carbonate units were analysed and classified following the modified Dunham (1962) scheme of Lokier & Al Junaibi (2016).

Finally, the spatial relationships and relevant proportions of each association across the aeolian-sabkha transition are quantitatively examined. From the detailed analysis and interpretation of facies, microfacies and facies associations, three-dimensional sedimentary models that describe temporal and spatial sedimentary relationships at multiple scales are generated.

Table 3.1 Summary of previous facies schemes of the Cedar Mesa Sandstone Formation

Author	Year of Publication	Facies Scheme and Finding
Mack	1978	Identifies mature facies, interprets Cedar Mesa Sandstone as having a shallow marine origin
	1979	Identifies cross-bedded sandstone, horizontally bedded sandstone and rippled sandstone facies. Interprets aeolian and shallow marine origin
Loope	1984	Identifies reverse graded laminations within cross bedding, the first full aeolian interpretation for the Cedar Mesa Sandstone.
	1985	Develops on previous scheme and presents a model for the accumulation and preservation of aeolian facies
Stanesco & Campbell	1989	Identify 6 facies: aeolian dune, interdune, sandsheet, palaeosol, fluvial and sabkha facies. Describe the sabkha facies as marine in origin
Langford & Chan	1988	Identify fluvial and playa facies within aeolian dune facies. Interpret this as coeval fluvial flooding of migrating dunes.
	1989	Identify facies belonging to aeolian dune, wet interdune, fluvial channel, overbank interdune. Identify deflationary and flooding surfaces.

Condon	1997	Builds on earlier work by Loope (1984; 1985) and Langford and Chan (1988;1989)
Mountney & Jagger	2004	Describes dune, interdune and fluvial facies and the interactions between marginal erg environments.
Mountney	2006	Described the aeolian facies and the mechanism for erg preservation and accumulation related to allocyclic controls
Langford & Massad	2015	Described the aeolian-sabkha transition. Identifies dune, interdune, palaeosol, fluvial, saline pan and sabkha facies.

Environment	Contained Facies	Contained Associations	Examples
Aeolian	Planar-crossbedded sandstone, Trough-crossbedded sandstone, Translatent ripple sandstone, Pinstriped sandstone, Convolute bedded sandstone, Massive sandstone.	Dune, Sandsheet, Dry Interdune, Wet Interdune, Damp Interdune.	
Fluvial	Intraformational conglomerate,Planar-crossbedded gravel,Planar-crossbedded moderate sorted sandstone,Horizontally laminated sandstone, Climbing-ripple sandstone,Calcrete rich palaeosol, Horizontally laminated palaeosol	Channelised Fill, Unconfined Flow	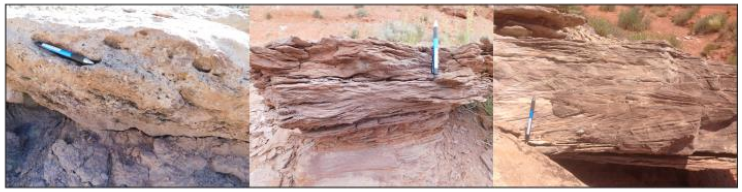
Lacustrine	Fine-grained carbonate, Clastic-rich carbonate, Wave-rippled sandstone, Massive mottled silt, Carbonate mudstone	Ponded Deposits, Settle from Suspension, Palaeosol	
Sabkha	Calcrete rich palaeosol, Horizontally laminated palaeosol, Crystalline gypsum, Gypsum-bound sandstone	Sabkha, Palaeosol	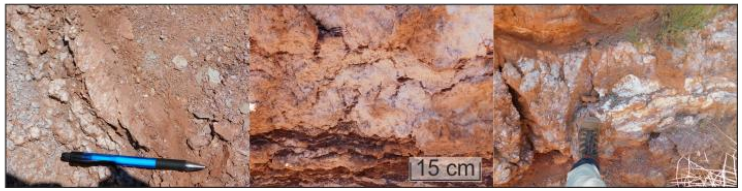

Figure 3.1 Summary table of facies, associations and depositional environments of the Cedar Mesa Sandstone Formation (from Pettigrew et al., 2018)

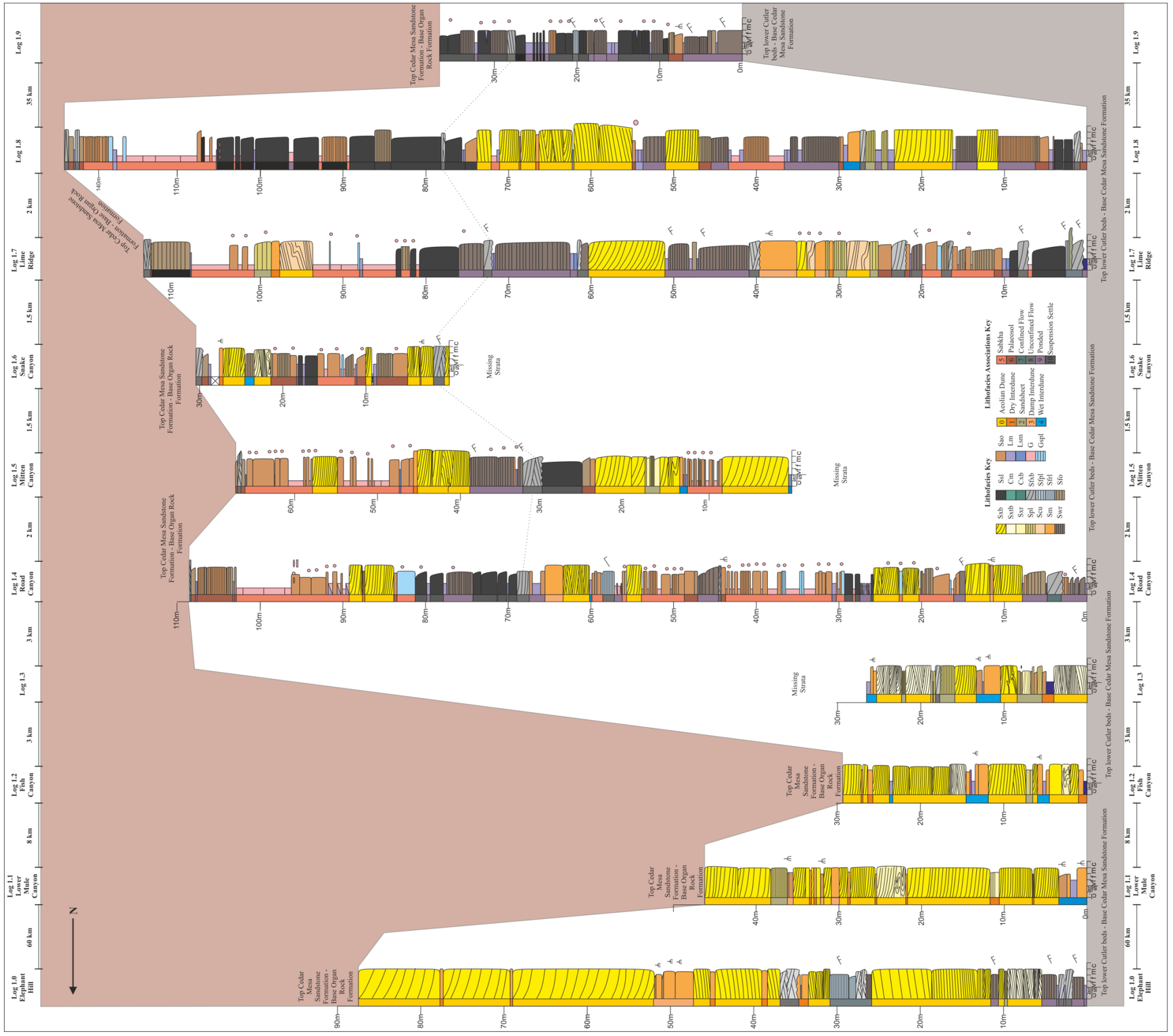

Figure 3.2 Attempted correlation of all logs within the study area. Logs are correlated from top lower Cutler beds to base Organ Rock Formation, traceable units within the Cedar Mesa Sandstone Formation are shown with dashed line. Logs are along a rough north-south transect with log 1.0 being the most northernly and 1.9 the furthest southerly log

3.3 Sub-aerial Lithofacies

Six lithofacies have been interpreted to have been formed in sub-aerial conditions within a suite of aeolian settings. These include: dunes, sandsheet and interdunes. The sub-aerial lithofacies are often easily-identified in outcrop due to a distinctive pale colour and weather into rounded bumps.

3.3.1 Planar cross-bedded sandstone-Sxb

Description. This lithofacies (Fig. 3.3) is characterised by yellow, white or orange, fine- to medium-grained sandstones. The facies is well-sorted, with a sub- to well-rounded texture. The facies displays planar cross-bedding arranged into simple (Fig 3.3D) or compound sets (Fig 3.3B) with a predominant south to south-eastern migration direction. Occasional inverse grading is found, which is separated by thin layers of finer grained laminae. Localised gypsum is occasionally present in the form of thin veins, 0.5-1 cm thick, precipitated along lower bounding surfaces, often near the contact with other lithofacies (Fig 3.3C).

The deposits range from 0.5 m to >10 m in thickness and are laterally extensive, often over distances of 10s of metres. The deposits are present in all logs, except Log 1.9, with the greatest thickness occurring in the north of the study area, shown in logs 1.0-1.3.

Interpretation. These cross-bedded homogenous sandstones represent the preserved deposits of straight-crested aeolian dunes (Mountney, 2006). Accumulated was achieved by the migration and climb of bedforms over one another with a predominantly south-eastern palaeo-wind direction (Mountney & Jagger, Loope 1984). The inverse grading within the inclined foresets represents the deposits of individual grainflow avalanches down a lee slope inclined at, or close to, the angle of repose (Hunter, 1977; 1981; Mountney, 2006). The individual grainflow

units are separated by thin accumulations of windripple and grainfall strata, which form the finer grained proportions of the facies (Hunter, 1981). Examples of packages within which cross-bedding occurs as compound cosets indicates the presence of smaller scale duneforms that migrated over larger bedforms, leading to the generation and preservation of multiple scales of aeolian bounding surfaces within individual units of this facies (Mountney, 2006; Rubin and Hunter, 1983).

The presence of gypsum along basal foresets, indicates solute rich water was drawn up preferential flow pathways in the sediments of the advancing dune as a result of capillary action at or soon after deposition (Banham & Mountey, 2013).

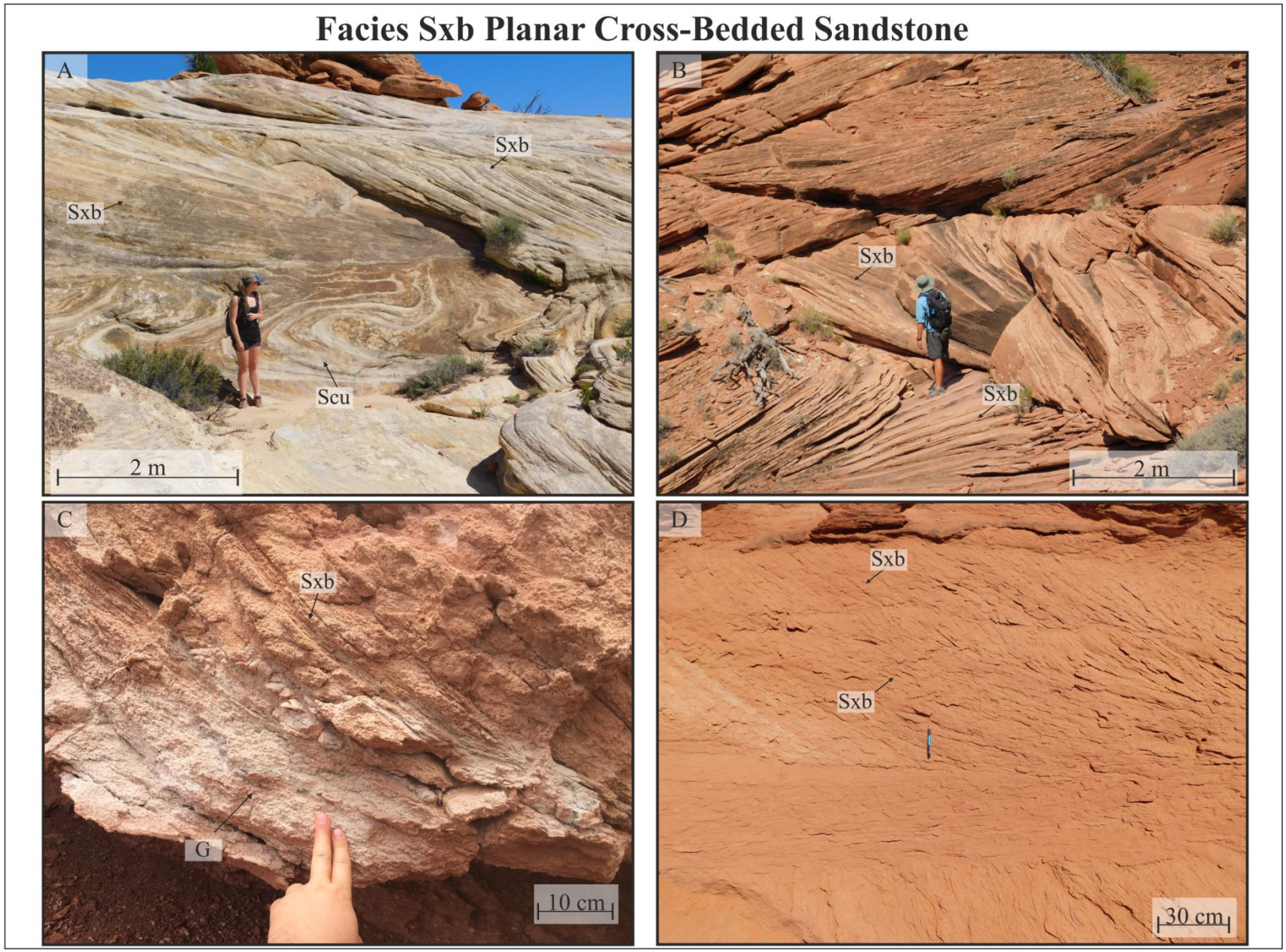

Figure 3.3 Facies SXB, planar cross bedded sandstone, on both a large (A-B) and small scale (C-D). (A) large scale planar cross-bedding over soft sediment deformation. (B) Compound planar cross-bedded sets in multiple directions. (C) Small scale planar cross-bedding, with gypsum precipitated along bounding surfaces leaving a white colour. (D) small planar cross-bedding

3.3.2 Trough cross-bedded sandstone-Stxb

Description. This lithofacies (Fig. 3.4) is characterised by yellow, white or orange coloured, fine- to medium-grained sandstones. The facies is well-sorted, with a sub- to well-rounded texture and displays trough cross-bedding arranged into large scale compound sets with a dominant migration direction towards the south-east. Occasionally, inverse grading is present, separated by thin layers of finer grained laminae.

The deposits range from 0.5 m to 5 m in thickness and are laterally extensive, often over distances of 10s of metres. The deposits are most prevalent within the north of the study area, i.e. logs 1.0-1.3. South of this, (logs 1.4-1.8) planar cross-bedded sandstone (Sxb) dominate, where present, Stxb is laterally and stratigraphically restricted, with thickness rarely greater than 2 m.

Interpretation. These trough cross-bedded homogenous sandstones represent the preserved deposits of sinuous crested aeolian dunes. The features are similar to the planar cross-bedded lithofacies (Sxb), however, the arrangement of many of these deposits into large-scale, trough cross-bedded sets indicates an origin via the migration of sinuous crested barchan or barchanoid dune forms, within a south-easterly palaeo-wind regime (Mountney, 2006; Mountney & Jagger, 2004). Most likely, the migrating dune trains were in an out of phase planform geometry, generating this trough cross-bedded pattern (Rubin, 1987; Rubin & Carter, 2006).

Figure 3.4 Facies Stxb, trough cross bedded sandstone. Large dish shaped troughs are highlighted in the figure (A) Large dish shapes trough-cross bedding highlighted in white, black shows smaller troughs migrating in different directions. (B) White shows large dish shaped trough cross-bedding

3.3.3 Translatent ripple sandstone-Sxr

Description. This lithofacies (Fig. 3.5) is characterised by shallowly-climbing (<8 deg) ripples (Fig 3.5B) composed of yellow, orange to white, fine- to medium-grained, well-sorted, sub- to well-rounded, quartz arenite.

The facies range from 0.2 m to 3 m in thickness and are laterally extensive, often over distances of 10s of metres primarily in stratigraphic relationships with facies Sxb, Stxb, Sm and Spl. The deposits are present in all logs, except Log 1.9, with the greatest thickness occurring in log 1.3.

Interpretation. Translatent strata inclined at low angles and found in thick units are indicative of deposition either: in response to the migration of an aeolian bedform that did not possess an active slipface (Biswas, 2005; Kocurek & Neilson, 1986); at the margins of the ergs where low sediment supply prevents the formation of larger dune forms (der Valle *et al.*, 2008); where periodic inundation of flood waters prevents the establishment of dunes, (Kocurek & Neilson,1986; Neilson & Kocurek, 1986); where vegetation, binds and inhibits sediment availability for aeolian transport (Bullard, 1997; Kocurek, 1999; Kocurek & Lancaster, 1999); sediment which has a grain size too coarse to become entrained effectively (Kocurek & Neilson, 1986); or a high watertable in contact with the sediment surface, entraining and limiting sediment availability (Fryberger *et al.*, 1988; Jagger, 2003; Mountney & Jagger, 2004; Stokes, 1968).

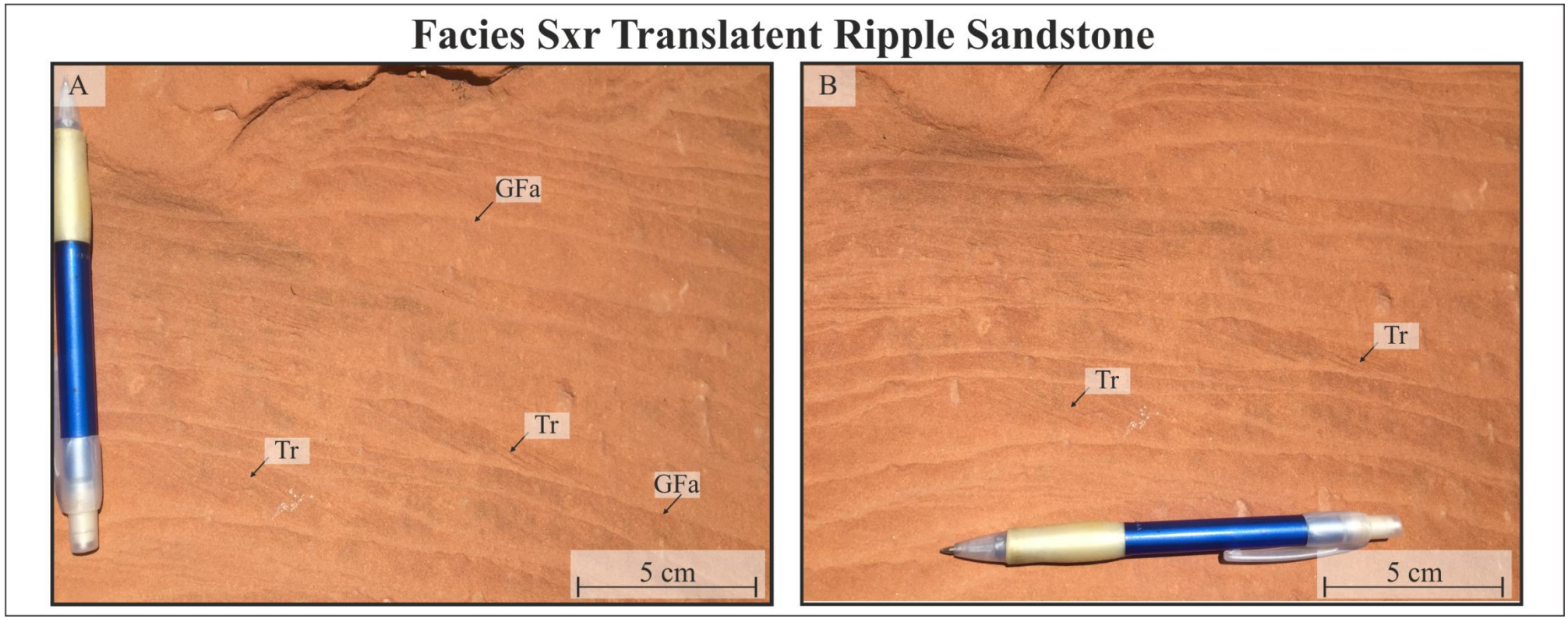

Figure 3.5 Facies Sxr, translatent ripple sandstone. Climbing translatent ripples are highlighted between alternating grain fall and grain flows

3.3.4 Pinstriped sandstone-Spl

Description. This lithofacies (Fig 3.6) is characterised by yellow, orange to white, fine- to medium-grained, well-sorted, sub- to well-rounded, quartz arenite. The lithofacies is horizontally laminated, occasionally undulose (Fig 3.6A), with bimodal (pinstriped) sorting (Fig 3.6B).

The facies range from 0.2 m to 1 m in thickness and are laterally extensive, often over distances of 10s of metres primarily in stratigraphic relationships with facies Sxb, Stxb, Sm and Sxrl. The deposits are present in all logs, except Log 1.9, with the greatest thickness occurring in log 1.3.

Interpretation. Aeolian grade sediment with well-developed bimodal laminations represents the migration of wind ripples, either along a sandsheet environment, where sediment supply is restricted and duneforms can't develop (Biswas, 2005; Kocurek & Neilson, 1986), or superimposed on aeolian bedforms, most commonly found along the toesets or due plinth of aeolian dunes.

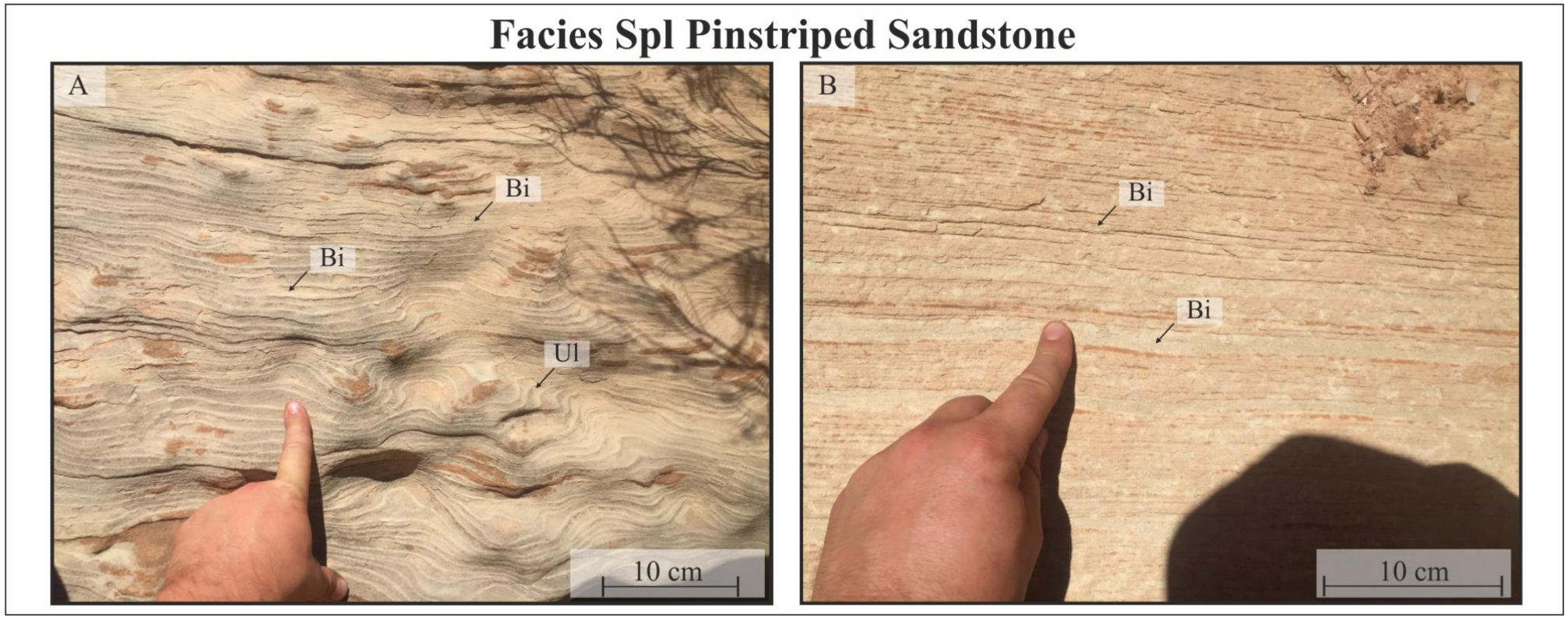

Figure 3.6 Facie Spl, pinstriped sandstone, (A) shows undulose laminations between alternating coarse and finer grainsizes. (B) shows bimodal sorting, coarser grainsizes weather proud and often have a more orange appearance.

3.3.5 Convolute bedded sandstone-Scu

Description. This lithofacies (Fig 3.7) is characterised by yellow, orange to white, fine- to medium-grained, well-sorted, sub- to well-rounded, quartz arenite. The facies shows convolute and undulose bimodally sorted laminations.

The facies ranges from 0.2 m to 1.5 m in thickness and is isolated, rarely greater than 1 m in laterally continuity. The facies occurs sporadically throughout the study area, primarily in stratigraphic relationship with facies Sxb, Stxb, or Sm.

Interpretation. The lithofacies is composed of aeolian grade material, the convolution and contortion results from variations in watertable elevation combined with the overburden pressure exerted by advancing dune forms that migrated over the water-laden facies (Collinson, 1994).

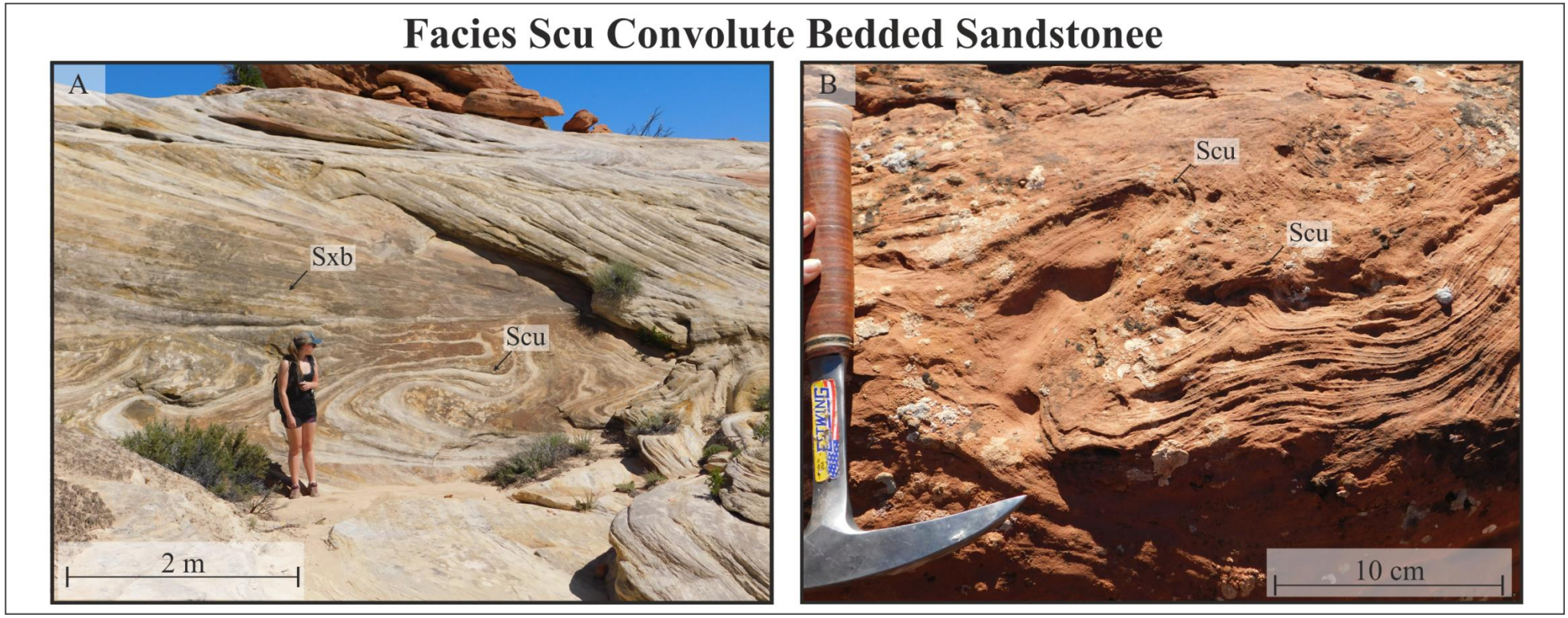

Figure 3.7 Facies Scu, convolute bedded sandstone, (A) shows large scale soft sediment deformation overlain by facies Sxb. (B) shows smaller scale convolute bedding within an aeolian dune.

3.3.6 Massive Sandstone-Sm

Description. This lithofacies (Fig. 3.8) is characterised by yellow, orange to white, fine- to medium-grained, well-sorted, sub- to well- rounded, quartz arenite. The facies has a massive appearance with sporadic mottling and occasional rhizoliths (Fig 3.8B).

The deposits range from 0.2 m to 5 m in thickness and are laterally extensive, often over distances of 10s of metres primarily in stratigraphic relationships with facies Sxb, Stxb, Sxr and Spl. The deposits are present in all logs, except Log 1.9, with the greatest thickness occurring in the north of the study area (logs 1.0–1.3).

Interpretation. This facies is composed of aeolian-grade sediment and appears massive due to the presence of very poorly defined translatent strata, where limited grainsize variations do not distinguish the bounding surfaces of each cross-laminated set (Kocurek, 1981). Rhizoliths and mottling indicate the occasional presence of water, most likely only short lived, and as a result in fluctuations in watertable elevation.

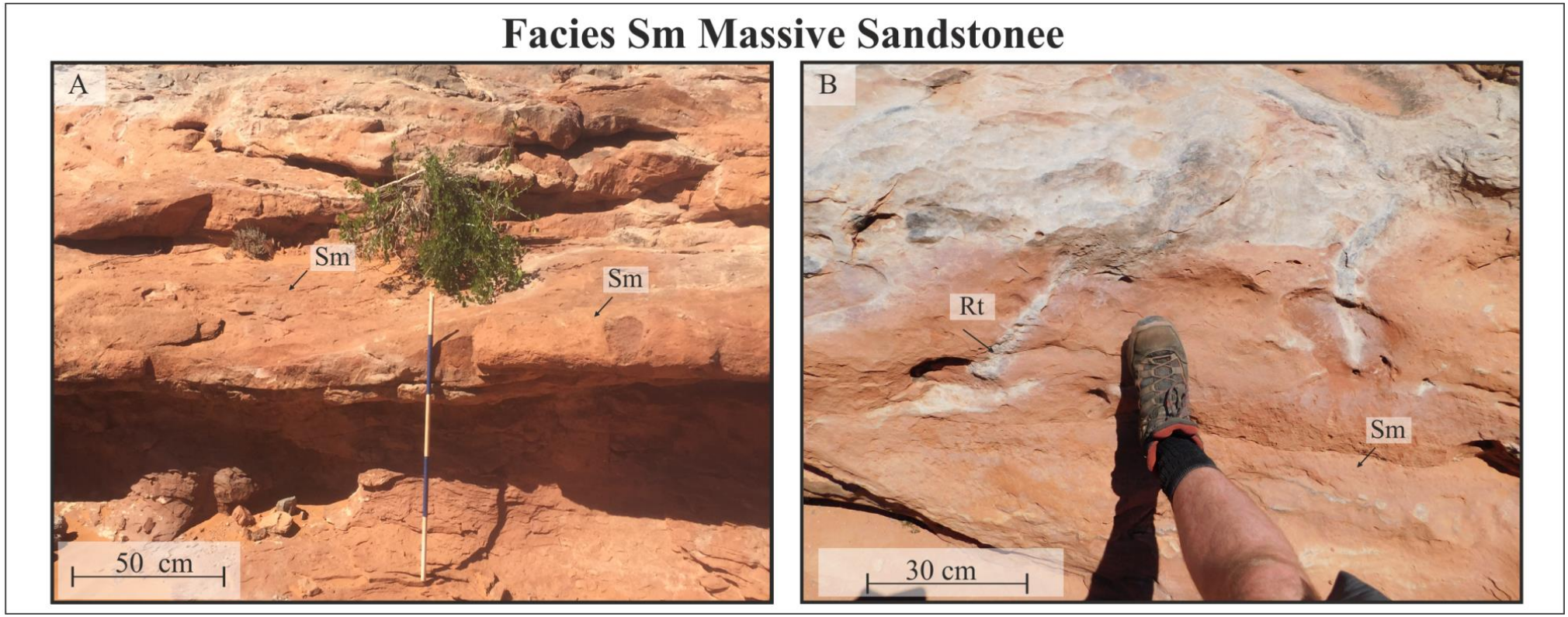

Figure 3.8 Facies Sm, massive sandstone. (A) typical appearance of massive sandstone facies within an aeolian interdune setting. (B) rooted appearance typically seen.

3.4 Sub-aqueous Lithofacies

Eleven facies are interpreted to have been formed in a sub-aqueous environment. These include deposits interpreted to form within either channelised or non-channelised aqueous flow, such as fluvial sheet flood deposits, or within standing bodies of water, such as puddles or lakes.

3.4.1 Wave-rippled sandstone-Swr

Description. This lithofacies (Fig 3.9) contains dark brown silt to very fine-grained moderately sorted sub-rounded sub-arenite. The facies is parallel laminated with a sporadic undulose texture and symmetrical wave ripple cross lamination. Sporadic rhizoliths, in the form of horizontal to sub-vertical root traces, localised bioturbation present in the form of thin (<10 cm) branched vertical and horizontal tube like-burrows, and localised mottling are also present.

The facies range from 0.2 m to 10 m in thickness and are laterally extensive, often over distances of 10s of metres. The deposits are absent in the north of the study area (logs 1.0-1.3), with the greatest thicknesses occurring in logs 1.7–1.9, in stratigraphic relationship with facies Ssl, Lm, Lsm or Sfxb.

Interpretation. This facies is interpreted as a low energy, sub-aqueous setting, where the deposits have settled out of suspension. Undulose and wave ripples form due to oscillating waters in response to wind action within shallow waters. Bioturbation and Rhizolith development indicates conditions able to support organisms, with the icnhnofacies suggesting *thlassinoides* and a localised bioturbation index of 2 (Taylor & Goldring, 1993).

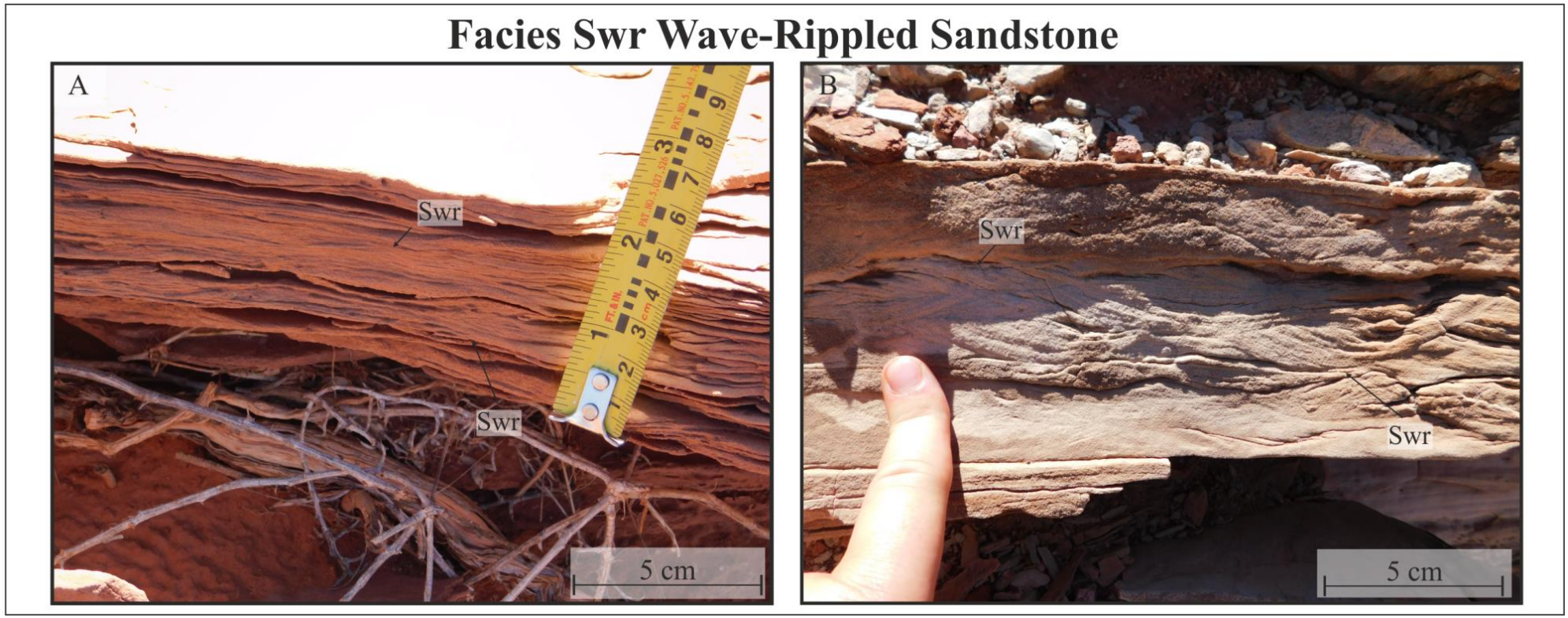

Figure 3.9 Facies Swr, wave rippled sandstone, symmetrical wave ripples shown in both (A) and (B)

3.4.2 Massive mottled silt-Ssl

Description. The facies (Fig. 3.10) varies between black to a dark grey, purple colour. The grain size varies as well between silt to very fine-grained sandstone. The facies has a slight structureless appearance however, fining upwards and parallel lamination can be observed sporadically. The facies often has a high organic content and often appears mottled. The deposits range from 20 cm– 1 m in thickness. The individual beds are laterally extensive and present throughout most of the logged sections, especially prevalent towards the south, with the thickest deposits seen in Log 1.8 and Log 1.9.

Interpretation. The extensive fine-grained–silt grade parallel-laminated deposits are representative of low energy sub-aqueous settings. Normal grading and parallel laminations indicate suspension settling dominates deposition (Tanner & Lucas, 2007; Fielding, 1984). Occasional evidence for high organic content could indicate water depths sufficient to cause thermal stratification, or anoxic conditions (Boehrer & Schultze, 2008).

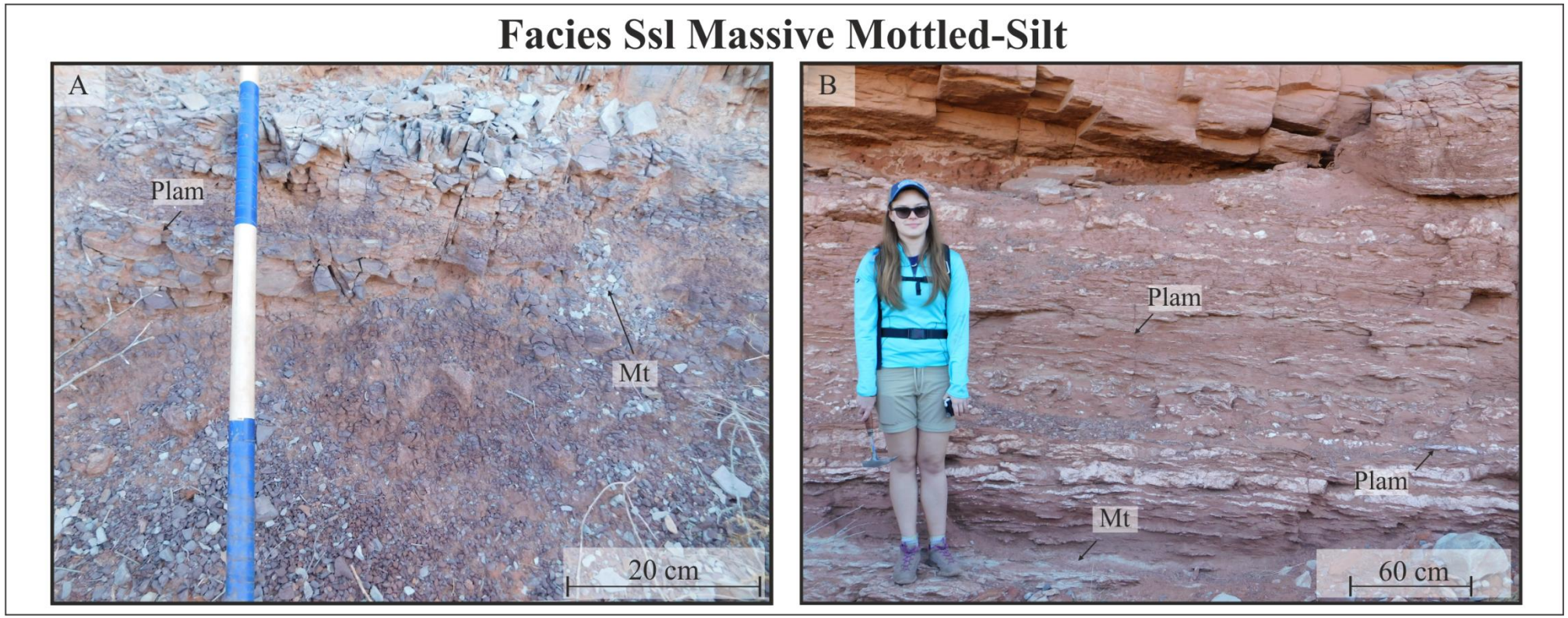

Figure 3.10 Facies Ssl, massive mottled silt. (A) shows laminations and the mottled appearance, (B) shows the often thick deposits of regularly spaced parallel laminated silts.

3.4.3 Intraformational conglomerate-Cm

Description. This facies (Fig. 3.11) is grey to brown in colour with a granule to pebble-sized grainsize. The facies is poorly sorted, sub-rounded to well-rounded, and is matrix supported. The facies fines upwards, clasts are polymictic, composed of grey to purple rip-up silts and fine sands from surrounding lithologies. The facies is rare within the study area, only present within the logs 1.0, 1.5 and 1.7, and occurs in isolated U-shaped bodies, frequently in conjunction with facies Cxb, Sfxb, Sfpl and Sfrl. The deposits range from 0.2 m to 1 m in thickness and are laterally restricted, often dying out over distances of less than 1 m.

Interpretation. The conglomeratic and isolated U-shaped nature of the deposit suggests deposition occurred within channelised confined flows able to generate high energy bedload transport, which reworked locally derived sediment as basal lags (*C.f* Pandita *et al.,* 2011).

3.4.4 Planar cross-bedded gravel-Cxb

Description. This facies (Fig. 3.11) is grey to brown coloured with a granule to pebble-sized grainsize. The facies is poorly sorted, with a sub-rounded to well-rounded texture. The facies is matrix supported, composed of fine-grained sandstone and normally graded. Sporadic, crudely developed planar cross-bedding is the dominant sedimentary structure with occasional pebbles lining the foresets. This facies occurs as isolated deposits with an erosional base. The facies range from 0.2 m to 0.5 m in thickness and are laterally isolated, often over less than 1 metre. The facies is rare, only present within logs 1.0, 1.5 and 1.7, and occurs occurring in conjunction with facies Cm, Sfxb, Sfpl and Sfrl.

Interpretation. The conglomeratic and channelised nature of the deposit suggests deposition occurred in similar setting to facies Cm, in confined flows able to generate high energy bedload transport, which reworked locally derived sediment as basal lags (*C.f* Pandita *et al.,* 2011). The texture and structure of the facies indicates depositional processes similar to facies Cm. However, the development of crude cross-bedding could indicate lower flow regime, dune scale bedform migration, under conditions of high sediment load.

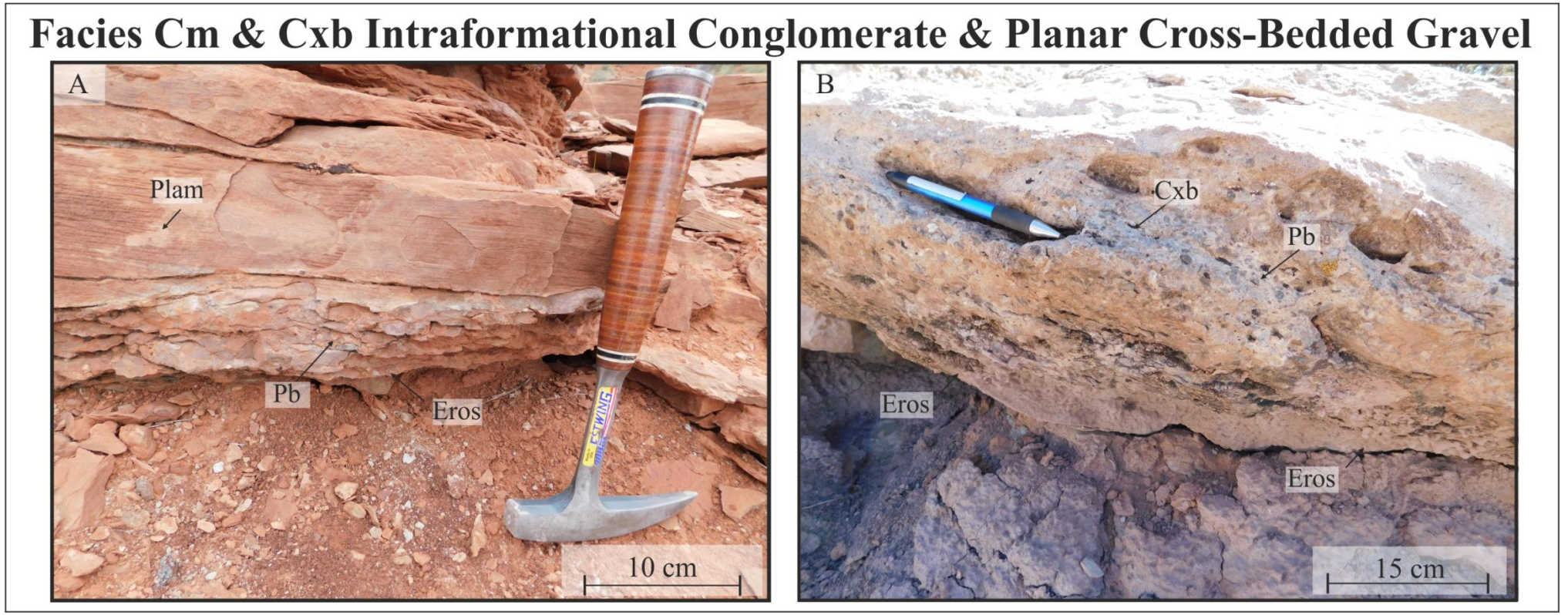

Figure 3.11 (A) Facies Cm, intraformational conglomerate, (B) Planar cross bedded gravel. Both show the erosional nature of the facies outlined in white, (A) fines rapily into parallel laminated sandstone (black line), (B) shows crude cross bedding with peddles lining of the foresets (black line).

3.4.5 Planar cross-bedded moderate sorted sandstone-Sfxb

Description. This facies (Fig. 3.12) is grey to brown in colour, composed of fine- to medium-grained sandstone. The sandstone is moderately sorted and sub-rounded. The main sedimentary feature of the facies is low angle planar cross-bedding, often in multiple sets (up to 1 m thick) and multiple directions, with a dominate palaeocurrent direction towards the south-west. In outcrop the vertical thickness of the facies is highly variable, and often branches, with thicknesses ranging from 0.5–1.5 m. The facies is laterally extensive, with distinct units being traceable over distances of 10s of metres.

Interpretation. Facies composed of moderately sorted, sub-rounded sub-arkosic arenites, suggest a fluvial derived source for the material. The planar cross bedding indicates accretionary migration of straight crested dune-scale bedforms under lower flow regime conditions (Miall, 2006).

The dominant south-westerly palaeocurrent direction is similar to that report by other authors (Langfrond & Chan, 1989; Moutnney & Jagger, 2004) and represents the fluvial transport of material shed from the Uncompahgre Uplift.

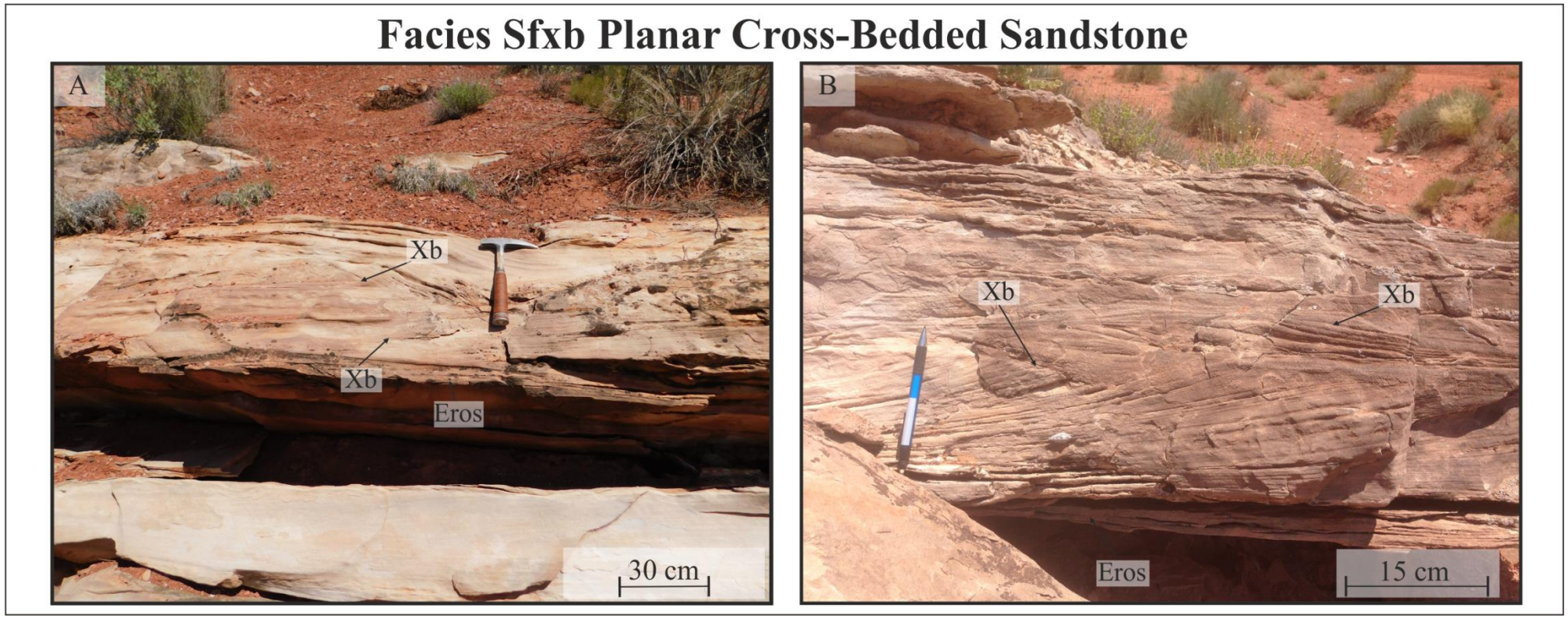

Figure 3.12 Facies Sfb, planar cross bedded sandstone, figure shows the multiple sets of cross beds in opposing directions.

3.4.6 Horizontally laminated sandstone-Sfpl

Description. This facies (Fig. 3.13) is a grey to brown coloured, fine- to medium-grained sandstone. The deposits are moderately sorted, normally graded, sub-rounded and formed of sub-arkosic arenite. The internal architecture of the facies is composed of well-defined planar laminations, 0.5 cm–1 cm thick, arranged into sets of 20–50 cm in thickness, with isolated lateral extents less than 1 m.

Interpretation. Facies composed of moderately sorted, sub-rounded sub-arkosic arenites, suggest a fluvial derived source for the material. Prevalent planar laminations represent upper plane beds deposited under upper-flow regimes (Miall, 2006).

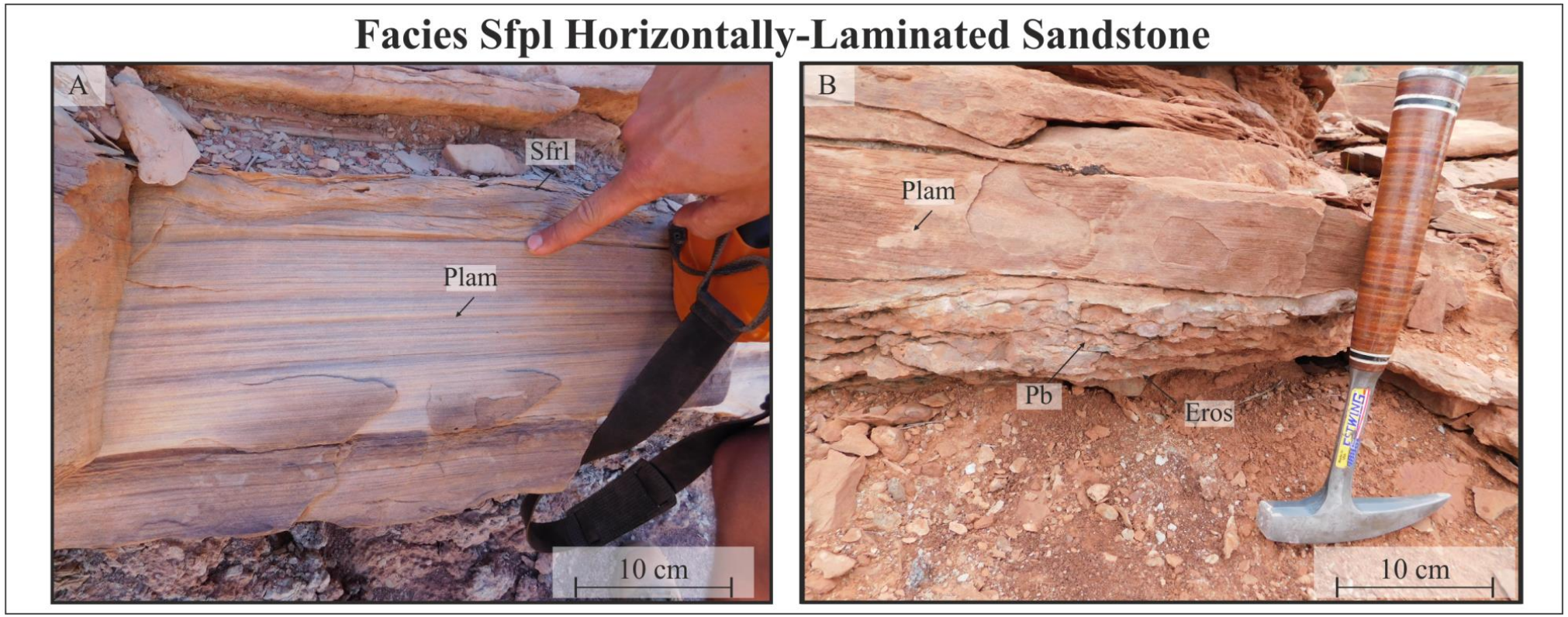

Figure 3.13 Facies Sfpl horizontally laminated sandstone (A) 30cm thick deposit of parallel laminations, (B) parallel lamination overlying conglomeratic facies Cm.

3.4.7 Climbing-ripple cross-laminated sandstone-Sfrl

Description. This facies (Fig 3.14) is formed of grey to brown, fine- to medium-grained, moderately sorted, sub-rounded, sub-arenites. The facies dominant feature is sub-critically climbing asymmetrical ripple laminations. The facies has thicknesses between 0.2-0.5 m and limited lateral extends of less than 1 m. The facies occurs primarily in stratigraphic relationship with Cm, Cxb, Sfpl and Sfxb.

Interpretation. This facies is interpreted to form under lower flow regime conditions, generating ripple scale bedforms as a result of unidirectional flow migration. The limited lateral extent of the facies and occurrences with related fluvial derived facies (Cm, Cxb, Sfpl, Sfxb) indicate formation and deposition within a channel fill succession (*cf.* Miall, 1978).

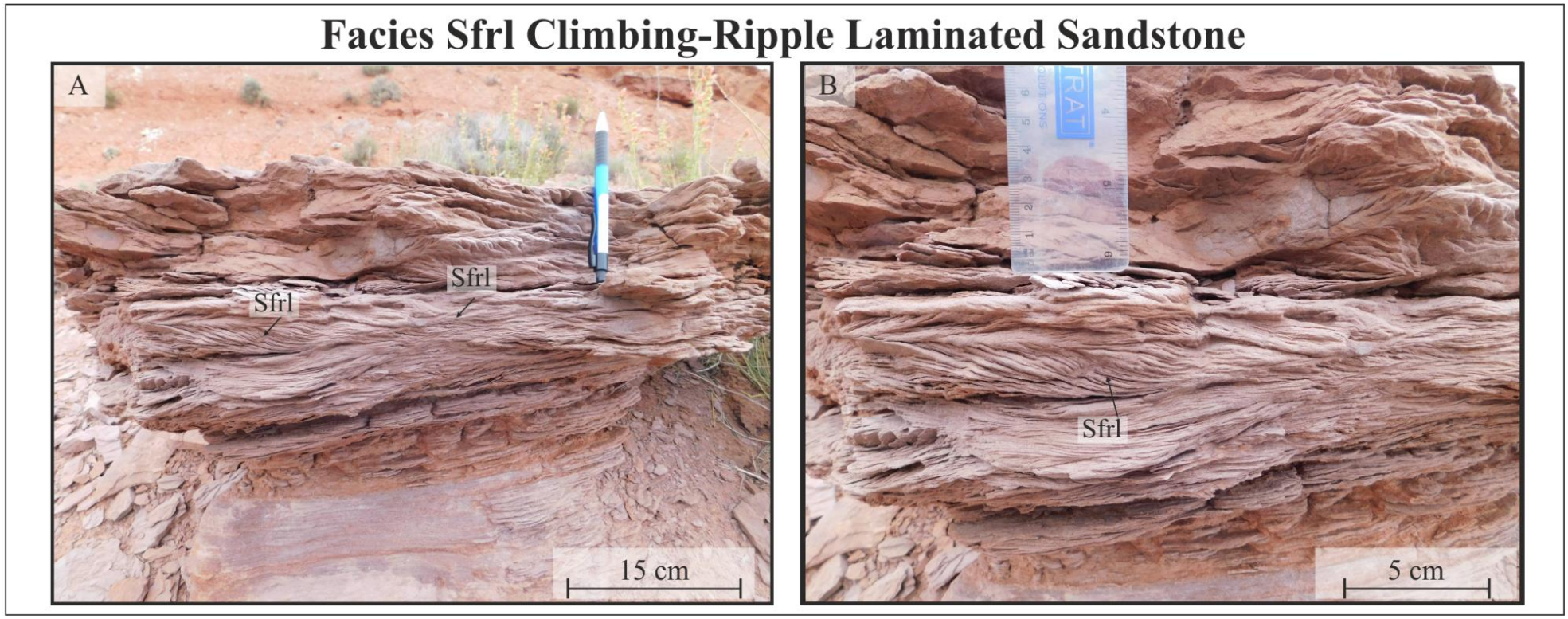

Figure 3.14 Facies Sfrl, Climbing ripple laminated sandstone

3.4.8 Calcrete rich pedogenic facies-Sao

Description. This facies (Fig 3.15) is characterised by a distinctive rooted and mottled appearance of light brown, grey to yellow very fine- to fine-grained, moderately to well-sorted, sub-rounded fining upwards sub-arenites 30–50cm in thickness, with lateral extents ranging between 1– 10s of metres occurring commonly in stratigraphic association with facies Sm ,Spl, Sxr, G and Gspl. Root traces are thin (5 cm width) sub-vertical (up to 50 cm in length), and often fine to a point at their base, mottling is highly localised, often around the root traces. The facies has a massive- to structureless appearance as a result of a disruption in primary depositional fabrics by root traces, frequent gypsum or calcrete nodules and veins (Fig 3.15B).

Interpretation. This facies indicates periods of surface stabilisation and soil development with sufficient moisture for vegetation to bind sediment. The presence of gypsum and replacement of roots within the calcrete-rich facies indicates an arid to semi-arid climate (e.g. Cecil 1990; Retallack, 1994; Kraus, 1999), with potential saline groundwater geochemistry precipitating gypsum within the vadose zone.

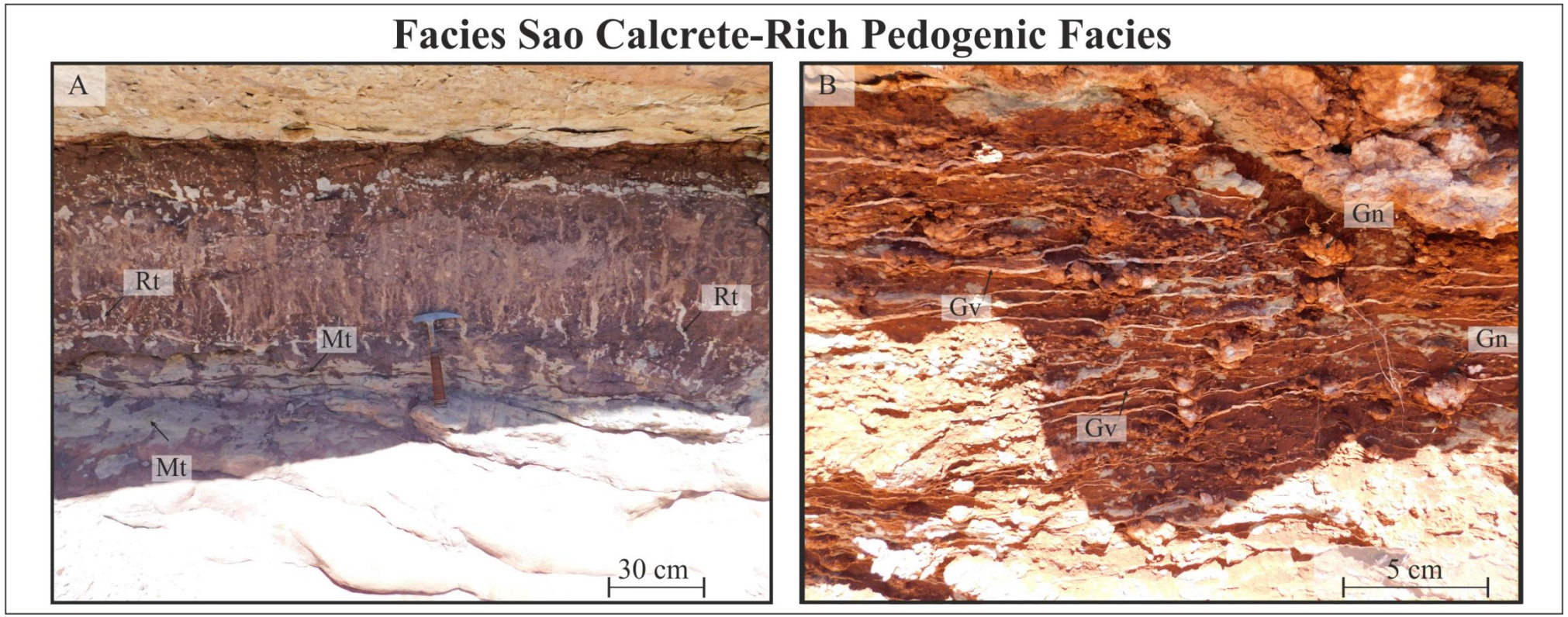

Figure 3.15 Facies Sao, calcrete rich pedogenic facies. (A) distinctive mottled and rooted appearance of the facies, (B) frequent appearance of gypsum nodules and veins.

3.4.9 Horizontally laminated pedogenic facies-Sfo

Description. This facies (Fig 3.16) contains purple to light brown, silt - to fine-grained, fining upwards sub-arenites. The facies is rarely greater than 30 cm thick with lateral extents between 1–5 metres, often occurring in stratigraphic relationship with Swr, Ssl, Sfxb, Sfpl, and Sfrl. The facies displays localised mottled with very fine horizontally lamination with rare and localised gypsum nodules and veins.

Interpretation. This facies represents periods of stabilisation and modification of fluvial derived sediment into a palaeosol. The presence of primary sedimentary features, such as laminations, indicates a relatively immature palaeosol most likely in proximity to fluvial channels or confined bodies of water (*cf.* Tooth, 2005). The rare occurrences of gypsum indicate a more humid climate.

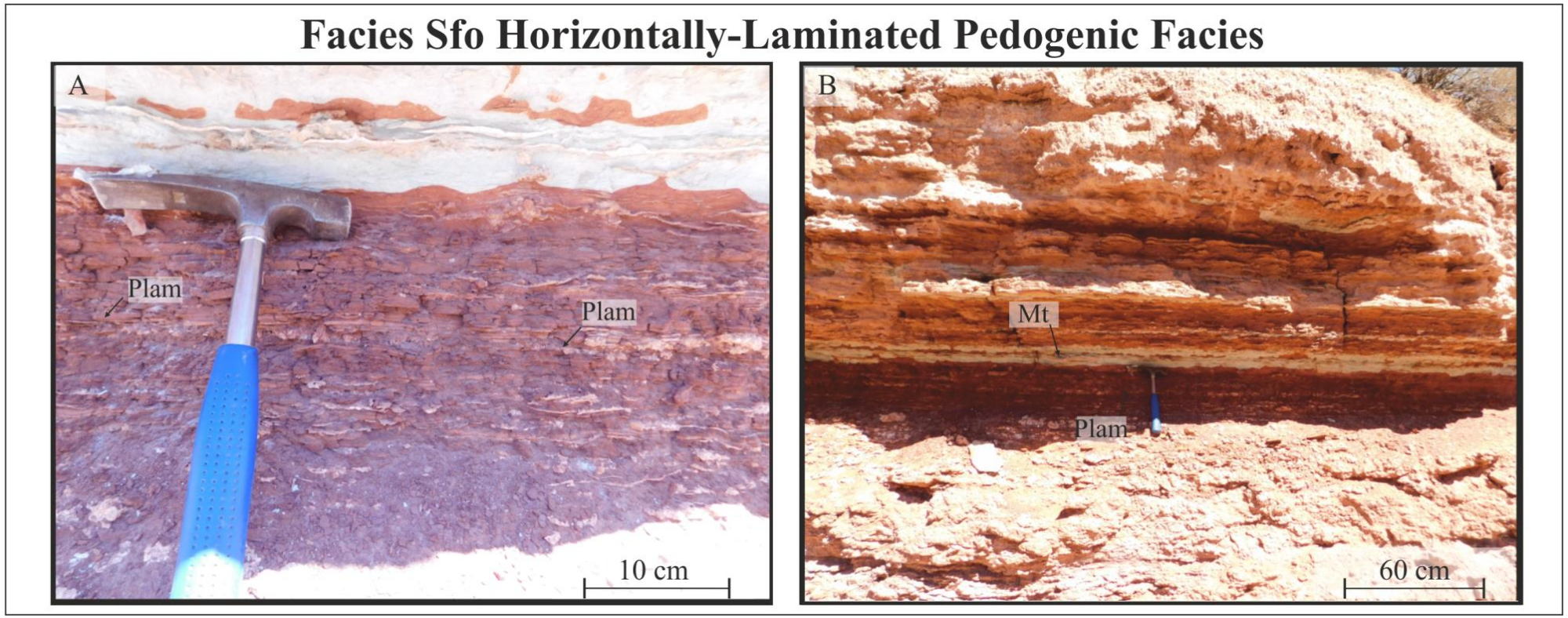

Figure 3.16 Facies Sfo, horizontally laminated pedogenic facies. (A) laminated appearance of the facies (B) typical thickness and appearance of the facies.

3.5 Evaporitic Lithofacies

Two lithofacies are identified to have been generated under evaporitic conditions: secondary gypsum lithofacies and gypsum-bound sandstone lithofacies. These are fully described below.

3.5.1 Secondary Gypsum Lithofacies-G

Description. In outcrop this lithofacies (Fig 3.17) is characterised by white to peach, very fine-grained crystalline gypsum (Fig 3.17B). The gypsum shows alabastrine and prophyroblastic textures and resembles white marble. The facies has either a clast supported brecciated and crudely bedded appearance (Fig 3.17E), or manifests as nodular (Fig 3.17C,D) to laminated-bands with enterolithic convoluted folds (Fig 3.17G,H), polygonal hummocks (Fig 3.17A) and chicken-wire structures (Fig 3.17F). Occasionally laminated layers show peach coloured elongate crystals.

Petrography of the Evaporites. Petrographic studies show (Fig 3.18, 3.19) that gypsum samples generally display alabastrine and prophyroblastic textures. Alabastrine textures show erratic migrating extinction shadows when rotated under cross-polarized light. Prophyroblastic gypsum forms small and large crystals with interlocking margins, with many of these larger crystals containing corroded anhydrite relicts. Satin spar hydration veins are also a common feature, and one sample contains large laths of secondary gypsum.

Interpretation. This facies results from the accumulation of primary anhydrite and gypsum by precipitation in saline shallow water conditions (Kendall, 1981; Handford, 1991; Warren, 1991). Enterolithic and chicken-wire structures indicate very early diagenetic (synsedimentary) displacive growth of anhydrite nodules which were partly or completely hydrated to secondary gypsum under post-sedimentary conditions i.e. early and/or late diagenesis and the exhumation process

(*cf.* Butler, 1970). Laminated layers with elongate crystals are indicative of selenite, signifying free growth of crystals from brine, which has been dehydrated to anhydrite during burial diagenesis and rehydrated to secondary gypsum during exhumation. Clast-supported brecciated alabastrine secondary gypsum is also present, potentially as a result of syndepositional dissolution. Polygonal hummocks form tepee structures due to desiccation of saline waters and fracturing of salt crusts into polygonal shapes (Warren, 2016).

Figure 3.17 Field photos of Facies G, crystalline gypsum (A) Tepee fracturing of salt crusts, (B) thin laminated gypsum crystals, (C) gypsum nodule, (D) bottom nucleating gypsum nodules (E)disrupted brecciated gypsum (F) chicken Wire structures (G) enterolithic folding of gypsum (H) multiple layered enterolithic folds

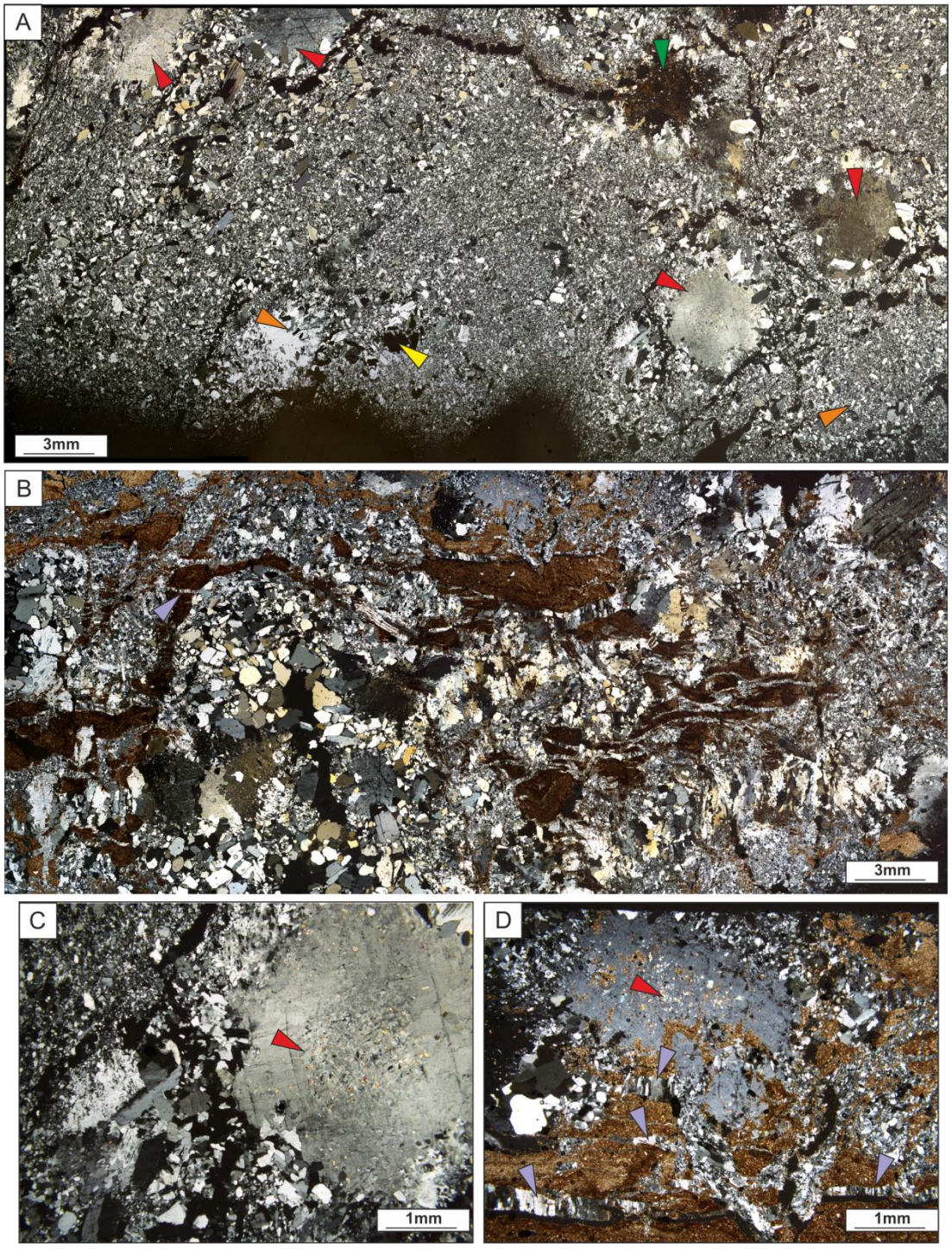

Figure 3.18 Photomicrographs of gypsum samples (A) Secondary alabastrine gypsum matrix with large prophyroblastic secondary gypsum crystals (red arrow) containing corroded anhydrite relics. Potential calcite replacement, highlighted by green arrow. Orange arrow shows anhydrite laths, yellow arrow highlight swallow tail habit. (B) Secondary gypsum composed of alabastrine matrix with frequent hydration veins filled with satin spar gypsum (purple arrow). Sample contains some clastic grains and calcite replacement of gypsum. (C) Close up of prophyroblastic gypsum in alabastrine matrix with corroded anhydrite relics highlighted by red arrow. (D) Close up of prophyroblastic gypsum in alabastrine matrix with corroded anhydrite relics highlighted by red arrow and satin spar hydration veins highlighted by purple arrow.

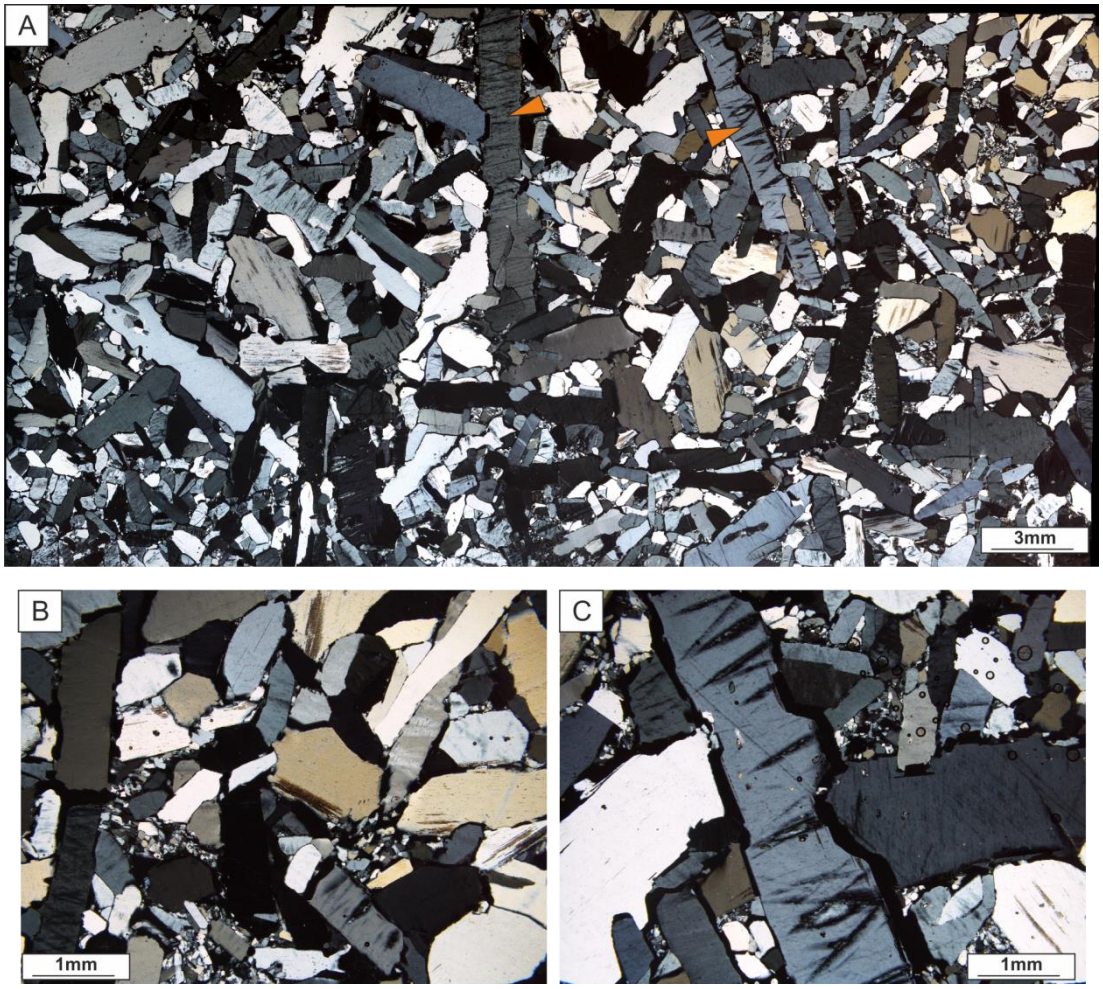

Figure 3.19 Photomicrographs of gypsum samples(A) Elongate secondary selenite gypsum crystals (orange) (B) Close up of elongate secondary selenite gypsum crystals highlighting the contacts between crystals. (C) Close up of elongate secondary selenite gypsum crystals highlighting the contacts between crystals and elongate crystal habits.

3.5.2 Gypsum-bound sandstone-Gspl

Description. This lithofacies (Fig. 3.20) is characterised by pastel blue, very fine to fine-grained, moderate to poorly sorted, sub-rounded sandstone within a gypsiferous matrix and cement. The facies is parallel-laminated to massive, and is often contorted by small gypsum nodules (Fig 3.20B).

Interpretation. This facies represents the flow of saline fluid and subsequent precipitation of gypsum in the pore space of sediment around the margins of saline lakes as water evaporated at the ground surface (Lowenstein & Hardie, 1985).

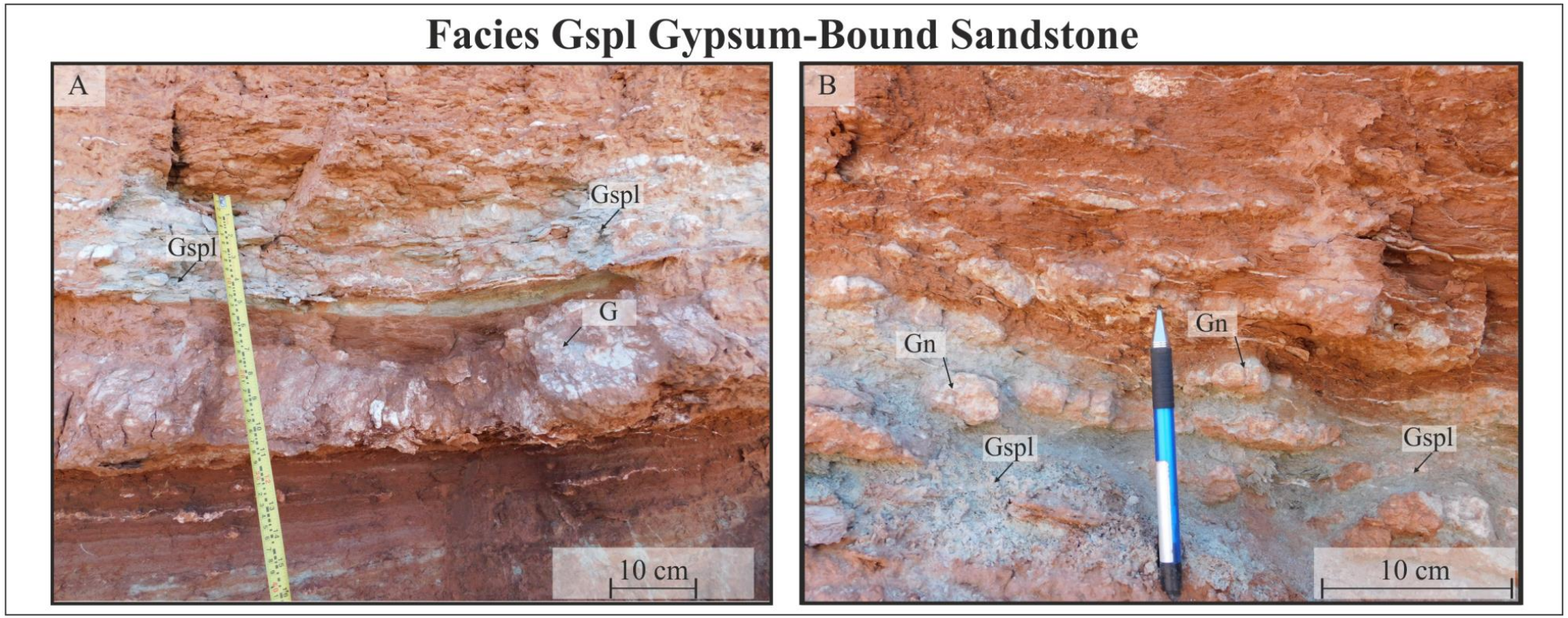

Figure 3.20 Facies Gspl, gypsum bound sandstone (A) distinctive pastel blue appearance of the facies, (B) blue appearance of the facies with interbedded gypsum nodules disrupting sedimentary fabrics.

3.6 Carbonate lithofacies

Two carbonate lithofacies were primarily identified within the field, however, when analysed under thin section six distinct carbonate microfacies have been identified. A summary table of the carbonates identified from field description is presented below (Table 3.2), followed by a full microfacies analysis of the thin sections. In the field, carbonates of the Cedar Mesa Sandstone Formation appear as dark grey to blue, homogenous carbonate mudstones. Outcrop specimens have a wavy–laminated (Fig. 2A) or nodular texture (Fig. 2D), these are classified as a wackestone, however some sand-grade-grain supported carbonates were classified as packstones (Fig. 2B, Fig. 2F). The carbonates occasionally appear interbedded with gypsum (Fig. 2D) or with chert nodules, but predominantly form blocky units in outcrop (Fig. 2B, Fig. 2E) between 20- 40 cm in thickness. The outcrop geometries vary from isolated lenses (Fig. 2B) to laterally continuous flatbeds (Fig. 2C, Fig. 2E).

Table 3.2 Field description of carbonate facies

Code	Facies	Description	Interpretation
Lm	Fine-grained carbonate	Dark grey to blue, carbonate mudstone/wackestone. Massive, sporadic blocky or stylotised with sporadic Ostracod microfossils and nodular red microcrystalline chert.	Sub-aqueous precipitation of carbonate.
Lsm	Clastic-rich carbonate	Dark grey to blue carbonate Wackestone/ Packstone with >10% fine grained sand within a carbonate mud matrix.	Sub-aqueous precipitation of allochthonous carbonate with siliciclastic input from neighbouring environments.

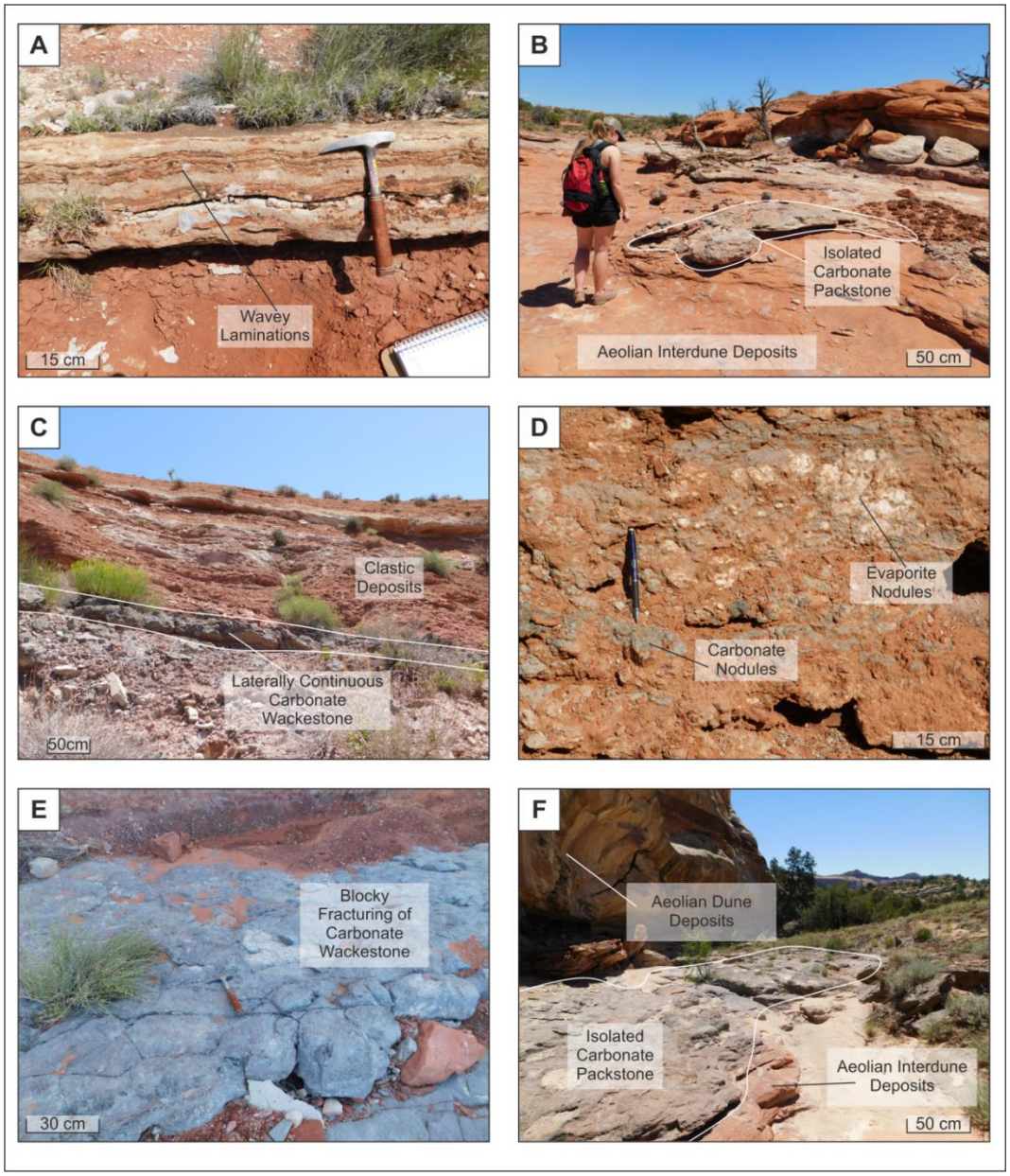

Figure 3.21 Outcrop photos showing the variety in carbonate deposits at field scale. (A) Alternating wavy laminations of carbonate wackestone, beds are laterally persistent and average approximately 40 cm thick. (B) Isolated lens of clastic-rich carbonate wackestone (circled) interbedded within aeolian interdune deposits, the carbonate lenses. (C) Thin laterally continuous dark grey carbonate wackestone, interbedded within lacustrine clastic deposits. (D) Interbedded gypsum evaporite nodules (white) and carbonate nodules (Grey) within a fine grained clastic matrix. (E) Blue carbonate wackestone, with distinctive blocky fracturing style. (F) Isolated carbonate packstone (circled) interbedded between aeolian dune and interdune deposits.

3.6.1 MF1: Clastic Influenced Carbonate Wackestone

This facies outcrops as isolated, dark grey to blue, siliciclastic, massive fine-grained wackestonee (Fig. 3.21B). The microfacies has a high clastic component (approx. 10–>50%) within a darker, homogenous dark brown carbonate mud matrix, with some poorly defined wavy laminations (Fig. 3.22A), but otherwise lacks any sedimentary structures. The carbonate mud matrix is composed of micrite with sparse microspar crystals. There are occasional isolated intraclasts of mudstone with a higher microspar component (these therefore appear slightly lighter than the background micrite-rich matrix), these grains are rounded and 'float' in the quartz-micrite matrix (Fig. 3.22,C). Quartz grains are dominantly well-rounded to sub-rounded, well sorted and fine to medium-grained (Fig. 3.22A, B, C). The majority of intraclasts have sporadic calcified tube-like structures, clotted micrite textures, and are found in association with micrite envelopes. A thrombolytic texture is sometimes preserved, where darker micrite appears to have enveloped "cauliflower"-like structures (Fig. 3.22C).

Interpretation

The high content of detrital well-rounded and sorted quartz material indicates deposition occurred in close proximity to a relatively mature clastic sedimentary system (i.e. aeolian dunes). The carbonate mud matrix along with the occasional carbonate grains, probably indicate extremely shallow (few centimetres) quiet waters. The presence of carbonate grains, formed of micro-spar may originate from reworked carbonate material, potentially transported into the system with the clastic component (cf. Lokier et al., 2017). The general lack of evaporites or of any desiccation structures suggest sufficient humidity that maintained long standing pools/puddles of water suitable for carbonate development. The lack of bioclasts,

and lensoidal outcrop relationships indicate an isolated depositional setting (Driese, 1985), lacking input or connectivity from larger bodies of water.

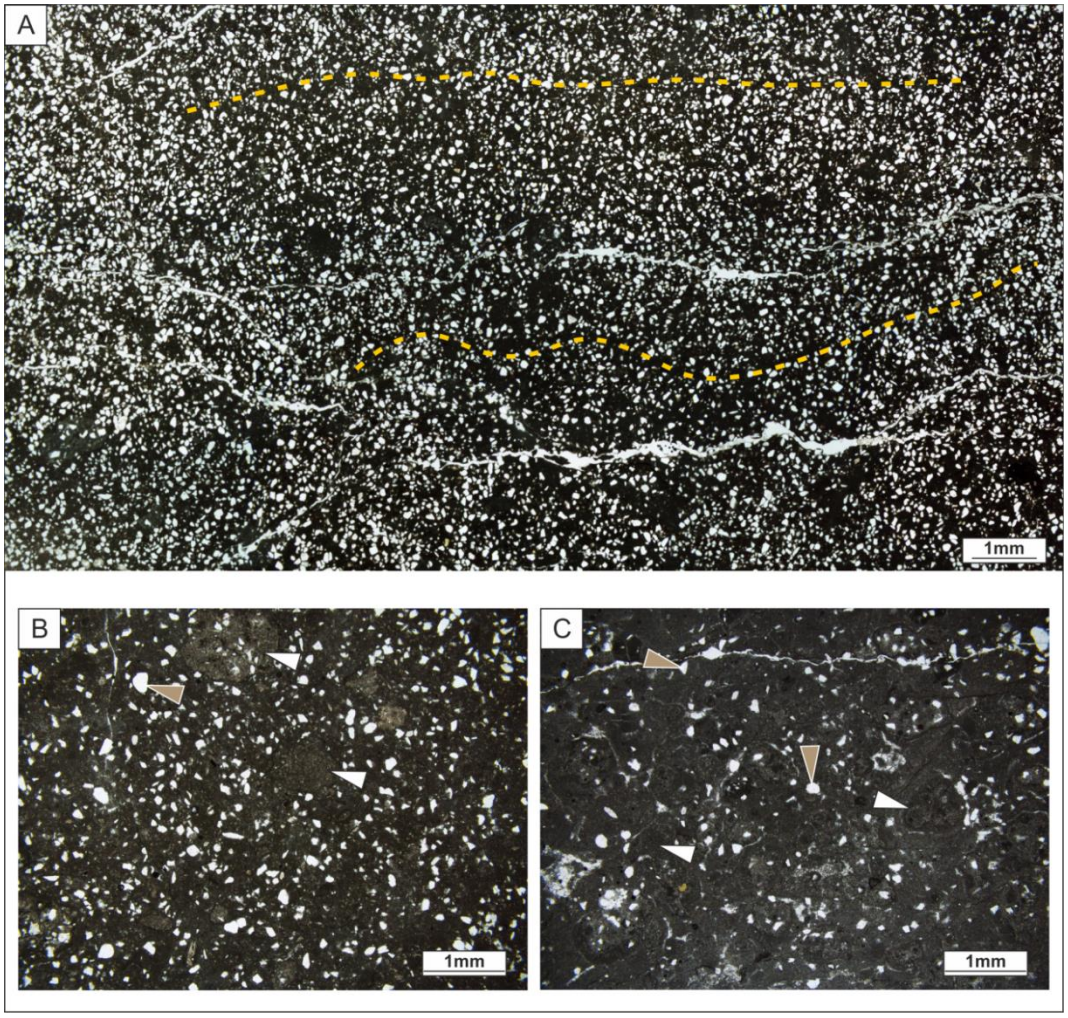

Figure 3.22 (A) Photomicrograph of MF1 showing the high quartz content and poorly defined laminations (dashed yellow line). **(B)** Close up of MF1 showing the dark brown carbonate mud matrix and occasional mudstone grains (white arrow) supporting clastic quartz grains (brown arrow). Clastic grains form up to 50–60% of the sample and are well sorted, with a sub-rounded to rounded texture. (C). Increased matrix/clast ratio and mudstone grains with microspar components (white arrow), quartz grains also highlighted (brown arrow). The mudstone grains appear to have micritic envelopes and occasional protostromate features are discernible.

3.6.2 MF2: Laminated Carbonate Wackestone/Packstone

MF2 is a siliciclastic rich (10–40% sand grains), dark grey to blue fine-grained wacke- to packstones, found as horizontally and laterally restricted lenses (approx. 2 m wide). The microfacies is characterised by bedding parallel laminations of dark-

brown carbonate mudstone matrix, alternating with either laminations of quartz grains or undulose laminations of light-brown to grey clotted microbial fabrics (Fig. 3.23A, B), these clotted micrites are regularly thrombolytic with peloidal and some protostromate features (calcified tubes) present. Quartz grains are moderately sorted and have a rounded to sub-rounded texture (Fig. 3.23C). Ostracods are present in very small numbers (Fig. 3.23B), but otherwise the microfacies is barren of metazoan skeletal grains.

In one sample horizontal laminations (approx.. 0.5-0.8 mm thick) of fine-grained quartz alternating with a thinner (approx.. 0.1-0.2 mm), flat-to undulose, brown carbonate mud matrix was observed. The laminations of quartz show slight normal grading with the thicker quartz bands being composed of medium to fine grained quartz which generally fine upwards (Fig. 3.23C), these laminar fabric is supported by the sand-grade grains (which are considered as extraclasts within the carbonate) resulting in a packstone classification.

Interpretation

The sedimentary framework of alternating laminations of fining upward, sub-rounded moderately-sorted quartz and clotted micrite fabrics within a more homogenous carbonate mudstone matrix indicates periodic influxes of clastic material, followed by a hiatus in detrital material input resulting in the clotted micrite carbonate precipitation, most likely mediated by microbial communities (as evidenced by the protostromate remains).

Normal grading of moderately sorted quartz shows suspension settling of a more immature detrital clastic sediment source than MF1. Isolated and lens shape geometry indicates isolated setting, however rare occurrences of skeletal grains suggest periodic connection to wider environments.

The presence of clotted and laminar microbial growth also indicate an environment which was wetter than that for MF1.

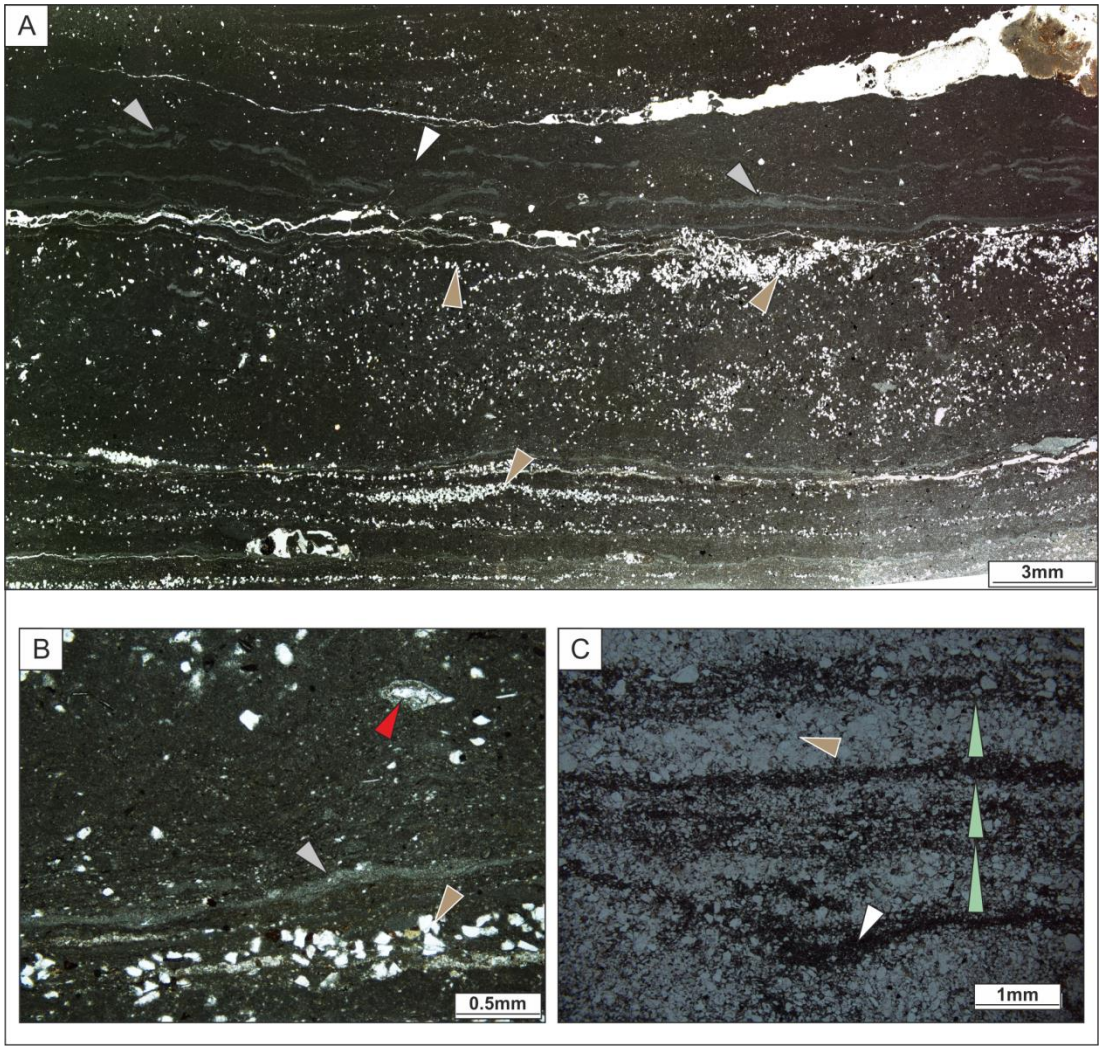

Figure 3.23 (A) Representative photomicrograph of MF2, the microfacies is characterised by horizontally laminated dark brown carbonate mudstone matrix (white arrow) alternating with laminated quartz grains (brown arrow) with occasional slight undulose laminations of light brown to grey microbial clotted fabrics (grey arrow). Quartz grains are reasonably well sorted and show a rounded to sub rounded texture. (B) The sample shows one example of an ostracod oriented with laminations (red arrow), but otherwise is barren of skeletal grains. Brown arrow shows sub rounded quartz grains, microbial laminations are also present (grey arrow) (C).This sample is dominated by bedding parallel laminations of quartz grains (brown arrow), these alternate with thin flat-to undulose brown carbonate mud matrix (white arrow). The quartz grains are moderately sorted and show a well-rounded to sub-rounded texture. The laminations of quartz show a slight normal grading with the thicker quartz bands being composed of coarser grains which normally grade upwards to finer material (green arrows point in the direction of fining).

3.6.3 MF3: Microbial Laminated Fenestral Bindstone

This facies outcrops over laterally continuous distances between 5-10 metres as a dark-grey to blue-grey laminated carbonate bindstone, beds of MF3 measure between 20-40 cm in thickness which are sandwiched primarily between evaporitic gypsum deposits, as well as wave-rippled sandstones and palaeosol s. The microfacies can be subdivided into 1) MF3a, characterised by a dominant laminoid fenestral (LF) fabric, LF-A (horizontally linked lateral fenestral fabrics), with some isolated areas of LF B-II (horizontal cavities with laminoid fabrics) consisting of elongate fenestrae and strings of regularly spaced birdseye-like voids between laminated, peloidal and oncoidal clotted fabrics. And: 2] MF3b, characterised by thinner, and more irregular fenestrae within laminated micrites, these often show an undulose habit. See Tebbutt et al., (1965) and Müller-Jungbluth & Toschek, (1969) for further information on laminoid fenestral fabrics.

MF3a - Fenestrae are arranged concordant to stratification, the dominant fabric consists of elongate fenestrae (Fig. 3.24A) which sit parallel to local contortions within the grain-supported sediment (LF-A), in places these fenestrae appear as strings or chains of regularly spaced birdseye-like voids (LF-BII) (Fig. 3.24A). Both of these void types appear morphologically related; the thickness of the voids are the same, they often occupy similar positions in sections (e.g. sit along the same laminations) and both are often encrusted (possibly scaffolded) by laminated, cyanobacterial and/or microbial structures (Fig. 3.24B,C). In places encrusting elements have been reasonably well preserved, with tube and chamber like structures observed (Fig. 3.24C,E), these encrusters are reminiscent of organisms such as Rothpletzella and Girvanella (Fig. 3.24E). The sedimentary framework of MF3 is dominated by oncoids and peloids (Fig 3.24D). Peloids occur as several to tens of micron sized mictite-grains that are often devoid of internal structures,

however, there are examples where tubular and rounded calcified tube-like structures are present (Fig. 3.24D). The porostromate features are more prominent in the larger (up to 300 μm in diametre) oncoids (Fig. 3.24D), which commonly display laminated features including similar tubular and rounded structures to those of the peloids. These grains are morphologically related (only differing in size), from herewith all of these grains are grouped as oncoids. The oncoids are often found in association with LF B-II fabrics and can be observed as internal sediments to the voids in places (Fig. 3.24C).

MF3b - Laminated (10–20 μm thick) undulose micrites (conspicuous as alternating lighter and darker laminae) with elongate fenestrae (Fig.3.24A,E) (these voids are both fewer and thinner than their MF3a counterparts). The micrite laminations commonly contain tube, chamber, sausage and bean shaped structures, often forming the lighter laminae. As in MF3a, these encrusting organisms resemble known encrusting forms like Rothpletzella (Fig. 3.24E).

Rounded lithic clasts (consisting of both carbonate and quartz grains) are found locally, these often exhibit thin (20–30 μm) micritic envelopes consisting of tubular structures, these are more commonly observed near to the boundary between the carbonates and the underlying clastic sediments; towards the top of these carbonate deposits, they are void of clastic grains. Evaporite pseudomorphs and casts are observed sporadically throughout these carbonates.

Interpretation

The sedimentary framework of this microfacies is dominantly micrite exhibiting pelloidal or oncoidal features (MF3a) with common evidence of laminar, encrusting modes of formation either within grains or, as laterally persistent laminations (MF3b). These grains are interpreted to be benthic peloids and oncoids, forming from similar mechanisms and processes (i.e. biochemical precipitation triggered by

microbial activity), but growing to various sizes. The encrusting nature of the laminar structures indicates that these are primary grains, rather than reworked components (MF3b, for example). The laterally continuous laminations of MF3b are interpreted to be algal and microbial mats, similar to those observed in modern day Abu Dhabi (Court et al., 2017). Undulations observed for these laminated components appear to be primary; there are no microstructures present to indicate secondary compression and the orientation of individual laminations can be seen to be columnar, bulbous and wavy in places (Fig.3.24B).

Fenestrae in this microfacies are interpreted as primary cavity networks. Sediments within cavities indicate that the cavities were part of a network through which currents were flowing at the time of primary deposition. The elongate voids common to MF3a are often sheathed in microbial structures, these are related to the primary construction of these voids, the chain-like cavities often display the same sheath like envelope, these encrusting features then join together from the base and roof of the voids forming column like structures; this results in their appearance as rows of spaced birdseye-like voids. Encrusting forms such as Rothpletzella and Girvanella have been observed to act as constructors of cavities in other microbially dominated carbonates (Rogers, 2018). Laminations and laminoid fenestrae indicate shallow/sub-aerial exposure, these features are often used as indicators of sea-level, however Bain & Kindler (1994) demonstrated that fenestrae should only be associated with sea-level where other features associated with inter- or peritidal characteristics exist. Here no further evidence for tidal influence is found, potentially indicating that the depositional environment was above sea-level. Birdseye cavities also generally occur in shallow (intertidal) marine, lacustrine and even in eolianite environments where rainwater induces cavities (Bain & Kindler, 1994). Shinn (1968) reported that birdseye structures never form in the subtidal zone. It is interpreted that this microfacies was deposited in extremely shallow

water that often experienced a certain amount of subaerial exposure. The cavities may have formed as desiccation related structures which were subsequently colonised by encrusting cyanobacteria, resulting in their preservation. The lack of skeletal metazoan grains suggests restricted depositional environmental conditions that were inadequate for other biota.

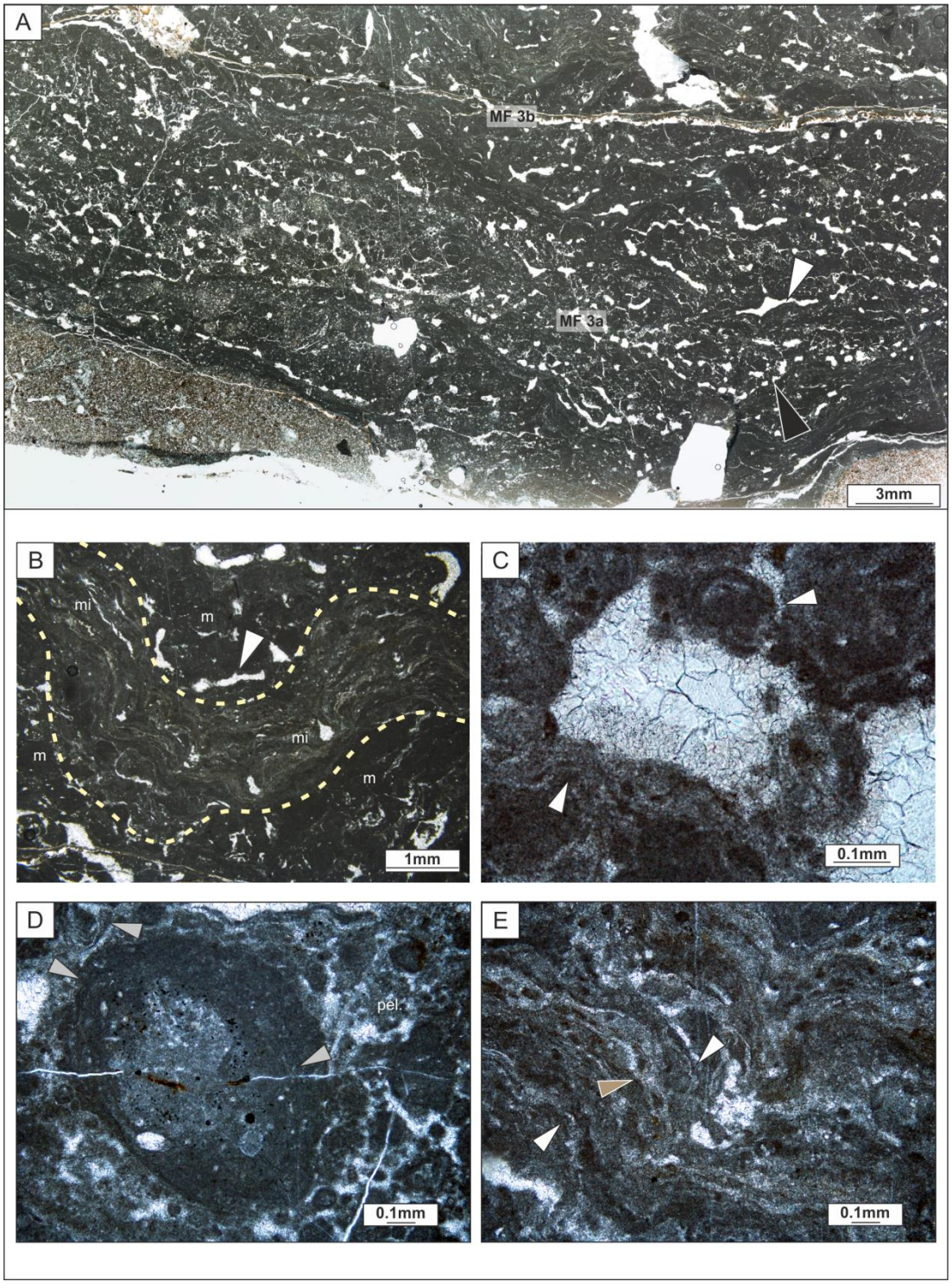

Figure 3.24 Photomicrographs of MF3. (A) image showing the multiple alternating undulose microbial bands and the change between the peloid and oncoid dominated MF3a in the middle of the figure and highly laminated MF3b. An example of an elongate fenestrae (typical of MF3a) is highlighted with a white arrow, an example of a chain-like fenestrae (also typical of MF3a) is highlighted with a black arrow (B) MF3b is highlighted (outlined by dashed lines and highlighted by 'mi'.) The sub-microfacies exhibits an undulose habit and lacks elongate fenestrae observed in MF3a. The homogenous matrix of MF3a is highlighted by 'm' an elongate fenestrae (typical of MF3a) is highlighted with a white arrow(C) A typical cavity showing late blocky calcite cement fill, with a possible fibrous isopachous rim. The cavity is framed by protostromate structures. The white arrows highlight tube like structures reminiscent of Girvanella (D) A typical oncoid found within MF3, the clast is surrounded by a matrix of peloids (pel.) which often show a clotted or thrombolytic texture. The cortex of the oncoid, and several of the peloids exhibit well preserved protostromate features (arrows), these are mostly tube like and as with the previous examples, resemble Girvanella.(E) Undulous laminations of MF3b the white arrows highlight tube like structures whilst the middle (brown) arrow highlights an encrusting form consisting of a chain of sausage or bean shaped chambers, this encruster is reminiscent of the calci-microbe Rothpletzella.

3.6.4 MF4: Rounded Mudclast Wackestone

MF4 outcrops as laterally continuous dark grey to blue mudstone to wackestone (Fig. 3.21). The matrix of this microfacies shows a dark brown carbonate muds matrix with rounded intraclasts of slightly lighter microspar mudstone dispersed throughout (Fig. 3.25). MF4 contains very few occurrences of bioclasts with minor appearances of ostracods (Fig. 3.25C). Isolated quartz grains are sporadically distributed. The matrix is generally homogeneous although evidence of poorly defined clotted textures have been observed (Fig. 3.25C). The mud clasts are commonly ~1 mm with fewer larger examples (up to 3 mm) present. The clasts account for up to 40% of the microfacies. The surfaces of these clasts are often the nucleation point for stylolites found throughout this microfacies, with some clasts surrounded by the compressional fractures (Fig. 3.25A). The stylolites are typically oriented parallel to bedding and occur sporadically spaced throughout the samples. Ostracods are irregularly distributed throughout the samples, although rare, they are more abundant than in MF2.

Interpretation

The rounded mud clasts within this microfacies have similar features (laminated micrites, ptotostromate features) as some of the other microfacies described here

(particularly MF3 and MF4), it is suggested that these clasts were likely reworked from partially lithified sediments from the proximal sedimentary environment. The reworking of this deposited material was coeval with the deposition of this sediment. The mudstone clasts composed of microspar grains may indicate reworking of a feature where carbonate sands may be present. The rounding of the clasts indicates transportation of the grains. The lack of lamination within the sediment and absence of cavities suggests that the deposition of this microfacies occurred in water that was deeper than that of the previously described microfacies (MF1, 2 and 3). The lack of laminar cavities is interpreted to indicate a lack of primary microbial mats and puckering/desiccation associated with sub-aerial exposure. The lack of Birds-eye cavities suggests that the microfacies was deposited sub-tidally. Ostracod occurrences, although in low numbers, are more frequent than the previously described microfacies (ostracods were absent from MF1 & 3). This may indicate a slightly less restricted or isolated depositional environment than those interpreted for MF 1, 2 and 3. Stylolites within this microfacies are not associated with primary tectonism, they are not regularly spaced and are oriented parallel to bedding, indicating they formed due to loading due to an applied sedimentary load and burial.

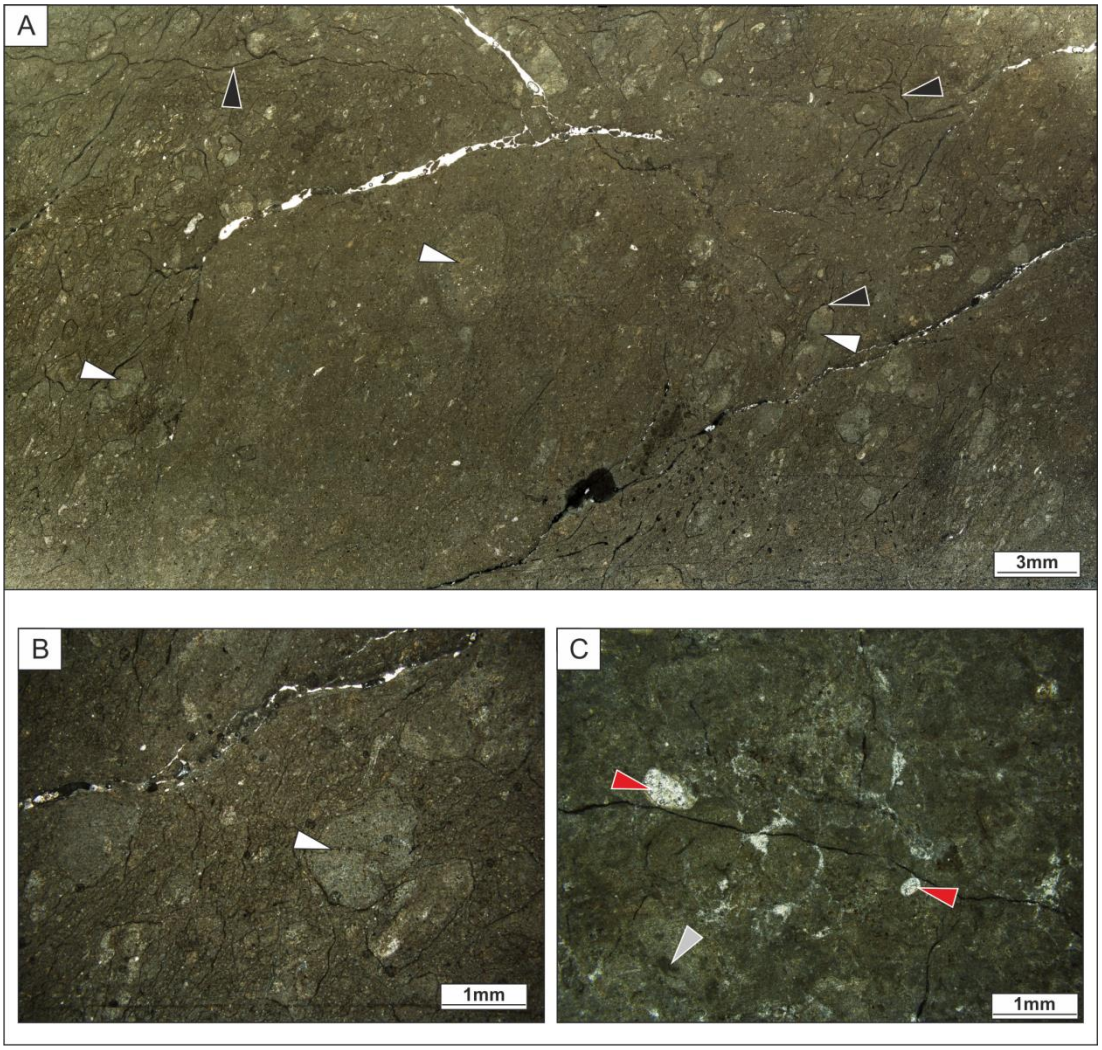

Figure 3.25(A) Photomicrograph of MF 4. This sample is characterised by a dominant background matrix of massive dark brown carbonate mudstone with a few mud grains, often lighter in colour (white arrow). Compressional fractures (stylolites) are also present (black arrow). (B) This sample shows the dominant dark brown carbonate mud matrix with few mud grains (arrowed). (C) This sample shows a homogenous matrix of brown carbonate mud with minimal skeletal ostracod grains (red arrow) between 30–70μm. Isolated clotted microbial textures are also present (grey arrow).

3.6.5 MF5: Laminated Bioclastic-Ostracod-Carbonate Wackestone

This facies outcrops as laterally continuous dark grey to blue coloured, fine grained carbonate mudstone to wackestone (Fig. 3.21E). The microfacies is characterised by a brown, laminated carbonate mud with a clotted textured matrix, interspersed laminations of microspar and some peloidal and clotted areas with a lighter grey/green thrombolytic textures. The thrombolytic textures often consist of clumped and tangles protostromate features, laminations or envelopes of micrite are often associated with this tube-like structures. The clumped features are arrayed

in a style reminiscent of thrombolytic growth forms. The bioclasts are dominantly composed of ostracod carapaces alongside some larger isolated shell-like fragments (Fig. 3.26A). Complete ostracods are mostly aligned with bedding and are between 30–60 μm in length. Ostracod tests appear white and the broken skeletal grains show a dominant convex upwards arrangement along a bedding horizontal plane (Fig. 3.26C). Isolated fenestral cavities are present, particularly within the more micritic layers; several stromatictis-like cavities were observed (Fig. 3.26B,E), exhibiting flat, sediment filled bases with an undulous cavity roof, a thin isopachous cement rim, with later blocky calcite cement fill (Fig. 3.26E). There is some evidence of 'wavy' laminations (Fig. 3.26D), however, this is much less frequent than in MF3. The microfacies is largely devoid of clastic grains, with minimal occurrences of isolated quartz grains.

Interpretation

The sedimentary framework of this microfacies is dominantly micrite with few microbially encrusted laminations or cavities present. The microfacies is similar to MF4. Relatively abundant ostracods are present indicating a less restricted environment than the previously described microfacies, indicating deeper water depths and/or better connected (less restricted) water bodies. Cavities are interpreted to be the result of gas bubbles (or have a biological origin) rather than desiccation (and subsequent encrusting biota construction) related, this may explain why they are less frequent than in MF3. The presence of stromatactis-like cavities is not indicative of any one setting as the formation mechanism of the cavities is still somewhat enigmatic (Monty, 1995; Aubrecht et al., 2002; Hladil, 2005). Two main hypotheses exists suggesting either a purely biological origin (Tsien, 1985; Flajs & Hüssner, 1993) caused by the collapse (Bourque & Gignac, 1983) or syndiagentic shrinkage of sponge bodies (Delecat & Reitner, 2005) with the coexistence of

stromatactis in sediments with bioclastic sand, large oncoids, and calcareous algae indicative of shallow-marine environments (Stenzel and James 1995). Or a physical origin (e.g. Wallace, 1987; Kukal, 1971) for stromatactis cavities, due to filling of cavity systems with cement and sediment (Bathurst, 1980) or formation during turbulent deposition and separation of unsorted clastic material within dispersed suspension clouds (Hladil, 2005, Hladil et al., 2007, 2006). However, the presence of stromatactis-like cavities does indicate that the depositional environment was quiet and sub-aqueous.

The low diversity, but high productivity of the microfacies suggests a restricted environment, and given the known setting of these deposits, it is likely that salinity played a restrictive role. This would make the formation mechanism of these stromatactis-like cavities by sponges seem unlikely, due to high salinity, restricted environments and lack of any evidence of remains. The laminated nature of the microfacies indicates suspension settling, often ostracods are disarticulated along bedding planes, which could indicate periodic reworking and detrital input into standing bodies of water during higher energy events, creating turbulent conditions and subsequent settlement, resulting in bedding plane parallel ostracods and turbulent flow generated stromatactis-like cavities (cf. Hladil, 2005, Hladil et al., 2006, 2007).

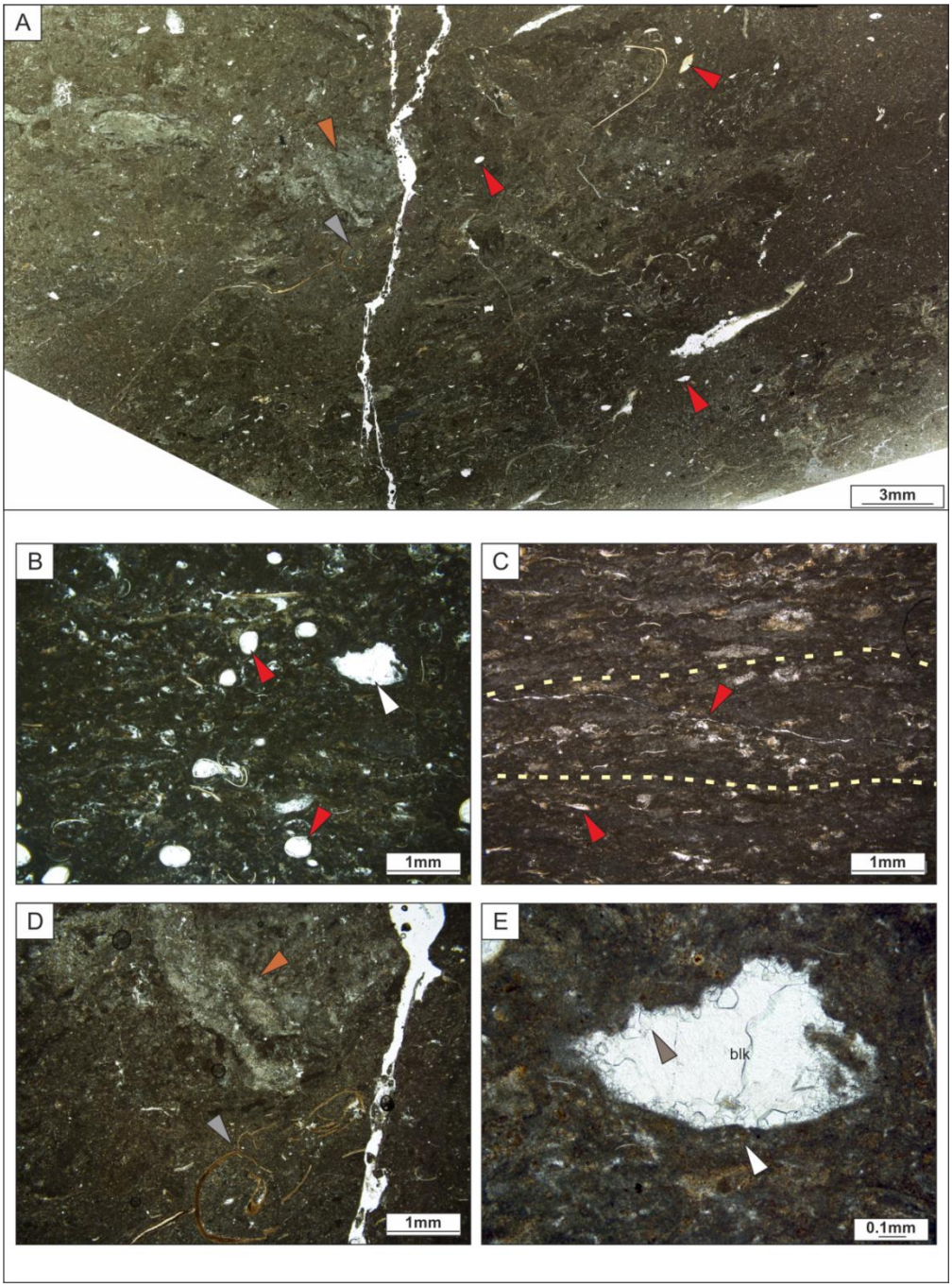

Figure 3.26 (A) Photomicrograph of MF5 showing the abundance of ostracods (red arrow) and occasional shell fragments (grey arrow), light clasts are shown by the orange arrow. (B) This sample contains abundant skeletal grains of both complete and broken ostracods (red arrow) and potential stomatactis-like cavities (white arrow) (C) The crudely laminated carbonate mud matrix interspersed with clasts of a lighter grey/green carbonate mud. Red arrow shows several complete ostracods (30–70μm) arranged in a bedding parallel fashion, the broken skeletal grains show a dominant convex upwards arrangement along a horizontal plane (Yellow) (D) The lighter clasts highlighted in (C) are shown in more detail here (orange arrow). These clasts show evidence of laminations and of a clotted (sometimes thrombolytic) texture, the example highlighted here is reminiscent of the undulous microbially dominated fabric observed in MF3b. shell fragment is highlighted by grey arrow (E) A stromatactis-like cavity, the flat base and undulous roof is apparent, as is the sediment fill at the base of the cavity (red arrow). Late blocky calcite cement fills the cavities interior, (blk.) whilst a rim of smaller calcite cement lines the cavity. It is this rimming cement that

distinguishes these cavities from 'true' stromatactis, voids, which bare isopachous, fibrous rims.

3.6.6 MF6: Microcrystalline Quartz

This facies outcrops as either isolated nodular bands of dark red chert or nodules. Samples are dominantly composed of microcrystalline quartz and show a variety of habits composed of microflamboyant quartz (cf. Milliken, 1979), random fibrous granular microcrystalline quartz (Fig. 3.27A), rimmed, radial, and undulose megaquartz (Fig. 3.27B). Evaporite inclusions are often present (Fig. 3.27C), frequently showing evidence for the displacement of the original carbonate material (Fig. 3.27D) in association with filled fractures of fibrous microquartz (Fig. 3.27C).

Interpretation

MF6 indicates the replacement of carbonate and evaporitic minerals by silica, most likely as a product of burial diagenesis (Scholle & Ulmer-Scholle, 2003). These features are commonly associated with silica fabrics in chert nodules, which have replaced evaporite minerals (Milliken, 1979: Hesse, 1989). MF6 is a post-depositional process, therefore it offers little help in determining the depositional story of the formation unlike the previously described microfacies (MF1-MF5).

Sulphate or chlorides are the most probable minerals to have been replaced, as these occur as either cements, displacive/replacive nodules, or as interbedded strata in carbonate rocks. Whether these minerals relate directly to the precipitation and deposition of primary evaporites from concentration of saline waters, or relate to the migration of evaporitic brines into underlying or adjacent stratigraphic units as displacive/replacive nodules, unrelated to evaporitic conditions, is unknown (Scholle & Ulmer-Scholle, 2003). Even after deposition and substantial burial, evaporite minerals can be remobilised and precipitated in distant, stratigraphically unrelated units (Scholle & Ulmer-Scholle, 2003).

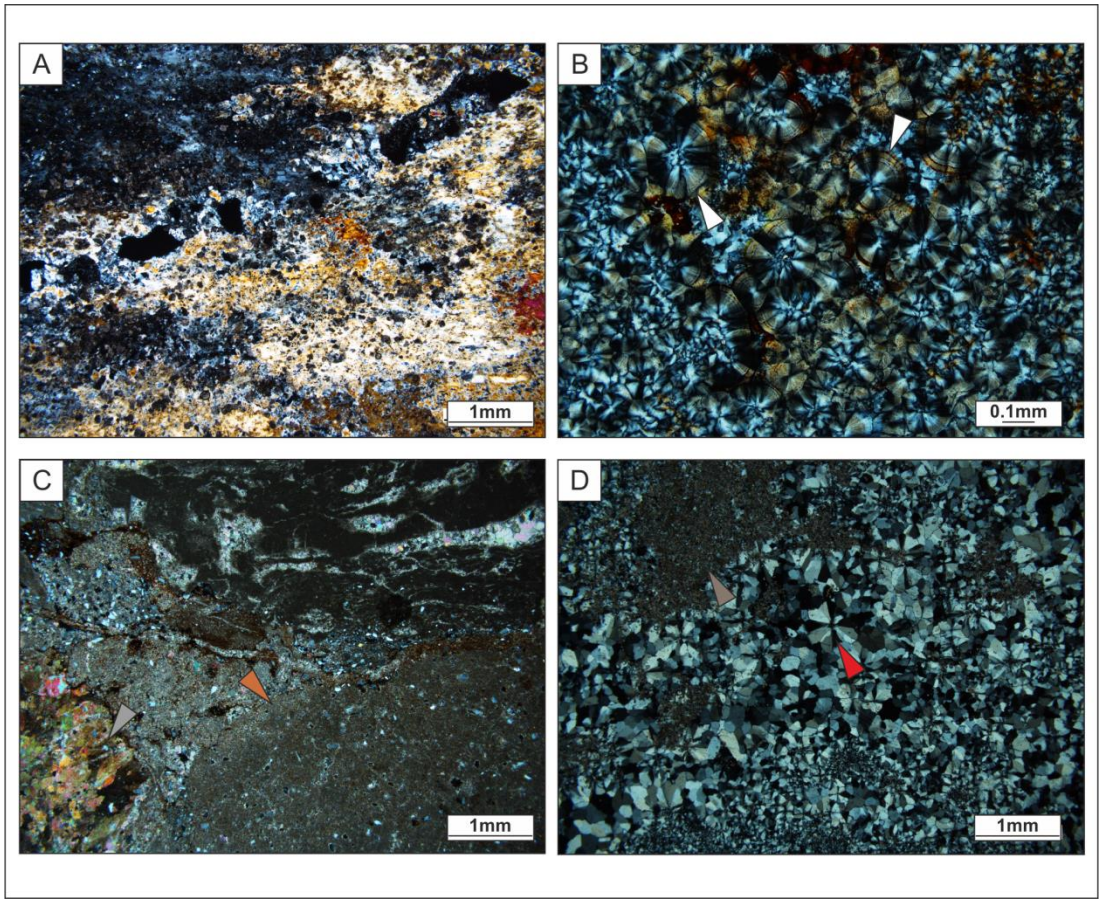

Figure 3.27 Photomicrograph of MF6 (A) High inference colours and fibrous nature under xpl. (B) Rimmed and radial nature of quartz crystals (arrowed) (C) Evaporitic inclusions (brown arrow) and displacement of original carbonate material (orange arrow), filled fractures of fibrous microquartz also present (arrow) (D) Radial megaquartz (red arrow) displaced primary carbonate (brown arrow)

3.6.7 Carbonate Depositional Environments

Microfacies analysis indicates five distinct primary depositional facies (MF1-MF5) and one microfacies resultant from secondary silicification (MF6). The depositional environment interpreted for MF1-MF5 are summarised in Table 3.3. The primary microfacies all indicate deposition within a shallow aqueous to sub-aerial and restricted environment where carbonate production was generally low. All the microfacies have a carbonate mud matrix, with evidence of microbial features common where detrital input is absent. MF1 and MF2 both have high clastic contents, whereas the rest of the microfacies are largely barren of detrital clastic grains. MF2 has isolated laminations of clastic material compared to the more uniform clastic distribution seen in MF1. Both MF1 and 2 are interpreted to be

associated with aeolian interdunes; MF1 is interpreted to belong to isolated deposits between dunes, whereas MF2 is placed in a similar environment, but one which is occasionally less restricted (e.g. the interdunes may be linked by fluvial systems during more humid periods). MF3 shows abundant evidence of shallow, restricted deposition. Undulous laminations associated with laminoid fenestrae are common and microbial mediation of micrite can be interpreted. MF3 is therefore interpreted to belong to a shoreline continental playa-lake sabkha environment. Bioclasts and ostracods are abundant only in MF5 with rare or sporadic occurrences within MF2 and MF4. The microfacies are laminated to varying degrees, except MF4; which has clear evidence of reworking of grains. MF4 and 5 are both interpreted to belong to a desert lacustrine system.

Table 3.3 Summary table detailing each microfacies and classification, as well as the environmental indicators present and the proposed depositional environment within the Cedar Mesa Sandstone Formation.

Microfacies	Classification	Environmental Indicators	Depositional Environment Within the Cedar Mesa Sandstone Formation
MF1	Clastic Influences Carbonate Wackestone	High detrital clastic content, carbonate mudstone matrix, occasional laminations. Clastic grains are well rounded and sorted. Limited lateral extent (<1m)	Isolated Aeolian Interdune
MF2	Laminated Carbonate Wackestone/Packstone	Carbonate mudstone matrix. Alternating laminations of clastic grains and clotted microbial textures. Clastic grains are normally graded, sub rounded and moderately sorted. Rare ostracods. Limited lateral extent (~2m)	Aeolian Interdune with occasional connectivity to wider environments

MF3 (subdivided into 3a and 3b)	Microbial Laminated Fenestral Bindstone	Laminated carbonate mudstone. Laminoid fenestrae, oncoidal and thrombolitic textures, protostromate features. **3a**, characterised by a dominant laminoid fenestral fabric consisting of elongate fenestrae and strings of regularly spaced birdseye-like voids between laminated, oncoidal and clotted micrite fabrics. **3b**, characterised by thinner, and more irregular fenestrae within laminated micrites, often with undulose habits. Laterally continuous.	Continental playa lake-Sabkha
MF4	Carbonate Mudstone, reworked grainstone	Carbonate mudstone matrix with rounded clasts of slightly coarser mudstones dispersed throughout. Very few occurrences of ostracods and rare isolated quartz grains. Laterally continuous	Desert Lacustrine System
MF5	Laminated Bioclastic-Ostracod-Carbonate Wackestone	Laminated carbonate mud forming a clotted textured matrix. Interspersed laminations of microspar and microbial thrombolitic textures. Frequent bioclasts dominantly comprised of ostracod carapaces alongside some larger isolated shell-like fragments. Laterally continuous	Desert Lacustrine System
MF6	Microcrystalline quartz	Chert	Diagenetic Alteration

3.7 Lithofacies Associations of the Cedar Mesa Sandstone Formation

Several of the previously-described facies share common relationships. This section integrates the facies observations described above and groups these into eleven facies associations. On the basis of broad-scale depositional environment (aeolian, fluvial, lacustrine and sabkha) and is summarised in figure 3.28.

Code	Log	Facies	Description	Code	Log	Facies	Description	Code	Log	Facies	Description
AD	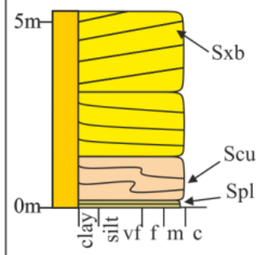	Spl, Sxb, Stxb, Scu	Laterally extensive (10s of metres) tabular bodies with planar bounding surfaces. Thin basal units of Spl and/or Sxc grade into either Stxb or Sxb arranged into sets (0.2-1 m) and cosets (5-10 m thick).	WI	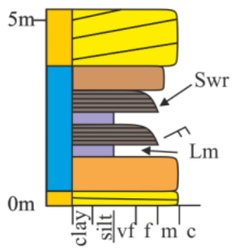	Lsm, Lm Swr	Isolated lenses which pinch out over small distances (< 5 m). Planar basal bounding surfaces with convex upper bounding surfaces. Deposits comprise of thin (20-40 cm) carbonate deposits (Lm, Lsm) interbedded with thin (< 50 cm)wave-ripple sandstone (Swr). Root traces, bioturbation and mottling are frequent throughout the sequence.	SA	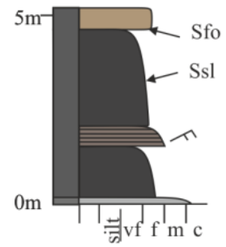	Ssl, Swr. Sfo	Laterally extensive (10s of metres) units with planar bounding surfaces. Units comprise thick (up to 10 m) deposits of fining-upwards silts (ssl), which lack internal structures, interbedded sporadically with wave-ripple sandstone (swr) the association is commonly topped by palaeosols (Sfo)
SS	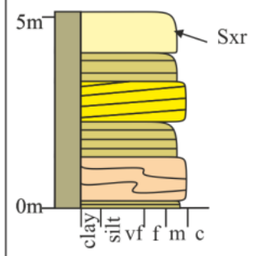	Spl, Sxr Sxb Scu	Laterally extensive (10s of metres) tabular bodies with planar bounding surfaces. Unit thickness between 1-2 m comprised of wind-ripple sand with minor components of aeolian dunes (Sxb) or convoluted sandstone (Scu)	FC	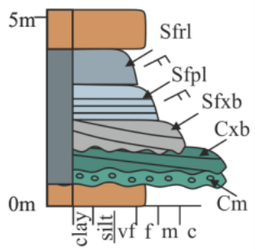	Cm, Cxb, Sfxb, Sfpl, Sfrl	Laterally extensive (10 s of metres) units with distinctive concave-up erosional basal bounding surfaces and sub-planar to- planar upper bounding surfaces. Basal units comprise conglomeratic and cross bedded gravels (Cm, Cxb) which fine-up in sequence into cross-bedded sandstones (Sfxb), planar (Sfpl) and ripple-laminated sands (Sfrl). Unit is typically less than 5 m in stratigraphic thickness and often lacks the full sequence	PS	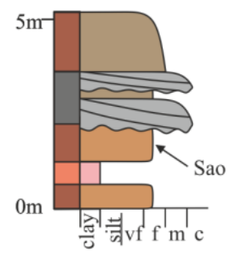	Sfo, Sao	Laterally extensive (10s of metres) units with planar upper and lower bounding surfaces. Deposits comprise of either horizontally-laminated (Sao) or calcrete-rich (sfo) pedogenic facies. Mottling and root traces common throughout, gypsum nodules and veins common within Sfo.
ID	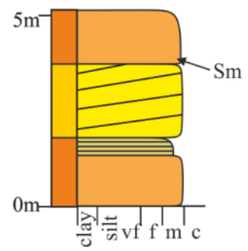	Sm, Spl	Laterally limited (<1.5 m) tabular bodies with flat lying bounding surfaces. Unit range between 1-5 m in stratigraphic thickness comprised primarily of massive and featureless sandstone (Sm) with occasional wind ripple strata (Spl)	UF	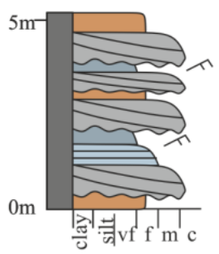	Sfxb, Sfpl, Sfrl	Laterally extensive (10 s of metres) units with distinctive erosional basal bounding surfaces and planar upper bounding surfaces. Unit is primarily composed of cross-bedded sandstone (Sfxb) overlain sporadically with either laminated or ripple- laminated sandstone. Stratigraphic thicknesses range from 0.2-1.5 m, deposits of Sfxb often thin and branch laterally.	SK	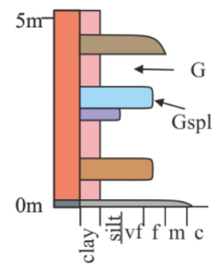	G, Gspl, Sao, Sfo, Lm	Laterally extensive (10s of metres) units between 0.2- 10m stratigraphic thickness with planar upper and lower bounding surfaces. Comprised primarily of gypsum deposits sporadically interbedded with gypsum sandstone (Gspl), palaeosols (Sao, Sfo) and carbonates (Lm). Gypsum nodules and veins common throughout associated clastic deposits.
DI	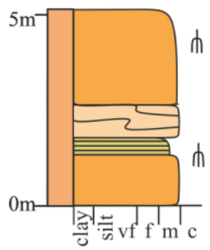	Sm, Spl, Scu	Laterally limited (<5 m) tabular bodies with concave-to planar bounding surfaces. Units range between 1-5 m in stratigraphic thickness and comprise massive sandstones (Sm) with occasion convoluted sandstones (Scu) and wind-ripple sandstone (Spl). Root traces are common throughout the massive sandstone deposits.	PA	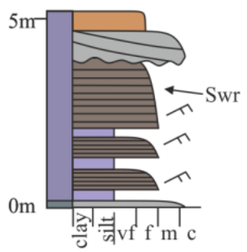	Lsm, Lm, Swr	Laterally extensive (10 s of metres) units comprising thin (0.2-0.5 m) carbonates (Lm, Lsm) and wave-ripple sandstone (up to 10 m in stratigraphic thickness). Root traces and bioturbation common throughout		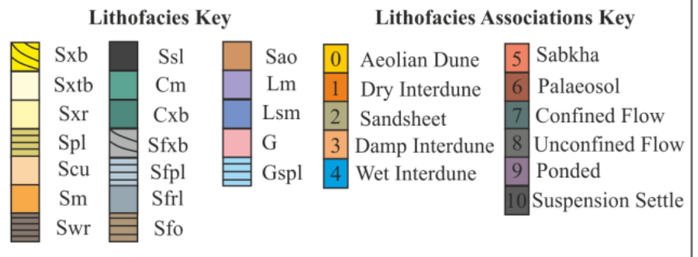		

Figure 3.28 Summary figure showing sedimentary associations and realated facies

3.7.1 Compound Aeolian Dune Association (AD)

Basal beds of this association are typically characterised by occurrences of pin-stripe laminated sandstone (Spl), no more than 20 cm thick, that are overlain by cross-bedded sandstones (Sxb) displaying foreset grainflows up to 3 cm thick, each draped with millimetre-scale grainfall laminae. Sporadically, foresets of basal sets are gypsiferous, with gypsum following the foreset surfaces (Fig. 3.3C). The cross-bedded sandstones are arranged into sets 0.2–1 m thick that climb subcritically and are bound dominantly by planar surfaces. The sets are stacked into cosets, typically 5 m thick, but sporadically reaching up to 10 m. Typically, the toesets of cross-bedded units grade into translatent wind-ripple-laminated sandstone (Sxr) along the foreset-bounding surfaces. Sets of cross-bedded sandstone are sporadically overlain by, or replaced by, sets of similar sized trough-cross-bedded sandstone (Stxb) that climb sub-critically. The set-bounding surfaces are typically slightly curvi-planar and concave upwards on the metre to decametre scale. Convolute bedded sandstone facies (Scu) are present sporadically at the base of the association and typically grade into, or modify, pin-stripe laminated sandstone, cross-bedded sandstone or trough-cross-bedded sandstone facies.

This association is interpreted as the deposits of migrating compound aeolian dunes. Cross-bedded sandstones displaying foresets of grainfall and flow indicate reasonably well-developed dune-forms with lee-slope slip-faces close to, or at, the angle of repose (Hunter, 1977; Kocurek, 1981, 1991, 1996; Mountney, 2006; Langford & Chan, 1989). Preservation of pinstripe lamination suggests well-developed dune plinths in front of the dune lee slopes from which ripples migrated up the toe of the lee slope to preserve translatent wind-ripple-laminated sandstone in a strong relationship with the toesets of cross strata. Dunes were dominantly straight-crested transverse forms, preserving planar cross-bedded sets with straight

bounding surfaces. Occasionally, sinuous-crested transverse forms developed, or straight-crested forms evolved into sinuous-crested bedforms, under localised conditions of increased sediment supply. Convolute bedded sandstone facies, typically preserved near the base of the association, indicates dunes migrated in the presence of a water table close to, or at the surface. Loading of water-saturated sediment as the dune advanced resulted in soft-sediment deformation of the dune plinth (McKee et al., 1971; Mountney & Thompson, 2002; Doe & Dott, 1980; Horowitz, 1982). The presence of gypsum along basal foresets (Sxb), indicates solute-rich water was drawn up preferential flow pathways in the sediments of the advancing dune as a result of capillary action (Banham & Mountney, 2013).

3.7.2 Aeolian Sandsheet (SS)

Most of the association is characterised by pin-stripe laminated sandstone (Spl), which typically grades upwards into translatent wind-ripple-laminated sandstone (Sxr), and sporadically into crudely developed cross-bedded sandstone (Sxb). This association is bound by laterally-continuous, planar bounding surfaces and forms units 1–2 m thick. Sporadically, convolute bedded sandstone facies (Scu) are present at the base of the association typically grading with, or modifying, pin-stripe laminated sandstone.

A lack of well-developed cross strata and combined with abundant pin-stripe and translatent wind-ripple-laminations suggests aeolian sandsheets formed under conditions of low sediment supply. Convolute bedding indicates a water table close to the surface, with deformation resulting from water table fluctuations and loading of the sandsheet by the following dune deposits (McKee et al., 1971). Wind-ripple-lamination and crude cross-bedding show some bedform development, but sediment supply was insufficient for full-scale dune development (Biswas, 2005; Kocurek & Nielson, 1986).

3.7.3 Dry Interdune (ID)

Associations of this type comprise almost exclusively structureless sandstone (Sm) with occasional beds of intercalated pin-stripe laminated sandstone (Spl). The association is of limited thicknesses (<1.5 m) and is bound by flat-lying upper and basal bounding surfaces.

Sediments of aeolian grain size and texture, deposited with a mostly structureless appearance, are interpreted as dry interdunes formed in settings where the water table lay significantly below the depositional surface and had negligible influence on the depositional processes. The structureless appearance resulted from translatent strata with limited grainsize variations which consequently did not form defined surfaces (Kocurek, 1981).

3.7.4 Damp Interdune (DI)

Associations of this type are often limited in their lateral extend and pinch out. The base of the association is characterised by slightly concave basal bounding surfaces, whilst the association comprises structureless sandstone (Sm) which is commonly overlain by pin-striped laminated strata (Spl). Some occurrences display sporadic convolute bedded sandstone (Scu) at their bases, and sporadic rhizolith development throughout.

Associations of this type containing facies indicative of wind-blown processes under conditions of low sediment supply (Spl), and evidence of subaqueous deposition (Sm) are interpreted as the deposits of damp interdunes, in which either flooding or a rise of the water table leads to direct contact of water with the depositional surface (Mountney 2006). Periodic influxes of water support plant life (Mountney & Jagger, 2004; Loope, 1984, 1988), whilst convolute bedding structures develop as subsequent dunes migrate over a water-laden substrate (Collinson, 1994). The isolated nature of the deposits and the shape of the basal bounding surfaces suggest

isolated, lensoid shaped interdunal areas probably associated with sinuous-crested dune-forms.

3.7.5 Wet Interdune (WI)

Associations of this type occur in isolated lenses bound basally by planar surfaces. In well exposed examples upper bounding surfaces are slightly convex up. The basal surfaces are typically overlain by 0.4–0.6 m beds of arenaceous-rich carbonates (Lsm), or fine-grained carbonates (Lm), which under thin section are representative of MF1 and MF2. These carbonates are typically overlain by wave-rippled-laminated sandstone (Swr) deposited in beds less than 0.5 m thick with a planar to undulose laminated appearance. Rhizoliths, bioturbation and mottling are frequently present throughout this association.

This association is interpreted as deposits of a wet interdune. Carbonate deposits have accumulated in long-lived shallow ponds of standing water above the depositional surface, close to an aeolian dune field (Langford & Chan, 1989; Loope 1981, 1984). Wave ripples form from wind shear over shallow water (Martell & Gibling, 1991). The isolated nature of the deposits signifies laterally restricted interdunes developing in an enclosed or semi-enclosed setting, either as a result of floodwaters trapped between surrounding sinuous-crested dunes or by rise in the water-table in topographical depressions (Loope, 1984; Mountney & Jagger, 2004; Purvis 1991).

3.7.6 Confined Flow Association (FC)

Associations of this type are characterised by concave-up, erosive basal bounding surfaces, overlain by intraformational conglomerates (Cm), and planar cross-bedded gravels (Cxb). Cross-bedding is poorly developed, with coarser gravel lining foresets. These facies are overlain by planar cross-bedded, moderately sorted sandstones that are massive to sporadically crudely cross-bedded (Sfxb), in sets no thicker than

0.5 m. The association fines upward into planar laminated sandstone (Sfpl), which is topped by climbing-ripple-laminated sandstone (Sfrl) below a planar to sub-planar upper bounding surface.

Associations with a characteristic concave-up erosive basal bounding surface and a fining upward fill are interpreted as the deposits of fluvial channels. Conglomeratic basal units with clasts lining crude foreset development represent channel lag deposits formed from bedload transport within high energy flows concentrated along the channel thalweg (Miall, 1985). Crudely developed cross-bedding with pebble lined foresets indicates supressed bedform development and migration due to the large grainsize of the bedload, within a high sediment load system (Bridge & Best, 1988; Todd, 1996). Sets of planar cross-bedded sandstone represent the migration of straight-crested dunes and dune trains along the base of a channel in times of lower sediment load and reduced grainsize (Miall, 1985). Planar-laminated sandstone followed by climbing-ripple laminated sandstones suggests rapid waning of flow and bedform aggradation.

3.7.7 Unconfined Flow Association (UF)

This association is characterised by a laterally extensive erosional base overlain by low-angle cross-bedded sandstone (Sfxb) with foresets in multiple directions arranged into sets with curved bounding surfaces. Set thicknesses range from 0.02–0.15 m within cosets of approximately 0.2–0.3 m. Cross-bedded sandstones are overlain by horizontally laminated sandstones (Sfpl), which are sporadically overlain by climbing-ripple laminated sandstone (Sfrl). The association is bound by a planar upper bounding surface and is often laterally extensive. In some occurrences, planar cross-bedded sandstones branch into composite thinner units, which maintain the same internal sedimentary structures.

The flat erosional base of this association represents a characteristic non-channelised flow incorporating either splay or sheetflood type architectures (Tunbridge, 1981; Sneh, 1983; Stear, 1985). Dominance of low-angle cross-bedding and planar-laminated sand indicates a transition from lower flow regime into upper flow regime as a result of a rapid reduction in depth associated with an ephemeral, sand-rich sheet flood, (Miall 1985). Facies that stack in a vertical section with dominant upper flow regime structures and fining upwards trends, suggest deposition within a high velocity flow that waned quickly, and thin units that split and branch represent the margins of individual sheet floods (Miall, 1996).

3.7.8 Ponded Water Association (PA)

Basal beds of this association typically comprise arenaceous-rich (Lsm) or fine-grained carbonate (Lm) facies, which under thin section are representative of MF4 and MF5. Wave-ripple laminated sandstone (Swr), when present, dominates the association forming thick units (up to 10 m) intercalated with thin beds (rarely great than 0.5 m) of arenaceous-rich carbonate, fine-grained carbonate or carbonate mudstone. Rhizoliths and bioturbation occur sporadically within the wave-rippled sandstone and fine-grained carbonate facies, however the carbonate facies are almost devoid of fossils, with only sporadic ostracod preservation. Both the top and bottom bounding surfaces of the association are planar and typically gradational with Unconfined Flow (UF), Suspension Settle (SA) or Palaeosol associations (PS).

A dominance of wave-ripple sandstone and fine-grained carbonates suggest a shallow ponded water setting. Wave-ripples have been generated by wind shear across the water surface (Martell & Gibling, 1991), whilst fine-grained carbonate facies suggest variations in clastic content and prolonged conditions of low energy standing water (Tucker, 1978; Platt & Wright, 1991). The development of rhizoliths indicates surface stabilisation around edges of these long-standing quiet waters

(Owen et al., 2008; Platt & Wright, 1991). Low diversity of fossil species within the carbonates suggests a high salinity or restricted environment (Flügel, 2004).

3.7.9 Suspension Settle Association (SA)

Associations of this type have planar, laterally extensive basal bounding surfaces that are overlain by a progressively fining upwards organic-rich siltstone (Ssl) intercalated sporadically with wave-ripple sandstone (Swr). The association is commonly topped by horizontally laminated pedogenic facies (Sfo) below a planar top bounding surface. The upper and lower contacts of the association are typically gradational with Ponded (PA) or Palaeosol (PS) associations.

Fine-grained deposits that lack internal sedimentary structures indicate deposition in lakes that were perennial and of greater extent than the deposits of the association Ponded Water Association (PA), in which suspension settling of sediment dominates deposition (Tanner & Lucas, 2007; Fielding, 1984). Occasional evidence for high organic content within the siltstone (Ssl) could indicate depths sufficient to cause thermal stratification (Boehrer & Schultze, 2008). Intermittent intercalation with wave-ripples (Swr) shows a shallowing of the water level, potentially caused by climate fluctuations, and an increasing influence from wind shear (Martell & Gibling, 1991). The occurrence of horizontally laminated pedogenic facies suggests stabilisation around the margins of a long-standing body of water (Eberth & Miall, 1991).

3.7.10 Palaeosol Association (PS)

This association is typically laterally extensive with planar upper and lower bounding surfaces and comprises calcrete-rich pedogenic (Sao) and horizontally laminated pedogenic facies (Sfo). Fining upwards, massive calcrete-rich pedogenic facies (Sao) forms the most common component of the association, frequently related to modification of aeolian and sabkha associations (AD, SS, DI, WI, SK). The

horizontally laminated pedogenic facies (Sfo) forms minor components occasionally interbedded with the calcrete facies (Sao) and is primarily associated with the modification of fluvial (UF, FC) and lacustrine associations (PA, SA). The association has a distinctive rooted and mottled appearance, with the calcrete-rich pedogenic facies (Sao) typically displaying nodules and veins of gypsum and calcrete. Calcrete is absent from the horizontally laminated pedogenic facies (Sfo) with only infrequent gypsum nodules and veins.

The pedogenic features shown within the association suggest periods of surface stabilisation and soil development, with sufficient moisture for plant colonisation. The presence of gypsum and replacement of roots within the calcrete-rich facies (Sao) supports an arid to semi-arid climate (e.g. Cecil 1990; Retallack, 1994; Kraus, 1999), with potential saline groundwater geochemistry precipitating gypsum within the vadose zone, defined as a Gypisol by Mack et al.,(1993). The horizontally laminated facies (Sfo) indicate an immature palaeosol, as primary sedimentary features are visible (laminations) and can be defined as either a protosol or vertisol (Mack et al., 1993). These are associated with more humid climatic conditions (Cecil, 1990) due to the lack of gypsum and calcrete and the modification of the previously described fluvial and lacustrine associations.

3.7.11 Sabkha Association (SK)

This association is bound by laterally extensive planar bounding surfaces, and comprises predominantly secondary gypsum (G) formed from the diagenetic alteration of primary anhydrite and gypsum. The evaporite facies (G) are regularly arranged into centimetre-scale, asymmetrical and overlapping folds, nodular, and chicken wire structures within a clastic matrix composed of fine to very fine sand, intercalated with planar and thin (1 cm) interlocking, crystalline pink to clear sheet-like gypsum selenite crystals up to 30 cm across. Tepee structures and massive

bedded/brecciated gypsum are also present, particularly at the top of the formation. The gypsum (G) is sporadically interbedded with gypsum-bound sandstone (Gspl), carbonates (MF3), calcrete-rich pedogenic facies (Sao) and horizontally laminated pedogenic facies (Sfo). The association has an inconsistent thickness ranging from 0.2 m up to 10 m.

The association is dominantly composed of folded and nodular crystalline gypsum and intermittent clastic material indicating deposition within an evaporitic sabkha environment (e.g. Kendall, 1978; Warren and Kendall, 1985; Clement & Holland, 2016; Raine and Smith, 2017). The asymmetrically folded nature of the evaporitic deposits is the result of either enterolithic growth within a saline-saturated ground water close to a shallow saline body of water (Warren 2016), or folding of subaerially exposed microbial matts by wind action (Escavy & Herrero, 2019). The presence and preservation of tepee structures suggests a calm low-energy environment (Lokier & Steuber 2008, 2009) consistent with a saline lake.

Thin planar interlocking crystalline evaporites indicate that primary gypsum formed in concentrated brines (Warren 2016). The intercalated nature of the selenite crystals within nodular, bedded gypsum and clastic material suggests periodic influx of fresh water, followed by a period of concentration. Eventually, crusts form from bottom nucleating salts as saline lake waters evaporate and desiccate (Warren, 2016). These cumulate salts often contain tepee structures as desiccation results in the polygonal fracturing of the evaporate crusts. These fractures trap sediment and infill the crusts, resulting in the interbedding of evaporites and clastic material (Kendall & Warren, 1987). Clast-supported brecciated alabastrine secondary gypsum present at the top of the formation is potentially a result of syndepositional dissolution. No halite occurrences are present in outcrop as halite is highly soluble and has a low preservation potential, this halite may have been leached by fresh

water resulting in solution-collapse breccia under synsedimentary conditions (*cf.* Gundogan *et al.,* 2005) and may indicate intense periods of evaporation and fully saline lake conditions.

Interbedded gypsum-bound sandstone with intercalated gypsum nodules and veins relate to saline pan deposition, occurring at the margins of saline lakes (Lowenstein & Hardie, 1985). The pedogenesis demonstrates a degree of hiatus, the presence of an emergent or near-emergent surface, and sufficient moisture for plant colonisation, probably formed from the modification of background sedimentation within or at the edges of saline rich lakes.

3.8 Regional Variation and Depositional Environments

The spatial sedimentology variation and distribution of facies is now examined. From these results, interactions, depositional environments and depositional models have been determined.

The styles of sedimentary interactions present within the distal sediments of the Cedar Mesa Sandstone Formation differ considerable spatially. This work examines the interactions of the distal deposits of a continental basin, specifically the spatial distribution and relationship of those interactions which involve sabkha sediments directly. Two distinct environmental interactions that involve evaporitic deposits have been identified, these are 'aeolian-sabkha' and 'lacustrine- sabkha' assemblages, and they are described in detail below.

3.8.1 Spatial Distribution of Facies Associations

To examine the nature of the interactions, three dimensional data and panels would usually be required complemented with in depth architectural element analysis. Unfortunately the outcrop of the distal sediments of the Cedar Mesa Sandstone Formation, in which the logged sections were collected, occurs within incised

canyons (Fig. 3.29), making it hard to see the three dimensional and spatial relationships of the facies and facies associations. To overcome this, the spatial distribution of the facies associations has been examined by plotting the percentage of each association within each log against each other (Fig. 3.30). Logs were conducted in a rough north-south transect in order to show the spatial changes in facies from the erg margin to the distal portions of the basin. The relationships of facies associations show there is a clear separation between aeolian associations in the north and lacustrine associations to the south, between which there is a mixture of aeolian, sabkha and lacustrine associations in varying amounts between each log.

The palaeogeography for the area (Fig 3.31) shows that the aeolian erg switches rapidly into sabkha sediments. This can be examined within the spatial distribution plot (Fig. 3.32). The switch to a dominant lacustrine setting or the degree of mixing between aeolian and lacustrine facies within the sabkha area however is not explained by previous paleogeographic reconstructions (Fig. 3.31). Logs (Fig 3.32) from the sabkha environment (logs 1.4-1.8) show a clear switch between groupings of aeolian-sabkha associations and aeolian-lacustrine associations. The styles of these interactions and the styles of sabkha sedimentology are very different and can be characterised as either an 'Aeolian-sabkha assemblage' or 'Lacustrine-sabkha assemblage' and are each described fully below. Spatial distribution of the microfacies (Fig. 3.33) is less clear, however it shows a transition from more aeolian related deposits (MF1 and MF2) within logs 1.2-1.3 to an increasing frequency and variation in microfacies, showing a progressive wetting of the overall environment towards the south.

Figure 3.29 Overhead drone model of locality 1.9, and photos showing the nature of the outcrop, forming within incised canyons.

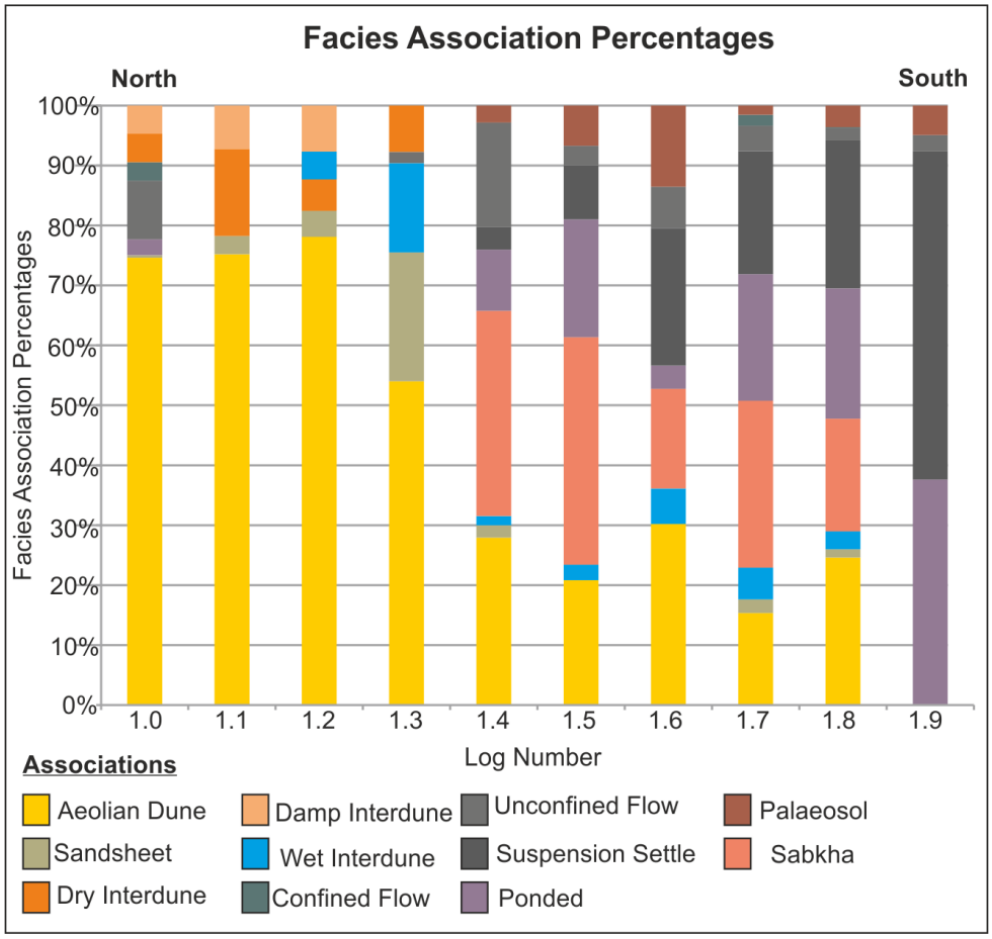

Figure 3.30 The histogram plot shows the percentage of each facies association in each log of the transect, which shows the spatial change from a aeolian dominated setting in the north through a sabkha setting and into a lacustrine dominated setting to the south

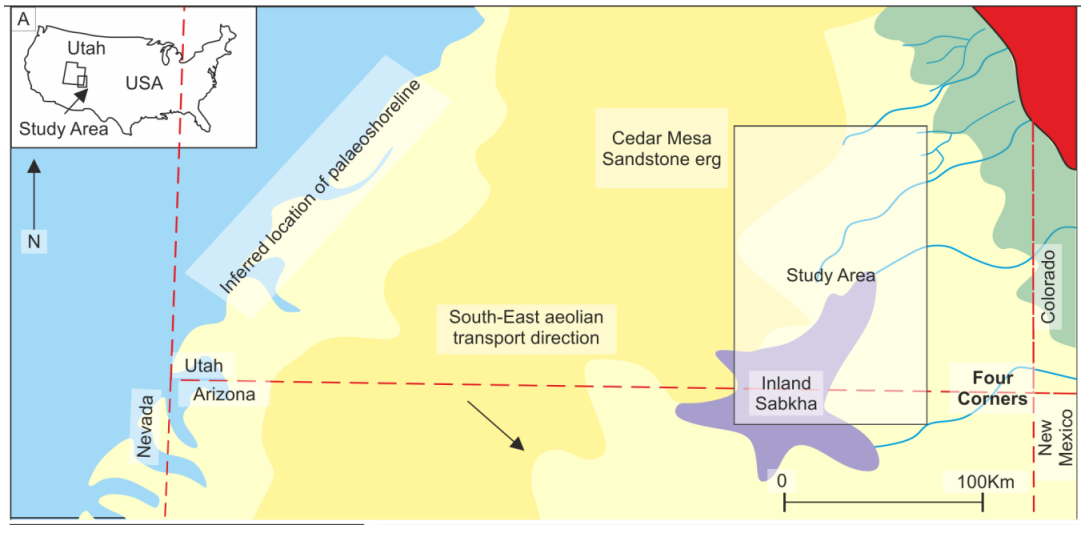

Figure 3.31 Reconstructed paleogeography of the Cedar Mesa Sandstone Formation during the early Permian Period (after Blakey et al., 1988). Location of the dune field is marked in dark yellow, with the location of sabkha sediments shown in purple against an inferred land surface (light yellow). Present day state boundaries are superimposed along with highlighted study area.

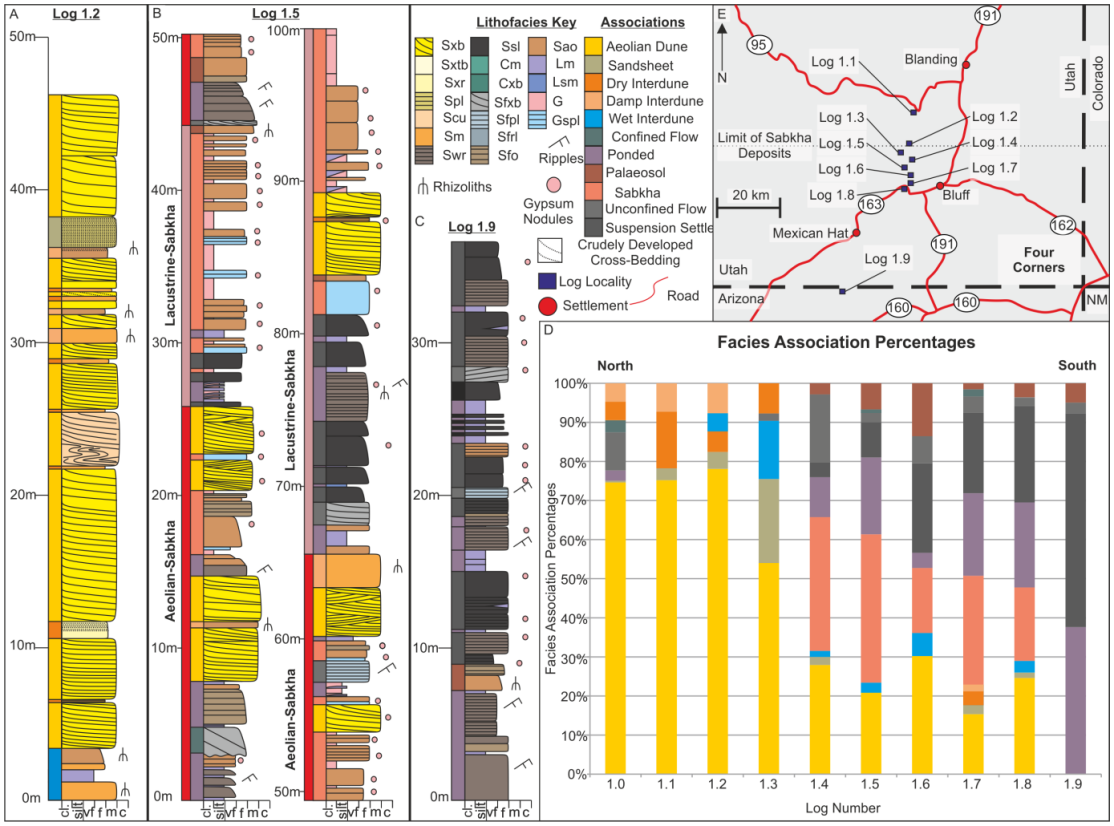

Figure 3.32 Figure showing the spatial variation in sedimentary characteristics. Three representative logs (A-C) are shown in a general north-south transect to highlight the spatial variability. Logs are coloured by facies, facies associations are indicated by the coloured bar along the side of the logs. Log 1.5 also highlights the alternating aeolian-sabkha or lacustrine-sabkha interactions by red or salmon boxes respectively. A) Log 1.2 shows dominantly sediments of an aeolian environment. B) Log 1.5 sediments of a sabkha dominated setting. C) log 1.9 sediments of a lacustrine setting. D) The histogram plot shows the percentage of each facies association in each log of the transect, which shows the spatial change from a aeolian dominated setting in the north through a sabkha setting and into a lacustrine dominated setting to the south. E) The positions of the logs are shown in against a map of the modern landscape with roads and state boundaries included.

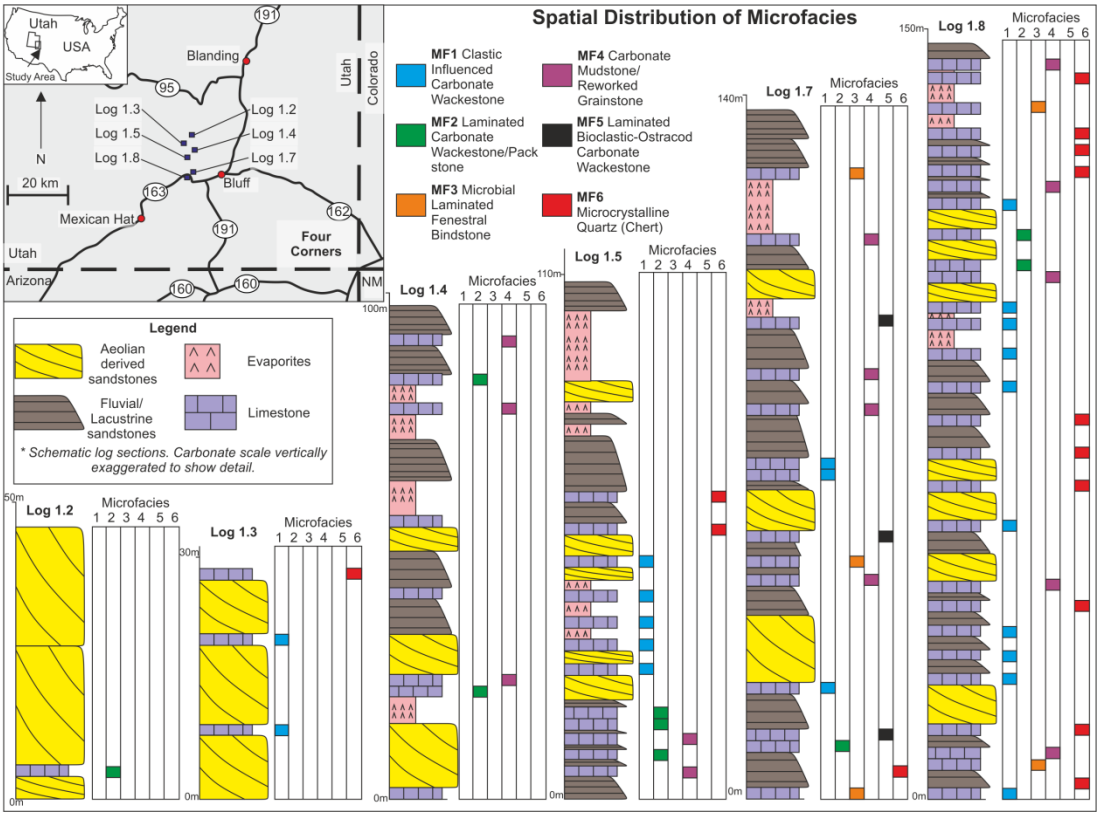

Figure 3.33 Schematic logs showing the spatial distribution of microfacies within the context of coeval clastic deposits. Insert in top left shows a location map, with individual log localities highlighted by blue squares, state boundaries are shown by dashed line, major roads are shown with solid black line. Logs are arranged in a north-south transect, from left to right. Logs are schematic and simplified, clastic and evaporitic bed thicknesses are true whereas carbonate beds have been exaggerated to highlight their spatial distribution. Corresponding microfacies related to the carbonate beds are shown to the right of each schematic log, Colours represent individual microfacies, explained in the key at the top of the figure. The type of deposit is explained in the legend.

3.8.2 Aeolian-Sabkha Assemblage

The dominant sedimentary style of the aeolian-sabkha assemblage is represented by aeolian associations of dune (AD), sandsheet (SS), and interdune (DI) are intercalated with sabkha facies resulting in aeolian sediments that are highly gypsiferous and contain gypsum nodules or veins (Fig. 3.34).

Dune associations (Stxb, Sxb), although common in this setting, are usually of limited vertical extent within logged data and cannot be correlated directly between logged sections, suggesting a limited lateral extent also. They generally lack the

large-scale set and coeset development seen in typical aeolian-dominated sediments (e.g. Rubin & Hunter, 1982; Kocurek, 1981). Dune associations typically overlie gypsum associations (G) and show gypsum precipitated along the bounding surfaces (Fig. 3.24). The thickest precipitates are found typically along set-bounding surfaces, with thinner deposits along foreset surfaces.

Thin units of gypsum (G) associations and carbonate facies (MF1, MF2) are interbedded frequently between sets of aeolian dune sand with soft sediment deformation developed along basal bounding surfaces. These units grade into pedogenic facies that are frequently gypsum rich, displaying enterolithic structures, gypsum nodules and evidence of haloturbation (Fig. 3.34).

Idealised sections through this assemblage (Fig. 3.34) typically begin with unconfined flow (UF) and ponded water (PA) associations, which dry up through aeolian dune (AD) associations with interdune (ID, Di, WI) or sabkha (Sk) associations sandwiched between. The top is commonly marked by palaeosol associations (PS) followed by associations that indicate a sudden wetting of the depositional setting. Aeolian associations dominate the vertical section, sabkha associations however are typically thin forming less than 10 percent of the section. However, aeolian facies are typically strongly influenced by evaporitic sediments.

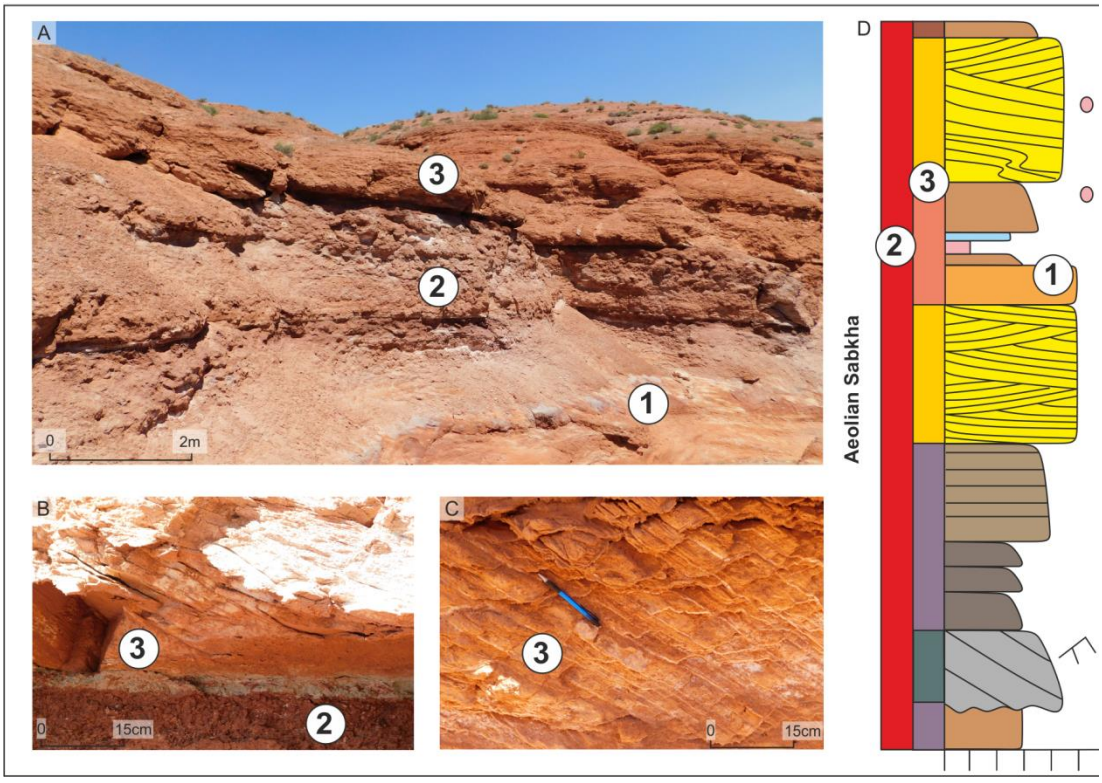

Figure 3.34 Representative sedimentary features, outcrop characteristics and schematic log for the aeolian-sabkha assemblage. A) Outcrop panel showing: Dry interdune deposits (1) overlain by a mixed sabkha setting consisting of pedogenic facies, gypsum-bound sandstone and gypsum (2), and gypsum rich aeolian dune sediments (3). B) Deformed gypsum rich aeolian dune sediments with frequent gypsum along bounding surfaces (3) overlying a sabkha related pedogenic facies (2). C) Close up image of gypsum within the bounding surfaces of aeolian dune sediments (3). D) Idealised log and relative humidity curve for aeolian-sabkha assemblage, log coloured by facies with association indicated by coloured side bar, red bar denotes the full aeolian-sabkha assemblage sequence

3.8.3 Lacustrine-Sabkha Assemblage

The lacustrine-sabkha assemblage is characterised by fluvio-lacustrine associations of confined and unconfined flow, suspension settlement, ponded and palaeosol occur in logs 1.4-1.8 intercalated with sabkha associations and individual occurrences of gypsum facies (G, Gspl, Sfo).

Thick sabkha associations of bedded gypsum (G) containing multiple polygonal crusts, crystals and cumulates (Fig. 3.35) are interbedded with thin unconfined flow associations (<1 m), along with gypsum-bound sandstone and pedogenic facies which contain frequent gypsum nodules and enterolithic structures (Fig. 3.35).

In all logged sections, these strata overlie suspension-settlement associations which are intercalated with unconfined flow associations and / or thin units of carbonate facies (MF4 MF5), both of which can be commonly correlated between adjacent logs (Fig.3.2=35).

Sections through this assemblage (Fig. 3.35) typically begin with unconfined flow (UF) and suspension settle associations (SA) which dry up through progressively thinner suspension settle deposits interbedded with ponded water associations (PA) containing carbonates and wave-rippled clastics. The top is marked by thick sabkha associations (SK) containing bedded evaporites and palaeosols with enterolithic growth followed by associations that indicate a sudden wetting of the depositional setting. Lacustrine and sabkha associations comprise approximately ninety percent of the vertical succession. Aeolian associations are somewhat limited in extent, and are largely unaffected by the presence of evaporitic sediments.

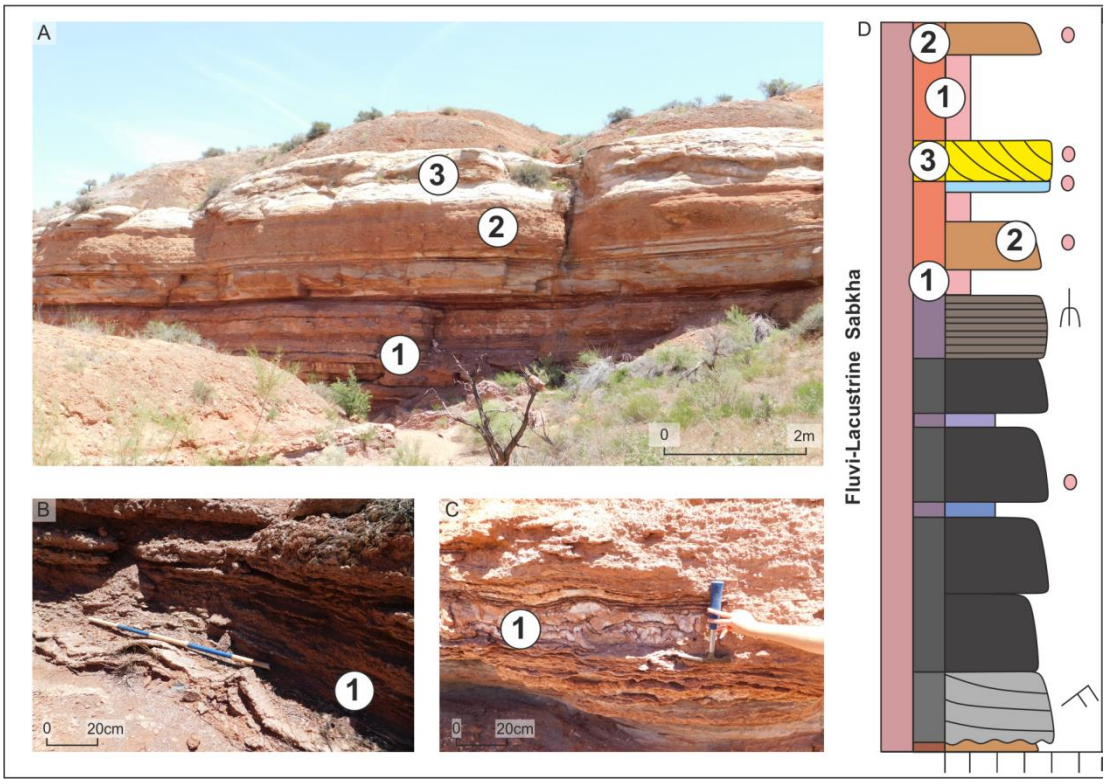

Figure 3.35 Representative sedimentary features, outcrop characteristics and schematic log for the lacustrine-sabkha assemblage. A) Outcrop panel showing: Interbedded gypsum and

pedogenic facies with frequent enterolithic growth overlain (1) by sabkha related pedogenic facies (2) and gypsum rich aeolian dune sediments (3). B) Deformed gypsum tepee structures (3). C) Enterolithic growth structures (3). D) Idealised log and relative humidity curve for lacustrine-sabkha assemblage log coloured by facies with association indicated by coloured side bar, salmon bar denotes the full aeolian-sabkha assemblage sequence.

3.9 Depositional Environments and Models

Analysis of facies, facies associations, facies relationships and their spatial distributions, indicate two end member depositional environments: an aeolian environment and a lacustrine environment. Sabkha environments form an intermediate stage occurring either as: an Aeolian-sabkha assemblage; or a Lacustrine-Sabkha assemblage. Schematic depositional models are here presented along with an explanation of the dominant depositional settings.

3.9.1 Aeolian Environment

The aeolian environment contains dune associations (AD), sandsheet (SS), interdunes (ID, DI, WI) minor fluvial elements (UF) as well as palaeosols (PS). Northern areas represent more central erg localities (Logs 1.0–1.2) where larger and more sinuous crested dunes are present, higher sediment supply from a more proximal locality to the sediment source has resulted in larger dunes, and well-developed slip faces with fewer interdunes. These interdune areas are isolated due to the sinuous nature of the dune and more likely to be dry or damp interdunes, wet interdunes, if long lasting, resulted in the isolated sand-rich carbonates of MF1.

Towards the erg margin (log 1.3), dune associations become smaller and are dominated by more straight-crested dunes, as sediment supply decreases. Interdune areas and sandsheets become more prevalent and are more interconnected due to the straight and in-phase nature of the dunes. These interdune areas are susceptible to flooding from fluvial associations (UF). Wet interdunes are more common and generate carbonates described from MF2, with surrounding areas becoming stabilised and modified into palaeosols.

3.9.2 Lacustrine Environment

In the south of the study area (log 1.9) deposits are primarily sub-aqueous associations (PA, SA) composed of parallel and ripple laminated silts and mudstones as well as fresh water carbonates. Palaeosol associations are also present. These deposits likely formed within desert lakes, from fluvial sheetflood influxes related to topographic lows and a perennially elevated water table (*c.f.* Gierlowski-Kordesch, 1998). Climatic fluctuations result in either contraction or expansion of lake levels and can alter clastic sediment supply, which can lead to the formation of lacustrine carbonates when the availability of clay-size particles is limited, such as MF4 and MF5 (Tanner & Lucas, 2007). Palaeosols have then formed around the edges of these lakes as a result of stabilisation and modification.

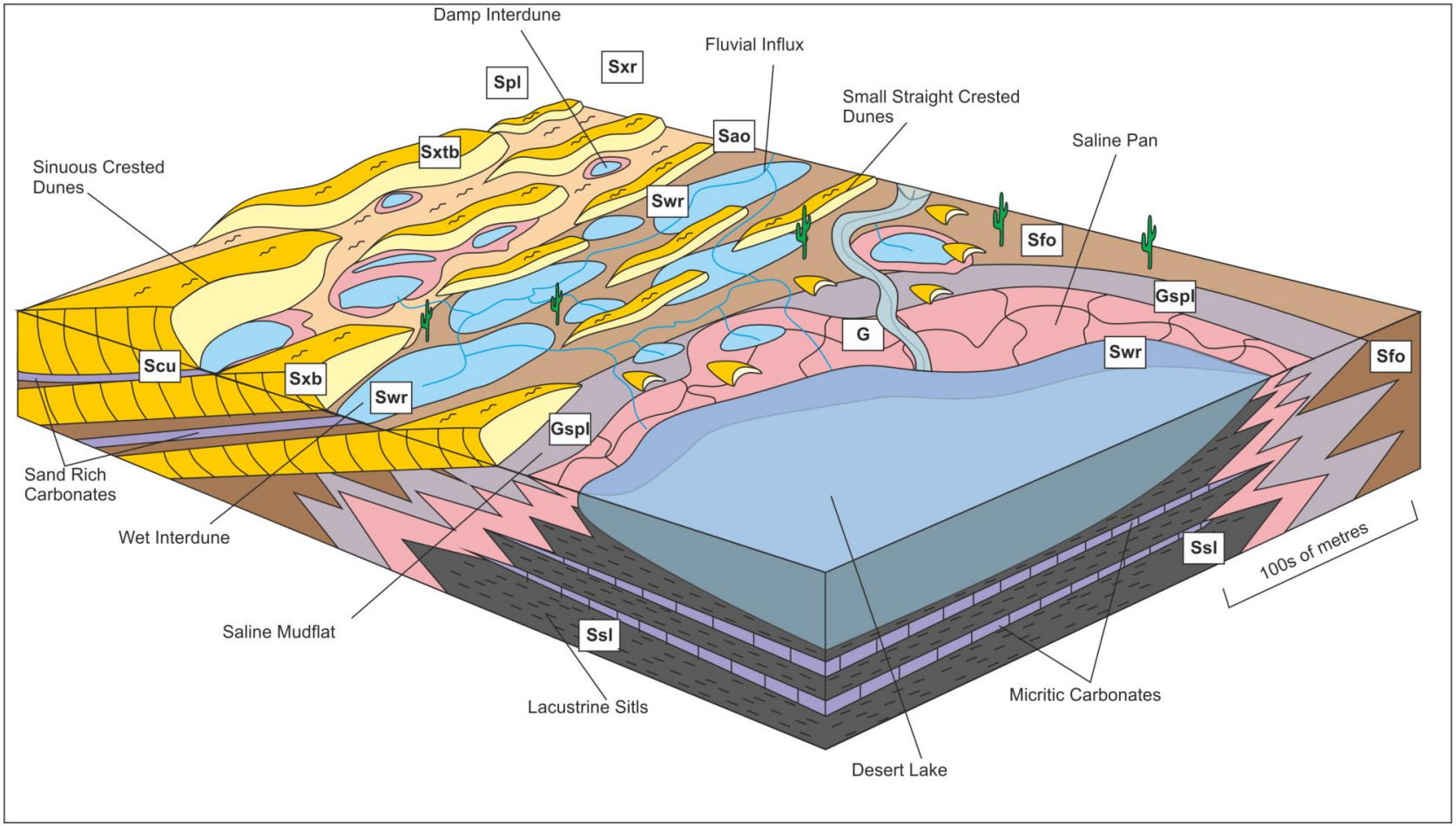

Figure 3.36 Summary depositional model showing the dominant end member environments. Facies are highlighted by codes

3.9.3 Sabkha Environment

The two assemblages described above related to sabkha sediments interacting with either a dominant aeolian setting or lacustrine system, two depositional settings are therefore interpreted as either an 'erg-margin sabkha' and a 'lacustrine-margin sabkha'.

Erg-margin Sabkha Setting

Within the erg-margin setting sabkha associations are present only in interdune areas and form relatively small deposits composed primarily of gypsum nodules and veins. Sedimentary relationships observed at both facies- and association-scale within the aeolian – sabkha assemblages suggest an erg-marginal setting (Fig. 3.37) in which small-scale sinuous-crested aeolian dunes migrated with damp to wet, solute-rich interdunal areas separating them. In some areas, the solute-rich substrate was wet enough for the direct precipitation of gypsum and carbonates (MF1), intercalated with aeolian-derived clastic sediments, to form evaporitic wet interdune deposits. In other areas, enterolithic growth of gypsum within the damp subsurface and evidence of haloturbation indicate damp interdune settings. A wet solute-rich substrate severely limited sediment supply to dunes and consequently dunes were isolated from one another, most likely barchanoid, and the damp interdunes are interconnected laterally.

As the dunes migrated over interdunal areas they deformed the underlying soft substrate and drew concentrated brine up the foreset bounding surfaces to deposit gypsum through capillary action. Thicker deposits of deformed gypsum that are present along set and coset bounding surfaces represent the migration and climb of wet or damp interdune facies with the migration and climb of dunes.

Although water played a role in the formation of sediments within the erg-margin sabkha, the dominant sediment transport processes were wind-driven, with

increases or decreases in the amount of water probably the result of variations in the elevation of the water table, rather than sustained surface flow from outside the system that fed significant and long-standing bodies of water.

Consequently, evaporitic associations within the deposited assemblages of this setting are thin and form a subordinate proportion of the vertical succession. They are intercalated with interdune associations and are typically of limited lateral extent despite lateral connectivity of interdune deposits themselves. However, preserved aeolian associations are strongly influenced by evaporitic sediments, and typically contain gypsum precipitated on bounding surfaces.

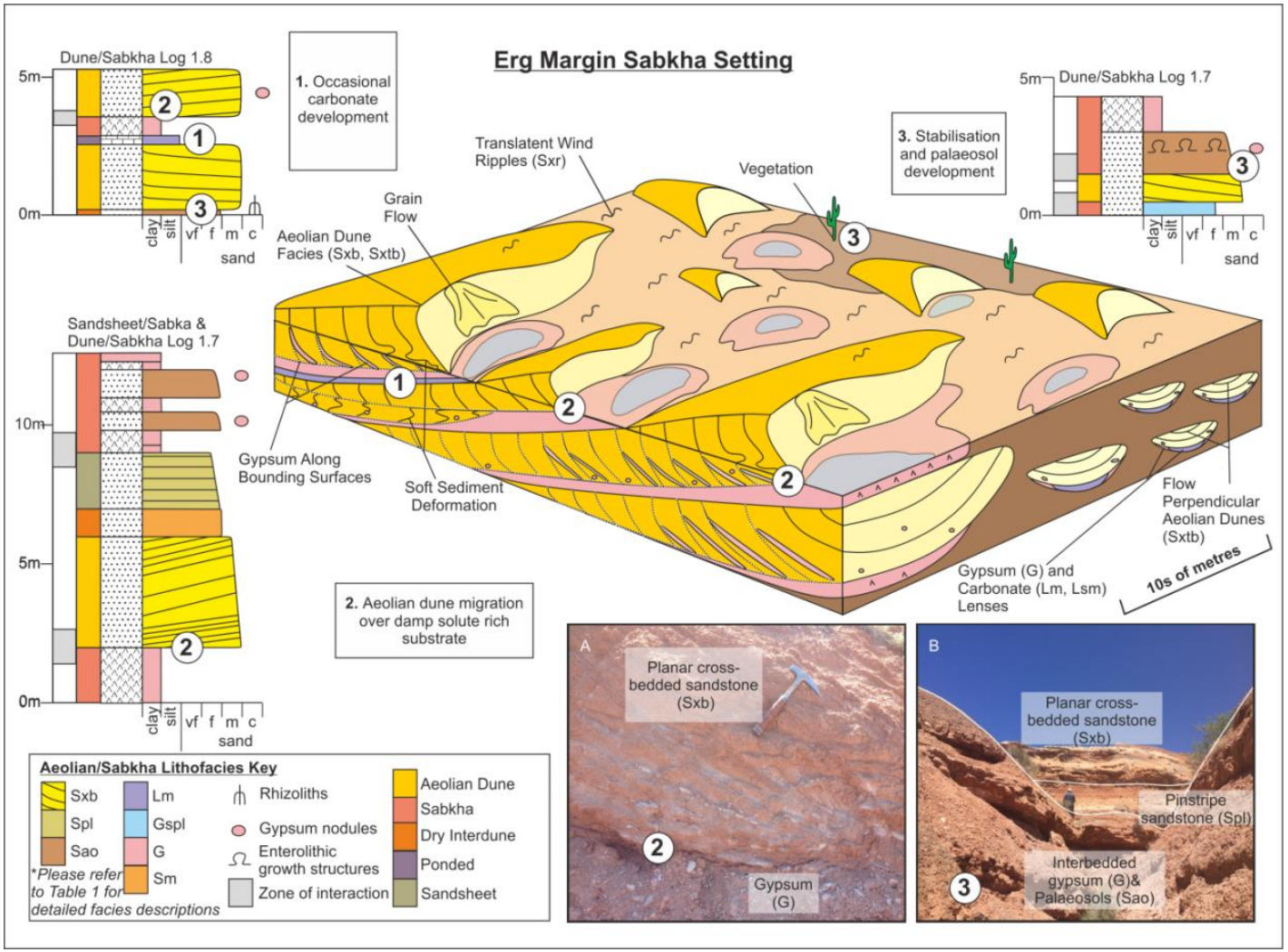

Figure 3.37 Conceptual depositional model for the erg margin setting of the Cedar Mesa Sandstone Formation. Three sections of field logs are shown, highlighting key characteristics of the erg margin sabkha setting, also highlighted on the depositional model, (1) The presence of occasional interdune carbonate deposits, (2) aeolian dunes with gypsum rich bounding surfaces overlying gypsum deposits, (3) development of palaeosols. Logs are coloured by facies, and associations are indicated by the colour bar alongside the logs. Key interactions are indicated by a grey box. The depositional model shows the three dimensional relationships between associations during deposition and the bounding surface relationships of preserved deposits. Field photos detail (a) gypsum precipitation up the bounding surfaces of aeolian dunes (b) the preserved nature of the deposits.

Lacustrine-margin Sabkha Setting

Sabkha associations within the lacustrine-margin setting are represented by thick-bedded successions of gypsum, gypsum-bound sandstone, occasional carbonates, tepee structures and palaeosols with significant haloturbation.

Sedimentary relationships observed within the fluvio-lacustrine – sabkha assemblages suggest an arid evaporitic lacustrine-margin setting (Fig. 3.38). Thick suspension settlement associations represent lacustrine sediment interbedded with either fluvial or carbonate sediments (MF4, MF5) depending on the rate of fluvial input and the magnitude of its clastic load. In dominantly submerged areas, thick arid saline pans of bedded gypsum formed from both surface nucleating halite rafts, and bottom nucleating salts, with eventual surface exposure indicated by polygonal growth structures. The gypsum bound sandstone and evaporite-rich palaeosols show capillary and phreatic growth of salts around the edges of an evaporitic lake from the infiltration of saline groundwater, indicative of a saline mudflat setting. Carbonate deposits (MF3) in this environment represent microbial matt development and preservation. Saline pans and mudflats are a recognized habitat for microbial life in desert environments as the interaction between the salt flat and the groundwater provides sheltered habitats for microbial life (McKay *et al.,* 2016).

In the preserved assemblages of this setting (Fig. 3.38), lacustrine and sabkha associations dominate, with subordinate aeolian sediments. Evaporitic sediments have limited influence upon the aeolian facies. This probably results from only local development of dune-fields of small size that formed in response to limited sediment availability.

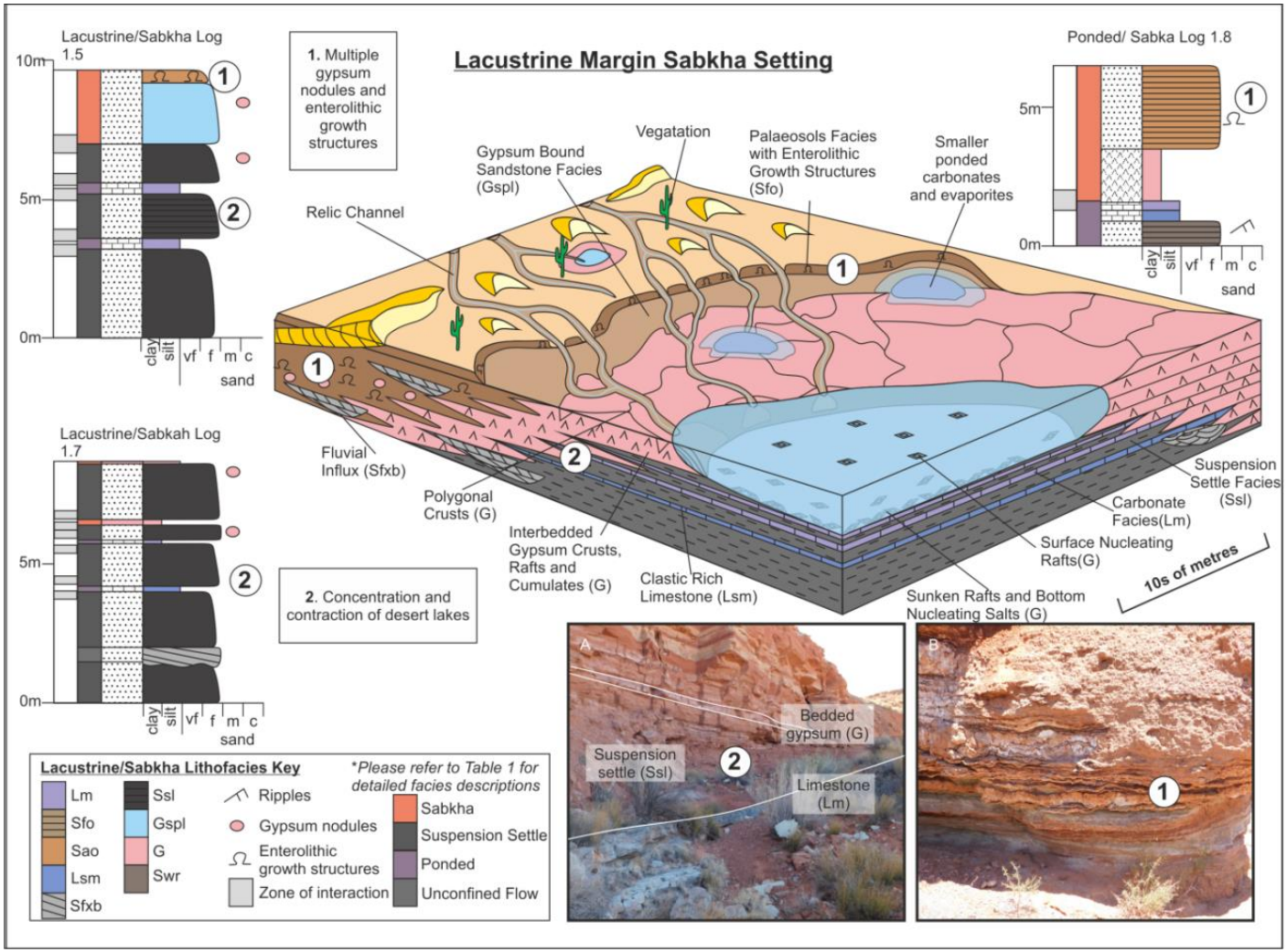

Figure 3.38 Conceptual depositional model for the lacustrine margin sabkha setting of the Cedar Mesa Sandstone Formation. Three sections of field logs are shown, highlighting key characteristics of the lacustrine margin sabkha setting, also highlighted on the depositional model, (1) multiple gypsum nodules and enterolithic growth, (2) the contraction and concentration of desert lakes. Key interactions are indicated by a grey box. The depositional model shows the three dimensional relationships between associations during deposition and the bounding surface relationships of preserved deposits. Field photos show (a) the lateral extent of deposits, (b) close up detail of the enterolithic growth structures seen within pedogenic facies.

3.10 Summary

This chapter has detailed the nineteen facies, six microfacies and eleven facies associations that have been identified within the Cedar Mesa Sandstone Formation, and builds upon previous facies schemes created by numerous authors within the Cedar Mesa Sandstone Formation. The nineteen facies are identified on the basis of their lithology and sedimentary structures present within. The facies have been further categorised based on their proposed depositional setting: sub-aerial, sub-aqueous or evaporitic.

Eleven facies associations have been recognised, these are grouped by the arrangement of commonly occurring sets of facies from logged vertical sections. The associations are recognised to fall into one of four broad scale depositional environments: aeolian, fluvial, lacustrine or sabkha.

The facies and facies associations observed are consistent with an ancient arid to semi-arid mixed aeolian/sabkha succession.

The spatial changes observed in sedimentology show a transition from an aeolian erg, through to a marginal erg, a sabkha setting and a lacustrine environment. Facies relationships within the sabkha setting depended on the relationship to either the lacustrine or aeolian settings, preserving either aeolian-sabkha assemblages or lacustrine-sabkha assemblages. These assemblages are traceable throughout the sabkha setting and have been interpreted to have formed in either an erg-margin sabkha or a lacustrine-margin sabkha depositional setting. The cyclic preservation mechanisms and temporal variations between dominant aeolian-sabkha or lacustrine-sabkha interactions seen have not been addressed and will be discussed in chapter five.

Chapter Four Spectral Gamma Ray Characterisation of an Arid Continental Sabkha

Gamma ray logging was conducted in five localities to complement sedimentological observations and interpretation. This chapter details the facies determined from gamma ray logging of outcrop sections of the Cedar Mesa Sandstone and compares them to sedimentological data.

4.1 Introduction

Geophysical logs have a wide range of techniques and methods and are frequently used to document and characterise subsurface and outcrop data. One of the most commonly conducted geophysical logging procedures is gamma ray (GR) logging, which measures the total radiogenic emissions from a rock and is primarily used to determine shale content and well log correlation (see Slatt *et al*., 1992). Spectral gamma ray (SGR) logging, whilst run less frequently, is a powerful tool as it divides the total radiogenic emissions from a rock into discreet spectral bands: Potassium (K); Thorium (Th); and Uranium (U). By studying the concentrations of these individual spectral signatures, and by plotting their mutual ratios of the signals against each other, detailed petrophysical and geochemical data can be gained which can be used as a tool for characterising stratigraphy (Doveton, 1994; Bristow and Williamson, 1998), mineralogical estimations, grain size, porosity, organic richness (Lüning *et al*., 2003), climatic regimes (Yan & Baumfalk, 1997; Sierro *et al.,* 2000), depositional environments (e.g. Myers & Bristow, 1989), stratigraphic surfaces and sequence boundaries (Ehrenberg and Svana, 2001; Davies & Elliot, 1996; Lüning & Kolonic, 2003).

Gamma-ray logs are widely used in subsurface stratigraphy to identify facies, borehole correlation and sequence-stratigraphic interpretation (e.g. Rider, 1996, Catuneanu, 2006, Hampson *et al.,* 2005). More recently, SGR and GR logging has been widely applied to outcrop studies, commonly focused on marine settings (e.g. Jordan *et al.,* 1993; Aigner *et al.,* 1995; Davies & Elliot, 1996) where it is used for correlation and facies mapping (Šimíček & Bábek, 2015), sequence stratigraphic and cyclostratigraphic research (Davies & Elliot, 1996). Much of this work uses Th and K values within marine calcium carbonate as a proxy for continental and marine influence (Postma & Ten Veen, 1999; Lüning et al., 2004; Hladil et al., 2006; Bábek et al., 2007; Bábek et al., 2013).

Continental GR and SGR studies have largely focused on its use at identifying unique facies, such as classifying fluvial/deltaic settings (Evans *et al.,* 2007; Myers & Bristow 1989). Application within arid continental setting has so far been proven difficult (North & Boering 1999) as it is often difficult to distinguish from the geophysical log trends individual facies due to signal overlap in the natural radioactivity of common continental facies (Rider, 1990). These problems can be overcome however by using an integrated approach, such as complementing spectral analysis with geochemical studies (Svendsen & Hartley 2001).

This chapter demonstrates the usefulness of spectral gamma ray measurements as an outcrop logging technique in determining quantifiable facies from arid continental sabkha sediments, by using the combined methods of K:Th cross plots (*Cf.* North & Boering, 1999) and interpreting unique log motifs from gamma ray signals (*Cf.* Martinius *et al.,* 2002). The Cedar Mesa Sandstone Formation of the Cutler Group in Utah, USA is used as a case study. This work demonstrates the unique facies within arid continental settings which can be distinguished based on

SGR outcrop logging, and the unique trends and values which can be quantified and used to correlate facies across the basin.

4.1.1 Gamma Ray Logging Principles

Gamma rays are bursts of high energy electromagnetic waves emitted during the decay of radioisotopes occurring naturally in rocks. Gamma rays have a slower attenuation rate than Alpha and Beta radiation allowing for gamma rays to travel several metres within the formation (Rider, 1996). The principal radioisotopes of interest in natural gamma logging are potassium-40 (^{40}K) and the daughter products of uranium and thorium decay series (Cripps & McCann 2000). The number and energy levels of the gamma rays associated with Potassium-40, uranium, and thorium, are distinctive (Belknap *et al* 1959). Potassium-40 decay, results in gamma photons of 1.46MeV (million electron volts) energy, and its spectrum shows a 1.46MeV photopeak. Uranium has peaks at 0.61, 1.12, and 1.76MeV, with the at 1.76MeV peak most commonly recorded. Similarly thorium shows peaks at 0.58, 0.91, 1.62 and 2.62MeV which is the preferred peak (Cripps & McCann 2000).

In sedimentary rocks gamma ray activity normally reflects the clay and finer grained components as these concentrate radioactive elements. Potassium-40 is abundant in micas and clay minerals most commonly associated with mudrocks. Thorium (Th^{232}) provides an indication of the detrital heavy mineral (for example, monazite and zircon groups) concentration (Herron & Matteson 1993). Uranium (U^{238}) is also present in heavy mineral groups but is used as an indicator of anoxic sediments and the presence of organic matter (Anderson *et al.,* 1989; Lovley *et al.,* 1991). It should be noted that diagenetic effects commonly have an impact on gamma ray signatures and this should be considered in their interpretation. Mud rich sediments account for the majority of gamma radiation in sedimentary rocks. Heavy radioisotopes also concentrate in clays due to absorption and ion exchange (Cripps & McCann 2000).

Gamma ray logs are not distinct to lithology, but will be consistent over an area. Sand rich lithologies will show low gamma counts whilst clay rich beds will give much higher counts, allowing for correlation between lithofacies and gamma logs.

4.2 Methods

A handheld BGO-Super-Spec 230 gamma ray spectrometer was used (Radiation Solutions, Inc., Canada) to log across five outcrop localities of the Cedar Mesa Sandstone Formation. This device offers convenient set up and portability resulting in negligible difference in the quality of logs obtained from larger vehicle mounted systems (Cripps & McCann, 2000). The tool uses a 103 ccm Bismuth-Germanate (BGO- $Bi_4Ge_3O_{12}$) crystal opposed to traditional thallium doped sodium-iodine crystal (NaI(Tl)), providing more sensitive spectral readings without the need for a Cs^{137} source to fix background (e.g. Zanzonico 2012).

Measurements were taken at 0.2m intervals over each section. Care was taking in achieving optimum tool position on the rock surface as convex angles give an underestimation of counts whilst a concave surface will give an overestimation, furthermore the tool position in relation to bedding can affect data collected (Fig. 5.1) (Svendsen & Hartley 2001). Due to the tool having no source the tool must be thermally stabilised prior to obtaining a reading, or this results in inaccurate thorium measurements, any time stabilisation was lost the measurement was repeated when stabilised.

Sampling was conducted with these limitations in mind and all possible efforts to ensure the most representative data was collected.

Three factors are required for a statistically representative concentration of radioactive elements (Svendsen & Hartley 2001): the amount of radioactive material in the formation; the size of the analysing crystal; and the counting time. The first

two factors are fixed resulting in the only variable being the count time of the survey.

Various count times were tested on representative sediments (Table 4.1) in the field and showed a ninety second count time was deemed to give a representative dose rate of the formation (e.g Løvborg & Mose, 1987). For optimum spectral data longer survey times are often required as reliable measurement of uranium concentrations are typically three to four times smaller than thorium concentrations (Løvborg & Mose, 1987), however Th:U ratios within continental setting have been shown to be somewhat ineffectual at determining continental provenance or facies (North & Boering, 1999; Zuchuat *et al* 2019). Shorter survey times allowed for more data to be collected during a limited field period with the U component largely ignored, due to the potential for measurement error from shorter survey times and unhelpful data. However, the shorter count times (Table 5.1) has had much less effect on the dose rate measurements than other studies which used NaI scintillation tools (see Hoppie *et al.,* 1994)

Five spectral gamma ray logs were collected at previously logged sections. These logs were chosen as they had good exposure and represent a spatial transition from the marginal aeolian erg and dominant sabkha setting. The results of which provide a data set which is able to characterise the full range of facies present in the distal portion of a continental basin and to examine the role evaporites play in altering the spectral signals of arid continental deposits. Total radioactive emissions are presented as well as the influence of the individual spectral elements of thorium (Th), potassium (K) and uranium (U). Dominant peaks of Th and K represent clastic influence and show evidence for the provenance of the rocks whereas U peaks are related more to post depositional fluid flow due to the soluble nature of uranium (Rider, 1996). Spectral gamma-ray data is collaborated with detailed

sedimentological field observations to aid in correlation and interpretation of depositional environments in order to generate quantifiable log data, and back up sedimentological interpretations.

Table 4.1 Table of results from different sample times on a representative rock sample from the Cedar Mesa Sandstone. Each measurement at the different time steps was repeated ten times, mean total counts, K%, Th and Uppm are shown.

Sample Time (Seconds)	***N***	**Mean Total Counts**	**Mean K %**	**Mean Th (ppm)**	**Mean U (ppm**
30	10	834.97	1.92	8.65	2.59
60	10	866.27	2.17	9.33	2.24
90	10	867.66	2.23	10.17	2.30
120	10	863.65	2.26	9.21	2.75
180	10	862.11	2.22	9.64	2.53

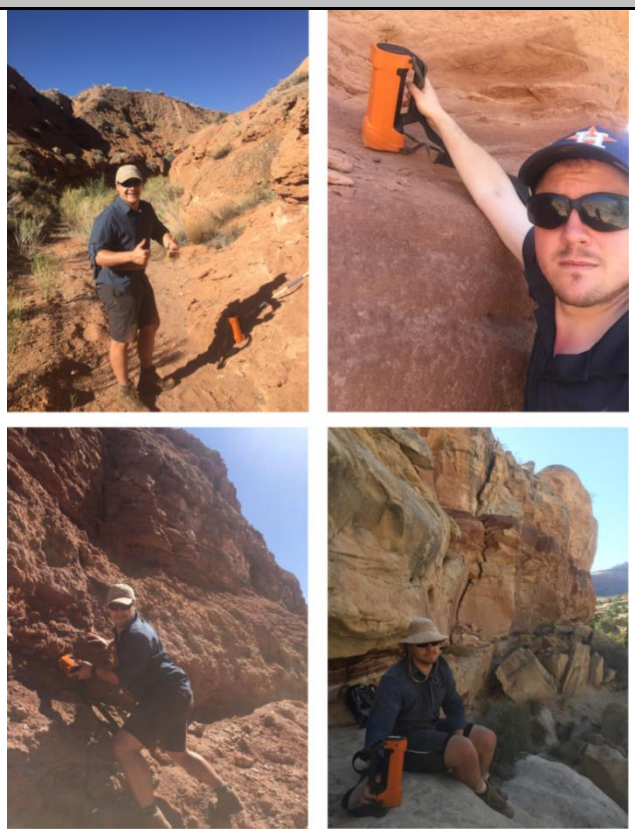

Figure 4.1 Field collection of spectral gamma ray day, range of tool positions chosen to reflect optimum data collection positions (see Svendsen & Hartley 2001).

4.3 Gamma Ray Results

Total counts (Fig. 4.2) and K:Th cross plots are presented below (Fig 4.3-4.4) Total count plots are correlated and positioned next to the associated sedimentological log and show the overall trends of each log and the variability of facies. K:Th cross plots have been plotted for all logs and have been separated on the basis of each of the known sedimentary facies (Chapter 3). This has been done as initial K:Th cluster plots show only one large cluster. This is helpful in discerning that the sediments are from one source, cross plots can give a crude indication of provenance, linear trends indicate one main source, whereas plots that are dispersed represent multiple sediment sources. However, from the limited data spread it is hard to determine unique facies from this trend alone.

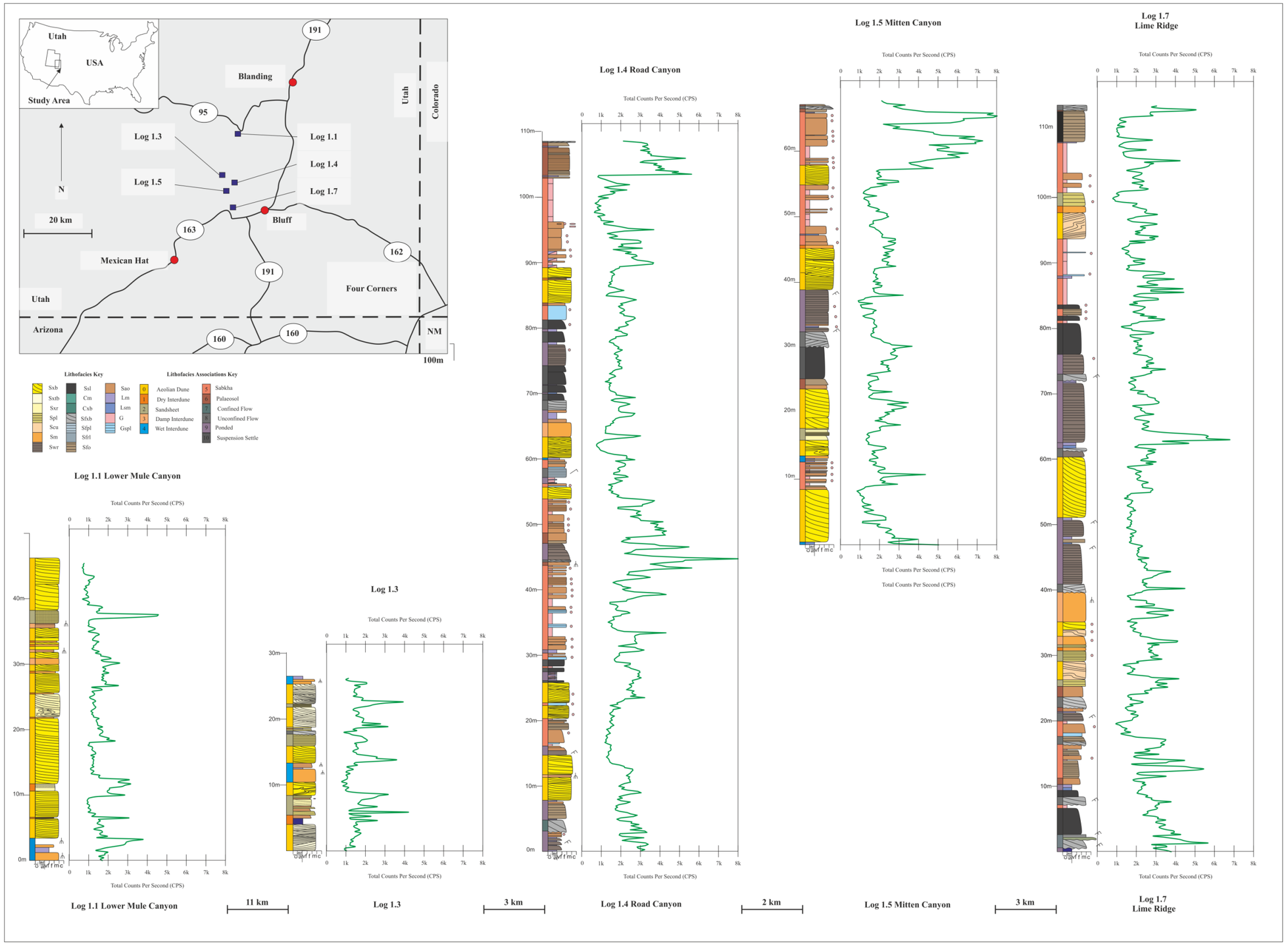

Figure 4.2 combined sedimentary and gamma ray logs.

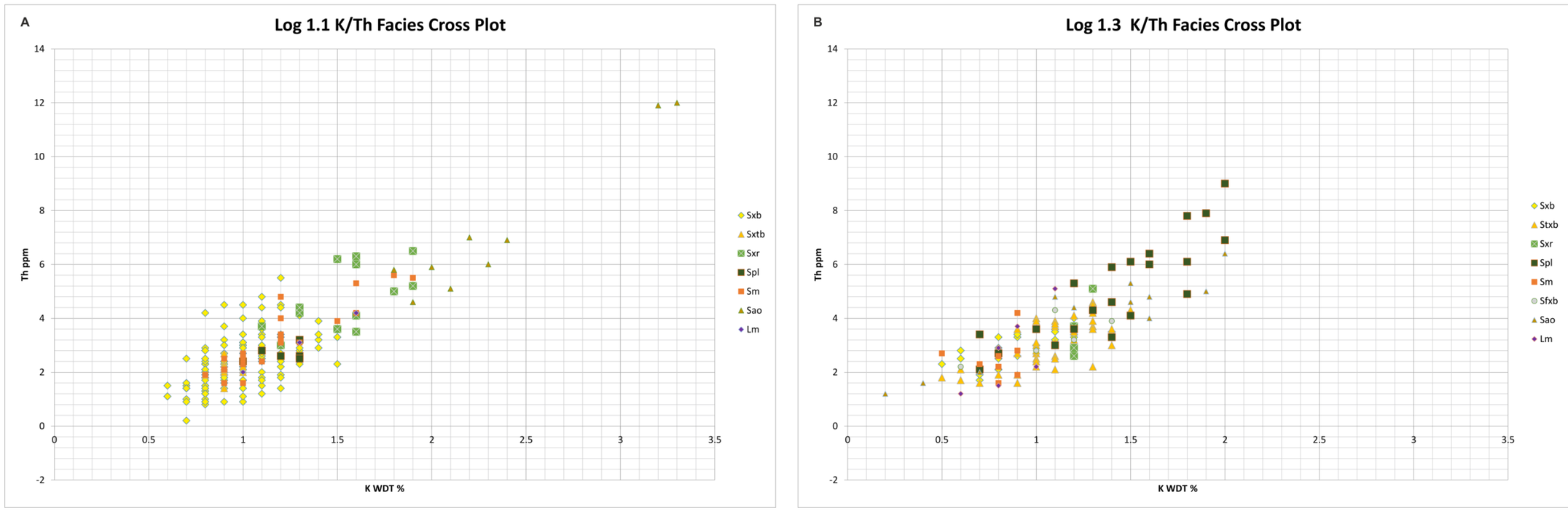

Figure 4.3 K:Th cross plots for logs 1.1 and 1.3, every facies is plotted on the same graph.

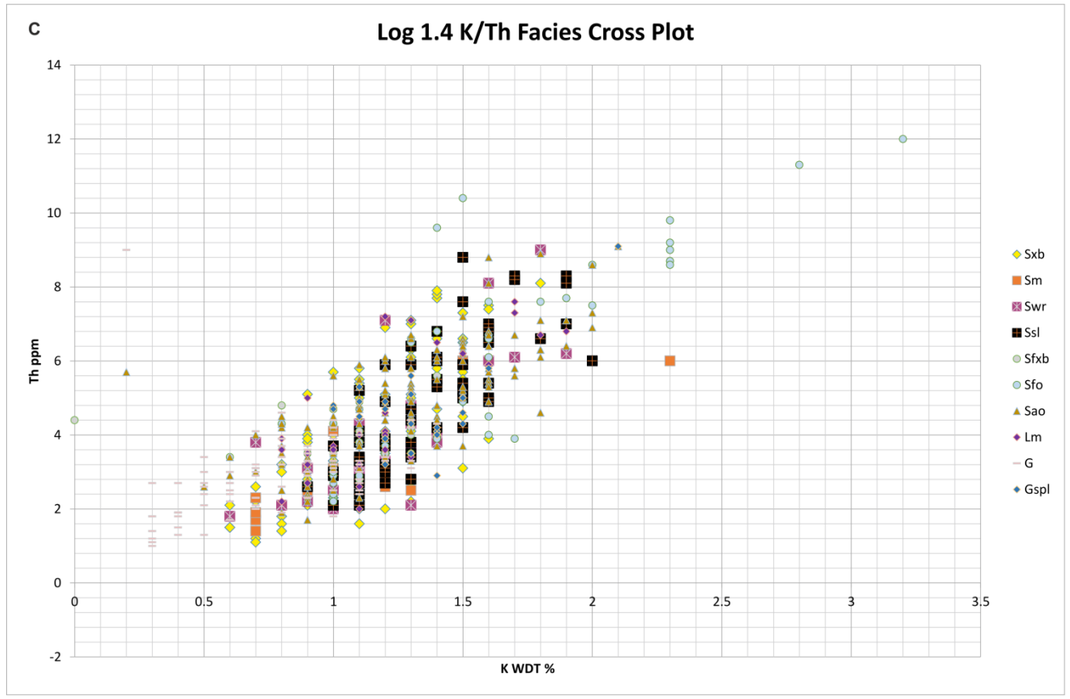

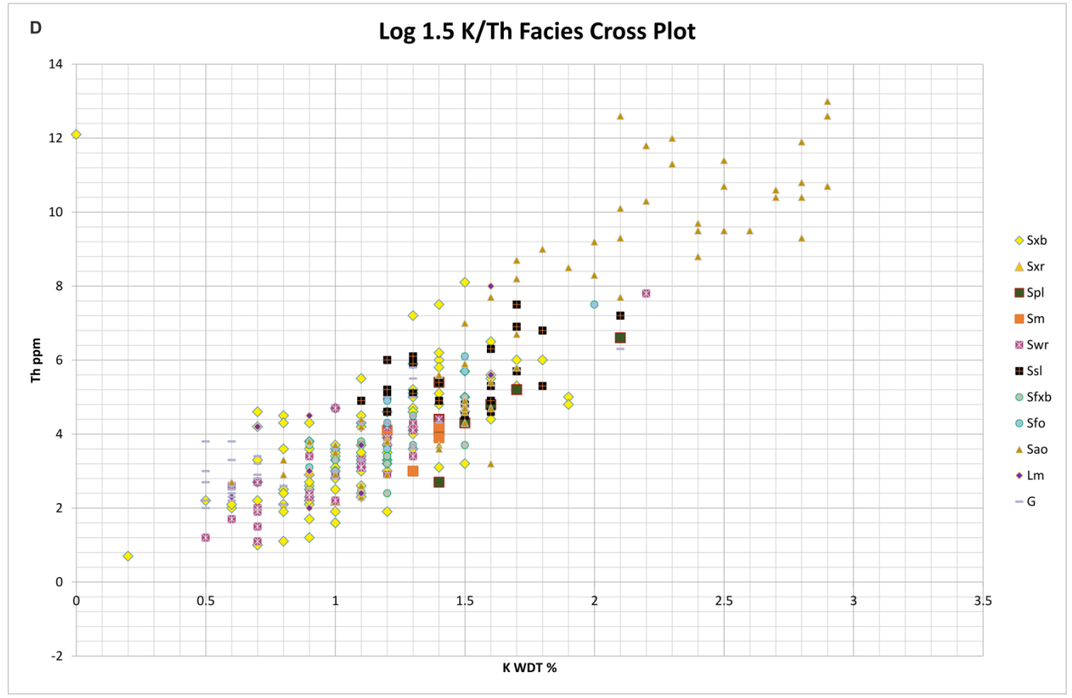

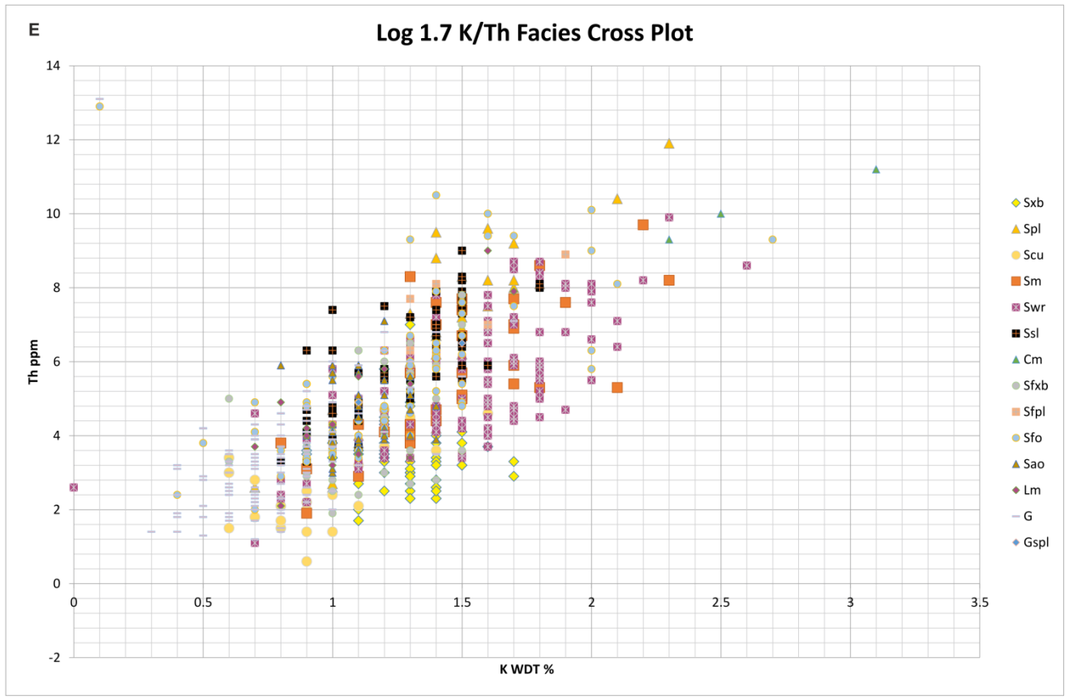

Figure 4.4 K:Th cross plots for logs 1.4, 1.5 and 1.7, every facies is plotted on the same graph.

4.4 Facies plots

Cross plots displaying all the facies within each log (Fig 4.3, 4.4) are scattered, therefore each facies has been separated and plotted together (Fig 4.5- 4.8). By doing this it allows for comparison between logs, ensuring facies have been interpreted correctly, and allows for easier comparison of the gamma ray signal for each facies.

Facies have been divided into broad scale depositional settings; aeolian, interdune and sandsheet, lacustrine, fluvial, palaeosol, and sabkha. These depositional settings are explained fully below.

4.4.1 Aeolian

Facies Sxb, Sxtb, and Scu (Fig 4.5) represent various dune types, and have very similar plots forming a distinct rounded cluster in the bottom left of each plot. Data points are limited for facies Sxtb and Scu. However, it is likely that with more points, cluster plots would be similar and largely indistinguishable based on this method alone.

4.4.2 Interdune/Sandsheet

Wind ripple facies (Sxr and Spl) and interdune sands (Sm) are relatively distinct from dune facies as they generally have higher counts and plot in a more dispersed and elongate shape in which diagonal trend lines could be drawn. Distinguishing between the types of wind ripple facies based on the cross plots alone is tricky, especially considering the small number of data points within facies Sxr. However, Sxr appears to have lower counts than Spl, and plots more in the left corner. Spl and Sm have similar cluster shapes. However, Spl has higher counts and a higher gradient when compared to Sm.

4.4.3 Lacustrine

Lacustrine facies (Swr, Ssl) are often present within interdune areas. The Swr plot shares similar count values, shape and gradient to interdune facies (Sm) which may make it tricky to distinguish based on cross plots alone. The plot of Ssl however, has a distinct circular shaped cluster based within the middle of the graph.

The lacustrine facies (Swr, Ssl) have a higher component of fine grained material (silts and clays, see chapter 3) than other facies. K:Th cross plots can be used to determine clay typing for fine grained material. Using the scheme of Quirein *et al.,* (1982), results show that both Swr and Ssl straddle the illite/montmorillonite boundary, with Ssl plotting slightly more within montmorillonite.

Limestone facies (Lm) are present within multiple environments. However, they are most commonly found within lacustrine dominated successions. Limestone cross plots generally plot in the left of the graph with a positive correlation which can be subdivide into one main circular cluster with lower counts, and a slighter less well defined circular cluster of higher counts.

4.4.4 Fluvial

Fluvial facies contain conglomerates (Cm) climbing ripples (Sfrl) and channel facies (Sfxb). Data points for Cm and Sfrl are low (Cm n=3, Sfrl n=5) yet distinct in count values and plot locations from each other and channel facies (Sfxb). Conglomerate plots have very high counts, plotting in to top right corner, whereas ripple facies have high counts which plot within the middle of the graph. Channel facies (Sfxb) plots in one central circular plot, with relatively low counts, with two smaller triangular shaped plots to the left and above the main circular plot.

4.4.5 Palaeosol

Palaeosol facies (Sfo, Sao) are characterised by a wide range of counts which plot with a strong positive correlation. Sao has higher counts than Sfo. However, both are fairly similar and hard to distinguish from each other. Palaeosol facies have the widest distributions out of any other facies, though the points would overlap many others if plotted together, obscuring detail.

4.4.6 Sabkha

Sabkha facies, (G, Gspl) both have low counts and cluster in distinct circles. Gypsum facies has the lowest values of any facies and a strong positive correlation. A number of evaporite minerals are potassium rich such as sylvite (Table 4.2), these minerals would give high readings when cross plotted, and would form clusters towards the right of the graph.

Evaporites generally lack feldspar and sources of potassium, thorium or uranium which would give higher counts. The low counts of the gypsum facies give some indication of the mineralogy of the evaporite deposits and shows that they are not potassium bearing (Table 4.2). Further geochemical analysis would be needed to fully quantify the mineralogy.

Table 4.2 Potassium bearing evaporite minerals (after Serra, 1984)

Name	Composition	K (% weight)
Sylvite	KCl	52.44
Langbenite	$K_2SO_4(MgSO_4)_2$	18.84
Kainite	$MgSO_4KCl(H_2O)_3$	15.7
Carnallite	$MgClKCl(H_2O)_6$	14.07
Polyhalite	$K_2SO_4MgSO_4(CaSO_4)_2(H_2O)_2$	13.4
Glaserite	$(KNa)_2SO_4$	24.7

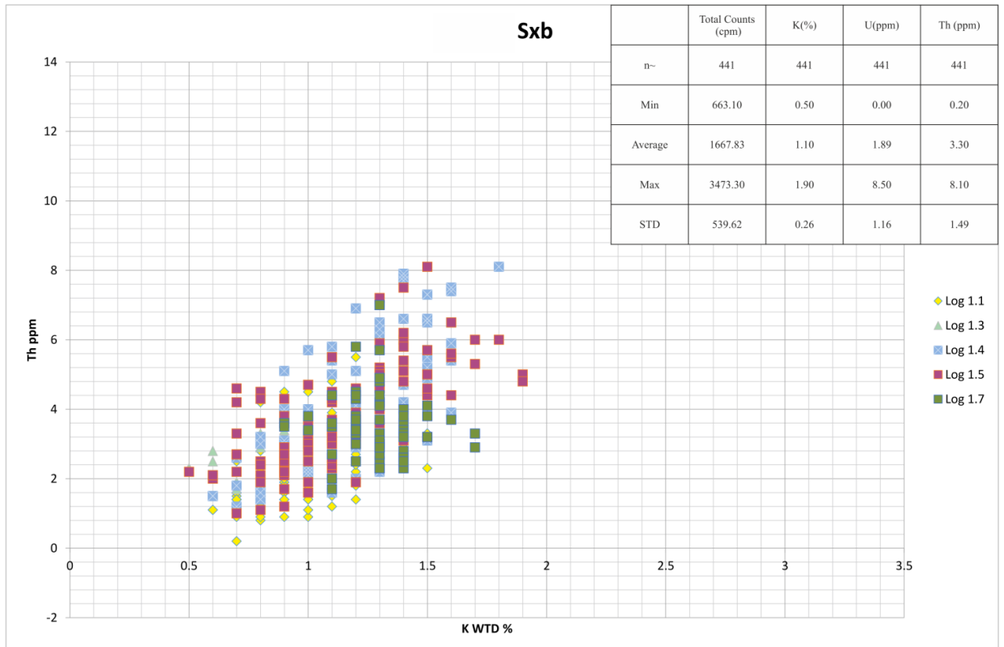

	Total Counts (cpm)	K(%)	U(ppm)	Th (ppm)
n~	441	441	441	441
Min	663.10	0.50	0.00	0.20
Average	1667.83	1.10	1.89	3.30
Max	3473.30	1.90	8.50	8.10
STD	539.62	0.26	1.16	1.49

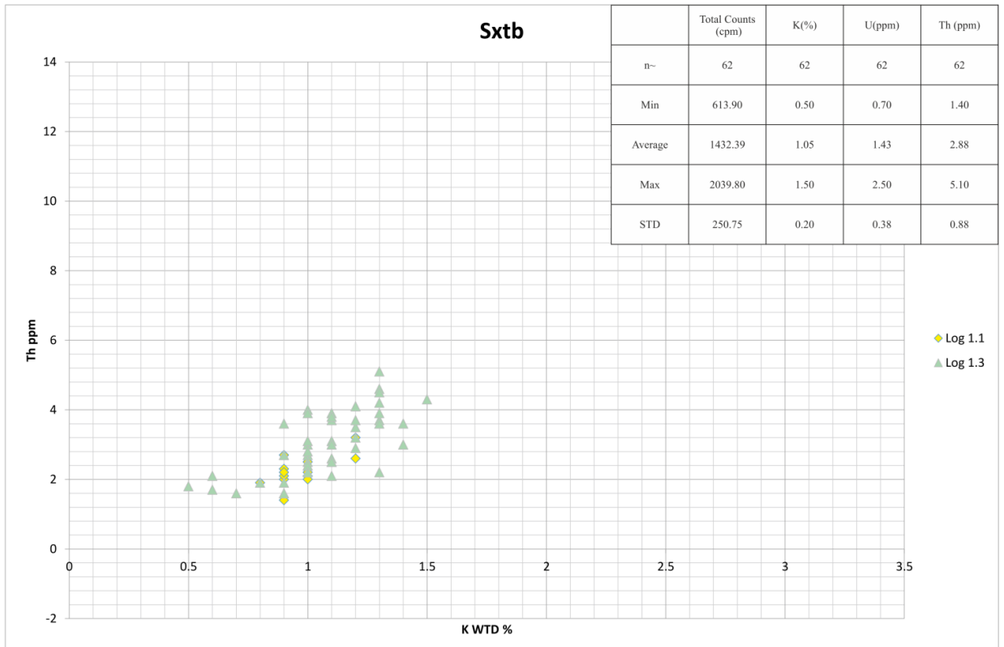

	Total Counts (cpm)	K(%)	U(ppm)	Th (ppm)
n~	62	62	62	62
Min	613.90	0.50	0.70	1.40
Average	1432.39	1.05	1.43	2.88
Max	2039.80	1.50	2.50	5.10
STD	250.75	0.20	0.38	0.88

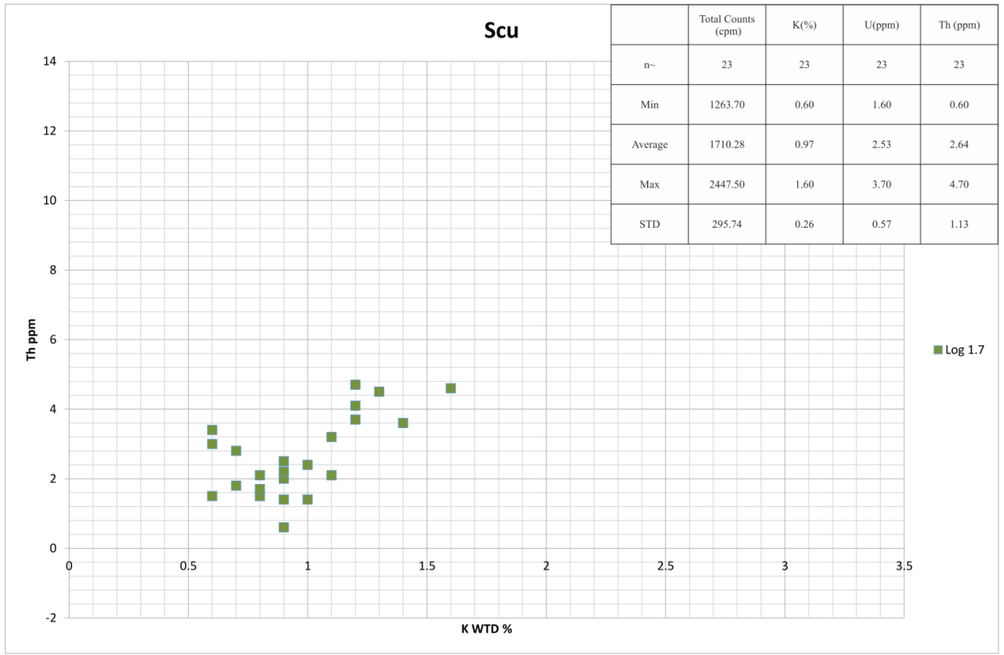

	Total Counts (cpm)	K(%)	U(ppm)	Th (ppm)
n~	23	23	23	23
Min	1263.70	0.60	1.60	0.60
Average	1710.28	0.97	2.53	2.64
Max	2447.50	1.60	3.70	4.70
STD	295.74	0.26	0.57	1.13

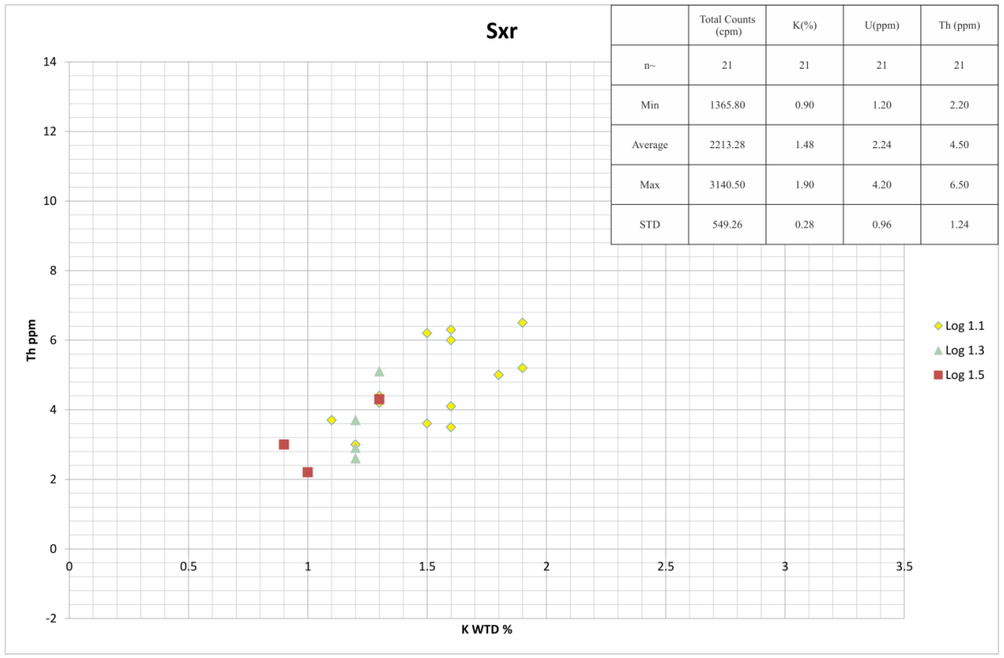

	Total Counts (cpm)	K(%)	U(ppm)	Th (ppm)
n~	21	21	21	21
Min	1365.80	0.90	1.20	2.20
Average	2213.28	1.48	2.24	4.50
Max	3140.50	1.90	4.20	6.50
STD	549.26	0.28	0.96	1.24

Figure 4.5 K:Th Cross plots for each individual facies, Location and log number is shown in the key on right hand side, values for counts, K, U and Th are shown in table, for facies codes see chapter 3.

	Total Counts (cpm)	K(%)	U(ppm)	Th (ppm)
n~	68	68	68	68
Min	1159.10	0.70	0.80	2.10
Average	2460.99	1.41	3.05	5.53
Max	4199.70	2.30	10.10	11.90
STD	696.73	0.34	1.66	2.31

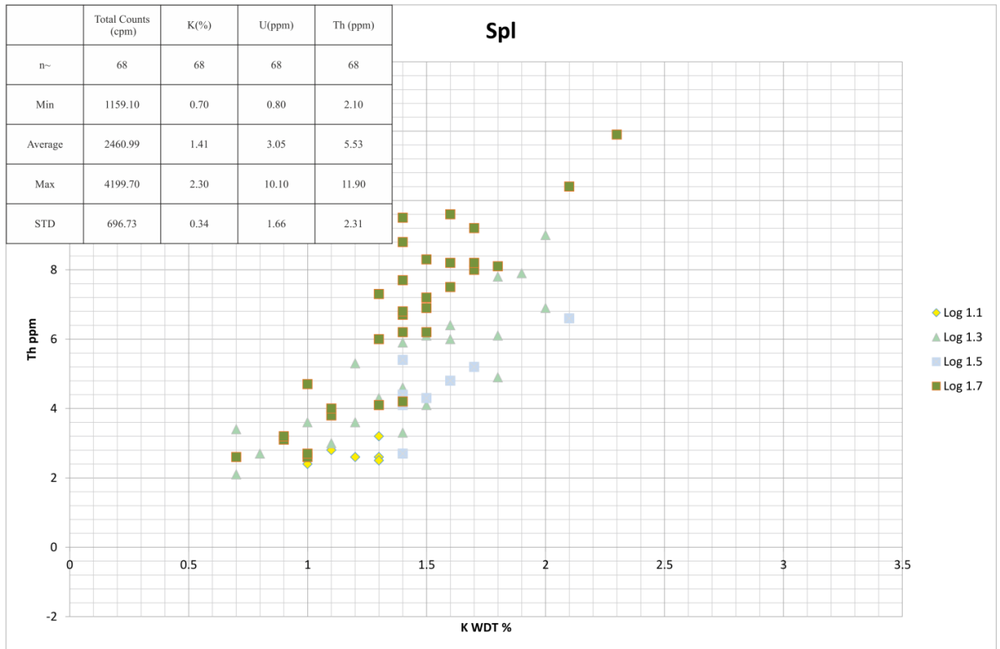

	Total Counts (cpm)	K(%)	U(ppm)	Th (ppm)
n~	88	88	88	88
Min	987.60	0.50	0.60	1.40
Average	2030.22	1.24	2.54	4.06
Max	4108.70	2.30	8.30	9.70
STD	775.75	0.39	1.51	1.96

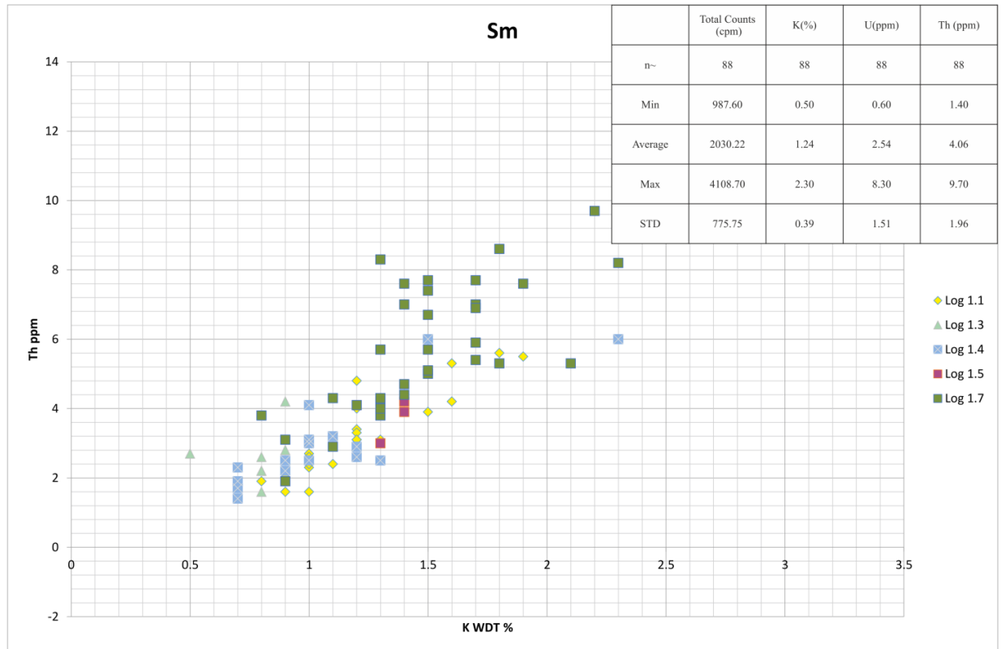

	Total Counts (cpm)	K(%)	U(ppm)	Th (ppm)
n~	185	185	185	185
Min	921.30	0.50	0.90	1.10
Average	2367.53	1.38	2.93	4.95
Max	6723.20	2.60	14.20	9.90
STD	883.27	0.38	2.16	1.85

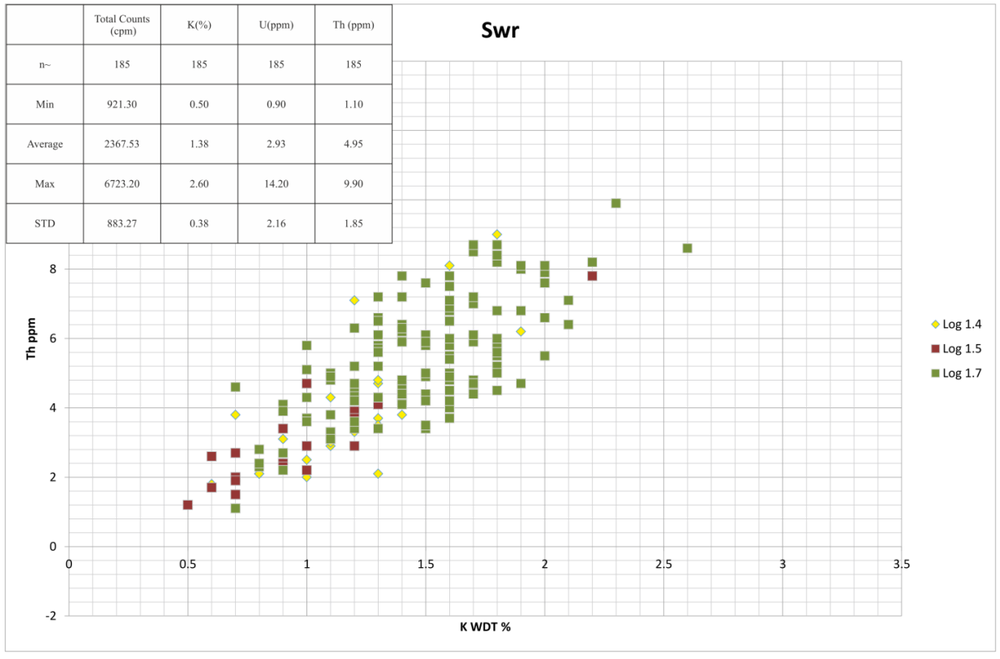

	Total Counts (cpm)	K(%)	U(ppm)	Th (ppm)
n~	137	137	137	137
Min	1395.50	0.80	1.00	2.10
Average	2434.34	1.35	3.12	5.52
Max	3940.30	2.10	6.70	9.00
STD	592.91	0.26	1.24	1.63

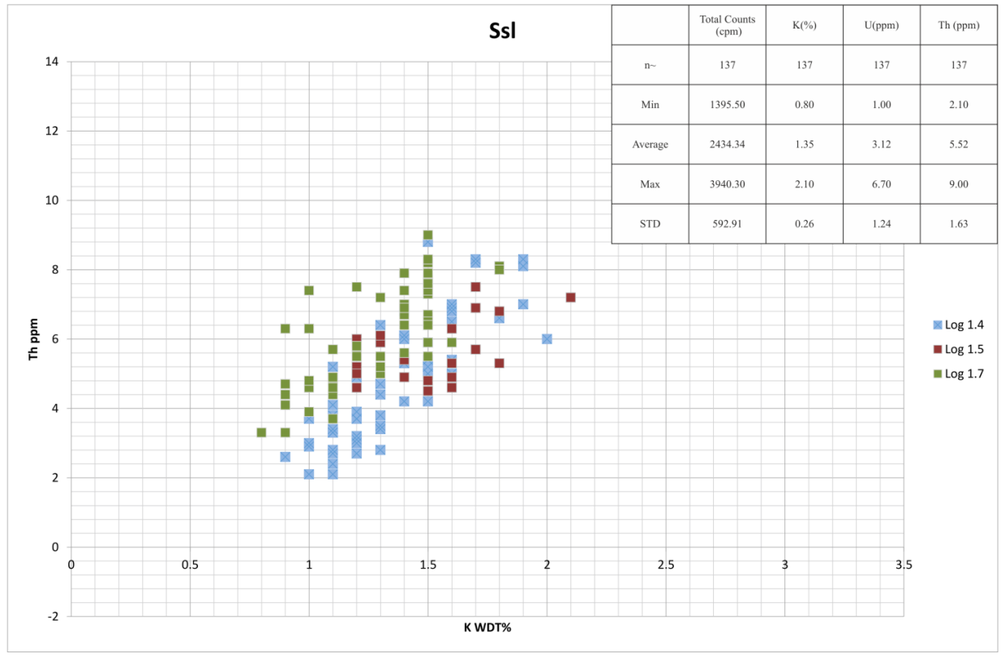

Figure 4.6 K:Th Cross plots for each individual facies, Location and log number is shown in the key on right hand side, values for counts, K, U and Th are shown in table, for facies codes see chapter 3.

	Total Counts (cpm)	K(%)	U(ppm)	Th (ppm)
n~	3	3	3	3
Min	4449.40	2.30	6.00	9.30
Average	4949.00	2.63	6.93	10.17
Max	5599.30	3.10	7.90	11.20
STD	481.39	0.34	0.78	0.78

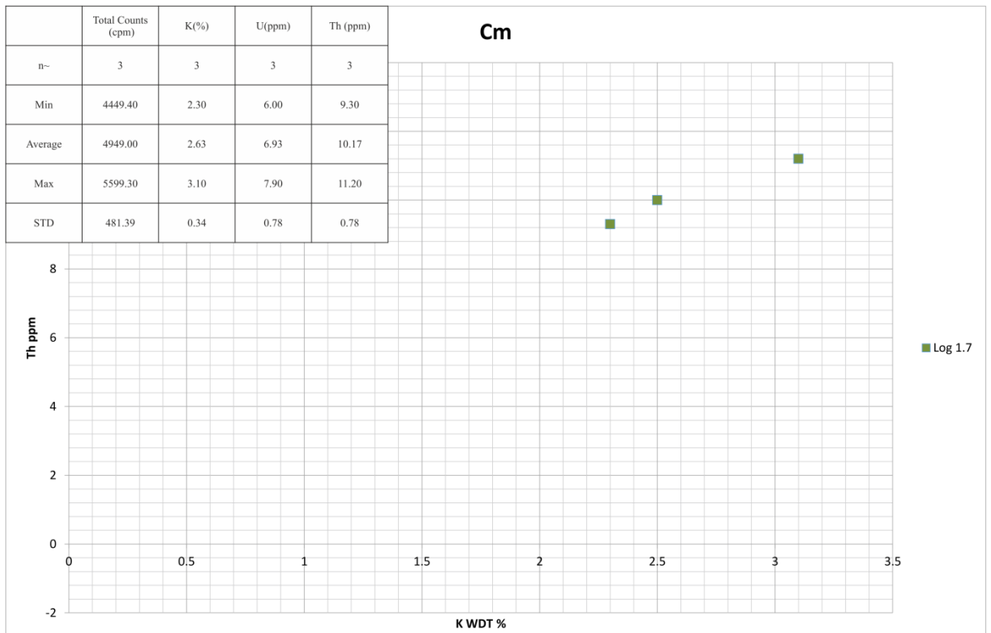

	Total Counts (cpm)	K(%)	U(ppm)	Th (ppm)
n~	66	66	66	66
Min	893.52	0.60	0.70	1.90
Average	2108.60	1.14	3.04	4.00
Max	3551.00	1.50	8.90	7.80
STD	557.26	0.22	1.67	1.21

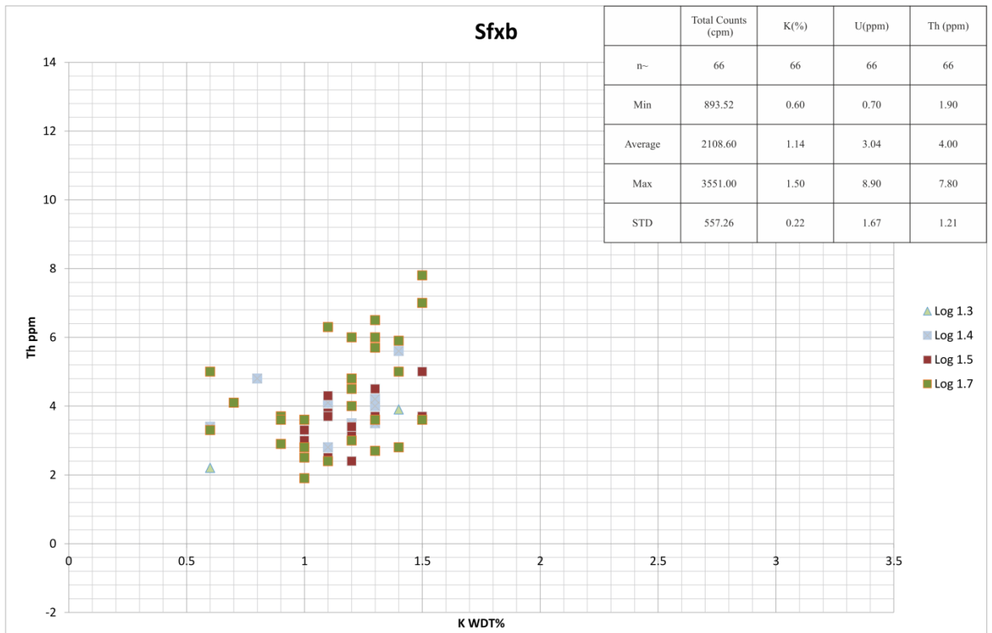

	Total Counts (cpm)	K(%)	U(ppm)	Th (ppm)
n~	5	5	5	5
Min	2878.10	1.30	4.10	6.30
Average	3713.96	1.50	6.18	7.60
Max	4245.40	1.90	8.20	8.90
STD	528.37	0.23	1.51	0.89

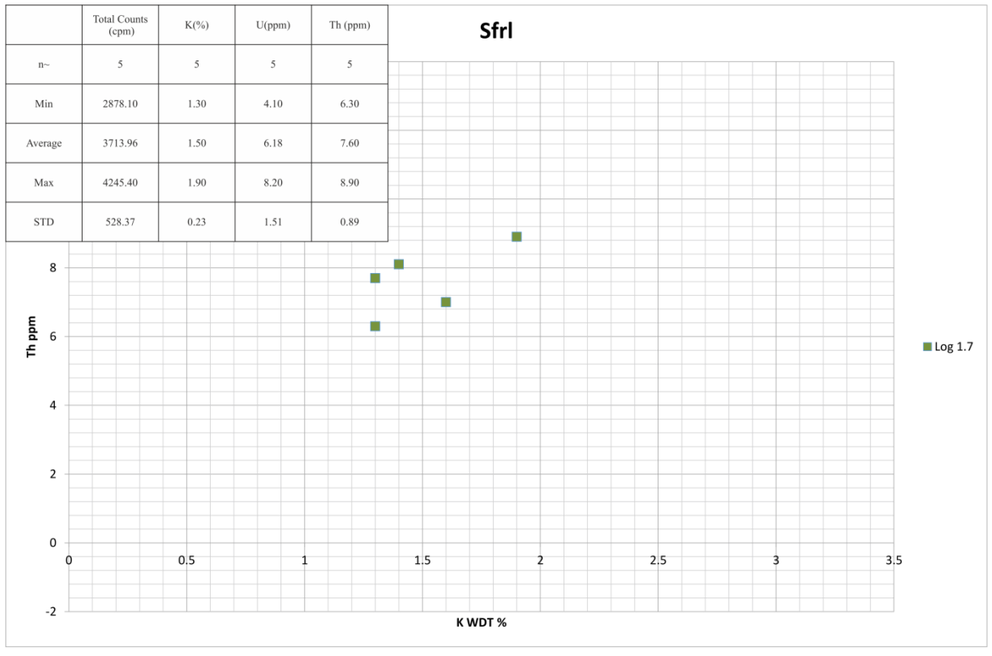

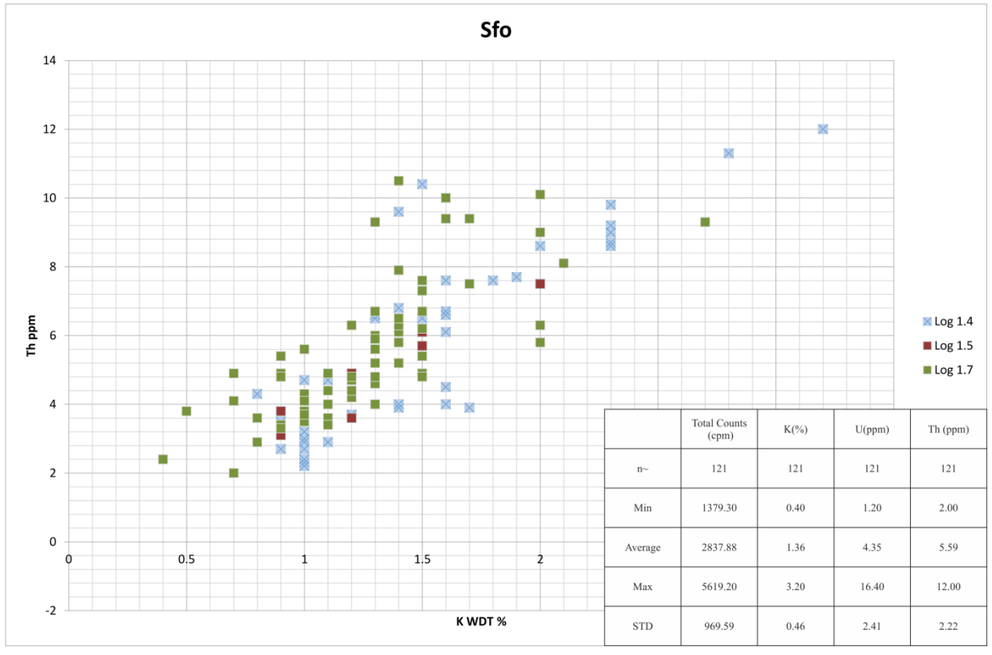

	Total Counts (cpm)	K(%)	U(ppm)	Th (ppm)
n~	121	121	121	121
Min	1379.30	0.40	1.20	2.00
Average	2837.88	1.36	4.35	5.59
Max	5619.20	3.20	16.40	12.00
STD	969.59	0.46	2.41	2.22

Figure 4.7 K:Th Cross plots for each individual facies, Location and log number is shown in the key on right hand side, values for counts, K, U and Th are shown in table, for facies codes see chapter 3.

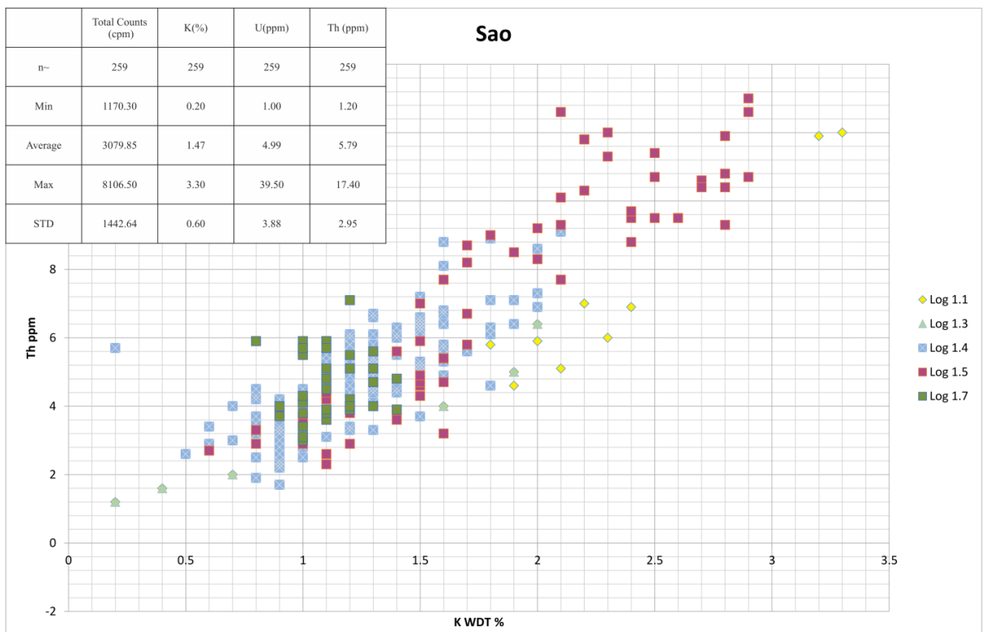

	Total Counts (cpm)	K(%)	U(ppm)	Th (ppm)
n~	259	259	259	259
Min	1170.30	0.20	1.00	1.20
Average	3079.85	1.47	4.99	5.79
Max	8106.50	3.30	39.50	17.40
STD	1442.64	0.60	3.88	2.95

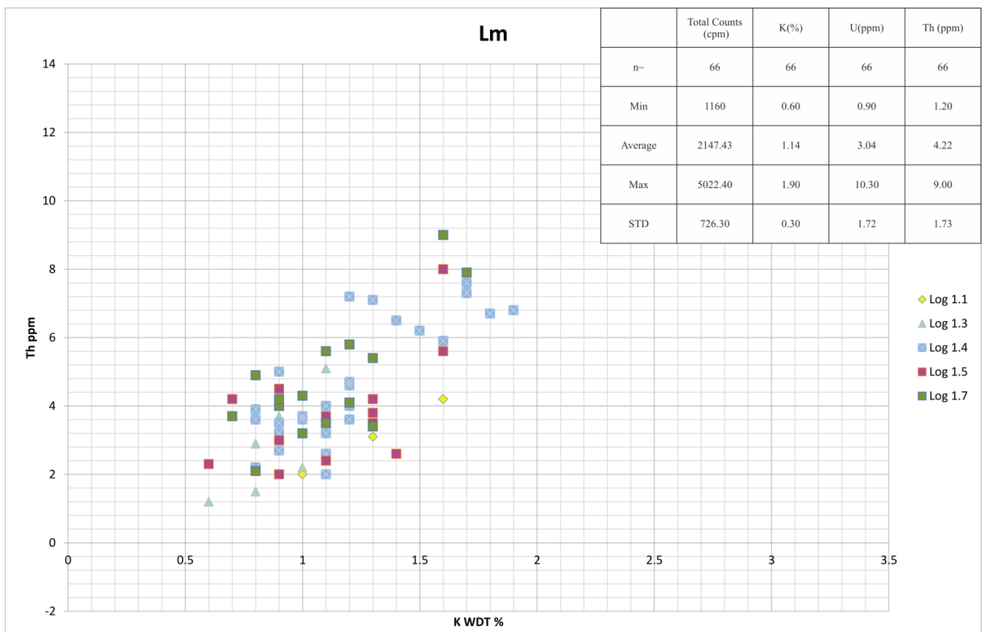

	Total Counts (cpm)	K(%)	U(ppm)	Th (ppm)
n~	66	66	66	66
Min	1160	0.60	0.90	1.20
Average	2147.43	1.14	3.04	4.22
Max	5022.40	1.90	10.30	9.00
STD	726.30	0.30	1.72	1.73

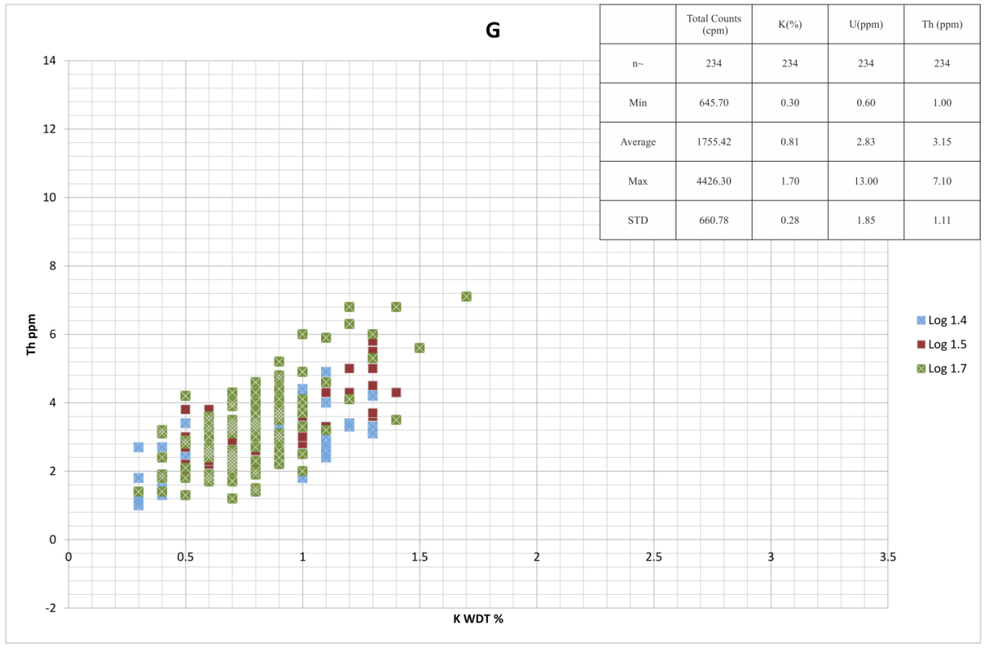

	Total Counts (cpm)	K(%)	U(ppm)	Th (ppm)
n~	234	234	234	234
Min	645.70	0.30	0.60	1.00
Average	1755.42	0.81	2.83	3.15
Max	4426.30	1.70	13.00	7.10
STD	660.78	0.28	1.85	1.11

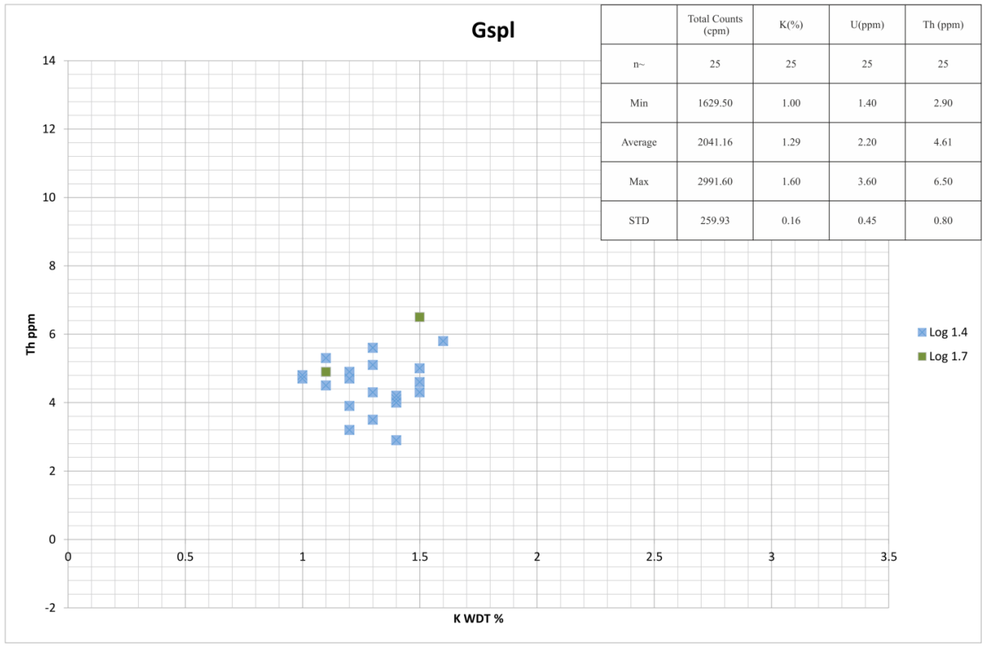

	Total Counts (cpm)	K(%)	U(ppm)	Th (ppm)
n~	25	25	25	25
Min	1629.50	1.00	1.40	2.90
Average	2041.16	1.29	2.20	4.61
Max	2991.60	1.60	3.60	6.50
STD	259.93	0.16	0.45	0.80

Figure 4.8 K:Th Cross plots for each individual facies, Location and log number is shown in the key on right hand side, values for counts, K, U and Th are shown in table, for facies codes see chapter 3.

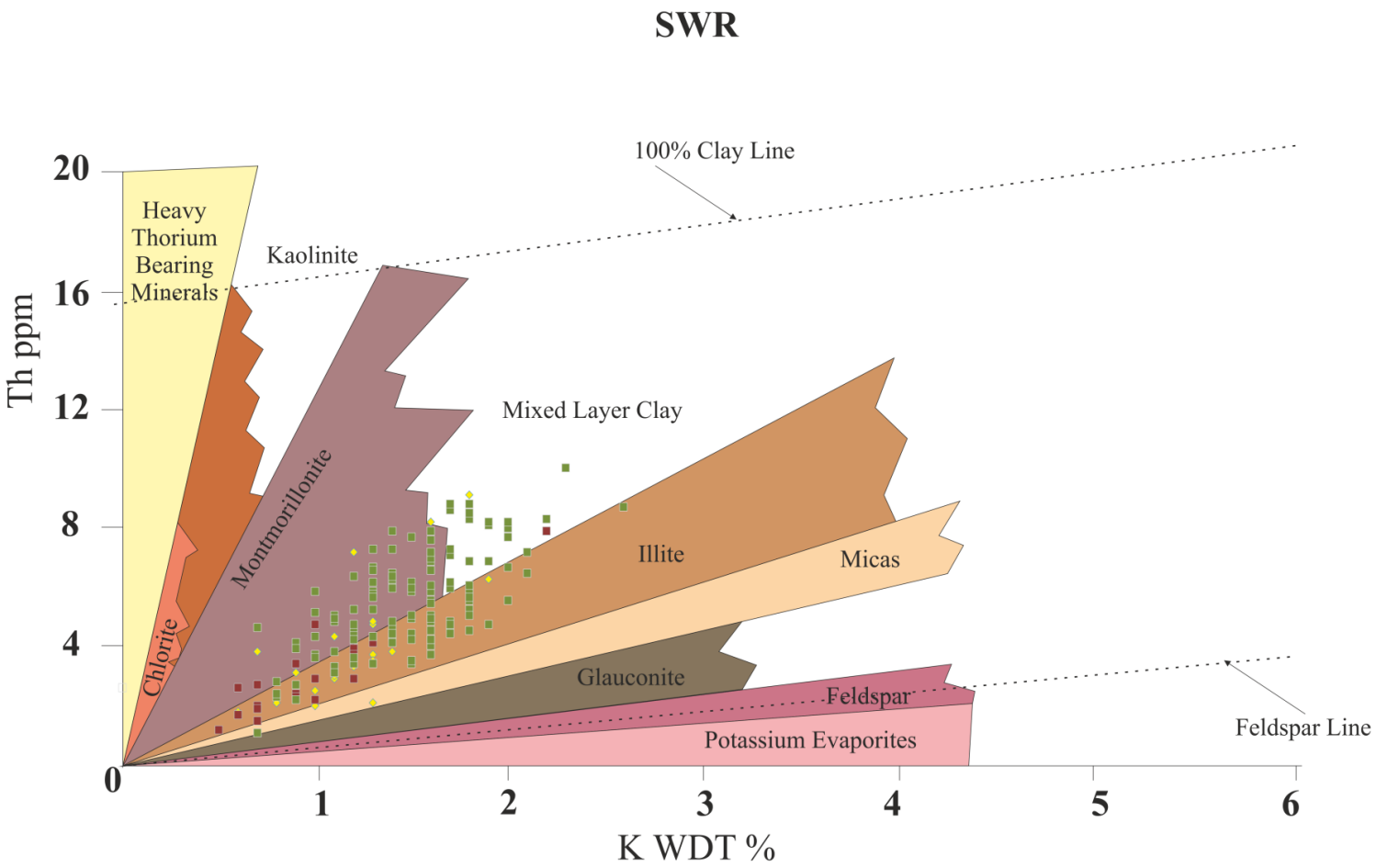

Figure 4.9 Clay typing for facies Swr

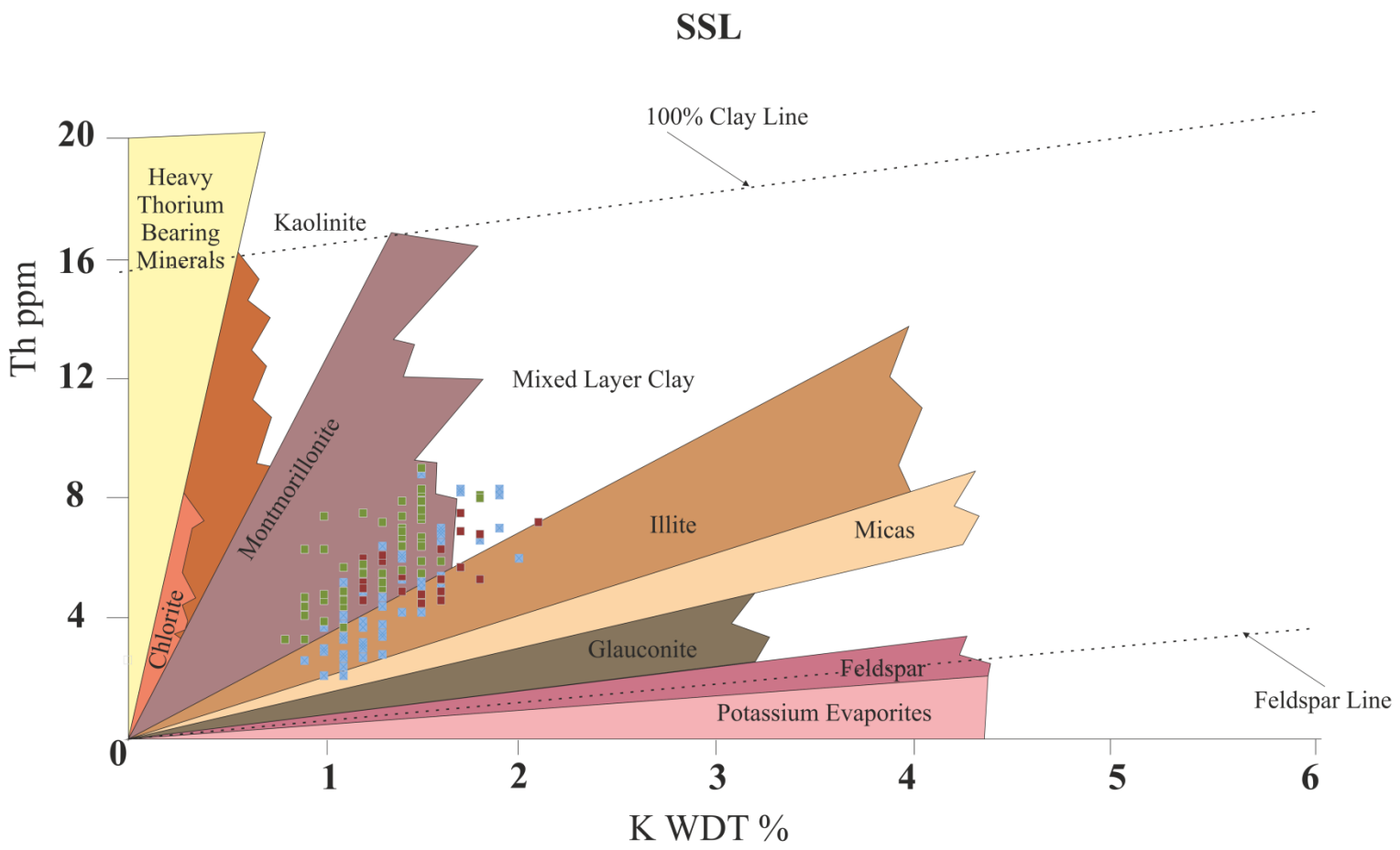

Figure 4.10 Clay typing for facies Ssl

4.5 Log Motifs

Due to the often overlapping nature and occasional lack of clear trends (Fig 4.3 4.4) in the ratios alone further gamma ray facies analysis has been conducted (Fig. 4.11, 4.12). This uses visual qualitative analysis of total counts to determine any recurring patterns and trends within the data (*Cf.* Martinius *et al.,* 2002). Unique patterns or 'log motifs' are classified from the total count curves. The shape of these motifs is determined by the natural radioactivity of the rock components and often reflects grain size trends or diagenetic effects. Grain size itself does not however, determine the gamma radiation from the rock (Rider, 1996; Martinius *et al.,* 2002). This technique coupled with the previous K:Th values cross plots provides a useful method to determine the statistical relevance of the qualitative interpretation (Myers & Bristow, 1989).

As before, the log motifs are split into broad scale depositional environments; aeolian, interdune and sandsheet, fluvial, lacustrine, sabkha, and palaeosol. These depositional environments are explained fully below.

4.5.1 Aeolian

Aeolian log motifs show generally low counts in aggrading or sweeping 'C' patterns. When compared to the sedimentary logs (Fig 4.11) the degree of foreset spacing also effects log response. Wider spaced, asymptotic foresets show log motifs with less count variability, often in a stronger 'C'-shaped pattern compared to tighter foreset bounding surfaces, which display motifs with more 'noisy' signals and that aggrade, often with higher overall counts. This is also the case with trough- cross-bedded dune forms, with have the same 'noisy' signal with slightly higher overall counts.

Bounding surface control is also picked up within the log motifs. Set, coeset, or bed bounding surfaces having higher counts, resulting in a single spike motif. This spike

is less than other similar signals resulting from interdune or sandsheet facies however. This allows the aeolian log spike to be detected fairly easily from the log signal.

Many of the aeolian dunes are strongly influenced by salt, especially within logs 1.4, 1.5 and 1.7. However, within the gamma ray signal and log motif there is a general lack of difference between the signals and counts of dunes unaffected by salt (logs 1.1, 1.3). This only manifests (see Fig 4.11) when thick veins of salt (~50 cm) are present and detected by the gamma ray tool.

4.5.2 Interdune/Sandsheet

Interdune log motifs are characterised by strong peaks (2.5k-3k counts), often singular, which fines upwards over larger deposits. Sandsheet wind ripple log motifs have similar style of log motif to that of interdunes, often arranged as signal peaks. However, the overall count ranges are greater than those of interdune deposits (3k-3k) and thicker sandsheet motifs aggrade rather than fine upwards. These log motifs also appear to match the corresponding sedimentary log response, with log signals aligning to the wind ripple laminations present within the sedimentary logs.

4.5.3 Fluvial

Small fluvial channels show an open 'C' pattern, whereas thicker deposits have a fining upwards log response. Count values are widespread and range between 1–4k. Conglomerate facies have high counts (5-6k) arranged into singular peaks, whereas ripples have lower counts (3k) in a trough style patter. However, both facies have limited data points.

4.5.4 Lacustrine

Lacustrine facies of silt (Ssl) and wave rippled (Swr) sediments have a generally aggrading trend between 2k-2.5k. However, wave ripple commonly shows

seemingly random and erratic spike in counts (up to 8k). Limestones show low counts and form trough motifs interbedded within the higher counts of Ssl and Swr facies, whereas thicker limestone deposits form wide open troughs with limited count variations.

4.5.5 Sabkha

Sabkha facies contain gypsum (G) which shows low counts and often forms blocky 'square like' log motifs. Gypsum is frequently interbedded with gypsum-bound-sandstone (Gspl) which has higher counts than gypsum (1.5-3k) and forms singular peaks which are often rounded and fairly 'open' or wide. Pedogenic (Sao) facies are also common within sabkha deposits which have high counts (3-5k) arranged into singular peaks. However, when influenced or interbedded with salt (G) the bleed effect of the measurement reduces the counts of Sao whilst often increasing the counts of G.

4.5.6 Palaeosol

Palaeosol deposits are formed of pedogenic facies (Sao, Sfo) and show high counts with a wide range (3-8k) than are most commonly present in single peaks. Where present, thicker deposits show fining upwards trends. The highest counts, present in singular peaks, are frequently associated directly with evidence of root traces and rhizoliths within the sedimentary logs.

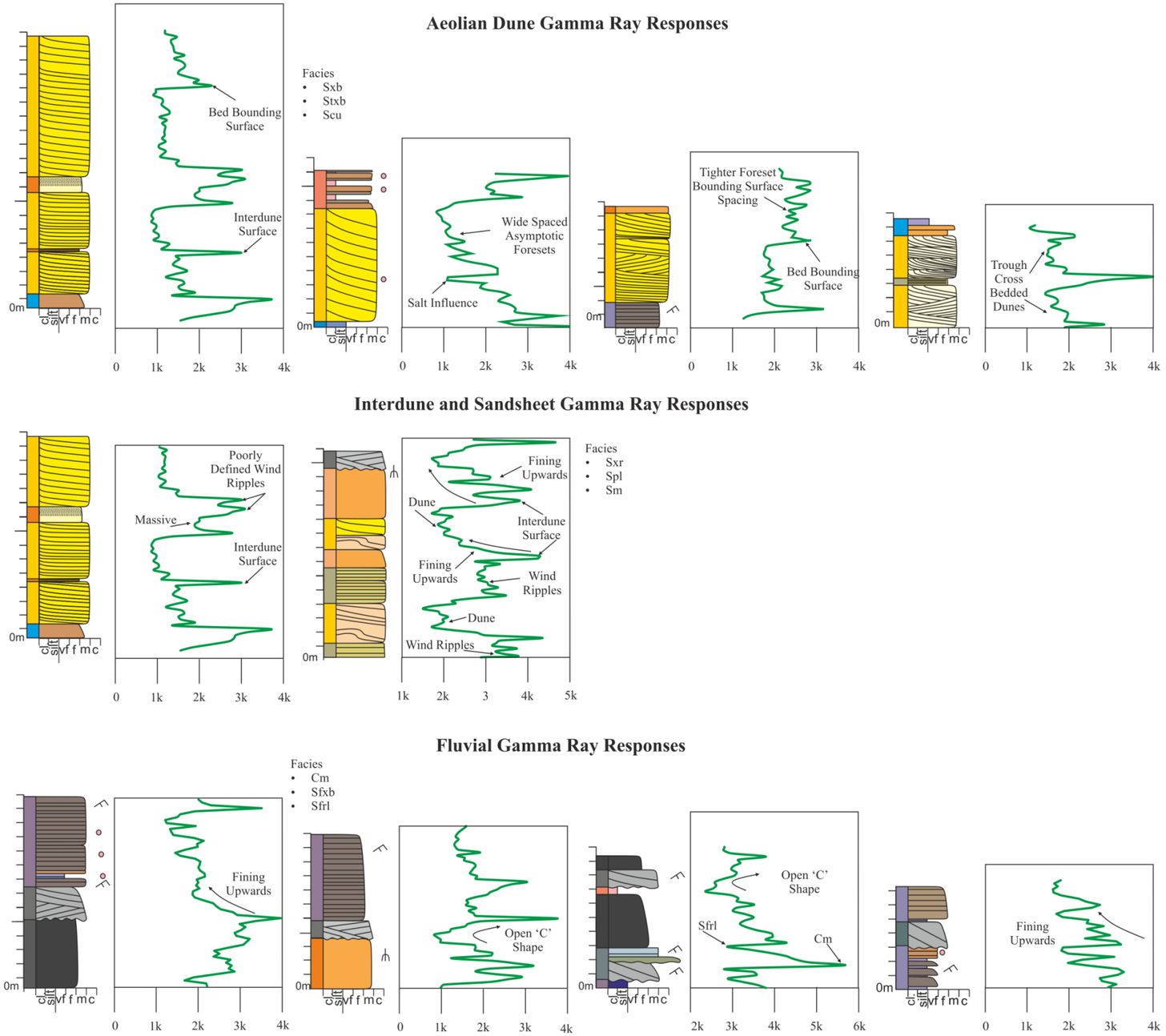

Figure 4.11 Typical log signals and motifs for aeolian dune, interdune/sandsheet and fluvial facies

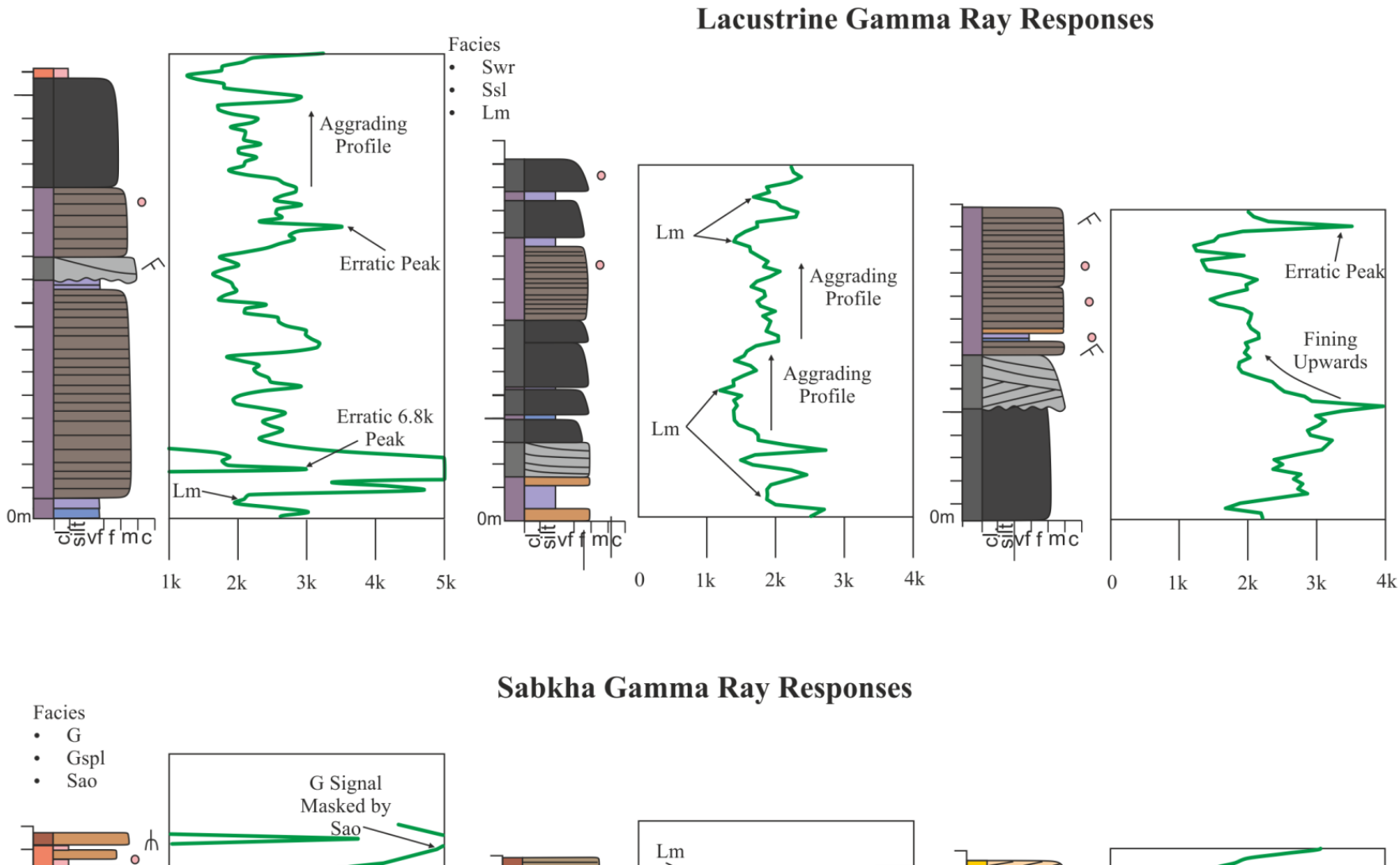

Figure 4.12 Typical log signals and motifs for lacustrine, sabkha and palaeosol facies

4.6 Link to Depositional Processes

4.6.1 Aeolian

Aeolian dunes are well sorted and composed primarily of quartz, rather than potassium bearing feldspars, reflecting the low counts present. Cluster plots of the different dune facies (Sxb, Sxtb, Scu) are hard to distinguish. There are some subtle differences within the log motifs of each facies. However, these two log motifs are still hard to distinguish from one another. Bounding surfaces and set, coeset and foreset surfaces are more easily distinguished. These surfaces act as fluid pathways and either allow or baffle flow, identification of which may be useful in reservoir evaluation. Interestingly, there is seemingly no salt influence on gamma ray results or clustering. Evaporites within the dunes associations is a common feature in log 1.4-1.7, however evaporites are completely absent in logs 1.1 and log 1.3. This is not detected within the clustering as examples from all logs are very tightly grouped together.

4.6.2 Interdune/Sandsheet

Interdunes form in areas between migrating dunes and within sedimentological data have been separated into dry, damp and wet. Within gamma ray data, this differentiation is not possible, however the generic interdune is easily identifiable by its log motif and K:Th clustering. Interdunes are regularly composed of similar material to dunes, and readily influence by water, either by rise in groundwater level or the influx of fluvial deposits through interconnected interdune corridors. This influence of water may explain the higher count values present in the interdune facies compared to dunes. Lithic and potassium bearing minerals are more common due to fluvial and water influence, and interdune sediments are often less mature than dunes as they lack many of the aeolian processes responsible for the well sorted nature of dunes. The high-low-high signature is most likely related to the opposing coeval environments, with ‘clean’ aeolian sediments being blown into interdune areas and reworked, coupled with regular influxes of potassium bearing immature sediments through fluvial processes.

Sandsheets are formed by aeolian process, where sediment supply is reduced and cannot for bedforms, often related to the margins of deserts. Although often indistinguishable from aeolian dune sediments in the field, the sandsheets have higher gamma ray values which have been previously described by North & Boering (1999), and most likely relates to increased lithic content.

4.6.3 Fluvial

Fluvial settings are common within arid basins, most often in the form of sheetfloods, which feed distal desert lakes. The material is often sourced from reworked aeolian material, but has a higher lithic content which leads to higher total counts within the gamma ray. The high counts encountered within the conglomerate facies may relate to mud rip up clasts present within, which have high potassium content, and/or from more exotic extra-clasts containing heavy mineral elements.

4.6.4 Lacustrine

Desert lacustrine systems are common within distal areas of continental basins fed by fluvial systems. The aggrading nature of the gamma signals relates to the dominant suspension settlement mode of formation of facies (Ssl, Swr). The high counts relate to higher organic content and to the more anoxic conditions found within desert lakes which often lead to higher uranium concentrations (Lüning & Kolonic, 2003). Random erratic high count spikes within Swr may relate to higher organic content and roots, due to the overall shallower depositional setting of the facies (see chapter 3). Montmorillonite and illite are commonly found within saline lakes (Brooks & Ferrell, 1970) with montmorillonite usually having the greatest concentration in higher salinity portions of lakes. Illite also commonly concentrates in the sediments of higher salinity areas (Brooks & Ferrell, 1970). Some of the illite may be authigenic, which may explain the higher percentage of illite within Swr facies, that occurs in interdune areas as well as purely lacustrine settings. Carbonates in their pure state are not radioactive, leading to their low

counts and easy to identify signals against the high background counts of the other lacustrine facies (Rider, 1996).

4.6.5 Sabkha

Sabkhas frequently contain evaporites and palaeosols. The readings for the evaporite facies (G) give the lowest counts within the study area indicating a lack of feldspar and sources of potassium, thorium or uranium minerals, Some evaporites contain potassium minerals (table 4.2). The low counts observed, however, indicate the dominance of evaporite minerals such as gypsum or anhydrite. Pedogenic facies (Sao) give high counts due to modification and frequently have higher thorium content than other facies. Within the sabkha setting pedogenic facies (Sao) are salt rich, with frequent nodules and bands of evaporites. This in turn reduces the overall signal and count range.

4.6.6 Palaeosol

Palaeosols are common features within arid continental settings and relate to modification and stabilisation of aeolian or fluvio/lacustrine sediment, often in relation to more humid conditions. Palaeosol associations have been split into two distinct facies, one more evaporitic (Sao) featuring evaporite and calcrete nodules and veins, and the other more immature (Sfo), associated with stabilisation around bodies of water. Separation of these two interpreted pedogenic facies based on either cluster plots or log motifs is difficult, as both have similar signals and responses. This may reflect the strong modification of the facies, with reworking of the previously described environments, mixing signals and creating the dispersed nature of the readings. It may be possible to interpret that the more evaporitic palaeosols plot in the lower corner of the cluster plots due to the reduced radiative emissions within them, though this is not certain.

4.7 Comparison with Recognised Sedimentary Trends

Two distinct sedimentary trends have been recognised within the study area (see chapter 3) either the erg-margin sabkha trend or lacustrine-margin sabkha trend. Using the idealised sedimentary logs from chapter 3 for each setting, an idealised gamma ray log based on the results of the work presented here has been created Fig (4.13). These trends are then compared to the complete gamma ray data set to see if comparable trends can be identified (Fig 4.14) with four potential trends from the data recognised.

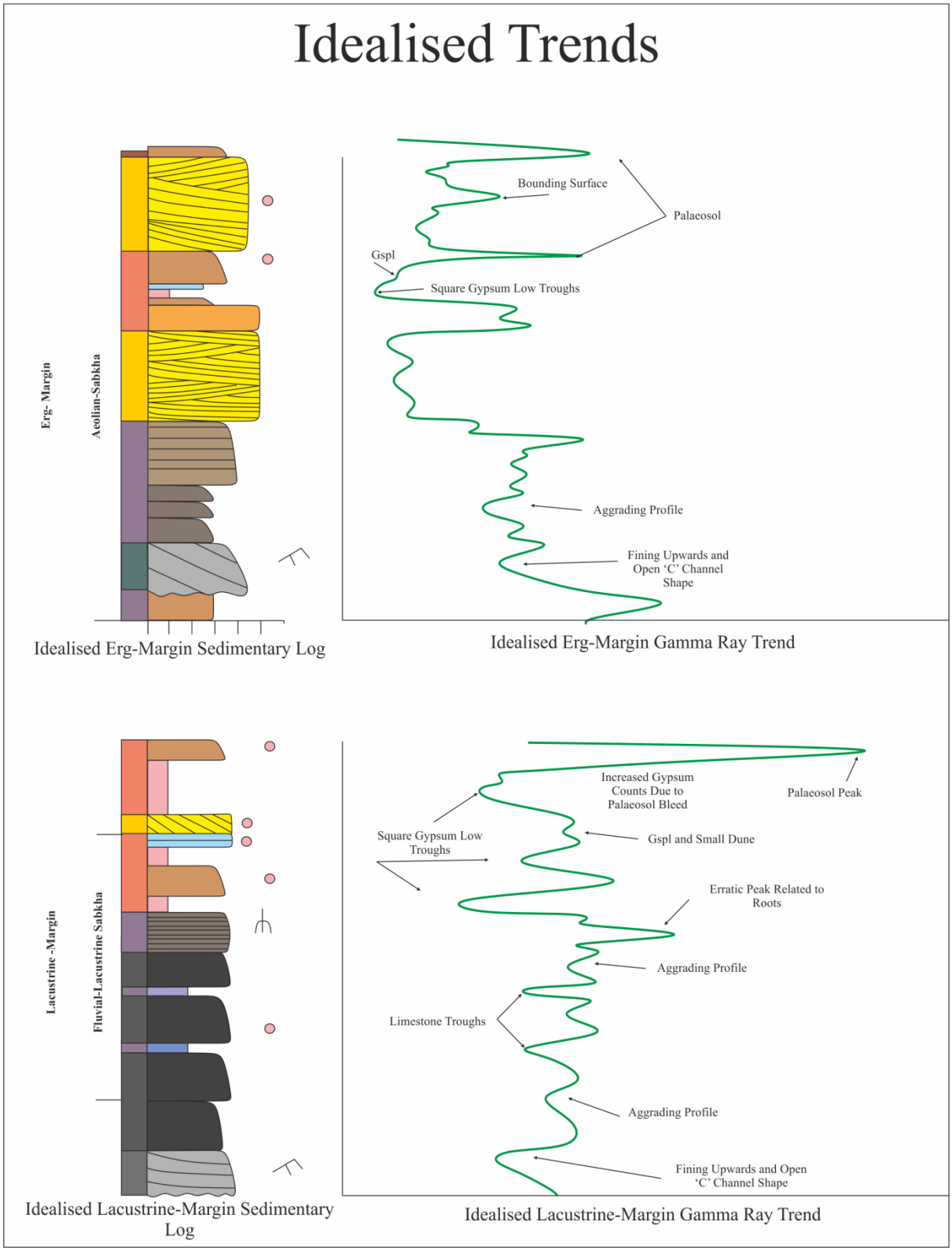

Figure 4.13 Idealised Gamma ray signatures of interpreted erg-margin and lacustrine-margin trends from the Cedar Mesa Sandstone Formation.

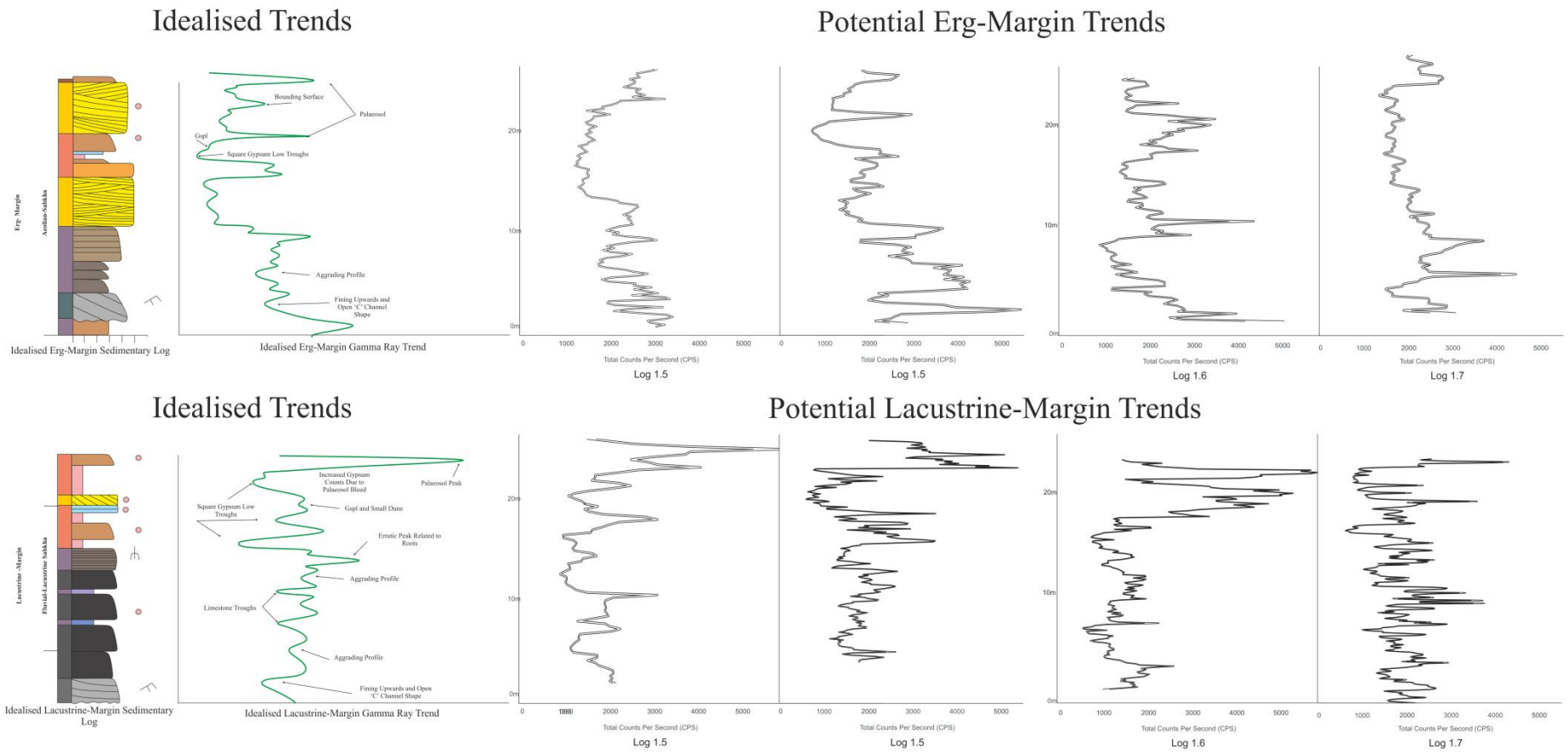

Figure 4.14 Idealised gamma ray signatures of erg-margin and lacustrine-margin trends and potential trends from the Cedar Mesa Sandstone Formation data.

4.8 Conclusions

Five spectral gamma ray logs were collected over outcrop sections of the Cedar Mesa Sandstone Formation, Utah, USA.

Determination of different facies from gamma ray logging within arid continental sediments has been shown to be difficult by previous workers (North & Boering, 1999). Initial cross plots of K:Th ratios encounter many of the same issues, and initially appears to be difficult to separate different facies (Fig 4.3–4).

With careful interpretation of the distinct log shapes and signatures or 'log motifs' (*c.f.* Martinius *et al.,* 2002) integrated with K:Th cross plots, however, distinct gamma-facies can be determined. Unique and recognisable facies have been interpreted from five logs within the Cedar Mesa Sandstone, which link to distinct depositional processes.

Cluster plotting of each facies from each separate logs shows that they are related and can be considered unique facies related to depositional processes that occur throughout the study area (Fig 4.6–8).

This work has shown that with an integrated approach it is possible to identify arid continental depositional settings and their sub environments, often down to a facies level. The primary use of gamma ray logs within the petroleum industry is for correlation. However, this is still tricky within the highly variable sediments of the Cedar Mesa Sandstone, even after gamma-facies are determined. Both the GR logs and sedimentology show evidence for cyclicity. Correlation on the basis of this cyclicity may help to smooth out some of the effects of highly variable lithology and preservation thicknesses. This is discussed in more detail in the next chapter.

This study shows spectral gamma-ray data is more useful than previously thought within arid continental settings and can be a powerful tool in interpreting basin wide facies changes in the subsurface when core or outcrop analogues are not available.

Chapter Five: Cyclicity in the Sedimentary Deposits of the Cedar Mesa Sandstone Formation

Cyclicity is easily detectable within the marine realm due to the high preservation potential, and, with the high abundance of biostratigraphical data, cycles can often be constrained temporally. In the continental realm cyclicity is typically more difficult to quantify and analyse. This chapter applies an integrated approach using gamma ray analysis and sedimentary logging, to quantifiably demonstrate the cyclicity within the Cedar Mesa Sandstone Formation and discuss it within the context of climatic and tectonic regimes.

5.1 Introduction

This chapter evaluates the temporal controls on the development of the Cedar Mesa Sandstone Formation. Lithological correlation has proven difficult as no clear trends are observed, however, within the sedimentology alternating temporal trends have been recognised and have been used as a means of correlation on the basis of the observed cyclicity.

Stratigraphical sequences and their development and evolution are controlled by the interaction of tectonic, eustatic and climatic processes (Vail *et al.,* 1991). Glacio-eustatic processes have previously been recognised as a driving mechanism for the controls on the proximal alluvial fan deposits (Gough, 2015) and the central and marginal erg deposits (Mountney & Jagger, 2004; Mountney 2006) of the Cedar Mesa Sandstone. This chapter examines, for the first time, the cyclicity detectable within the distal sabkha deposits of the formation and places them in the context of autocyclic and allocyclic controls. Time series analysis of the gamma ray data has been used to complement sedimentological interpretations and attempt to quantify

the cyclicity observed. This integrated method helps explain the roles that allogenic and autogenic processes have had in the development and evolution of the Cedar Mesa Sandstone Formation.

5.1.1 Controls on Continental Depositional Systems

Tectonics and climate are the primary controls on continental depositional systems (Qugley *et al.,* 2007), controlling both the type and amount of sediment supplied to the basin and the rate at which accommodation space is created and filled (Vail *et al* 1991). Tectonic activity creates elevated landscapes, as well as generating structural lows and depocentres, while climate influences the discharge and sediment availability.

5.1.2 Tectonics and Accommodation

Tectonics are recognised as a primary control on sabkha formation by generating tectonic lows related to subsidence and sagging in which water can pool and subsequently evaporate (e.g. Mertz & Hubert, 1990). Tectonic uplift increases the potential for subsidence derived accommodation creation via flexural subsidence (Qugley *et al*., 2007).

Deposition of the Cedar Mesa Sandstone Formation coincided with a reduction in the subsidence rate and accommodation space generation of the Paradox Basin. A maximum of ~2.7 km of sediment was deposited at an estimated sedimentation rate of 84 m/myr by the end of the Pennsylvanian (Huntoon *et al.,* 1996; Nuccio & Condon, 1996) compared to 1.8 km of deposited sediment at a rate of 40 m/myr during the Permian as a result of the Paradox Basin being overfilled (Condon, 1997; Barbeau, 2003; Huntoon *et al.,* 1996; Nuccio & Condon, 1996). This overfilled state resulted in a basinward progradation of facies due to limited accommodation space (Mountney & Jagger, 2004) and may indicate that basin-scale tectonics has a

negligible effect on the preserved deposits, acting only as a means of generating accommodation space through a relatively constant subsidence rate.

5.1.3 Climate

Climatic variations play a key role within arid continental settings, effecting the preserved architecture, facies distributions and stratigraphy of a succession.

During periods of relative humidity, increased discharge rates leads to higher water table levels and deposits indicative of fluvial and lacustrine systems. Fluvial systems prograde resulting in increased channel facies, which feed the expansion of desert lacustrine systems, characterised by fine grained suspension settle facies. Aeolian deposits are often supressed by high water tables resulting in deflation and increased sandsheet development (Howell & Mountney, 1997).

During arid periods, discharge rates fall and fluvial systems are shut down, desert lakes are starved and contract, often becoming hypersaline resulting in the formation of continental sabkhas in the form of saline pans and mudflats. Water table levels drop, resulting in a large increase in sediment supply, often in the form of re-worked fluvial material, available for aeolian transport which fuels the expansion and growth of aeolian dunes and dune fields (Howell & Mountney, 1997).

Response of sabkhas to climatic change

Sabkhas are very susceptible to climate change, and within a typical arid continental basin, the migration of facies belts related to climatic shifts can be predicted (Fig 6.1). Sabkhas form around the edges of desert lakes during arid periods with frequent adhesion structures from wind-blown sand and mud (Nagtegaal, 1973; Olsen *et al.,* 1989) and haloturbation and enterolithic structures (Glennie, 1970). Increased aridity results in contraction of playa lakes and a basinward migration of sabkha facies (Howell & Mountney, 1997). Vertically this is represented by a

transition to sandier facies, commonly sandsheets, which show evidence of wind rippling. Dependant on sediment supply, aeolian dunes may also be present as they migrate over the former sabkha (Howell & Mountney, 1997). A switch to more humid conditions leads to water table rise and flooding by expanding lakes where suspension facies will dominate, with fluvial facies also likely due to increased run-off from the basin hinterland (Howell & Mountney, 1997).

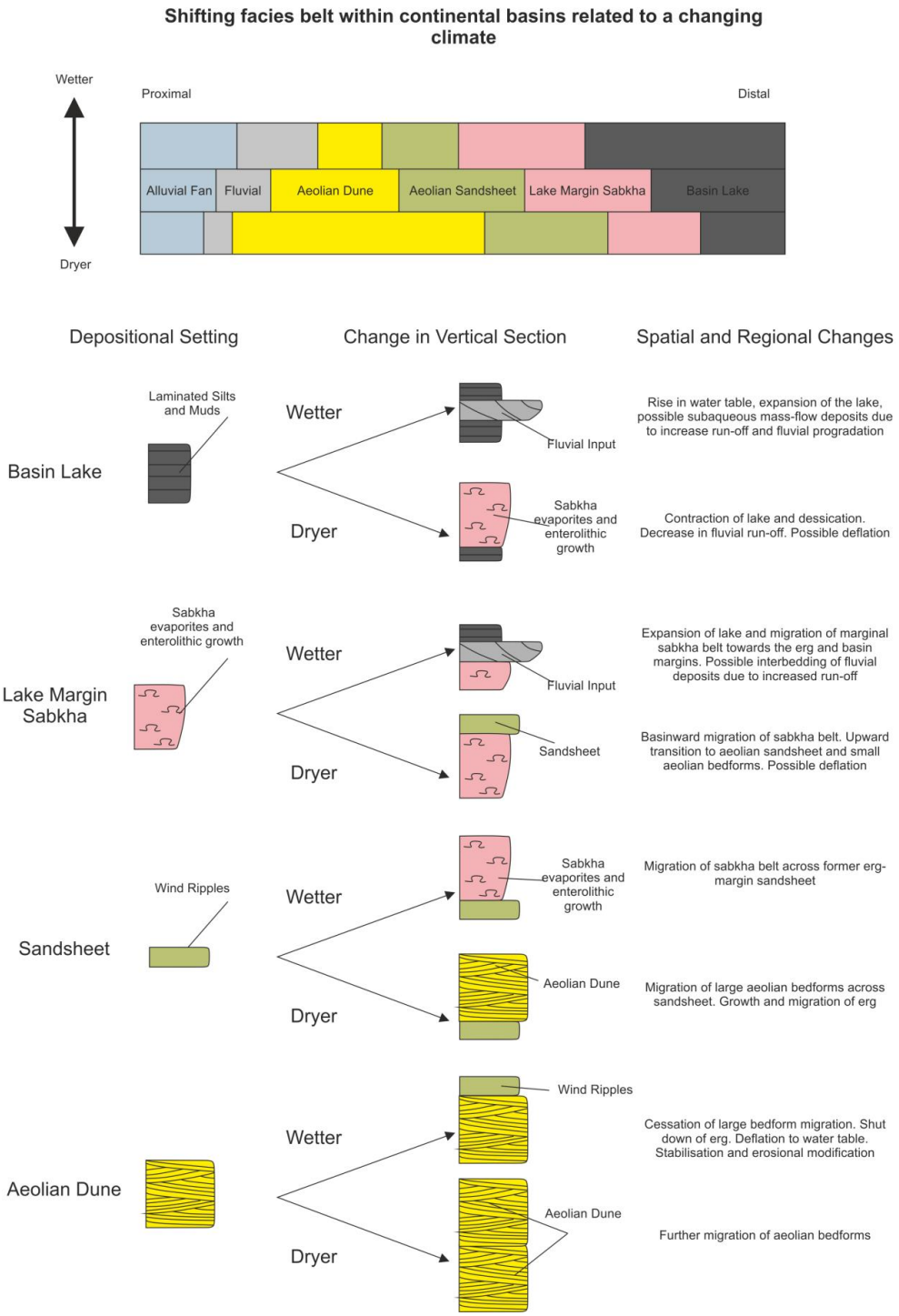

Figure 5.1 Response of arid continental basin sediments to shifts in climate (after Howell & Mountney, 1997).

Theoretical models to account for the sediments preserved within arid continental basins have been developed by Howell & Mountney (1997) (Fig 5.2) by plotting

accommodation creation and sediment supply against a time scale in which relative climate fluctuates cyclically for both erg and sabkha settings.

Within these models subsidence is treated as a constant and time is considered in the context of absolute changes in climate. Each environment will result in predictable but different changes in net sediment flux, modelled as sinusoidal curves. Sediment supply is directly related to the depositional process and the climate, with periods of positive and negative budget shown, where the supply curve is above or below the accommodation line. Idealised preserved sediment columns and the expression of preserve climatic cycles are also shown (Howell & Mountney, 1997).

Within the erg environment (Fig. 5.2A) during humid periods sand is stabilised by vegetation due to high water tables, resulting in the creation of more accommodation space than sediment accumulation. During subsequent arid periods, large aeolian bedforms rapidly prograde into the area and fill the space created. When accommodation space is filled further sediment is bypassed and an erosional supersurface may form at or close to the point of maximum aridity (Howell & Mountney, 1997; Kocurek, 1988), or the erg retains a positive relief until the ensuing wet period, where erosional modification and subsequent stabilisation will form a supersurface (Loope, 1984; Talbot, 1985). In both cases a sandsheet is deposited above a supersurface through the subsequent wet period (Howell & Mountney, 1997).

This interaction between climate and sediment supply preserves depositional cycles that show drying upward motifs, where the majority of sediment is deposited during short periods of time with most of the time encapsulated within the supersurface and the overlying sandsheet (Howell & Mountney, 1997; Havholm & Kocurek, 1994).

In the lake and marginal sabkha settings (Fig. 5.2B) sedimentation is usually slow with little variation. Aggradation occurs where sediment infilling more or less matches accommodation space creation, which results in symmetrical preserved cycles as the accommodation space is not always exceeded (Howell & Mountney, 1997). Drying upwards motifs indicate that accommodation space has been exceeded, and will occur at or near the dry maxima (Howell & Mountney, 1997).

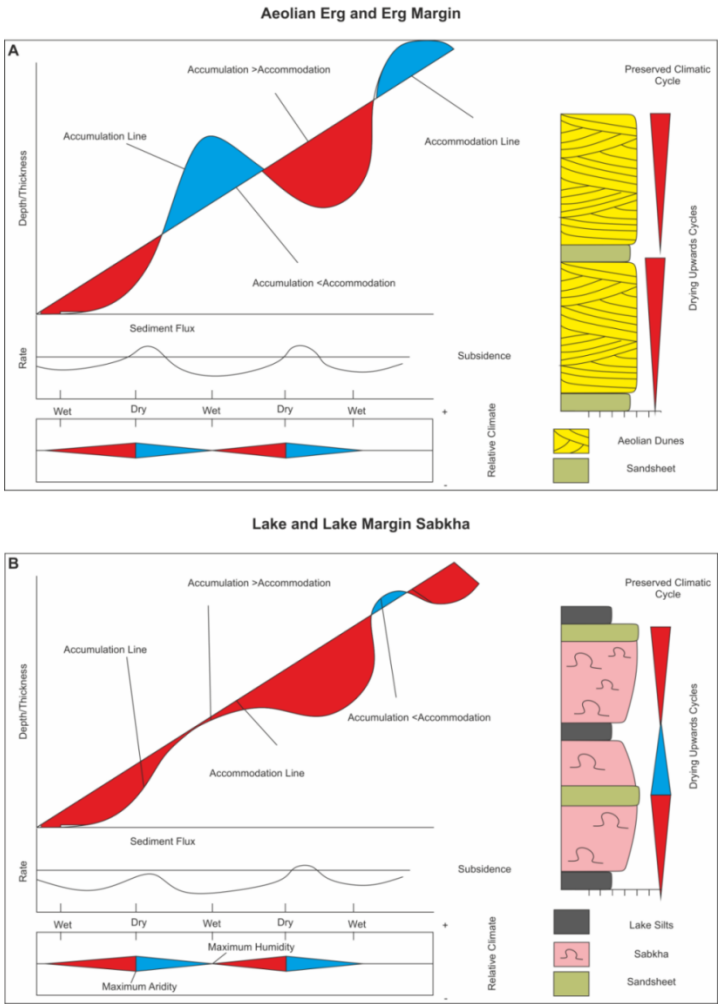

Figure 5.2 theorethical modles exaplaning how climate cyclicity affects the deposits preserved in arid continental sequences. (A) Model showing erg response to climatic shift and the resulting changes in sediment supply on accomodation and accumulation. (B) Model detialing the response of desert lakes and sabkhas to climatic shifts (After Howell & Mountney, 1997)

5.2 Temporal Evolution of the Cedar Mesa Sabkha

Temporal changes in sedimentary style within arid continental basins reflect episodic variations in allocyclic-controls combined with autocyclic processes of deposition (Cecil, 2003). The logged sedimentary successions through the sabkha-dominated succession of the Cedar Mesa Sandstone show marked and cyclic variations between water-derived or non-water-derived sediments that describe cycles of wetting and drying of the environment.

Two sabkha trends have been identified and described in Chapter Three, the 'erg-margin sabkha' and 'lacustrine-margin sabkha'. Each model shows temporal changes related to deposition within more arid or humid conditions. These trends are described below, with interpretative models of their temporal evolution.

5.2.1 Temporal Changes in the Erg-Margin Sabkha Trend

At a time of high humidity, the erg-margin sabkha was influenced by a wet marginal aeolian erg interacting with limited ephemeral fluvial systems (e.g. Mountney & Jagger, 2004) that fed small saline lakes in interdunal areas. Sabkha development was limited, with lake-marginal areas characterised by vegetation and the formation of soils. Evidence for the evaporitic nature of the system as a whole is limited to gypsiferous nodules and calcrete development within soils (facies Sao and Sfo). As the climate dried, aeolian dunes increased in magnitude and frequency, and became contiguous, forming dune fields dominated by straight-crested dunes evolving through time into sinuous-crested forms with well-developed dune plinths. Water-derived sediments were deposited within laterally restricted and isolated interdune areas surrounded by sabkha facies.

Although water plays a role in the formation of sediments within the erg-margin trend, the dominant sediment transport processes are wind-driven, with increases

or decreases in the amount of water, which are likely the result of variations in the elevation of the water table, rather than sustained surface flow feeding significant and long-lived bodies of water. Most evaporite deposits within this trend are thin and isolated, hosted within interdune areas.

In the preserved deposits of this setting (Fig. 5.3), aeolian and lacustrine sediments dominate. Sabkha associations are typically extremely limited to absent, despite the fact that preserved aeolian sediments indicate their coeval presence through evidence of extensive aeolian–sabkha assemblages. This suggests that sabkha deposits in this setting have low preservation potential, perhaps as a consequence of the high mobility and erosional potential of migrating aeolian dunes as the environment dries.

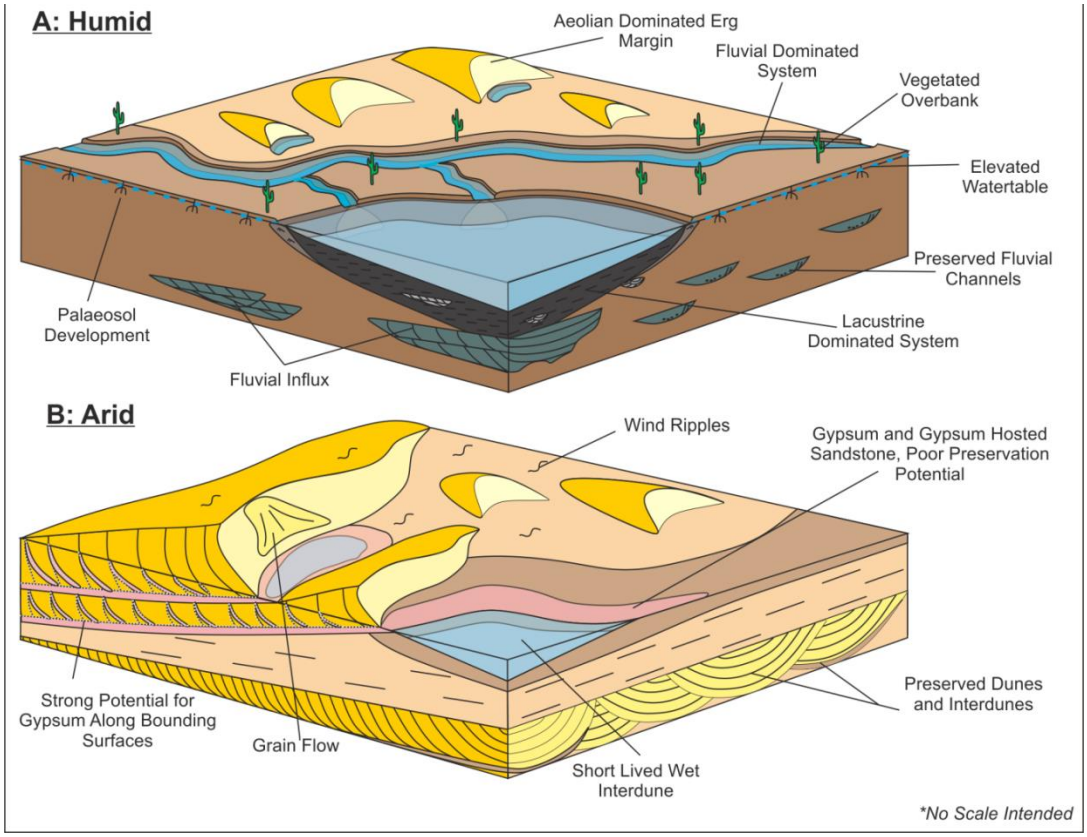

Figure 5.3 Temporal variations between humid and arid times within the erg-margin sabkha trend

5.2.3 Temporal Changes in the Lacustrine-Margin Sabkha Trend

At a time of high humidity, the lacustrine-margin sabkha was dominated by fluvio-lacustrine systems. Aeolian dunes were small-scale, barcanoid and strongly isolated between well-developed fluvial systems and associated vegetated overbank. Around the lake margins, the fluvial deposits of unconfined flow produced sediments conducive to vegetation growth, and distal lacustrine settings were dominated by clastic sediment from fluvial input, despite the salt concentration in the water. As the environment dried, the lake contracted. By a time of maximum aridity extensive lake-marginal saline mudflats developed over the edges of the lacustrine depression. Surface and enterolithic mineral growth in these areas severely limited the sediment that is available for aeolian transport, and trapped much wind-blown sediment on damp surfaces. Consequently, the dune field showed little to no growth as the environment dried. Fluvial systems incised and straightened in response to lake base-level drop, isolating the surrounding sabkhas from fluvial flooding, severely reducing clastic dilution of the evaporitic sediments, and further restricting the aeolian sediment budget. In the lake, a lack of clastic input from fluvial systems, coupled with concentration of dissolved salts as the water evaporated, produced a saline pan with lacustrine carbonate precipitation, followed by gypsiferous sediments dominated first by rafts formed on the lake surface and later by bottom nucleating sediments. Finally, lacustrine derived gypsum deposits are superseded by those of the aggrading sabkha as the lake contracts completely.

In the preserved deposits of this setting (Fig. 5.4), lacustrine and sabkha sediments dominate with somewhat limited preserved evidence for aeolian sediments. This is despite the switch to arid conditions portrayed by the succession and evidence for significant drying displayed by lacustrine-sabkha assemblages. This most likely results from a lack of significant dune-field development because of limited

sediment available for aeolian transport, rather than poor dune preservation potential.

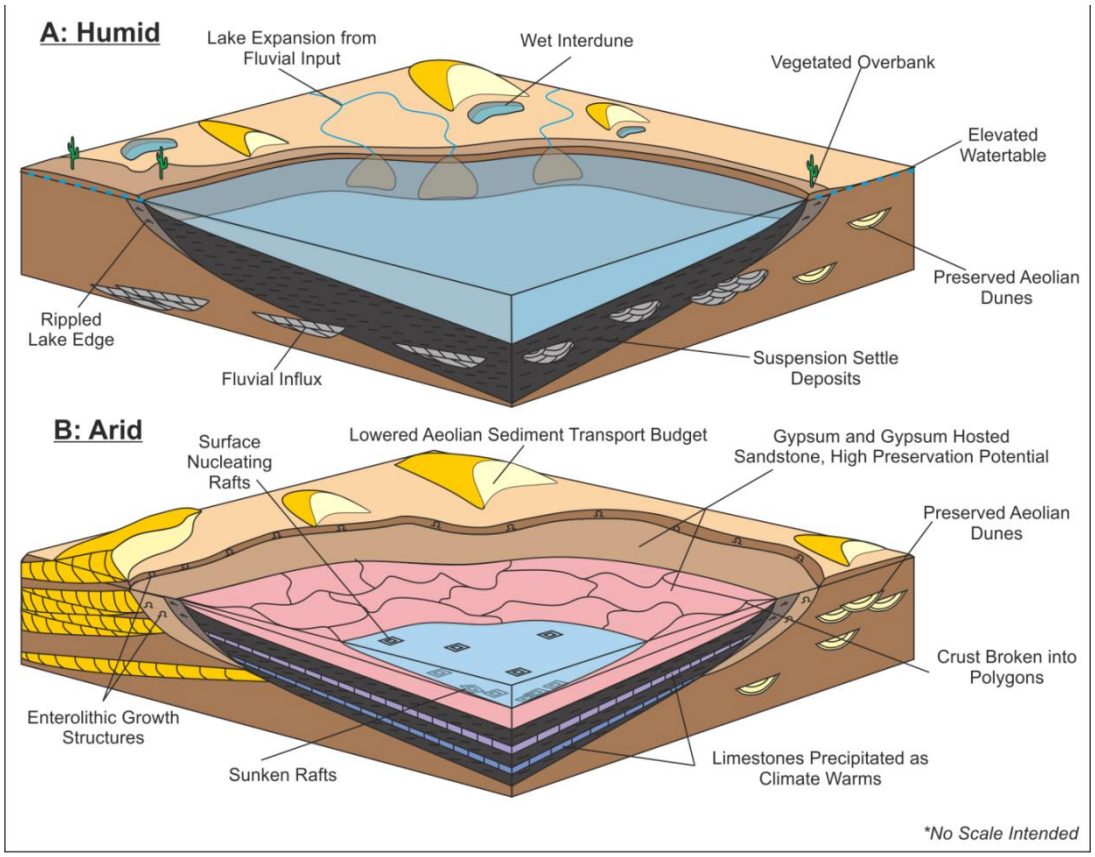

Figure 5.4 Temporal variations between humid and arid times within the lacustrine-margin sabkha trend

5.3 Arid Continental Cyclicity

Lithostratigraphy and sequence stratigraphy have limited application in arid continental settings due to the combined influence of localised autogenic and sedimentation variations and larger allocyclic processes, which can lead to spatial and temporal variations within the depositional system (Fig 5.5).

Multiple depositional environments may also exist within continental basins, the Cedar Mesa Sandstone Formation for example has coeval proximal alluvial fans, aeolian dune deposits and distal sabkha settings. Each setting is spatially

constrained and lacking lateral continuity, thus hindering lithostratigraphical correlation.

Periods of depositional hiatus or erosion are often prevalent within continental settings (Shanley & McCabe, 1994), present as supersurfaces within aeolian deposits (Langford & Chan, 1989). These frequent time gaps coupled with lack of reliable biostratigraphical and dating markers in arid continental settings again pose problems for lithostratigraphical correlation (Fig 5.5).

To overcome these limitations cyclostratigraphical models are used (Miall 1990). These models use climatic alterations to establish a context in which correlations can be conducted and used to interpret cyclicity on a basin scale. The environmental interactions observed in field data, and temporal variations interpreted from log data provide a means of characterising a range of sedimentary relationships and their deposits that typify evaporitic/clastic interactions involving sabkhas locally. However, to determine these larger scale relationships within a regional context, cyclicity must be used to provide a framework for recognising contemporaneous deposition.

Associations have been assigned a relative dryness number from driest 0 (aeolian dune) to wettest 10 (suspension settle) in order to generate a relative humidity curve (Fig 5.6).

By examining breaks (sudden wetting) within the relative humidity curve and the changing pattern of sedimentary style, up to five cycles can be recognised across the study area. Complete cycles show drying upwards trends only and consist of a lower wetting portion, which dries upwards until a sudden break and wetting, representing the start of the next cycle (Fig 5.5). Within the dominant erg (logs 1.0–1.3) and lacustrine settings (log 1.9) generic and often subtle drying upwards trends occur, which represent gradual shifts in facies due to climate fluctuations between

wet and dry periods. However, the host environment (lacustrine or erg) remains constant. Within the sabkha margin (logs 1.4–1.8) two distinct drying upwards trends exist with well-defined sedimentology.

These represent either lacustrine-margin or erg-margin sabkha trends bound by points of maximum aridity, and can be recognised and correlated across the sabkha margin (Fig. 5.6). Wetter periods of time are characterised more readily by lacustrine-margin sabkha systems and dryer periods of time by erg-margin-hosted sabkha systems. Spatial changes in deposits are also seen, with the dryer portions of the cycles thinning towards the lacustrine dominated section (Log 1.9) and the wetter portions increasing. (Fig. 5.5). Furthermore, if each site is considered in isolation, each of the five drying upward cycles displays sedimentology that indicates a progressively wetter setting than that of the previous and underlying cycle, suggesting a large-scale wetting-upward trend for the Cedar Mesa succession as a whole (Fig. 5.6).

A correlation of this nature provides a basis for interpreting coeval settings across the study area. It demonstrates that the temporal trends recognised and the environmental interactions they contain, are not separate distinct sabkha settings but reflect end member settings for a continuous spectrum of coeval sedimentary interactions from an aeolian dominated setting in the north of the study area, to a fluvio-lacustrine dominated one in the south.

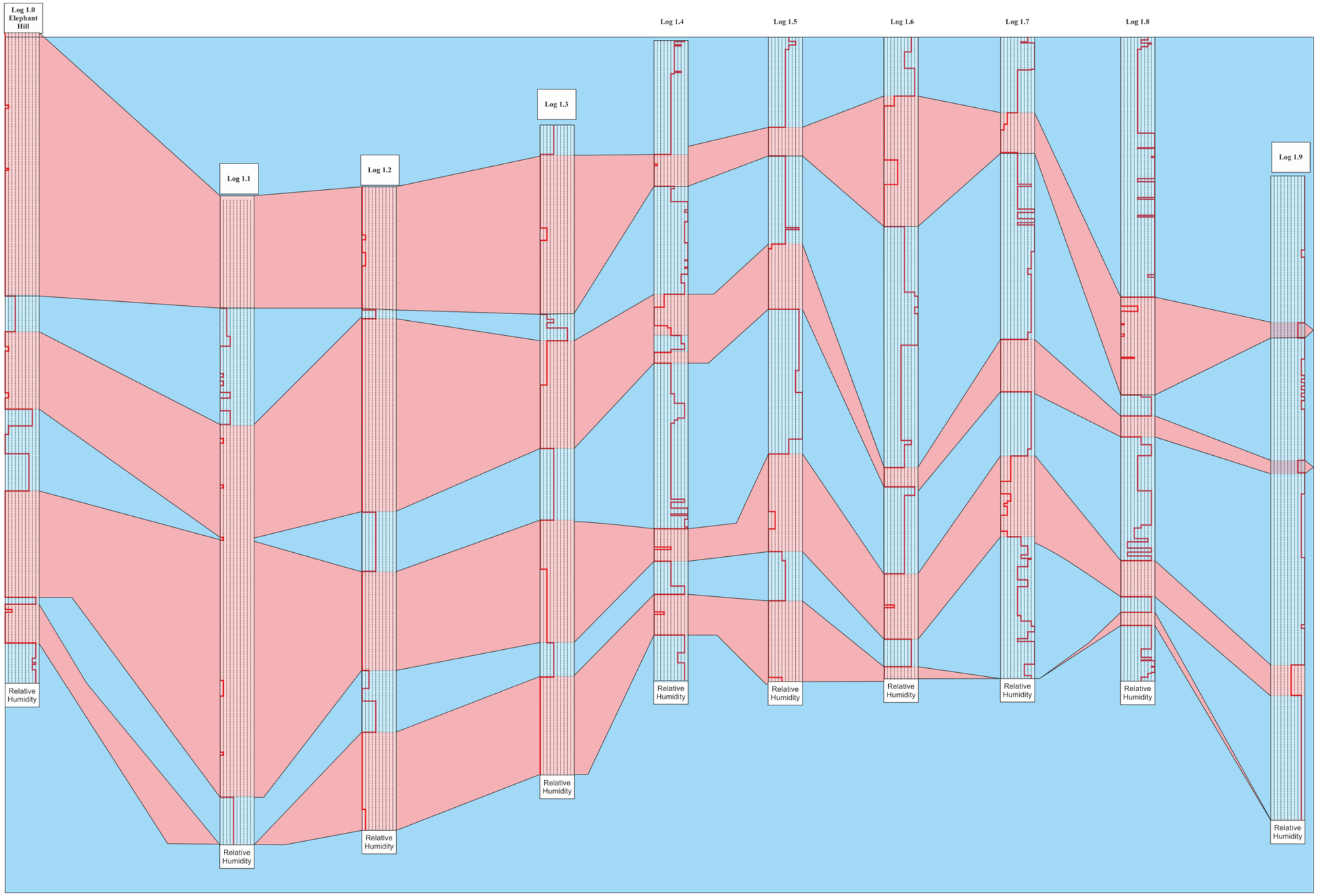

Figure 5.5 Correlation of wet and dry shifts across each log based on changes in relative humidity. Blue shows wet. Pink indicates dryer sediments. Each log has been normalised in length to aid interpretation.

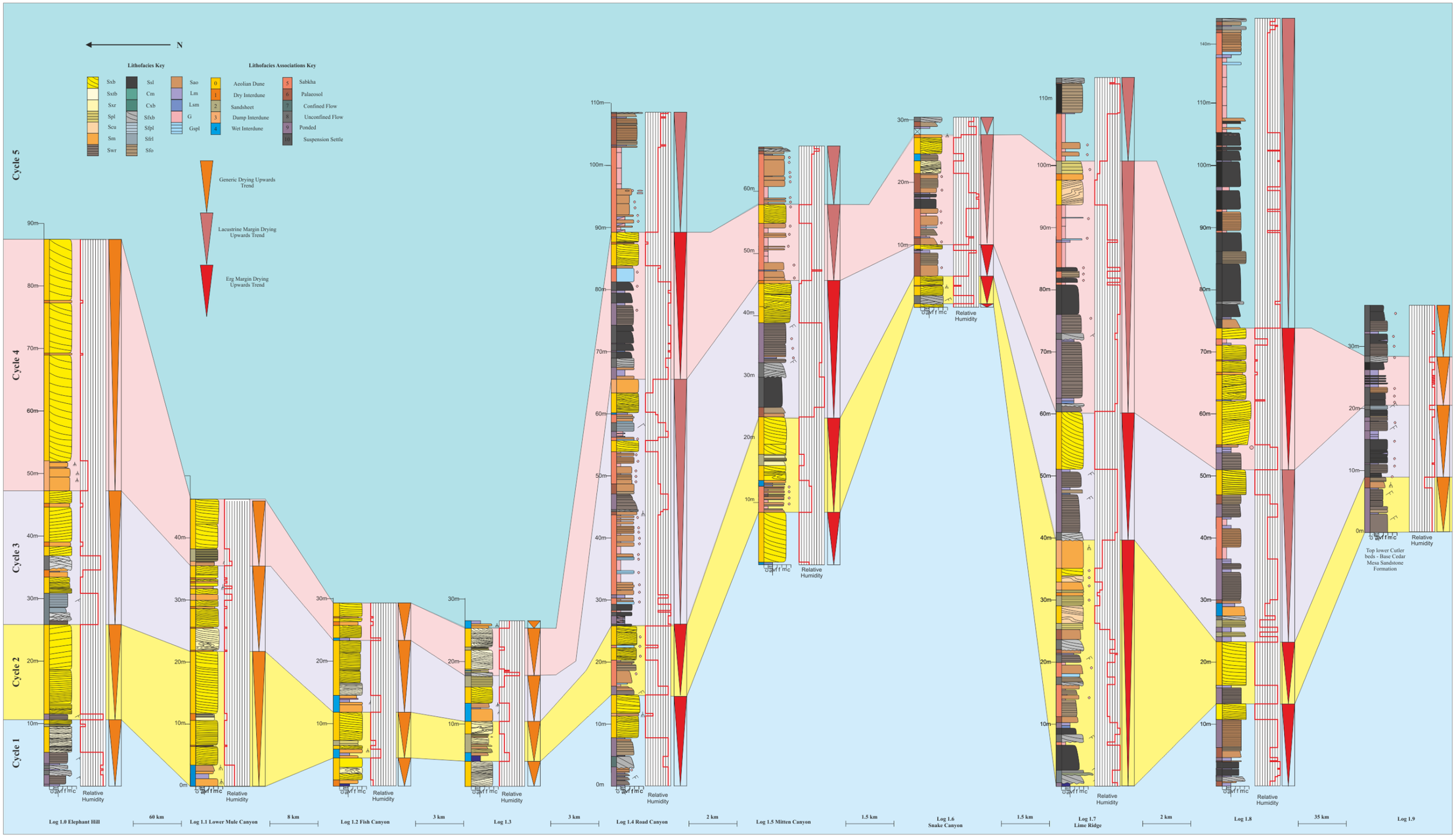

Figure 5.6 Four representative sedimentary logs (logs 1.5, 1.6, 1.7, 1.8) from the sabkha depositional setting have been correlated across the study area by formational relationships and key lithological units. Logs are coloured by facies, facies associations are indicated by the colour bars to the side of the logs. A rolling average relative humidity curve from maximum aridity to maximum humidity is shown. The humidity values are shown next to corresponding associations within the key, 0 indicates most dry whilst 10 is the wettest. Interpreted drying upwards successions are indicated by coloured arrows, red arrows indicate erg margin assemblages, whilst salmon arrows show the lacustrine margin assemblages.

5.3.1 Controls on Preservation of Cyclicity in the Sabkha Margin of the Cedar Mesa Sandstone Formation

Examination and analysis of the sabkha-influenced sediments of the Cedar Mesa sandstone Formation demonstrates a number of drying upward successions of genetically related sediments. Each succession is separated from the succeeding one by a depositional break represented by a sudden wetting of the setting in which succeeding associations were deposited. All successions contain sabkha associations, but the distinctive character of the associated clastic sediments and their relationships to the evaporitic sediments describe two distinct assemblages of aeolian-sabkha and fluvial-lacustrine-sabkha. In each log, successions alternate in character and a correlation of drying upward successions describes cycles of sedimentary deposition and preservation that form in an erg-marginal sabkha setting and in a lacustrine-marginal sabkha setting.

The preservation potential of sediment in any environment is controlled by the interaction between sediment accumulation (a function of environment, supply and climate), and developing accommodation space through time (tectonics) (Howell & Mountney, 1997; Cecil, 2003).

With a constant rate of subsidence, the preservation potential of continental sediments responding to cyclic changes in climate is governed by the relationship between the rate of creation of accommodation space and the independent rate of sediment flux (the difference between the rate at which sediment enters and leaves the system) under different climatic conditions within the depositional setting (Howell & Mountney, 1997). If sediment is supplied continually, but the rate is insufficient to overfill the developing accommodation, then the preserved sedimentary succession may reflect both wetting and drying of climate. If rates of

sediment flux are sufficiently high enough during part of the climate cycle to over-fill the accommodation space the sediment deposited above accommodation is transient and will not be preserved; it will be reworked during periods of lower sediment flux and redeposited under different climatic conditions. Consequently, preserved sedimentary successions may represent deposition during only part of the climate cycle (Howel & Mountney, 1997; Mountney, 2006).

The deposited sediments of continental sabkha settings are influenced by separate clastic and evaporitic sediment fluxes that respond differently to climatic change, but combine to deposit sediment in the developing accommodation space. The likely effects of climatic variability upon both clastic and evaporitic sediment fluxes in erg-marginal and lacustrine-margin sabkha settings are discussed below, and combined subsequently with developing accommodation space to produce a theoretical model that accounts for the preserved successions observed in the Cedar Mesa sediments.

Erg-marginal sabkha settings are dominated by aeolian deposition. During climatic drying, the clastic sediment flux rate is likely to be comparatively high and significant volumes of sediment accumulate, typically to well above base level. Accommodation is exceeded by clastic deposition at or near the point of maximum aridity (Howell & Mountney 1997). Interdune brine pools evaporate, concentrating solutes and producing evaporitic sediments in pools and in subsurface sediments surrounding them. Evaporitic sediment flux rates increase rapidly from zero to a maximum relatively early in the climatic drying cycle once solute concentration in the spatially restricted pools of evaporating water exceeds the threshold for precipitation. Once water is exhausted, the rate of evaporitic sediment deposition falls rapidly to zero. As the climate wets, a rise in the water table significantly reduces the clastic sediment available for aeolian transport, with material removed, producing a negative clastic sediment flux and the dunes deflate to, or near, the

water table. Small saline puddles and lakes form, solutes are diluted and evaporitic sedimentation flux remains near zero and may fall to negative as some deposited evaporites are dissolved.

In lacustrine-marginal sabkha settings, as the climate dries, evaporitic sediment flux rates are near zero until the large volumes of water within lakes are reduced sufficiently to concentrate solutes (e.g. Handford, 1982; Gunatilaka & Mwango, 1987; Lowenstein & Hardie, 1985; Hardie et al., 1978) and promote precipitation of evaporite minerals. With continued drying, evaporitic flux rates increase dramatically toward the point of maximum aridity for as long as water remains in brine pools or within the shallow subsurface. Evaporitic sediment may accumulate to slightly above accommodation space as the brine pool dries completely and surface evaporitic sediments form. A wetting climate dilutes evaporite concentration in surface and subsurface water and reduces evaporitic sediment flux rates significantly. In the initial stages of climatic wetting, areas inundated with water may experience negative evaporitic flux rates as some evaporitic crusts are dissolved, while areas above water may experience a slightly positive evaporitic flux as evaporites are reworked by aeolian dunes. Clastic sediment flux rates are probably greatest at the point of maximum aridity when the lake is completely dry and the exposed bed supplies sediment to aeolian dunes. However, the magnitude of the flux at this point is low, because most clastic sediment is bound by evaporitic precipitation on or within the former lakebed. With wetting, clastic flux rates fall further, fall rapidly, and may become negative as the lake expands rapidly over areas of former clastic sediment source.

The effects of these variations in both clastic and evaporitic flux rates can be investigated using theoretical models that build upon the approach of Howell and Mountney (1997) (Figure 6.2). In the models (Fig 6.7), subsidence rates are

considered constant over a defined period time during which the climate cycles between wet and dry. Clastic and evaporitic sediment flux rates are modelled independently with shapes and variations in magnitude described by the preceding discussion.

A constant rate of subsidence produces linearly increasing accommodation space through time (Fig. 5.7). The cumulative accumulation of sediment through time is independent of accommodation space and is the cumulative total of the clastic and evaporitic flux rates combined (Fig.5.7). Over periods of time where the rate of total sediment flux is less than the rate of subsidence, the accommodation and accumulation lines diverge and newly created accommodation space is under filled. Over periods of time where the rate of total sediment flux is greater than the rate of subsidence, the accommodation and accumulation lines converge: accommodation space is filled, and may be over filled. When the rate of total sediment flux is negative, previously accumulated sediment is eroded and accommodation space may be created. Sediment that is deposited below the accommodation line, and that is not subsequently eroded by a negative sediment flux, is preserved. Sediment deposited above the accommodation line is transient and ultimately is not preserved.

In an erg margin setting, the model demonstrates that a large amount of sediment from both clastic and evaporitic sources is likely to accumulate during the drying phase, and accommodation space may be significantly overfilled. During the wetting phase the total sediment flux reduces and may fall negative as clastic sediment is removed and evaporitic sediment is not produced. Much of the sediment deposited during the drying phase is not preserved, sediment accumulation falls below accommodation, and new accommodation space is generated for deposition to fill during the next drying phase. Consequently, erg margin sabkha settings preserve

drying-upwards only motifs. By contrast to typical erg-centre drying-upward successions (Howell & Mountney, 1997), the base of each drying upward cycle is characterised by sediments deposited in sabkha ponds of limited spatial extent within interdune corridors. These sediments represent accumulation during the earliest stages of drying, at or soon after the point of maximum humidity, when significant water is still present. As the climate dries and water evaporates, subsequent deposition evolves rapidly to become dominated by aeolian sediments. Consequently, sabkha associations constitute only a small proportion of the sediments preserved in aeolian-sabkha assemblages, but their intimate association with dunes means that significant interaction at the facies scale takes place, and dune associations in this assemblage are strongly influenced by evaporitic sediments.

Drying-upward motifs in lacustrine-margin sabkha settings occur because significant evaporitic sediment is precipitated during the latter half of the drying phase when solutes become concentrated in the remaining lake water. Clastic sediment flux increases with drying, but is comparatively low and contributes comparatively less to the sedimentary succession. Rapid switching to evaporitic deposition occurs when evaporation of lake waters is sufficient to concentrate solutes and precipitate evaporites. A generally low clastic flux severely limits facies-scale interactions between clastic and evaporitic facies, and when evaporitic sediments are deposited they quickly dominate the succession. With wetting, sediment flux from both evaporitic and clastic sources is severely curtailed.

The simple models presented demonstrate that in both erg-marginal and lacustrine-marginal sabkha systems, drying upward motifs will be observed in the preserved assemblages if sediments completely fill accommodation space during each climatic cycle. The relative timing of the points of maximum clastic and evaporitic production

on the climate curve provide arguments for relationships between clastic and evaporitic sediments, and for the relative proportion of each observed within the preserved assemblages.

However, these interpretations come with caveats of both temporal and spatial scale. The two models undoubtedly represent end-members of a continuous spectrum of sabkha influenced settings that were present across the study area during Cedar Mesa times and that can be observed in many similar modern settings. This factor may be responsible for some of the sedimentary variation observed in the assemblages, but distinct assemblages representing intermediary settings between erg marginal and lacustrine marginal settings are not clearly observed in the data. The extent to which any intermediate setting would preserve drying upward sedimentary trends is also unclear.

The preservation of continental sediments is a function of the depositional process intrinsic to the sedimentary setting, coupled with the spatial and time scales over which the sedimentary environments evolve, and the frequency of climatic change. It may be possible that the depositional processes intrinsic to the aeolian and lacustrine settings have a dominant influence on deposition and preservation of the sediments of sabkha settings, such that intermediate settings are less likely to be preserved, or are preserved with signatures that reflect one of these end members, biasing the sedimentary record. Alternatively, preservation of intermediate settings may require different spatial or temporal scales of evolution to those examined in this work. Higher frequency oscillations in climate may produce wet and dry trends if the period of the oscillation is insufficient for sediments to fill accommodation space, or in settings where the processes of deposition can respond quickly enough. In other settings, high-frequency scales may be overprinted by lower frequency ones depending upon sedimentation rates (Havholm & Kocurek, 1994).

The models assume constant subsidence with time. Furthermore, a correlation of depositional assemblages across the sabkha influenced Cedar Mesa (Fig 6.6) based upon the nature of the assemblages and their thicknesses assumes constant subsidence spatially across the study area. However, sabkhas form in topographical depressions and the effects of differential subsidence across the depositional system should not be dismissed. The correlation of assemblages and their boundaries is less evident, and thickness of assemblages more varied, in the lower Cedar Mesa than in the upper two thirds. This may be the signature of independent rates of subsidence across the study area that resulted in isolated and independently evolving sabkha systems in the early stages of Cedar Mesa development, with each system responding to its own accommodation space and localised sediment supply.

The models provide an explanation for the sedimentology of individual depositional cycles within the succession. However they do not provide explanation for the alternating nature of the preserved assemblages in any given log, or for the overall apparent wetting upward in each log. These trends may result from longer term and higher amplitude oscillations in climate that drive similar scale oscillations in sediment supply to the system. The effects of these scales cannot be investigated conclusively within the sedimentological data alone and are discussed later.

Nevertheless, the models presented provide valuable insight into the distributions of preserved sediments across erg-margin to lacustrine margin sabkha settings. They provide means of predicting distributions of evaporitic and clastic strata in the subsurface, their relative volumes, and the relationships between them. As such they have useful economic potential for evaluating the possible volumes of exploitable evaporites in the subsurface, or the effects at a variety of scales that evaporitic sediment have upon their contemporary and coeval clastic sediments.

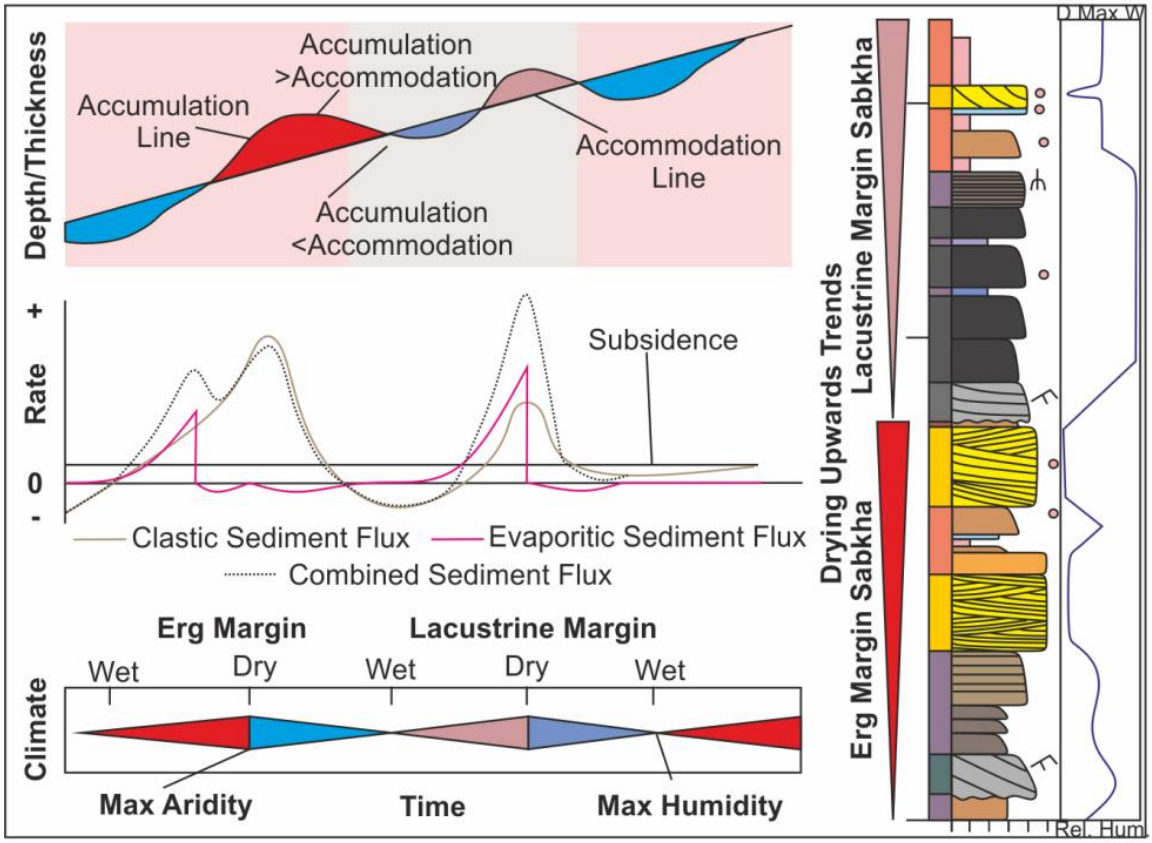

Figure 5.7 Theoretical sediment accumulation and accommodation space development with time that could account for the deposits observed in the Cedar Mesa Formation. A) Cumulative accommodation and cumulative total sediment accumulation. Sediment accumulation below the accommodation line is preserved, accumulation above the accommodation line is transient and ultimately not preserved. B) Relative clastic (brown) and evaporitic (pink) sediment flux curves with time, that combine to give a total flux curve (dotted) from which the cumulative accumulation curve in (a) is calculated. Positive flux rate results in deposition of sediment, whereas a negative rate results in erosion. C) The variations in climate with time over which sediment flux rates in (b) and the cumulative sediment accumulation (a) are modelled. Over the first climatic cycle, sediment fluxes for the erg-margin setting are modelled; over the second climatic cycle, sediment fluxes for the lacustrine-margin setting are modelled. D) Idealised sedimentary logs for erg margin and lacustrine margin sabkha settings are presented alongside, logs are coloured according to facies, with associations represented by the coloured bar. See Fig. 4 for key to the colours. Idealised relative humidity curves are also plotted against the sedimentary log from maximum aridity on the left to maximum humidity on the right.

5.3.2 Driving Forces of Climatic Cyclicity

Sedimentological analysis indicates a primarily climatic control on the preservation of drying upwards cycles of both the erg-margin sabkha and the lacustrine-margin sabkha. The relatively thin sedimentary packages (~25 m) within each cycle indicate more short term cyclicity attributed to glacio-eustatic origins, rather than long term

tectonic cycles, which most often occur over large amplitudes (Dickinson *et al*., 1994). Mountney (2006) has identified 12 separate erg accumulations within the aeolian deposits of the Cedar Mesa Sandstone related to 412 kyr cyclic changes in climate and glacio-eustatic sea-level variations attributed to Milankovitch orbital periodicities.

Milankovitch cycles (Fig. 5.8) are caused by changes in the ellipticity of Earth's orbit known as eccentricity, as well as changes in the tilt (obliquity), and the precession of Earth's rotational axis. (Van Wagoner *et al.,* 1987; Van Wagoner *et al.,* 1990; Mitchum & Van Wagoner, 1991; Catuneanu, 2006; Miall, 2010). These periodic changes in the Earth's orbit and rotation lead to rhythmic layering in strata, which reflect these processes. The values for precession and obliquity have been worked out for the geological past (Berger *et al,* 1989*;* Waltham, 2015) and provide a direct link between aspects of climate change allowing for biological, chemical and physical change in the Earth's past to be constrained (Meyers, 2019).

Milankovitch processes are the most likely cause of the variations in sedimentology previously mentioned, with changes in levels of solar radiation reaching the Earth, leading to more arid or humid periods, and associated sedimentology.

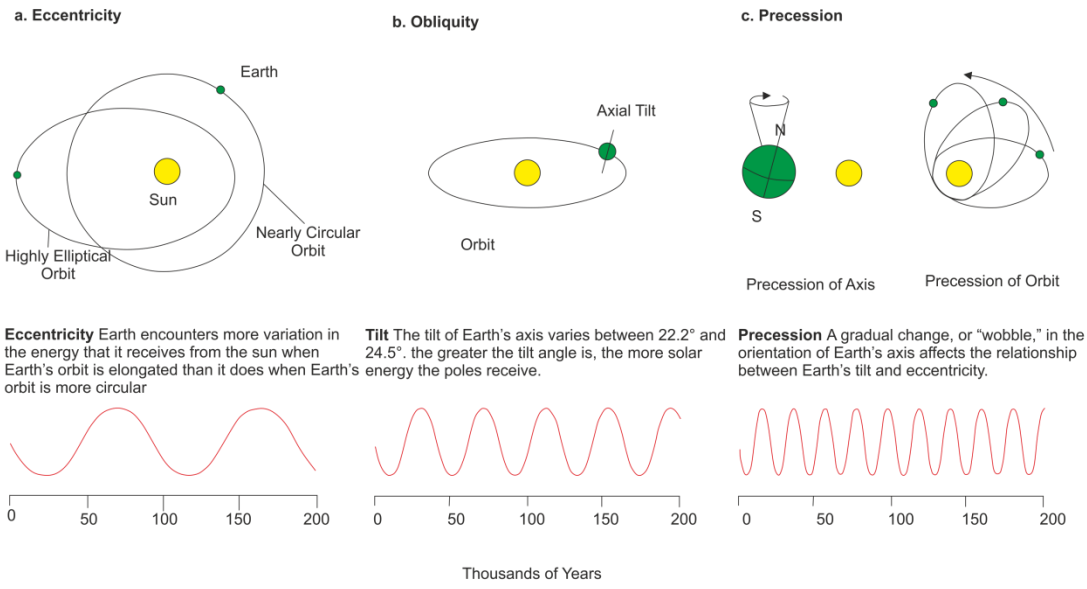

Figure 5.8 Milankovitch theory (after Van Wagoner et al., 1987)

5.4 Quantifiable Cyclicity

With the probable method of cyclicity determined, cyclo-stratigraphic analysis can be conducted to try and examine any quantifiable Milankovitch markers preserved within the sediments deposited. Cyclo-stratigraphic analysis is most commonly applied to marine strata, due to the high preservation potential of quantifiable stratigraphic markers in both a biostratigraphic and sequence stratigraphic context. Such high abundance and preservation of quantifiable stratigraphic markers in the marine setting has led to a wealth of studies analysing the cyclic nature of deposition in the geological record (Hays *et al.,* 1976; Hilgen *et al.,* 1995; Shackleton, 2000; Lisiecki & Raymo, 2005; van Dam *et al.,* 2006; Gradstein *et al.,* 2012; Crampton *et al.,* 2018). More recent undertakings have studied cyclicity within the continental lacustrine setting and have had similar success (Steenbrink *et al.,* 2003; Wang *et al.,* 2018; Shi *et al.,* 2019), attributing variations in high and low water depths to periods of humidity and aridity on a Milankovitch scale. The analysis of cyclical stratigraphy in an arid continental setting is notoriously difficult as these environments do not

typically host continuous standing water and stratigraphic markers are sparse or altogether absent due to processes such as oxidation, which destroys palynological markers (Joannin *et al,.* 2010; Herczeg & Chapman*,* 1991). Previous work however has demonstrated that continental sabkha successions readily preserve Milankovitch signals and are suitable environments for the study and interpretation of these processes (Yang & Baumfalk, 1994).

Cyclo-stratigraphical analysis has been conducted on five logs, three within the sabkha, and two from the aeolian/sabkha margin. First the gamma ray data is examined using time series analysis which is then compared to log and microfacies data. This integrated approach helps to quantify and confirm the hypothesis that the cycles recognised previously and the general cyclicity described within the Cedar Mesa Sandstone (e.g. Mountney, 2006; Loope, 1984) is attributed to climatically controlled Milankovitch orbital processes (eccentricity, obliquity and precession).

5.4.1 Time Series Analysis of Logs

Time series analysis can be conducted on many data sets, either continuous-signal records which have sample intervals chosen by the investigator, or discrete-signal records, in which the sample intervals are dictated by the process forming the strata. However, to ensure meaningful time series data is generated, the environmental conditions must remain reasonably consistent, and the variable measured is representative of the environment (Weedon, 2003).

Methods

The gamma ray logs have been chosen for time series analysis due to the systematic sampling interval of 0.2 m providing a discrete-signal record, and the lack of any unintentional bias or interpretation which may be present in sedimentary logs. Orbital forced climate cycles can be recorded within gamma ray logs only when, the depositional process is continuous; and the sediment accumulation rate is constant

(Yang & Baumfalk 1994). These conditions are not always met, which may result in some discrepancies between ratios of Milankovitch cycles and those recorded within the logs.

The most important approach for identifying periodicities such as eccentricity, obliquity, and precession in a time series is spectral analysis. This is used to estimate the power (strength) of periodic components at all possible frequencies. These are assumed to be sinusoidal, each with a certain amplitude and phase. Power is proportional to amplitude squared.

Fourier analysis is then used, which splits the time series into a complete set of sine and cosine components. Any evenly spaced time series of length N is represented precisely and completely as a sum of $N/2$-1 sinusoids, each with an amplitude and a phase, and in addition one constant ('bias', or zero frequency component) and one amplitude for a fixed phase sinusoidal at the maximal frequency as limited by half the sampling frequency (the *Nyquist* frequency). The first of these sinusoids has a period of N samples, the second a period of $N/2$, the third $N/3$ etc. up to the Nyquist frequency with a period of only 2 samples. Spectrums can be plotted for much more than $N/2$-1 frequency values, but is regarded as interpolation as the spectral resolution is limited by N and cannot be increased (Hammer, 2010).

Power spectrums of each complete log were plotted utilising Fourier analysis using the software Past (Hammer *et al.,* 2001), which displays the frequency of each peak against its power (strength). The red dashed lines are $p<0.01$ (upper line) and $p<0.05$ significance levels, below which the data should be considered uncorrelated noise.

Ratios between the spectral peaks and corresponding wavelengths have then been determined by using $1/(n_1+1):1/(n_2+1):1/(n_3+1)=$

These ratios are then compared to Milankovitch periodicities for the early Permian (Fig 5.10).

A worked example of the method is shown in figure 5.9, this shows the values and related periodicities when using the method of Yang & Baumfalk (1994). Alternative peaks are also considered as the potential 100ka peak. However, this gives values which do not relate to Milankovitch periodicities. In each example alternate peaks have been considered as the potential 100ka peak, but in each case, the first strong peak relates most strongly to reported Milankovitch periodicities (Fig 5.10).

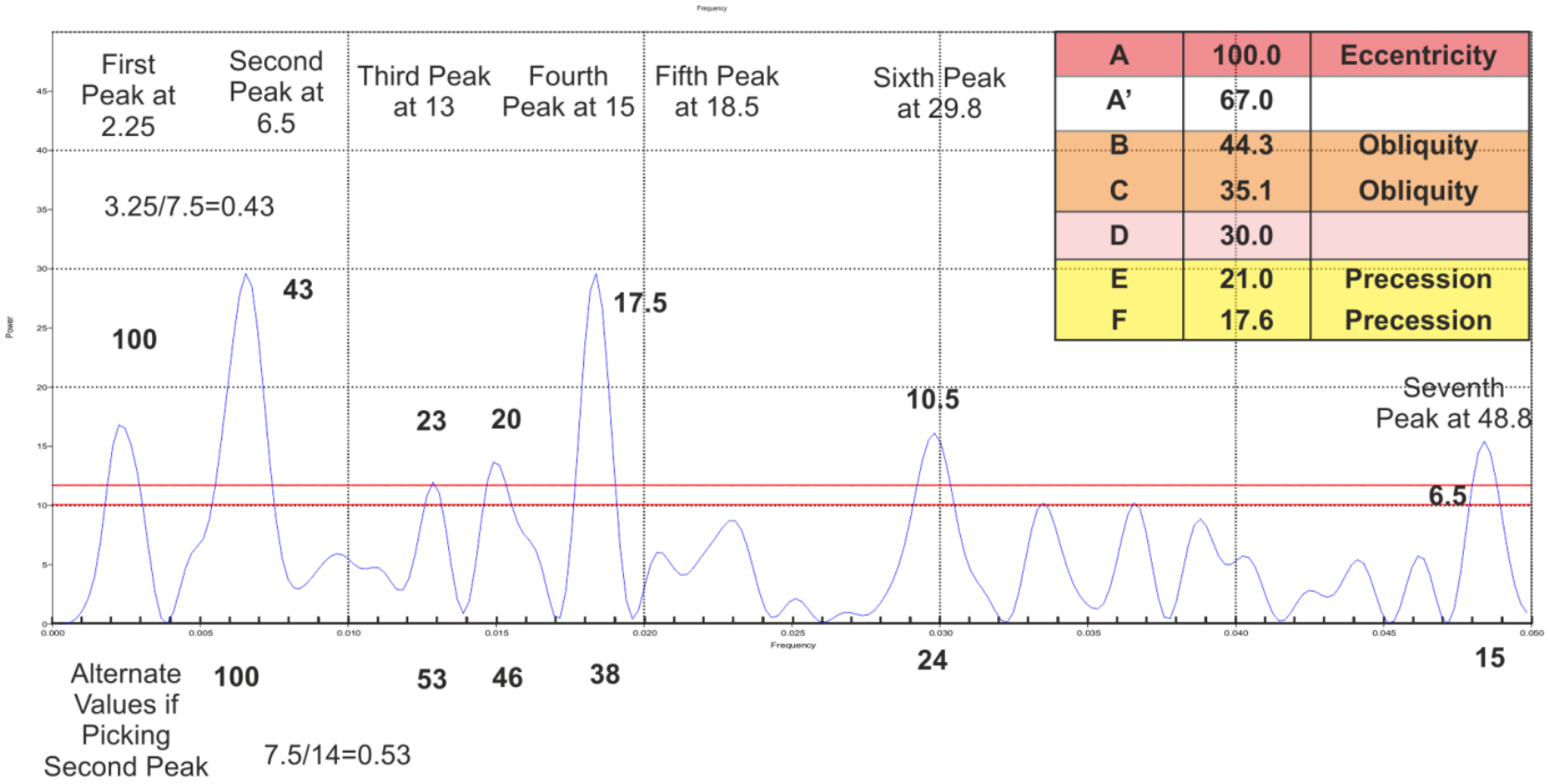

Figure 5.9 Worked example using the technique of (Yang & Baumfalk 1994). The 'frequency' value is plotted for each peak, with the first peak assumed to be the 100ka peak, by adding 1 then dividing by the frequency value of the next peak +1 a ratio is generated for that peak (plotted in bold), this is then compared to the known Milankovitch periodicities for the Permian period. Along the bottom row the second peak is considered as the 100ka peak and related ratios are shown (bold) these however do not relate as closely to Milankovitch periodicities as when you consider the first peak as the 100ka cycle.

A	100.0	Eccentricity
A'	67.0	
B	44.3	Obliquity
C	35.1	Obliquity
D	30.0	
E	21.0	Precession
F	17.6	Precession

Figure 5.10 Milankovitch Ratios of the early Permian after (Berger et al., 1989)

Results

Results from time series analysis of five gamma ray logs are plotted below, spectral peaks are then compared to known Milankovitch ratios following the methods of Yang & Baumfalk (1994).

Log 1.7

Results from spectral analysis of log 1.7 (Fig. 5.11) shows seven peaks (0.002, 0.006, 0.013, 0.015, 0.018, 0.029, 0.048) above the noise threshold with ratios of 100 : 43 : 23 : 20 : 17.5 : 10.5 : 6.5.

The ratios between the first four wavelengths are very close to the ratios between Milankovitch periods for the early Permian (Fig.6.9) and represent the 100ka eccentricity cycle, 44.3ka obliquity cycle and the 21ka and 17.6ka precession cycles.

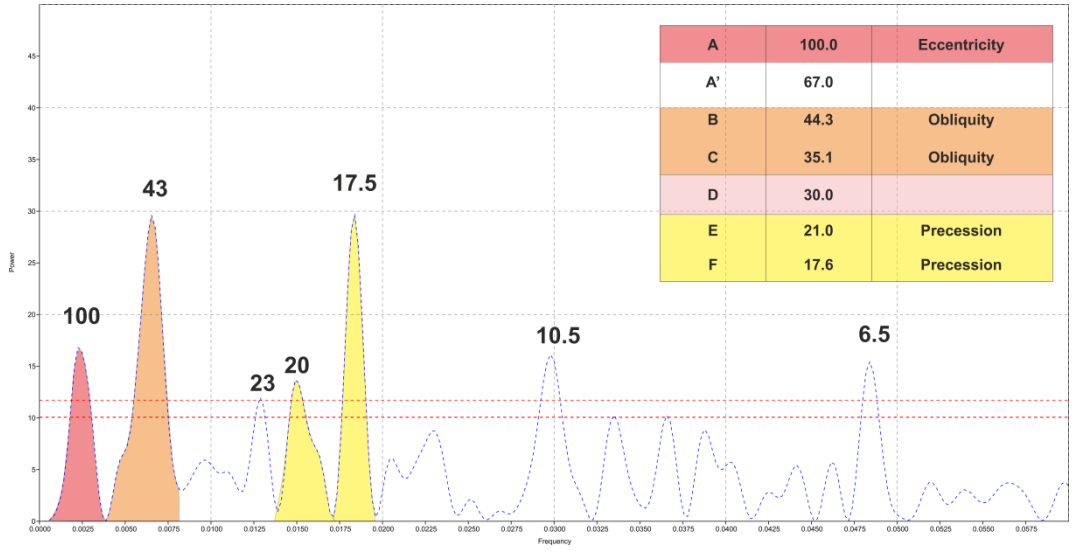

Figure 5.11 Power spectrum for log 1.7, peaks and corresponding Milankovitch ratios are coloured and correspond to table on the right of diagram, dashed red line represents confidence level, any peaks below which can be considered as noise

Log 1.5

Log 1.5 shows four peaks (Fig. 5.12) (0.003, 0.006, 0.0105, 0.013) with ratios of 100 : 57 : 35 : 29. Three of these relate to the 100ka eccentricity cycle, 35.1ka obliquity cycle and the 30ka 'D' cycle

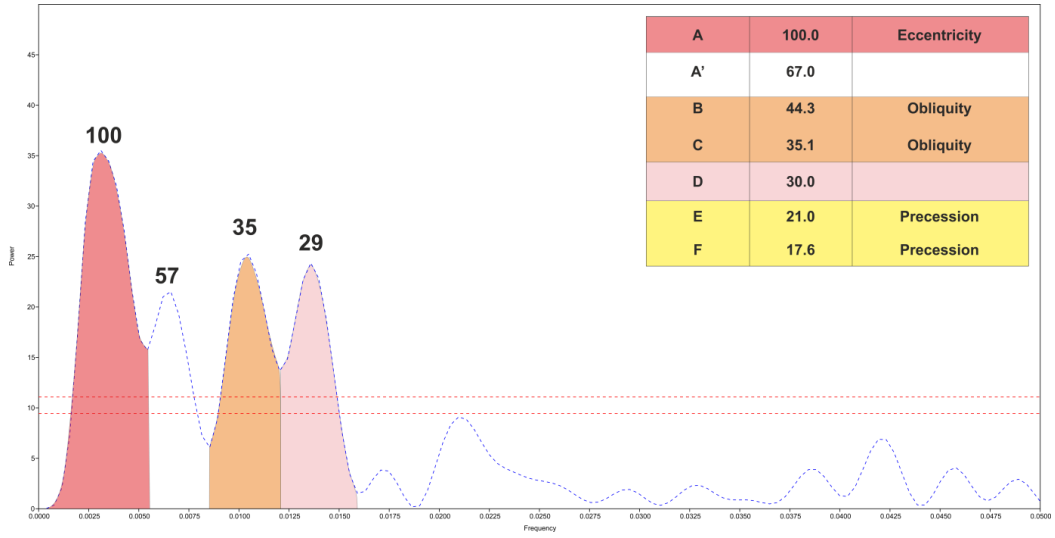

Figure 5.12 Power spectrum for log 1.5, peaks and corresponding Milankovitch ratios are coloured and correspond to table on the right of diagram, dashed red line represents confidence level, any peaks below which can be considered as noise

Log 1.4

Log 1.4 (Fig. 5.13) shows seven peaks (0.0035, 0.0055, 0.0075, 0.0105, 0.0130, 0.0155, 0.0170) with ratios of 100 : 71 : 55 : 42 : 36 : 29 : 27. Three of these relate to the 100ka eccentricity cycle, 44.3 and 35.1 obliquity cycles.

Log 1.3

Log 1.3 shows three peaks (Fig. 5.14) (0.015, 0.026, 0.0425) with ratios of 100 : 59 : 42.5

Two of these could relate to the 100ka eccentricity cycle, 35.1ka obliquity cycle however they all occur below the threshold for noise.

Log 1.1

Log 1.1 shows five peaks (Fig. 5.15) (0.006, 0.018, 0.025, 0.0325, 0.0425) with ratios of 100 : 37 : 27 : 22 : 16

Four of these could relate to the 100ka eccentricity cycle, 30ka 'D' cycle and the 21ka and 17.6ka precession cycles, however like log 1.3 most of the peaks fall below the threshold line for noise with only the 0.025 peak above.

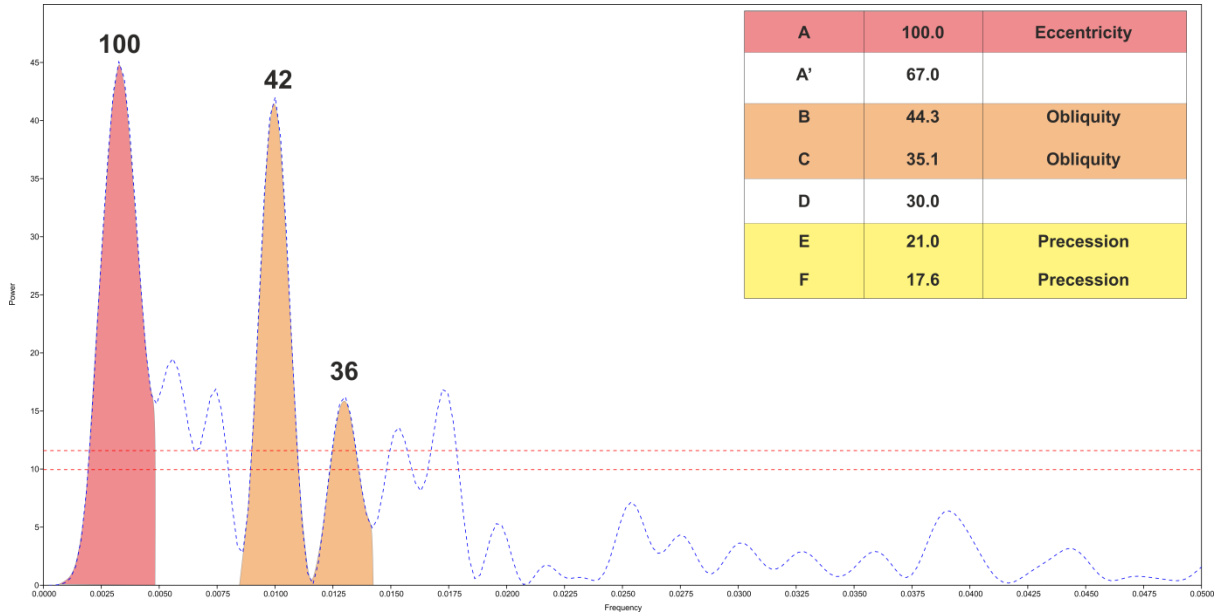

Figure 5.13 Power spectrum for log 1.4, peaks and corresponding Milankovitch ratios are coloured and correspond to table on the right of diagram, dashed red line represents confidence level, any peaks below which can be considered as noise

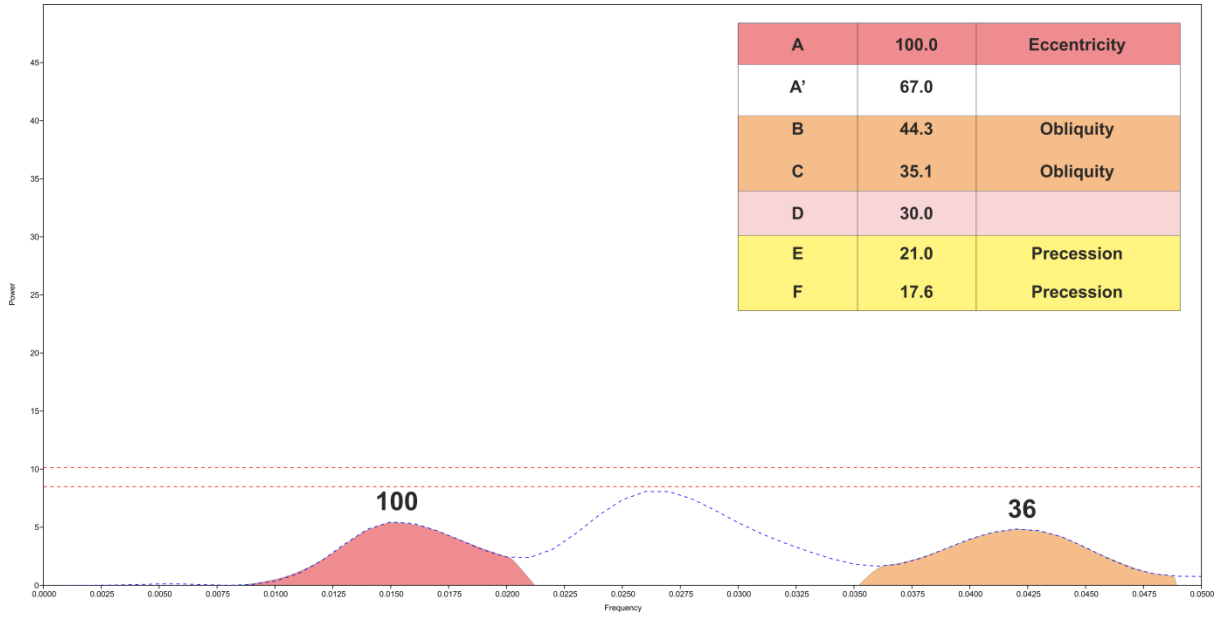

Figure 5.14 Power spectrum for log 1.3, peaks and corresponding Milankovitch ratios are coloured and correspond to table on the right of diagram, dashed red line represents confidence level, any peaks below which can be considered as noise

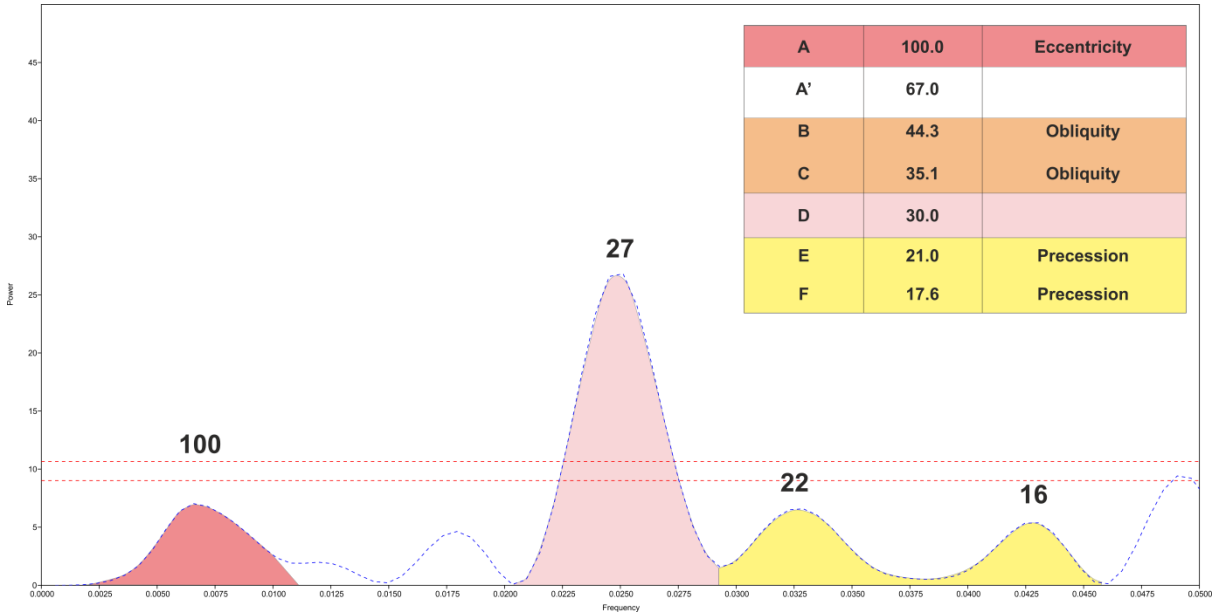

Figure 5.15 Power spectrum for log 1.1, peaks and corresponding Milankovitch ratios are coloured and correspond to table on the right of diagram, dashed red line represents confidence level, any peaks below which can be considered as noise

Comparison to Sedimentary Cyclicity

This method provides a useful means in analysing cyclicity within sabkha settings, however some of the charts have peaks unrelated to Milankovitch periodicities and the use of time series analysis within a pure aeolian environment is somewhat limited. These peaks may be the result of signal noise, signal repetition or ratios which are previously unknown. Each individual cycle interpreted from sedimentological data, is now tested with time series analysis to see if any one driving factor is responsible for its cyclicity and to assess the impact of noise on the previous results.

Log 1.7

Log 1.7 (5.16) has four interpreted cycles, two erg-margin and two lacustrine-margin trends. Within all cycles the peaks are relatively muted, this may be a result of the shorter signal which is processed and combined with the abundance of aeolian and evaporite material which mute the gamma ray signal. Only two of the cycles show more than one peak, both of which are greater than 40m.

The lowest erg-margin trend has four peaks, which relate to eccentricity and peaks at 35, 18 and 15. These most likely related to 35ka obliquity and 17ka precession cycles. The lower lacustrine-margin trend shows four peaks at 100, 62, 45 and 35. These related to 100ka eccentricity, 44ka and 35ka obliquity. The 62ka peaks origin is unknown, however it may be a combination of the 44ka obliquity with 17.5ka precession (44+17.5= 61.5)

Results from individual interpretation of cycles indicate that the lacustrine-margin trends were potentially driven more by 44ka and 36ka obliquity processes, whereas the aeolian-trend is driven by 35ka obliquity as well as 17.5ka precession.

Compared to the time series analyses of the whole log (Fig. 5.11, log 1.7) there are fewer peaks, and only ratios of periodicities present, which may confirm that the other peaks are a product of noise. A 21ka precession peak is present within the whole log, however this is missing within the individual cycle analysis, this may be due to the signal being hidden by other processes, or it was a peak related to noise, as it is barely over the threshold line within Fig. 5.11(log 1.7).

Log 1.7

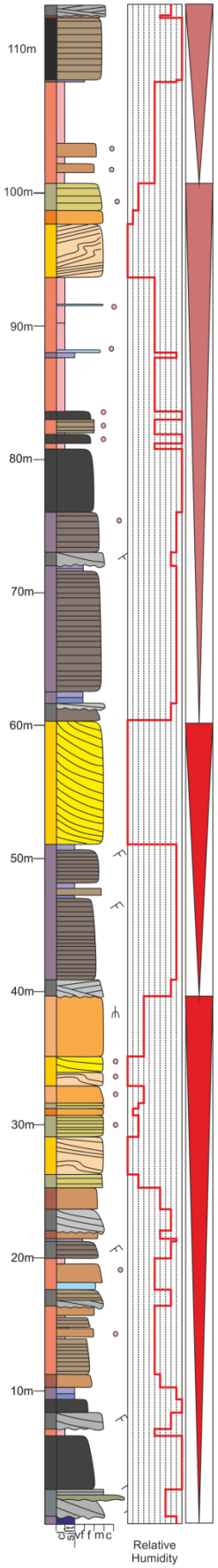

Log 1.7 Upper Lacustrine-Margin Cycle

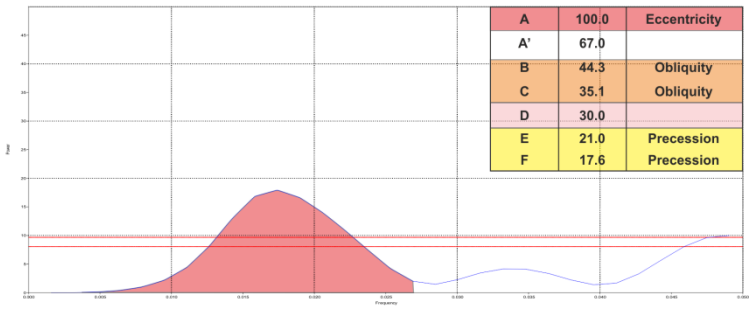

Log 1.7 Lower Lacustrine-Margin Cycle

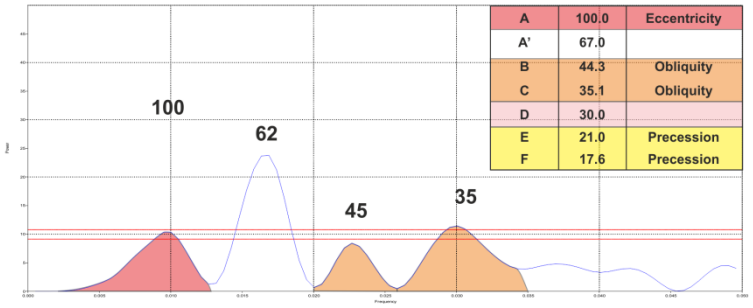

Log 1.7 Upper Erg-Margin Cycle

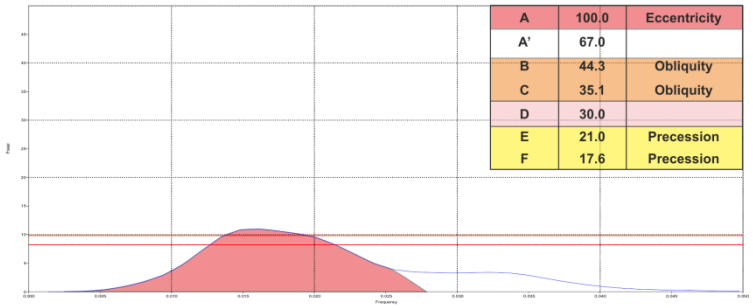

Log 1.7 Lower Erg-Margin Cycle

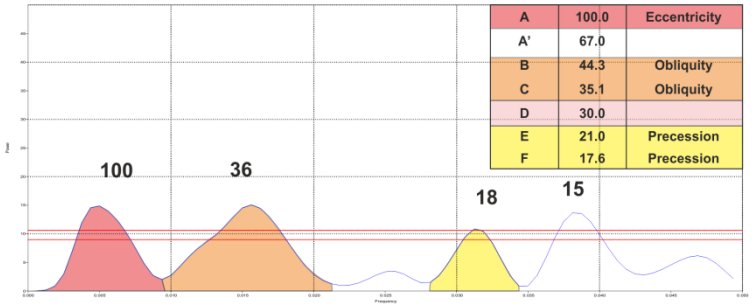

Figure 5.16 Combined sedimentary log, with interpreted drying upwards cycles, either erg-margin (red arrow) or lacustrine-margin (salmon arrow) for log 1.7. Relative humidity cure is plotted within square box. Power spectrum for each individual interpreted cycle is shown next to equivalent cycle. Peaks and corresponding Milankovitch ratios are coloured and correspond to table on the right of each power spectrum diagram, dashed red line represents confidence level, any peaks below which can be considered as noise.

Log 1.5

Log 1.5 (Fig 5.17) has five interpreted sedimentary cycles each less than 30m. No cycles generate more than one peak. When the lowest two erg-margin trends are combined a second peak at 50ka is present. This may be a masking of the combined 17ka and 35ka cycles or the 30ka and 21ka cycles.

When compared to the whole log signal (Fig. 5.12 log 1.5) none of the peaks seen in the individual cycles related to peaks seen within the whole log. This may be due to signals masking each other's peaks, or that the processes occur over long timescales and at points unrelated to the sedimentological interpretations.

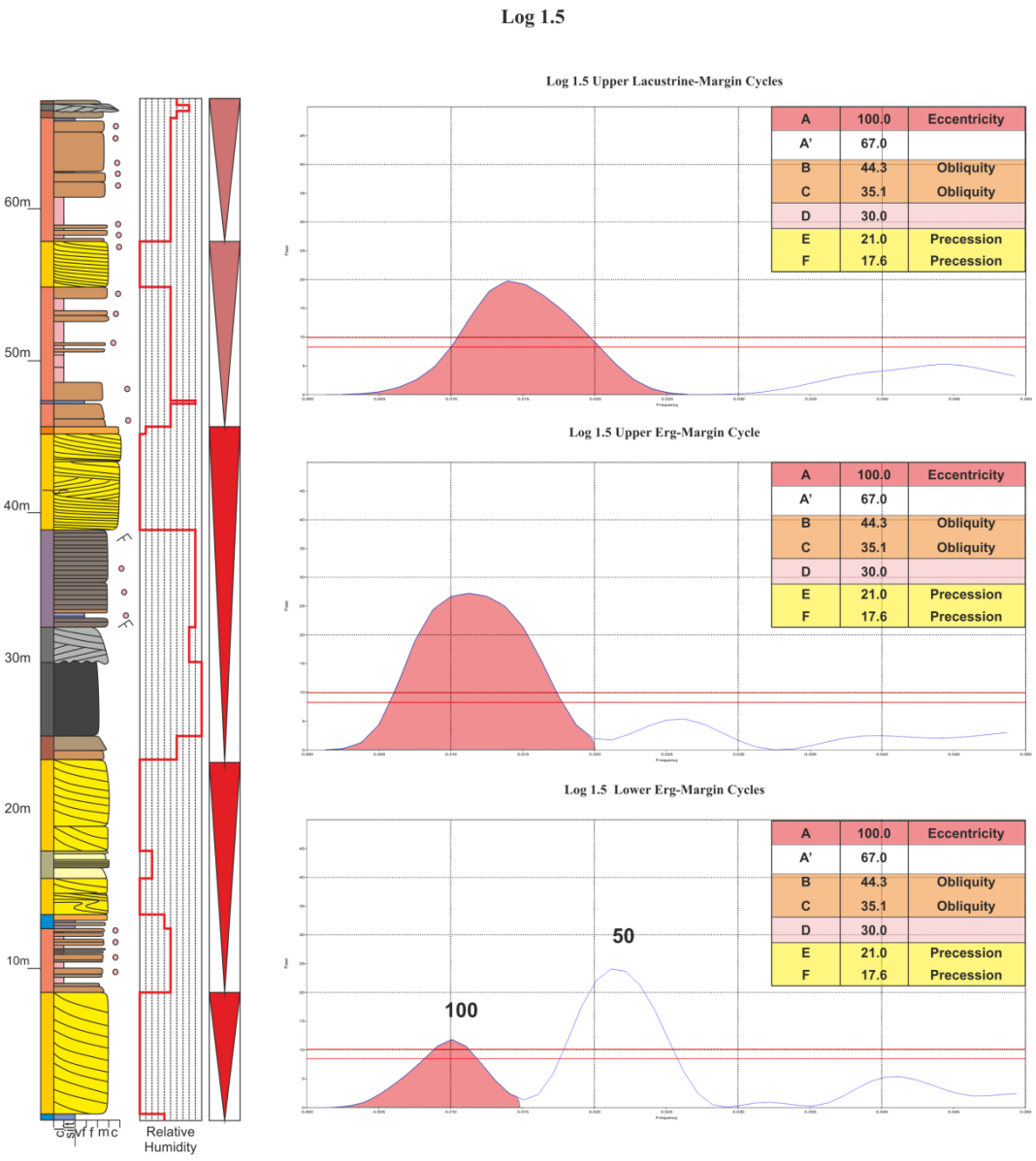

Figure 5.17 Combined sedimentary log, with interpreted drying upwards cycles, either erg-margin (red arrow) or lacustrine-margin (salmon arrow) for log 1.5. Relative humidity cure is plotted within square box. Power spectrum for each individual interpreted cycle is shown next to equivalent cycle. Peaks and corresponding Milankovitch ratios are coloured and correspond to table on the right of each power spectrum diagram, dashed red line represents confidence level, any peaks below which can be considered as noise.

Log 1.4 Road Canyon

Log 1.4 (Fig 5.18) has five interpreted sedimentary cycles alternating between erg-margin trends and lacustrine-margin trends. The signals are all muted compared to the whole log analysis, due to a combination of a smaller sample size and lithology effects.

As with log 1.5 few cycles show a second peak (50ka) and is only present within the erg-margin trend, again this could be either a combination of the 17 and 30ka cycles or 35 and 21ka cycles.

Within the whole log signal the 36ka obliquity curve is present, however this is not present within any of the individual cycles, pointing to the fact that this may occur over long timescales and at points unrelated to the sedimentological interpretations. The muted signal response for all cycles in log 1.4 may be a factor of its positioning. Log 1.4 is closer to the dune field than the previous two logs, and has a higher aeolian sand content, which is represented in the more muted signal responses than the previous two logs.

Log 1.4 Road Canyon

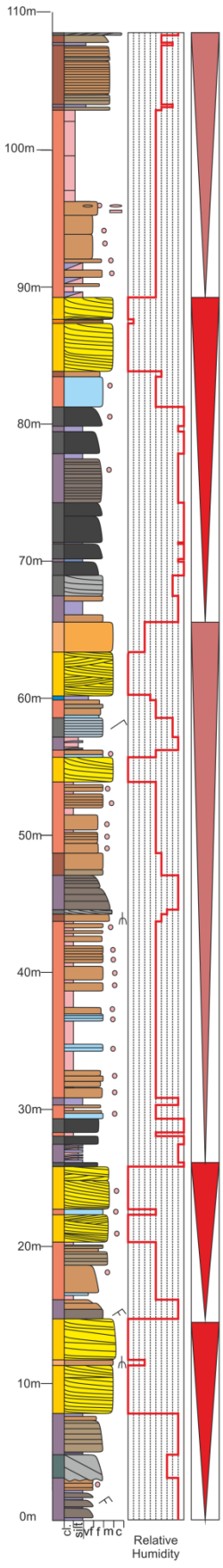

Log 1.4 Road Canyon Upper Lacustrine-Margin Cycles

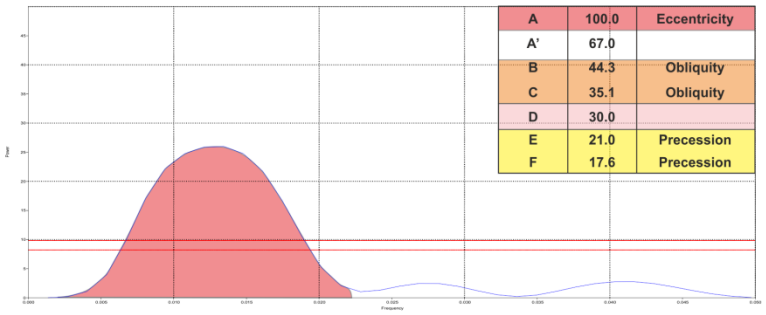

Log 1.4 Road Canyon Upper Erg-Margin Cycles

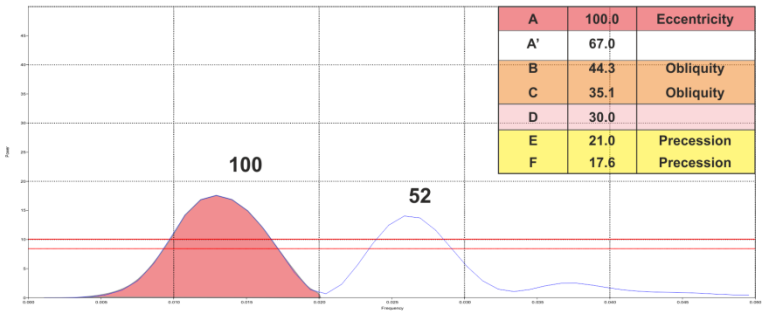

Log 1.4 Road Canyon Lower Lacustrine-Margin Cycles

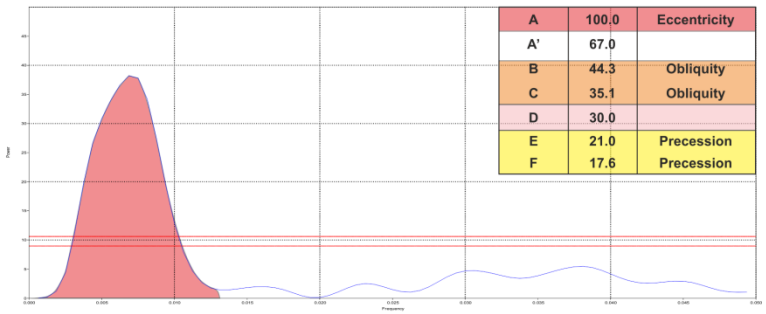

Log 1.4 Road Canyon Lower Erg-Margin Cycles

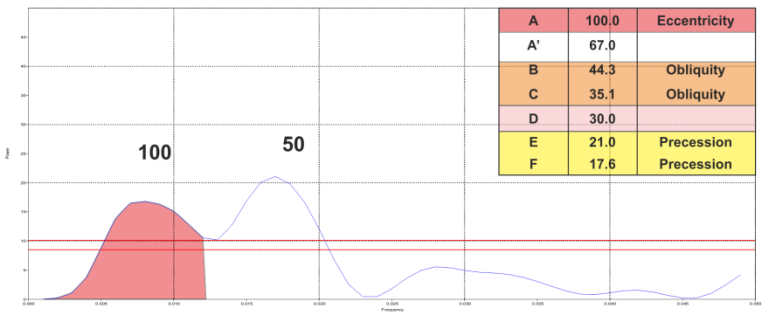

Figure 5.18 Combined sedimentary log, with interpreted drying upwards cycles, either erg-margin (red arrow) or lacustrine-margin (salmon arrow) for log 1.4. Relative humidity cure is plotted within square box. Power spectrum for each individual interpreted cycle is shown next to equivalent cycle. Peaks and corresponding Milankovitch ratios are coloured and correspond to table on the right of each power spectrum diagram, dashed red line represents confidence level, any peaks below which can be considered as noise.

Spatial comparison of Cycles

Within each log the combined values for all erg-margin or lacustrine-margin cycles and values have been plotted for comparison (Fig 5.19). While results are far from conclusive, they suggest that lacustrine-margin cycles are more influenced by the 35ka obliquity cycle compared to erg-margin cycles which are more influences by the 41ka cycle as well as either 21 or 17ka precession cycles.

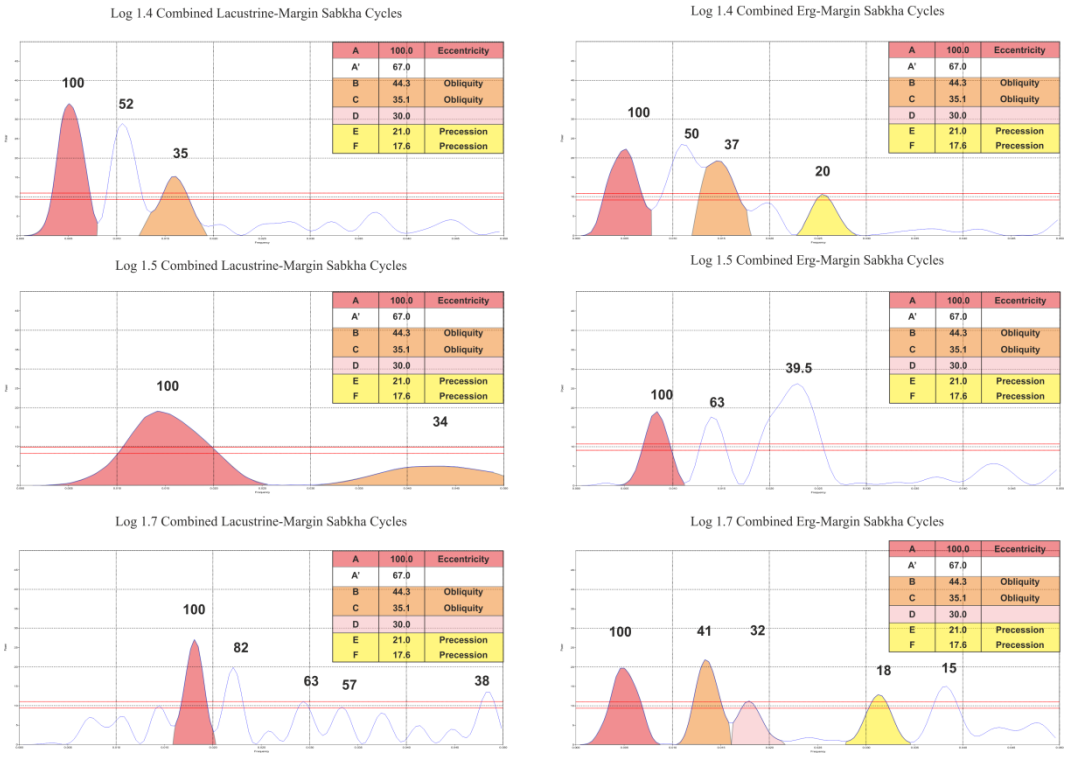

Figure 5.19 Comparison between lacustrine-margin and erg-margin cycles. Results from each log are combined and the power spectrum of this combined data is plotted. Peaks and corresponding Milankovitch ratios are coloured and correspond to table on the right of each power spectrum diagram, dashed red line represents confidence level, any peaks below which can be considered as noise.

5.4.2 Discussion of Time Series Analysis

Time series analysis has shown clear Milankovitch periodicities within each log. Analysis of the complete logs however often showed multiple seemingly random peaks which are most likely attributed to noise.

By splitting signals into cycles interpreted from sedimentology, the noise peaks were eliminated and the dominant controlling factor for each cycle became clearer. This approach however has limitations as some peaks present in the whole log are absent and likely represent processes that are on longer timescales or do not reflect the distinct changes in sedimentary style in which the cycles are determined. Occasionally signals may have been masked by occurring together giving the '52' peak.

Attempts to compare correlated cycles together was somewhat limited, often raising more questions than answers, however it was possible to split some cycles hidden by the 52 peak, though to properly compare cycles against each other, statistical manipulation of the data may be needed.

The signal strength has shown a clear correlation between higher signals and lacustrine facies, and a much more muted response within aeolian settings. Sabkha settings with high evaporite content also have a muted signal response. The spatial changes in facies can be shown by this as log 1.7 has the strongest signals, which decrease with each log as they get closer to the dune field.

Link to Sedimentology

Attempts to astronomically tune deposits and relate the power spectrums back to the sedimentology are difficult due to the lack of precise dates. However, the interpreted sedimentation rate of the formation has been estimated at 40 m/myr during the Permian (Condon, 1997; Barbeau, 2003; Huntoon *et al.,* 1996; Nuccio &

Condon, 1996). Within Log 1.7 two cycles are 40 m in length, assuming constant sedimentation rate, however unlikely, for each 40 m cycle the influence of each cycle and the frequency of occurrence can be plotted. For the erg-margin cycle (Fig 5.20), the 100ka eccentricity peak will occur every 4 metres, the 35ka obliquity and 17ka precession cycles will therefore occur multiple times within this 4 m section. Within the lacustrine-margin cycle (Fig 5.2), the 100ka peak occurs every 8 metres. These cycles have then been compared to the sedimentological data (Fig 5.22, 5.23). Within both the erg-margin and lacustrine margin settings, the 100ka cycle is related to the switching of facies, and coincides with bedding planes between different facies. By integrating time series with sedimentological data, tentative conclusions can be drawn that the 100ka eccentricity cycle is the primary driver of changes in facies, and therefore climate is the dominant driver of change in the sedimentary environments. The differences in frequency of occurrences of this cycle also suggest that the lacustrine-margin cycles accumulated over longer periods of time than the erg-margin cycles and is more likely to be effected by longer scale processes such obliquity, although evidence of obliquity cycles would only preserved within sediments which encapsulate a large amount of geological time, such as interdune, sandsheet or lacustrine silts.

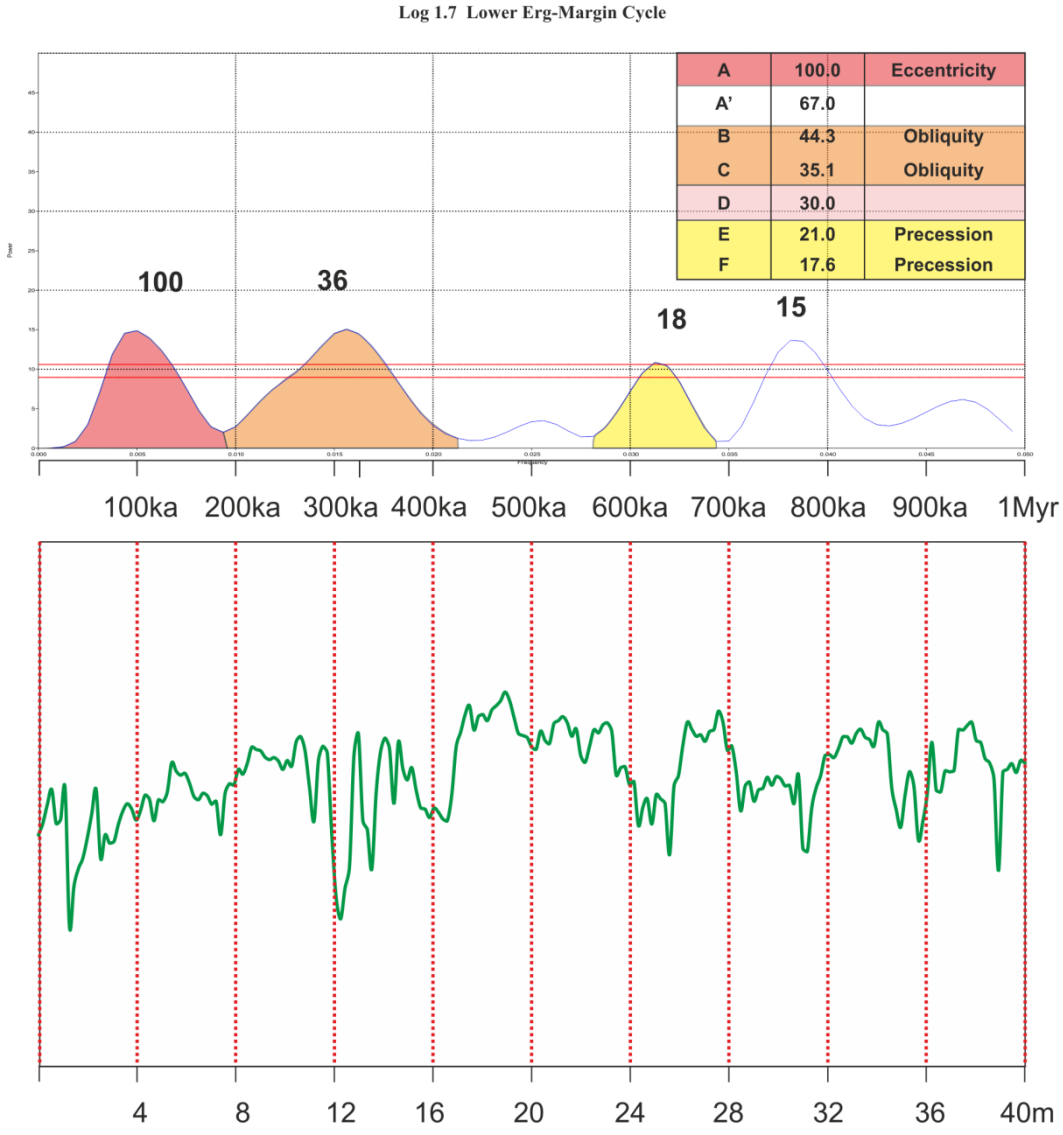

Figure 5.20 Linked power spectrum to sedimentation rate per Myr. Red dashed line shows frequency of 100 ka eccentricity cycle.

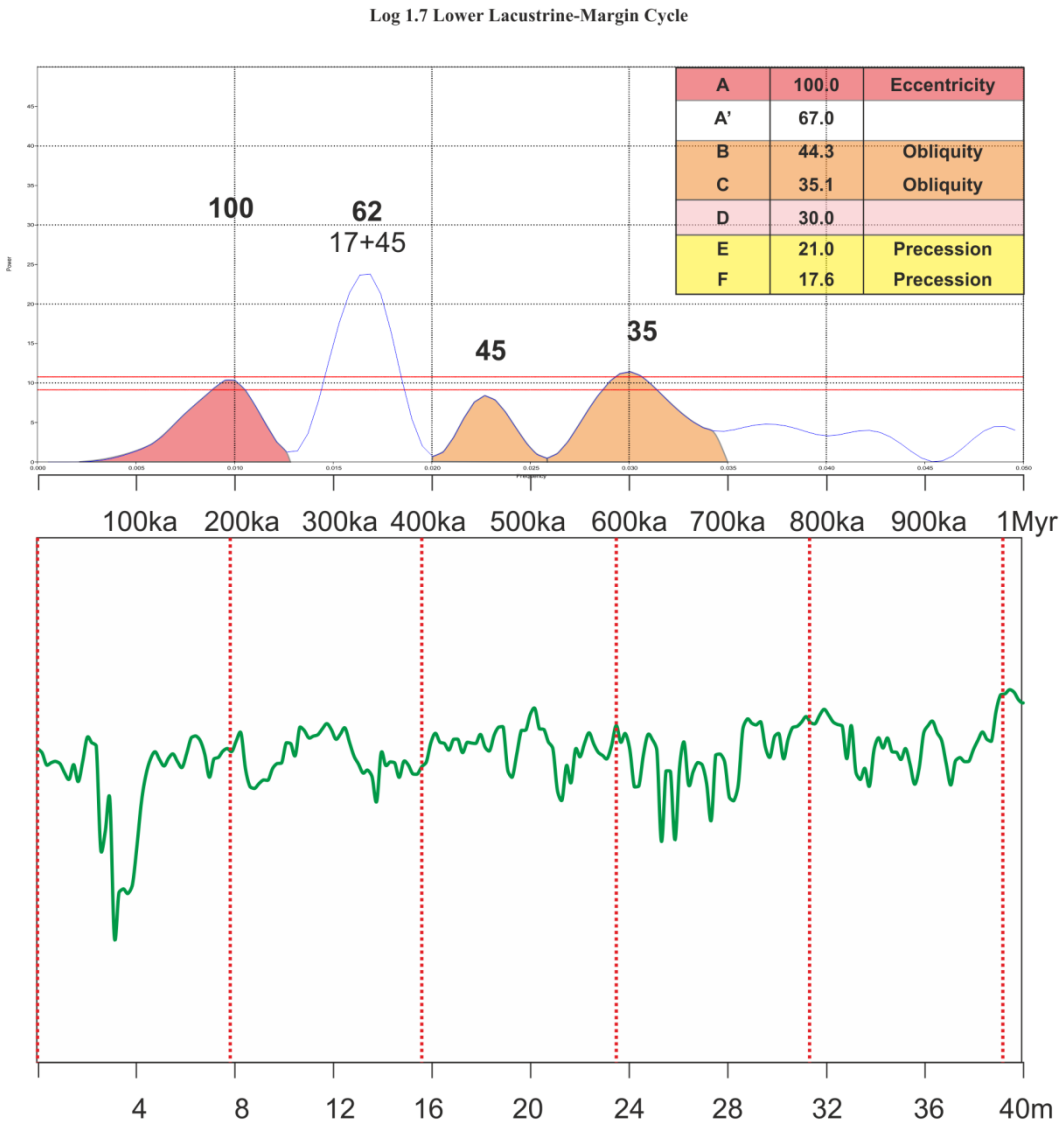

Figure 5.21 Linked power spectrum to sedimentation rate per Myr. Red dashed line shows frequency of 100ka eccentricity cycle.

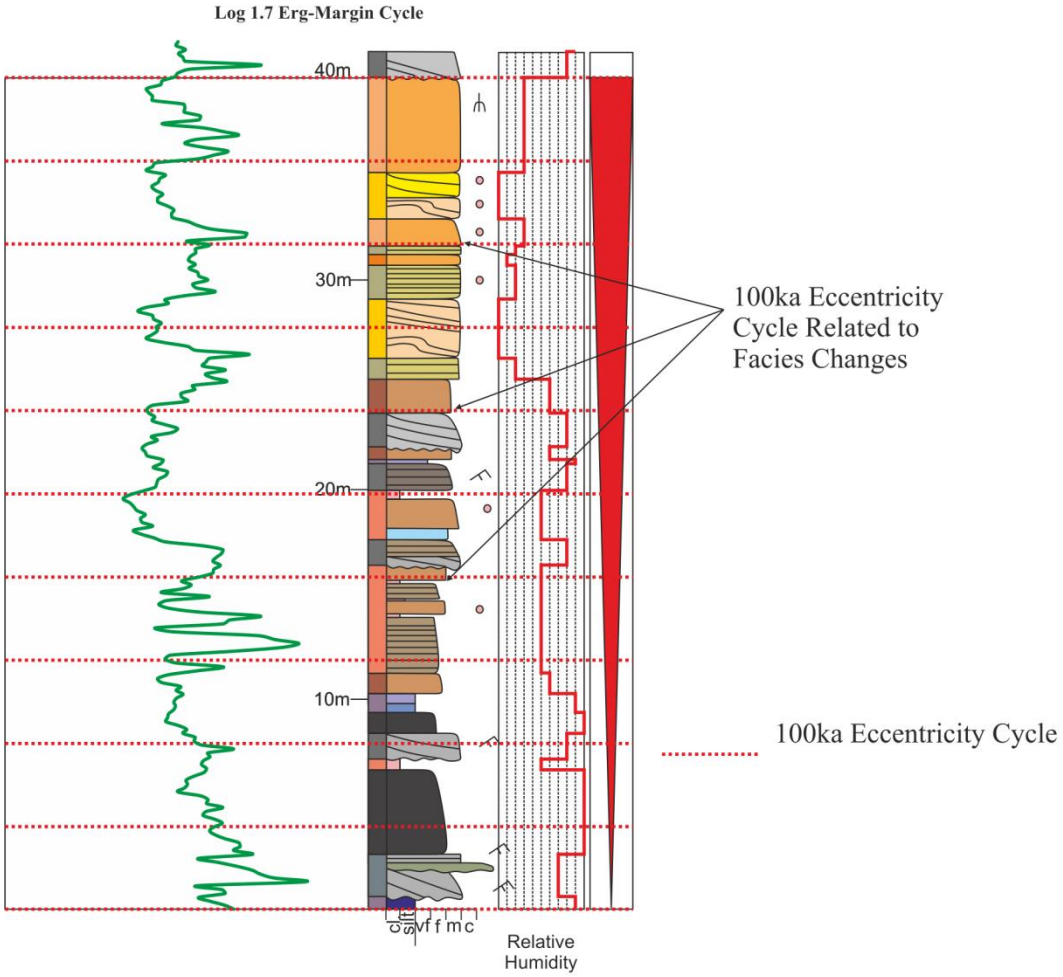

Figure 5.22 Linked sedimentology to interpreted Milankovitch ratio frequencies for the Erg-Margin cycle.

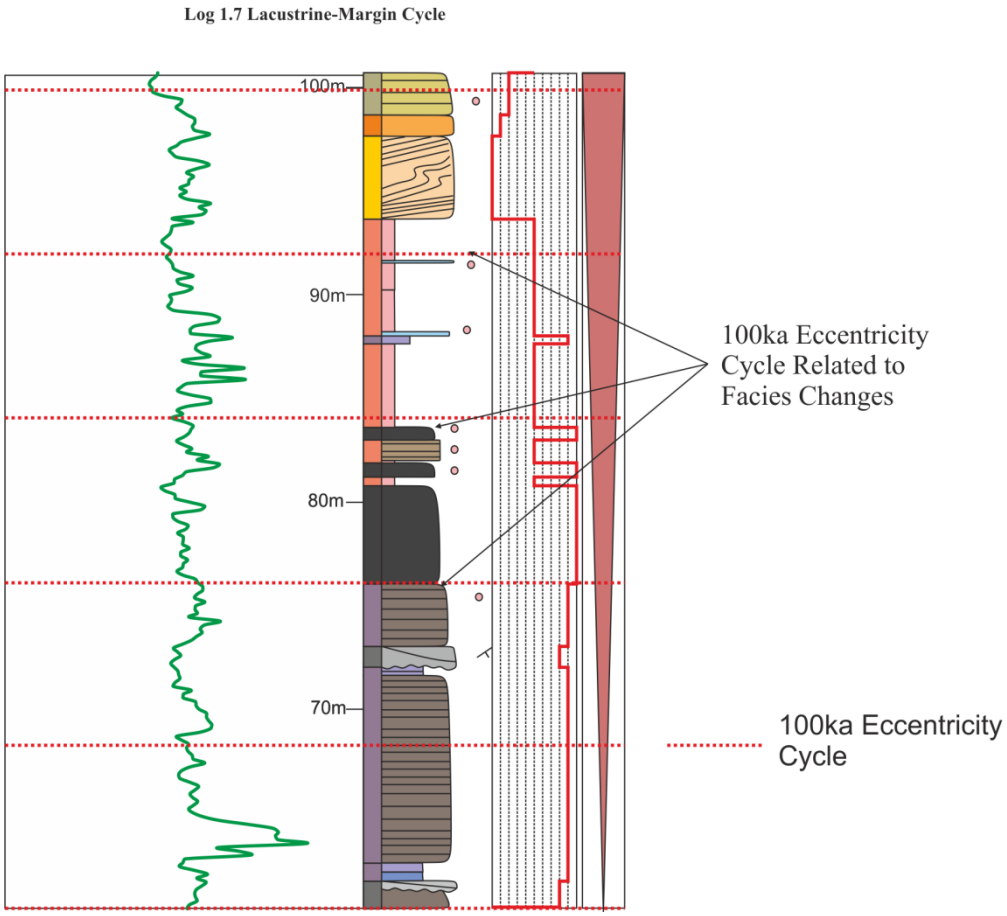

Figure 5.23 Linked sedimentology to interpreted Milankovitch ratio frequencies for the Lacustrine-Margin cycle.

5.5 Discussion

The previous section has described the climatic influence on the deposited and preserved sedimentary architectures seen. However the influence of other processes such as tectonics cannot be ruled out. The location of the inland sabkha deposits (Fig. 1.1) occur between two faults present today as the Comb Ridge and Raplee Ridge monoclines formed as a result of Laramide structural inversion (Mynatt *et al.,* 2009; Hilley *et al.,* 2010; Kelley 1955: Davis, 1999; Huntoon, 1993). The arrangements of the Comb Ridge and Raplee Ridge monoclines would have been present pre-inversion as two antithetic extensional faults, forming a graben-like structure (Fig. 5.24). These faults have been dated as inherited Precambrian

basement structures with multiple movement throughout geological time (Huntoon, 1993; Kelley, 1955). This fault arrangement likely resulted in a structural low which coincides with the sabkha deposits.

Tectonics are recognised as a primary control on sabkha formation by generating tectonic lows in which water can pool and subsequently evaporate (cf. Mertz & Hubert, 1990) and these faults likely generated localised topographic depocentres within the graben-like structure allowing for the pooling and subsequent evaporation of water during climatic fluctuations, creating the transition from aeolian to sabkha-like depositional environments.

These fault generated topographic lows may have allowed fluid to flow through the faults and spill out into a hot desert climate and pool (i.e. modern day Death Valley), with potentially deeper facies such as suspension settle lacustrine associations to occur near the point of maximum displacement. Isotopic analyses of gypsum samples give a marine signature (Stanesco & Campbell, 1989) whereas recent findings (Langford & Massad, 2014) and the results of this work point squarely to a continental depositional environment. The underlying Paradox Formation is composed of marine salts, which could have been recycled due to fluid flow along these faults (*cf.* Taberner et al., 2000) resulting in the marine geochemical signature.

The abrupt shift in facies from predominantly aeolian, to sabkha/lacustrine and limited distribution of the sabkha facies indicate that the fault control was most likely a local effect which is governed by the larger climatic allocyclic controls switching between varying degrees of either arid and humid conditions relating to changes in precession (Fig 5.25) or obliquity (Fig 5.26).

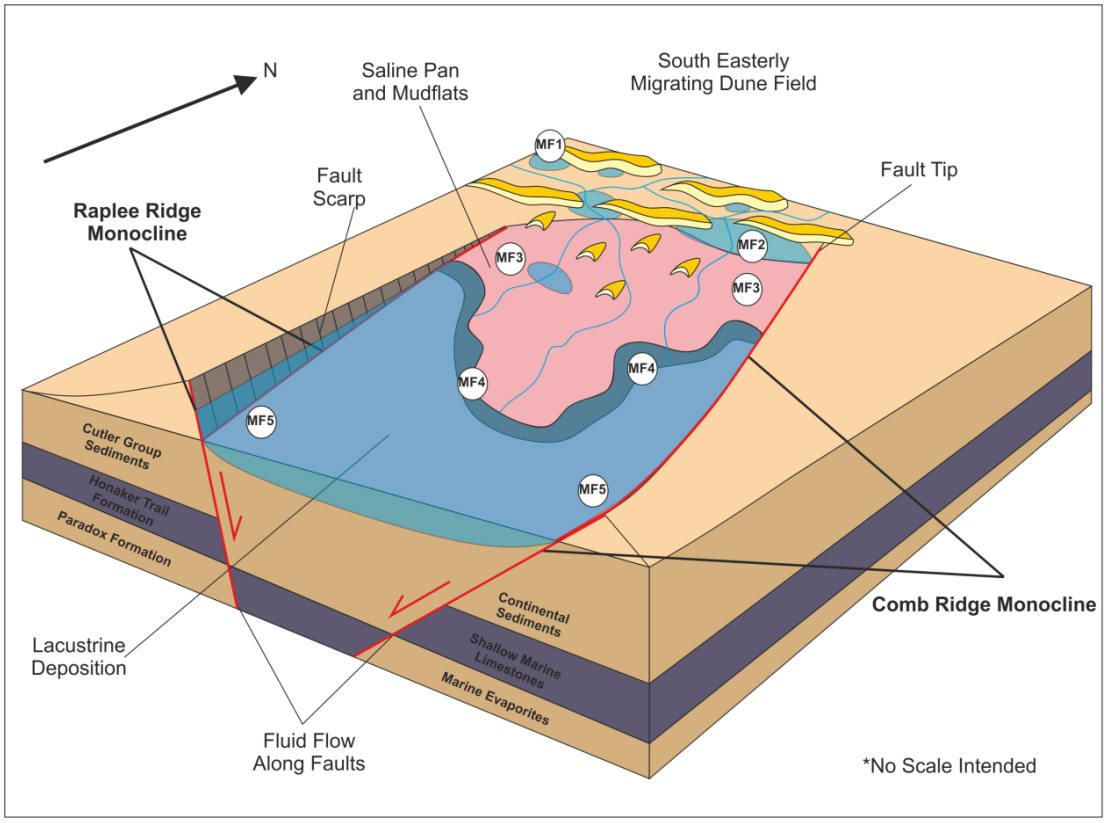

Figure 5.24 Schematic depositional model depicting the possible role that fault generated topography played on the arrangement and deposition of facies of the Cedar Mesa Sandstone Formation. The faults are shown in red with the interpreted depositional environments between. The location of each microfacies are marked with white circles, and the number of the microfacies within. The sabkha environment is shown in pink, lacustrine environment in blue, dunes are drawn in yellow.

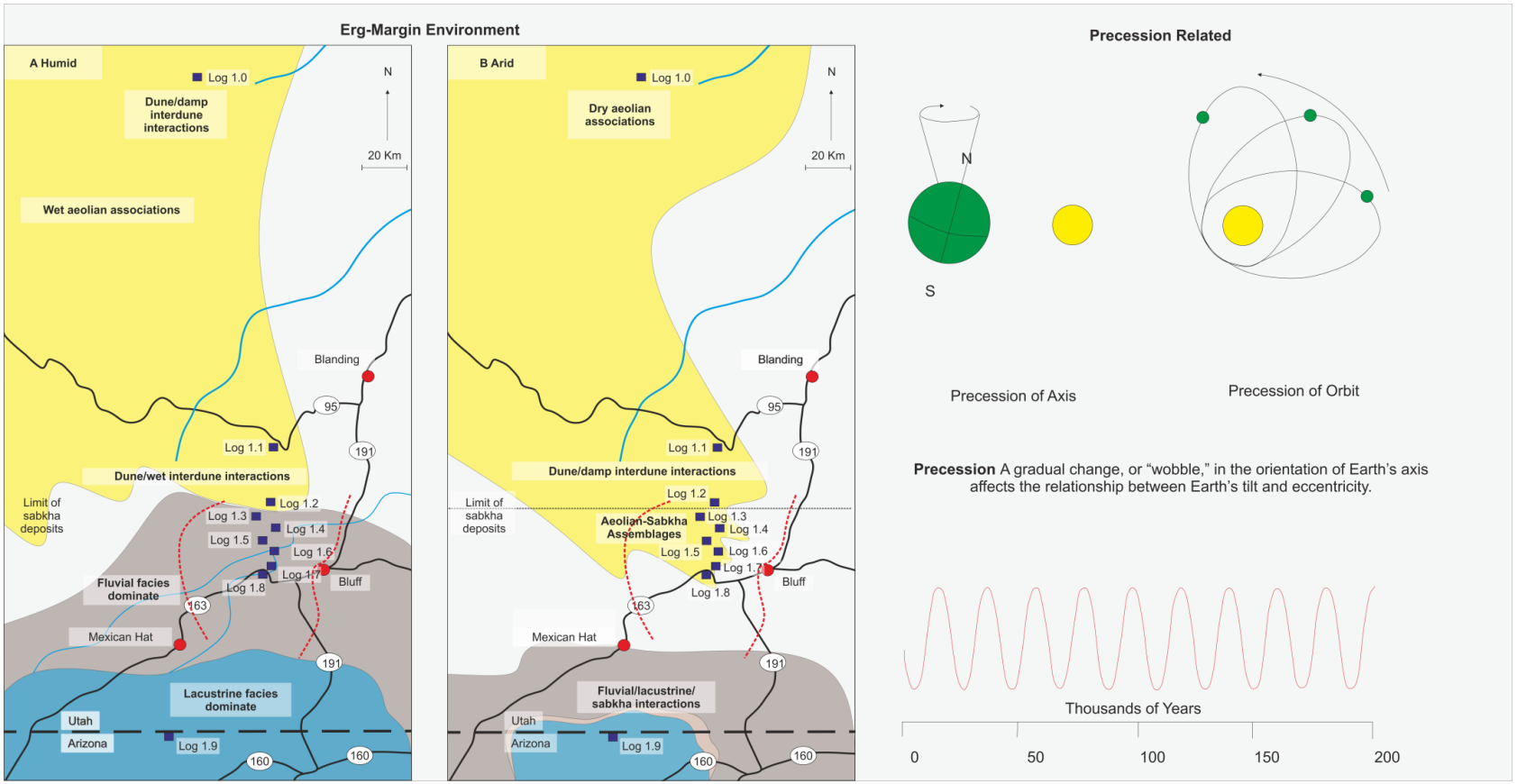

Figure 5.25 Paleogeographic reconstruction of the erg-margin environment during either humid (a) or arid (b) conditions. Dune sediments are represented by yellow colour, blue indicates lacustrine depositon. Pink shows location of evaporitic facies, grey is the fluvial plane. Location of the Raplee Ridge and Comb Ridge monoclines are shown by dotted red lines. Modern day roads are shown in solid black lines, state boundaries are highlighted with dotted black lines. Modern settlemets are shown with red circles. Location of each log is labelled and marked with dark blue square. Inferred Milankovitch process which resulted in the sedimentary deposits and variations between arid and humid conditions is shown to the right of the diagram

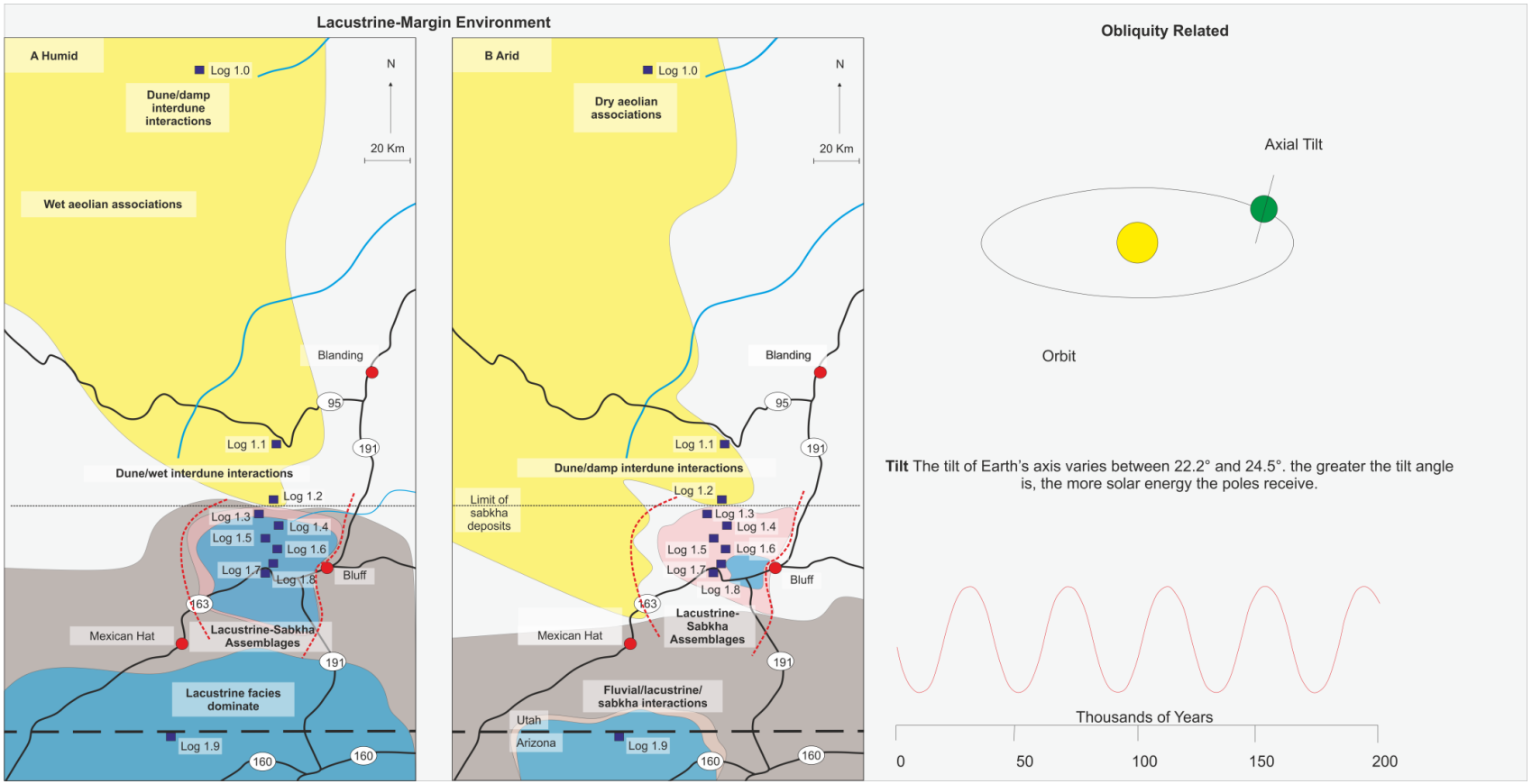

Figure 5.26 Paleogeographic reconstruction of the lacustrine-margin environment during either humid (a) or arid (b) conditions. Dune sediments are represented by yellow colour, blue indicates lacustrine depositon. Pink shows location of evaporitic facies, grey is the fluvial plane. Location of the Raplee Ridge and Comb Ridge monoclines are shown by dotted red lines. Modern day roads are shown in solid black lines, state boundaries are highlighted with dotted black lines. Modern settlemets are shown with red circles. Location of each log is labelled and marked with dark blue square. Inferred Milankovitch process which resulted in the sedimentary deposits and variations between arid and humid conditions is shown to the right of the diagram

5.6 Summary

This chapter has demonstrated that the deposits of the Cedar Mesa Sandstone Formation show cyclic temporal changes in sedimentology between either the erg-margin or the lacustrine-margin setting. These changes are governed by changes in climate and related sediment supply, which result in the preservation of alternating drying upwards cycles of each trend. The preservation of drying upwards only trends is due to the lack of accommodation space. Time series analysis of gamma ray data suggest that these cyclic changes are influenced by Milankovitch cycles. When gamma ray signatures are compared to the interpreted sedimentary logs, further time series analysis indicates that the erg-margin setting is primarily influenced by precession style processes compared to the lacustrine-margin trend which is influenced by obliquity, most likely as a result of differences in sedimentation rates between the two settings. Local fault control also played a role, and is the most likely explanation of the facies shift from erg to sabkha style deposits.

Chapter Six: Application of the Cedar Mesa Sandstone Field Analogue to the Leman Sandstone and Silverpit Formation of the Southern North Sea

This chapter details the application of the previous chapters work to subsurface data of the Leman Sandstone and Silverpit formations of the southern North Sea, a proven gas play. Gamma ray well data is reinterpreted using the results of field analogue study to aid in the correlation of potential reservoir units and to build depositional models.

6.1 Introduction

Field analogues are a well-used and useful technique in geology to help better understand subsurface geology. Subsurface data is usually in the form of seismic, core, or wireline well logs. While useful, this data is often limited in quantity and represents only a two-dimensional view of the rocks. Field analogues can offer a more comprehensive study, in more detailed resolution, and help gain insights into the three–dimensional architecture, enabling more accurate interpretations of the limited downhole data.

The early Permian Rotliegend Group of the Southern North Sea, UK, is composed of coeval mixed aeolian/fluvial deposits known as the Leman Sandstone and mixed evaporitic/clastic sabkha deposits of the Silverpit Formation. These deposits are commercially viable and have been producing hydrocarbons since the 1970s. While most of the hydrocarbons are contained within the aeolian erg deposits, significant resources also lie within the transition zone between the erg and the sabkha, where dune sediments encroached into the sabkha during periods of climatic aridity. These

dune sediments are often small and isolated, making them hard to detect in downhole data, and, thus, a risky prospect.

This chapter will use the detailed outcrop study of the Cedar Mesa Sandstone Formation of Utah, to demonstrate that the results have application to the similar depositional system of the Rotliegend in the North Sea, UK. Downhole Gamma Ray data is used from several wells, which span this transition to compare with trends seen from the Cedar Mesa Sandstone Formation. This work will test the conclusions of the outcrop study, with the aim of potentially enhancing hydrocarbon recovery by demonstrating that correlations on the basis of drying upwards climatic cycles can pinpoint periods where dune sediments are most likely to be present.

6.2 Geological Setting

The early Permian Rotliegend Group of the Southern Permian Basin is composed of the mixed aeolian/fluvial deposits of the Leman Sandstone Formation and the mixed evaporitic/clastics of the Silverpit Formation. The Rotliegend Group is underlain by the Carboniferous Westphalian coal measures and overlain by the upper Permian Zechstein salt Supergroup (Fig 6.1)

6.2.2 The Silverpit Formation

The Silverpit Formation was formed within an extensive desert lake which at its apex extended over 1200 km eastwards from the North Sea through Germany and Poland with a width of over 200 km (Glennie, 1986; Cameron *et al.,* 1992). The deposits of the Silverpit Formation consist of lacustrine clays and silts interbedded with halite and anhydritic mudestones. The basal halite interval within the type-well of the Silverpit Formation (44/21-1), located within the lake centre, is 50 m thick (Rhys, 1974), however, the evaporite beds progressively thin and become less numerous up section and towards the lake margins. This suggests the lake was

relatively shallow and subject to more extreme fluctuations in salinity at the start of its formation during the early Permian, with increased freshwater discharge into the lake, followed by less intense evaporitic conditions leading to an expansion of the lake southwards over the Leman Sandstone Formation (Cameron *et al.,* 1992).

Lacustrine facies are characterised by monotonous sequences of red-brown, silty anhydritic mudstones, with occasional beds of grey silts (Cameron *et al.,* 1992). Interbedded halite occurs at the base of these mudstones and is termed the Silverpit Halite Member.

Lake margin facies comprise a complex interfingering of lacustrine, sabkha, aeolian and fluvial sediments, with succession up to 50 m thick consisting of interbedded clays, silts and sandstones, often in upwards fining cycles which have been correlated between wells (Butler, 1975). Sandstones are interpreted to have been deposited by distal sheetflood deposits entering the desert lake, with shoreline sabkha facies represented by adhesion-rippled sands and nodular anhydrite within clays and silts (Glennie, 1972). Rare interbedded aeolian and fluvial deposits indicate periods of lake retreat, however the sabkha and lacustrine deposits are gradational so the lateral limits of the sabkha facies is not easily determined (Cameron *et al.,* 1992). Long term expansion of the lake is seen within the south of the basin, as the lacustrine facies prograde over the lake margin aeolian/fluvial deposits of the Leman Sandstone Formation (Butler, 1975). Short term fluctuations are also seen within the lake margin facies, with complex interbedding of lacustrine, sabkha, aeolian and fluvial deposits (Cameron *et al*., 1992).

6.2.1The Leman Sandstone Formation

The Leman Sandstone is composed almost entirely of fluvial and aeolian sediment (Cameron *et al.,* 1992) each of which is relatively distinct in core and wireline logs (Glennie, 1972).

Fluvial facies comprise of conglomeratic layers which interfinger with laminated or homogeneous red-brown sandstones and dark red muds and clays (Cameron *et al.,* 1992). The fluvial facies occur interbedded or in distinct packages above or below aeolian facies. The thickest fluvial deposits occur in a north-east trending belt from the coast of East Anglian to the margin of the Silverpit desert palaeolake (Marie, 1975). Distinct deposits of fluvial strata are 100 m at their thickest, and intercalated with aeolian sandstones, elsewhere fluvial deposits average ~50 m in thickness (Glennie, 1986).

The sedimentary structures observed from core (Glennie, 1972) indicate an ephemeral fluvial system. Deposits are either structureless or have gently inclined laminae, with occasional rip up clasts of red clay and pebbles, interpreted as being scoured from underlying deposits of ephemeral lakes within a wadi style system with occasional desiccation features suggesting sub-aerial exposure (Glennie, 1972: Cameron *et al.,* 1992). Conglomerates of 1.5 m thickness are occasionally present, and interpreted to have been formed around the basin margins (Goodchild & Bryant, 1986).

The fluvial sediments of the southern North Sea were deposited in alluvial plains and floodplains by rivers flowing northwards from the Variscan highland towards the Silverpit desert palaeolake in the centre of the basin (Marie, 1975). Rainfall was most likely seasonal, occurring in violent storms with floodwaters following interdune corridors between sand dunes eroding and reworking aeolian and previously deposited fluvial sands. During dry periods aeolian sediment encroached over these wadis but did not become well-established (Marie, 1975).

Aeolian sandstones dominate over the fluvial facies towards the top of the Leman Sandstone Formation, indicating a progressively drier environment (Cameron *et al*., 1992).

Aeolian facies occur in sequences up to 200 m thick, of dune sets and cosets. Dune sediments form almost the entire components of the Leman Sandstone Formation in the east and south-east area of the basin (Marie, 1975; van Veen, 1975). Towards the west of the basin these aeolian deposits interfinger with fluvial deposits described previously (Glennie, 1972). Within core data the aeolian sediments are represented by alternating planar and trough cross laminations of fine and coarser grained sandstone (Glennie, 1986). These laminations are inclined between 20-25 ° before being truncated by the following dune set, and have been interpreted to represent both transverse and seif dunes (Glennie, 1972). Occasionally, thin packages of silty sands, with wavy laminations are encountered, and are interpreted to be the deposits of damp interdunes, where sediment has adhered to the damp surface caused by an elevated water table (Glennie, 1972; Conway, 1986).

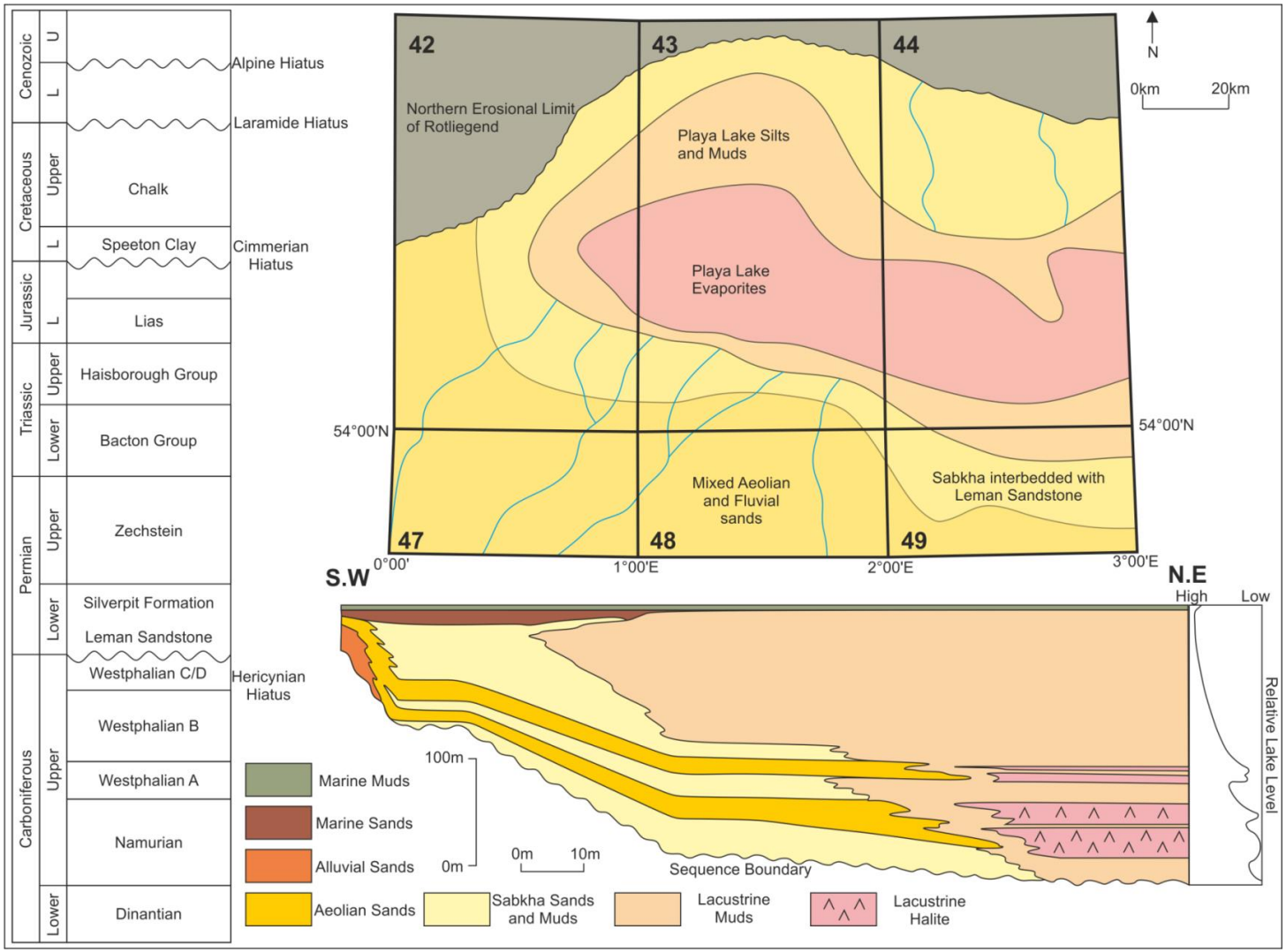

Figure 6.1 Stratigraphy of the southern North Sea (after) Cross section and paleogeography of the Silverpit/Leman formations of the southern North Sea, UK license blocks are shown in bold (after Bailey *et al.,* 1993)

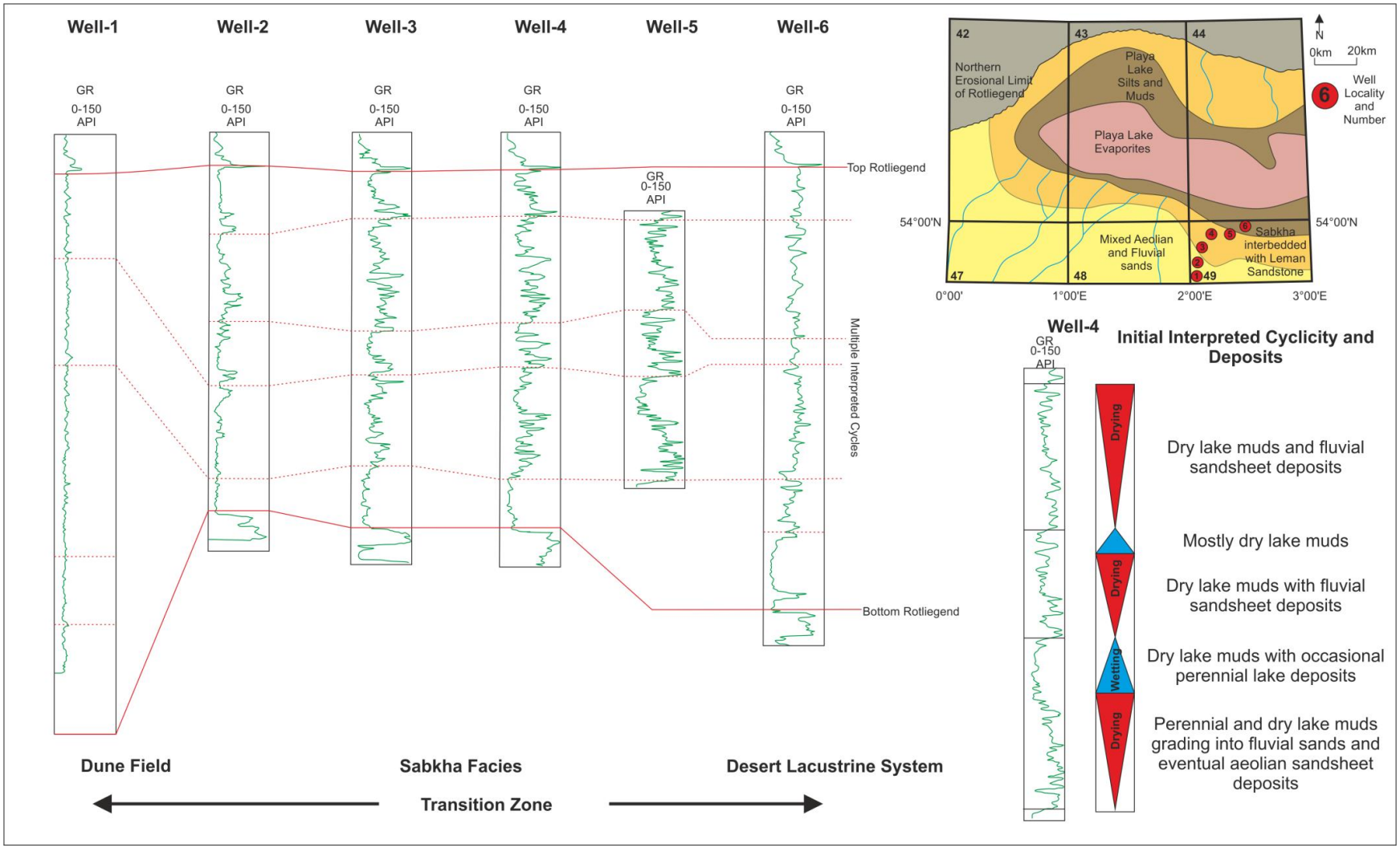

Figure 6.2 Well logs and initial correlation over the erg-lake transition zone, location of well logs are shown on paleogeographic map. Interpreted cyclicity and deposits of well-4 are shown on the right hand panel

6.3 Methodology

This work uses six gamma ray well logs over a South West-North East transect along the south of the basin, which spans the main transition zone between the Leman Sandstone and the Silverpit Formation (Fig 6.2). This area was targeted as it has been recognised that both-long and short-term fluctuations of lake retreat and expansion are present, represented by complex interbedding of aeolian, fluvial, lacustrine and sabkha facies (Butler, 1975). An initial correlation of the well logs (Fig. 762) is presented, which shows the top and bottom Rotliegend interval and an initial lithographic interpretation of the deposits based on drying and wetting cycles.

Idealised log trends for the erg-margin and lacustrine-margin sabkha trends have been determined from the Cedar Mesa Sandstone Formation (Chapters 3 & 4), these trends are subsequently compared to downhole signals in the transition zone of the Rotliegend, to see if comparisons can be made and refine the initial interpretation. Due to the commercial sensitivity of the logs, well names and depths are omitted.

6.3.1 Idealised Log Trends from the Cedar Mesa Sandstone Formation

Comparison of the gamma ray results to the interpreted drying upwards cycles within the Cedar Mesa Sandstone for both the erg-margin trend and the lacustrine-margin trend, allows for the observation of unique gamma ray trends for the cycles (Fig. 4.13). Comparison of the trends from each of the various interpreted cycles has led to the development of idealised trends for each setting (lacustrine-margin or erg-margin) which can be related back to idealised sedimentary successions (see chapters 3 and 4).

The erg-margin trend shows overall low counts, with a drying upwards section towards the bottom of the trend, which relates to fluvio/lacustrine sediments as the

climate dries, followed by a large curved 'C' as dune sediments dominate the sequence.

The lacustrine-margin trend shows an initial coarsening upwards sequence related to the dominance of lacustrine deposits, followed by intermittent high and low counts as the climate dries and sabkha deposits composed of interbedded palaeosol and evaporite deposits become dominant.

These trends are subsequently compared to downhole data from the Rotliegend to test their applicability.

6.4 Results

Previous work (e.g. Howell & Mountney, 1997) has focused mainly on interpreting cycles from wireline logs and core based on wetting and drying (Fig. 6.2), however outcrop studies from the Cedar Mesa Sandstone, detail that cycles may only preserve drying-upwards cycles, with the lower, wetter, part of the cycle being misinterpreted as part of a wetting trend (chapters 3,5).

When interpreted as overall drying-upwards trends, similarities between the idealised gamma ray successions for both the erg-margin and lacustrine-margin sabkha can be seen (Fig. 6.3-6.7).

At least five distinct drying-upwards cycles which correspond to either the lacustrine-margin or erg-margin trend are seen in Wells 2-6.

Well-1 (Fig 6.8) shows no relationship to either the erg-margin or the lacustrine-margin trend, however when compared to core (Fig 6.9) work (Priddy *et al.,* 2018) it is clear that these wireline responses match signatures for the mixed aeolian-fluvial Leman Sandstone Formation, and so it can be interpreted that the Silverpit Formation had no influence upon its deposition and represents a central erg

paleogeographical position away from any influence of a sabkha or lacustrine deposition (Fig 6.10).

Correlations are subsequently made on the basis of these drying upwards cycles (Fig 6.11) with the aim of identifying climatic trends and potential zones for hydrocarbon exploration.

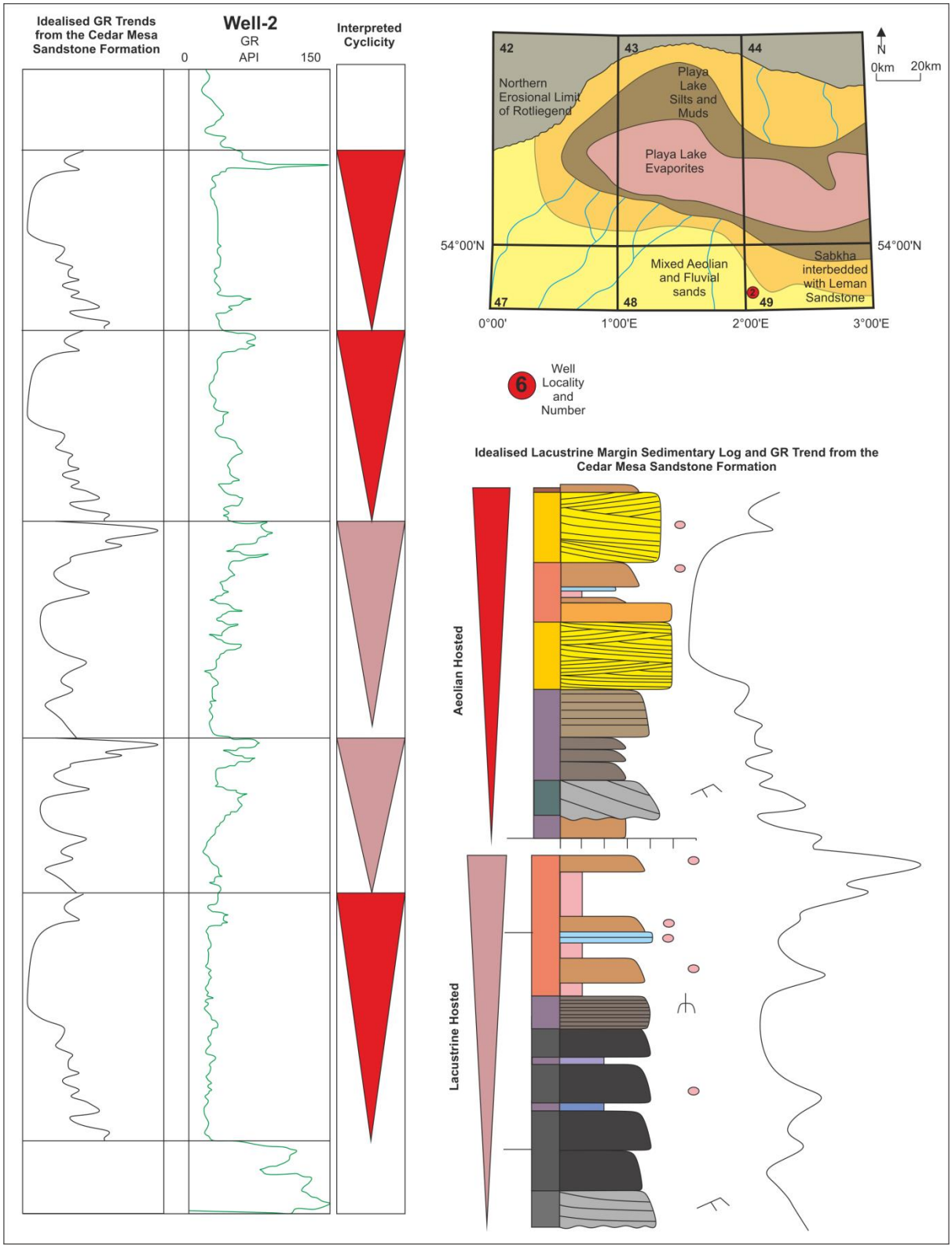

Figure 6.3 Gamma ray log of Well-2 shown in green, the best fit idealised trend is shown in the left hand column. Interpreted cyclicity is shown by arrows, red arrows indicate drying upwards trends of erg-margin trend, salmon arrow indicates lacustrine-margin trend. Idealised sedimentary logs are shown in right hand side. Location of well log is shown in upper right corner over paleogeographic map.

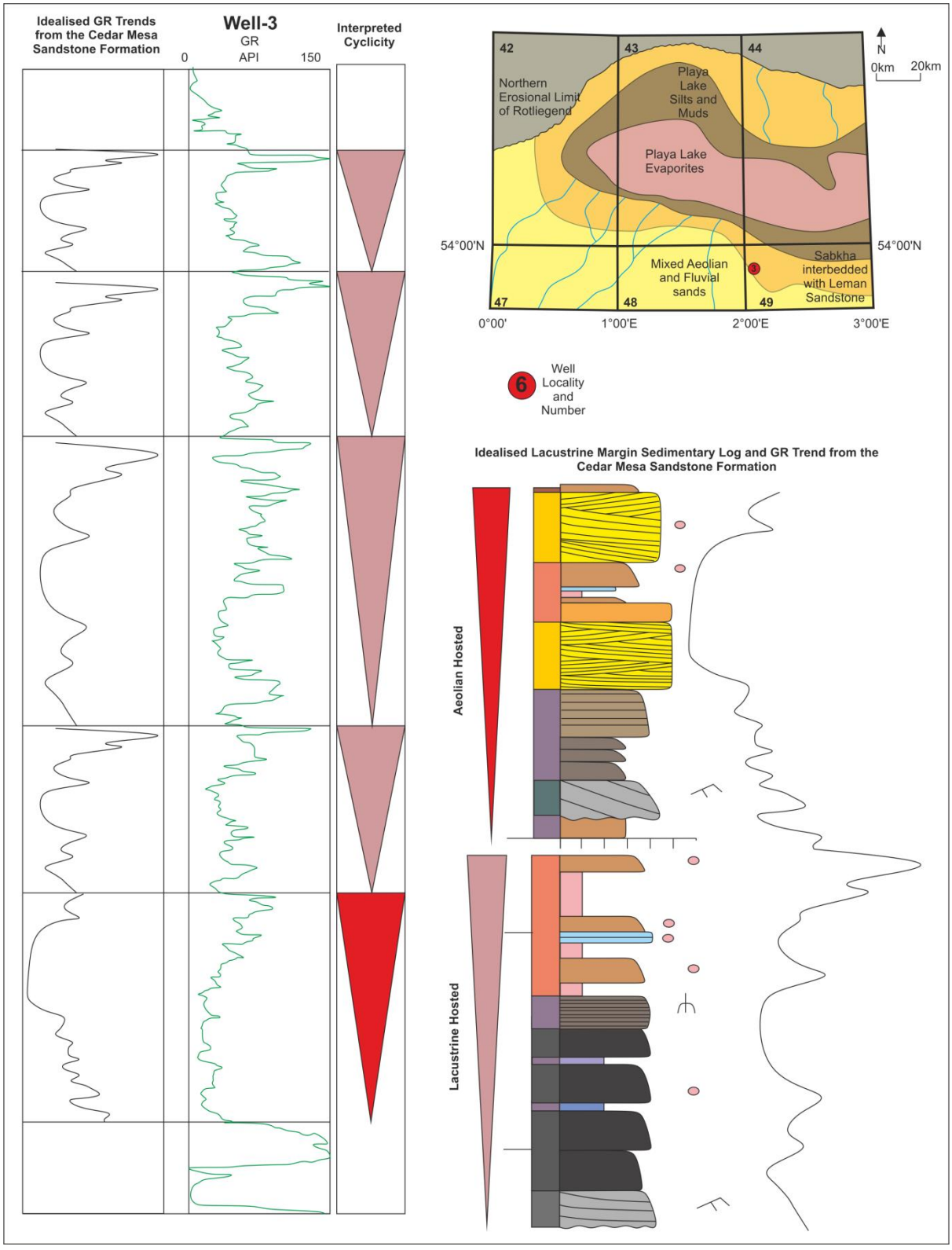

Figure 6.4 Gamma ray log of Well-3 shown in green, the best fit idealised trend is shown in the left hand column. Interpreted cyclicity is shown by arrows, red arrows indicate drying upwards trends of erg-margin trend, salmon arrow indicates lacustrine-margin trend. Idealised sedimentary logs are shown in right hand side. Location of well log is shown in upper right corner over paleogeographic map.

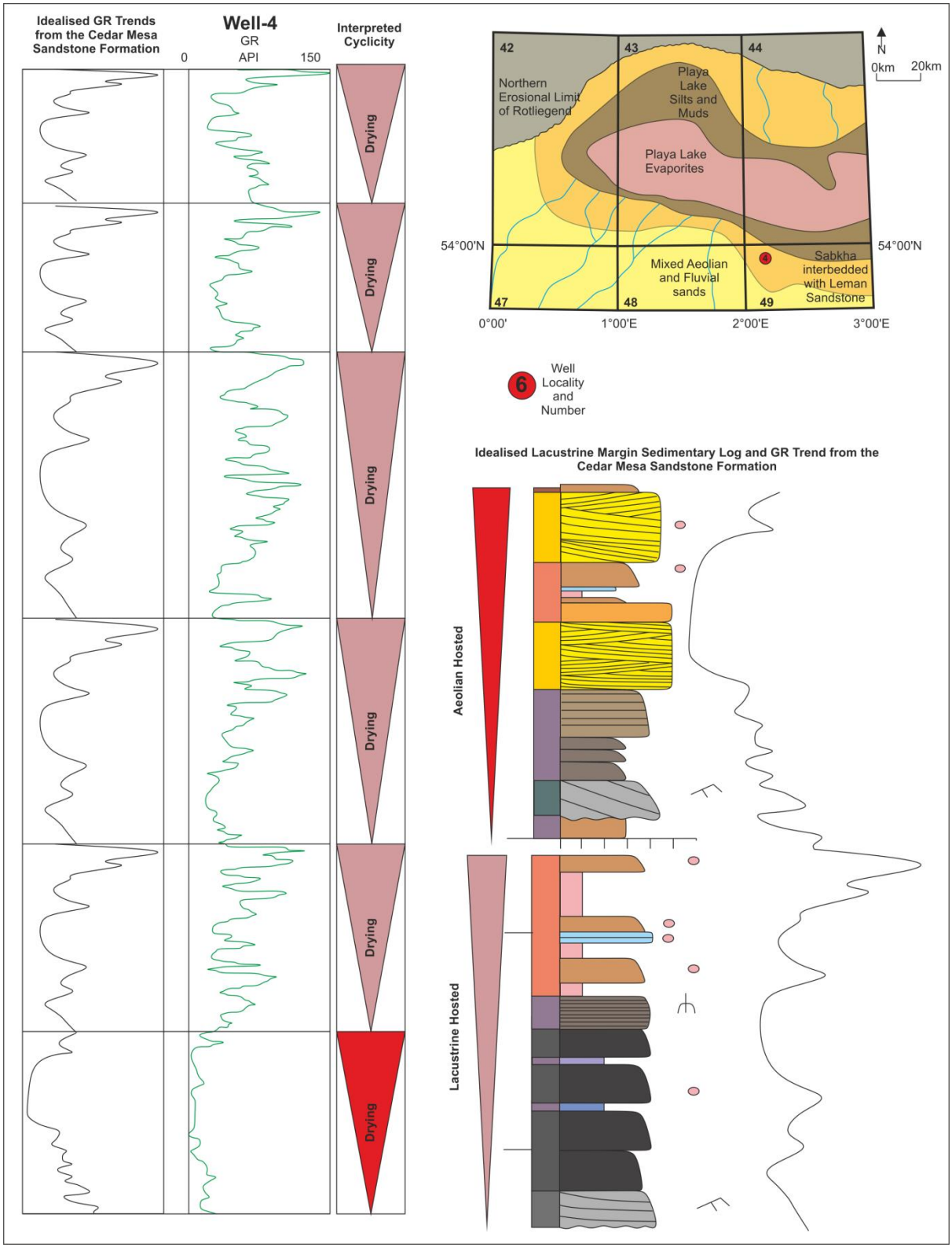

Figure 6.5 Gamma ray log of Well-4 shown in green, the best fit idealised trend is shown in the left hand column. Interpreted cyclicity is shown by arrows, red arrows indicate drying upwards trends of erg-margin trend, salmon arrow indicates lacustrine-margin trend. Idealised sedimentary logs are shown in right hand side. Location of well log is shown in upper right corner over paleogeographic map.

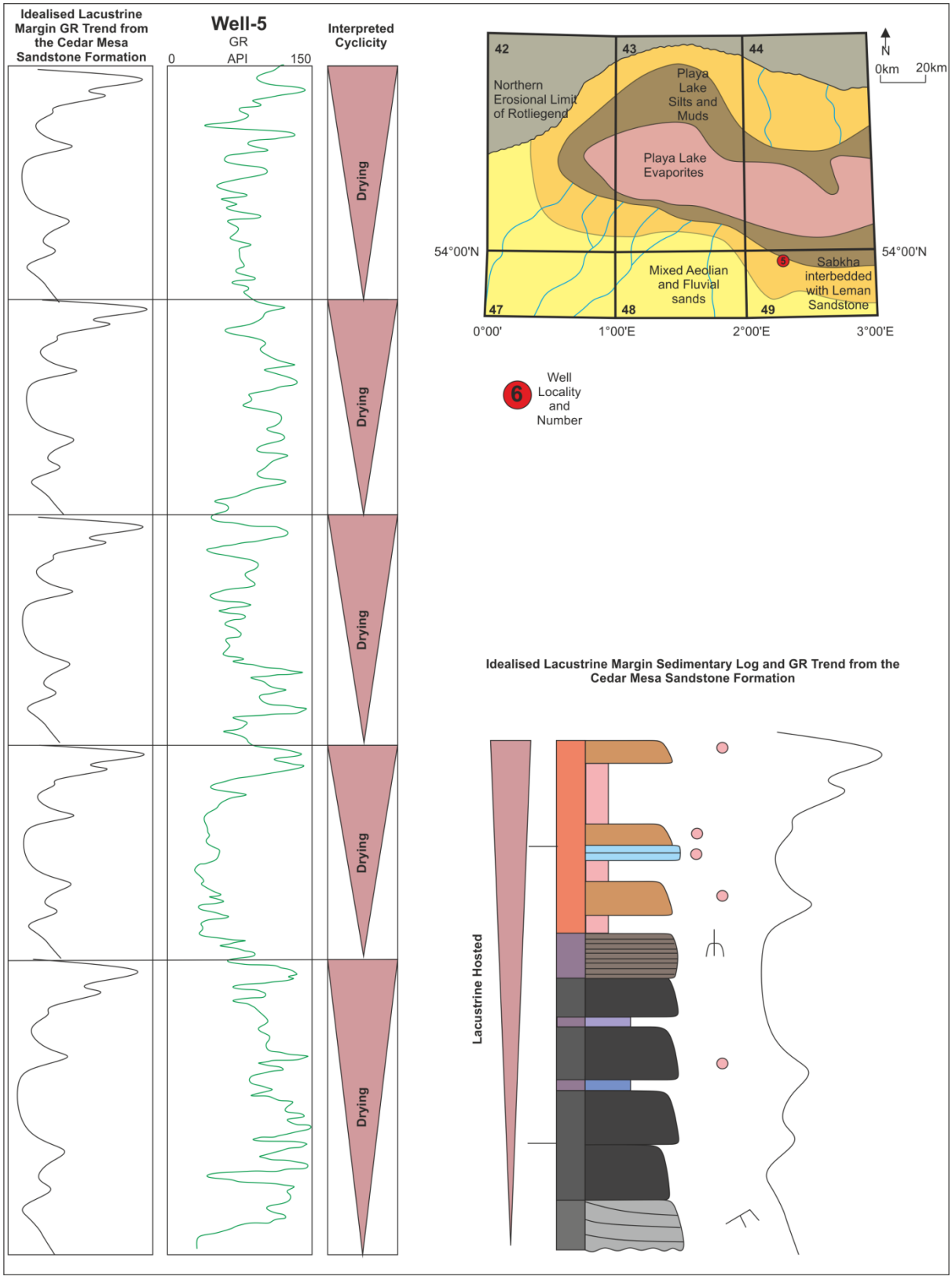

Figure 6.6 Gamma ray log of Well-5 shown in green, the best fit idealised trend is shown in the left hand column. Interpreted cyclicity is shown by arrows, red arrows indicate drying upwards trends of erg-margin trend, salmon arrow indicates lacustrine-margin trend. Idealised sedimentary logs are shown in right hand side. Location of well log is shown in upper right corner over paleogeographic map.

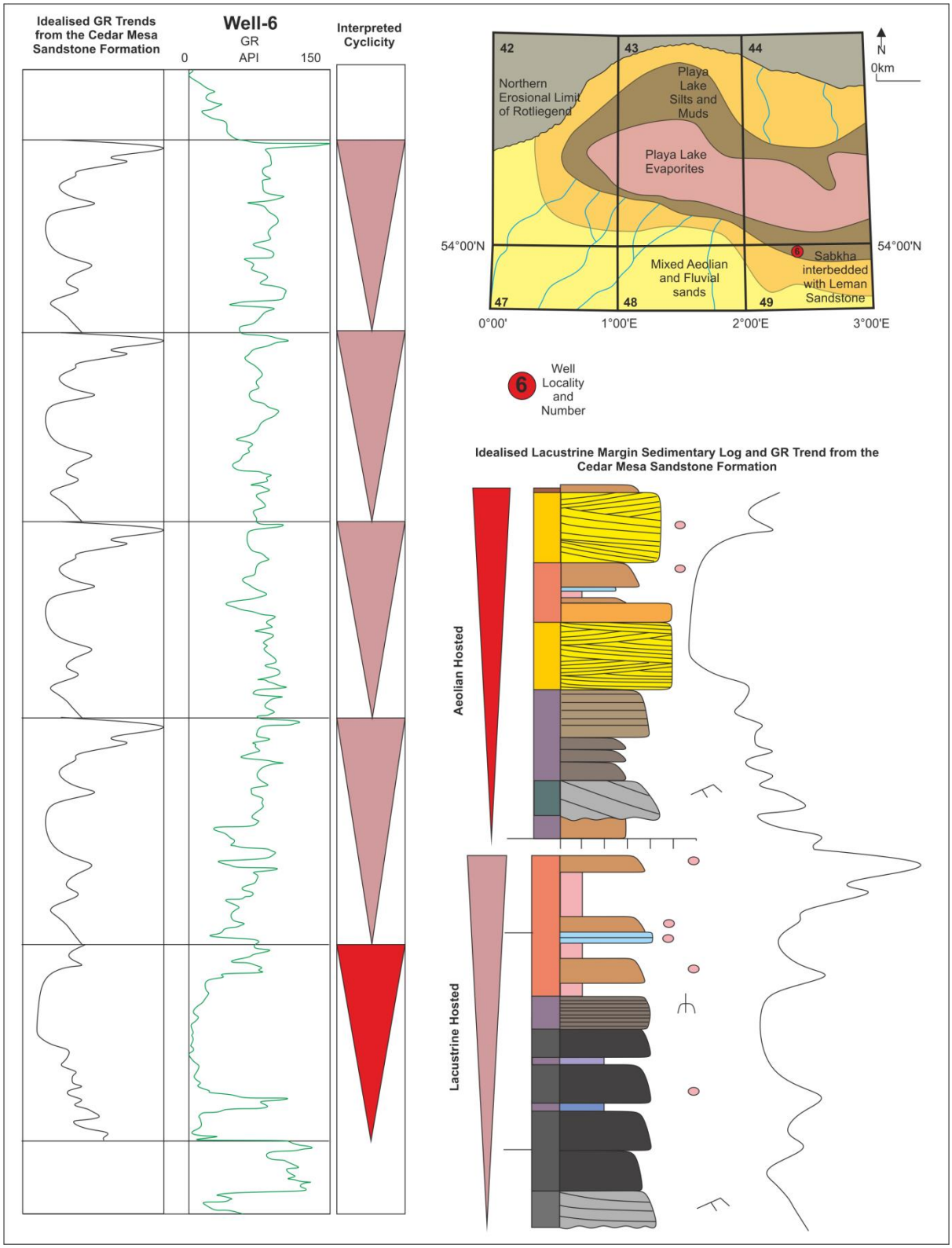

Figure 6.7 Gamma ray log of Well-6 shown in green, the best fit idealised trend is shown in the left hand column. Interpreted cyclicity is shown by arrows, red arrows indicate drying upwards trends of erg-margin trend, salmon arrow indicates lacustrine-margin trend. Idealised sedimentary logs are shown in right hand side. Location of well log is shown in upper right corner over paleogeographic map.

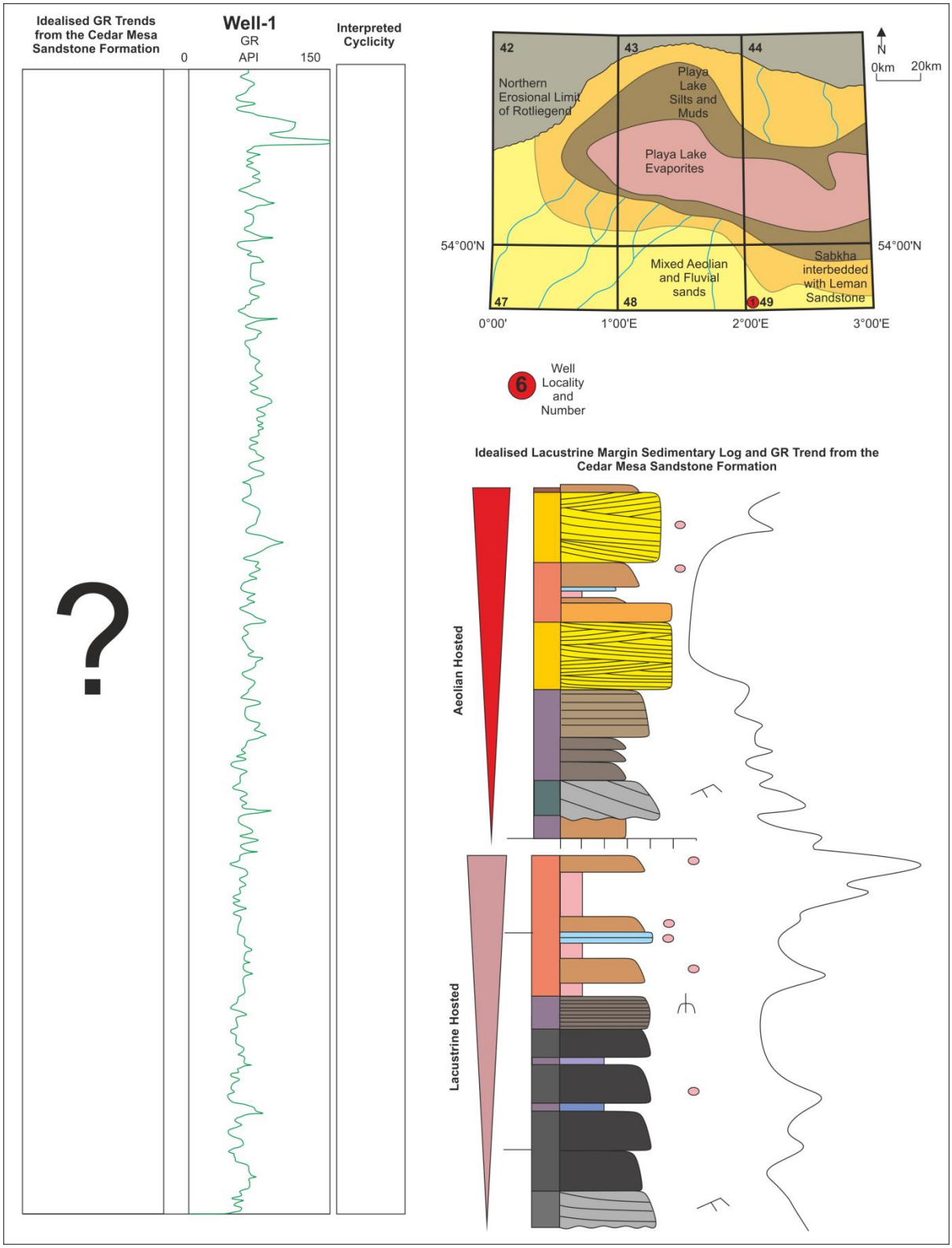

Figure 6.8 Gamma ray log of Well-1 shown in green. Log does not fit any of the idealised trends, shown in the right hand side. Location of well log is shown in upper right corner over paleogeographic map.

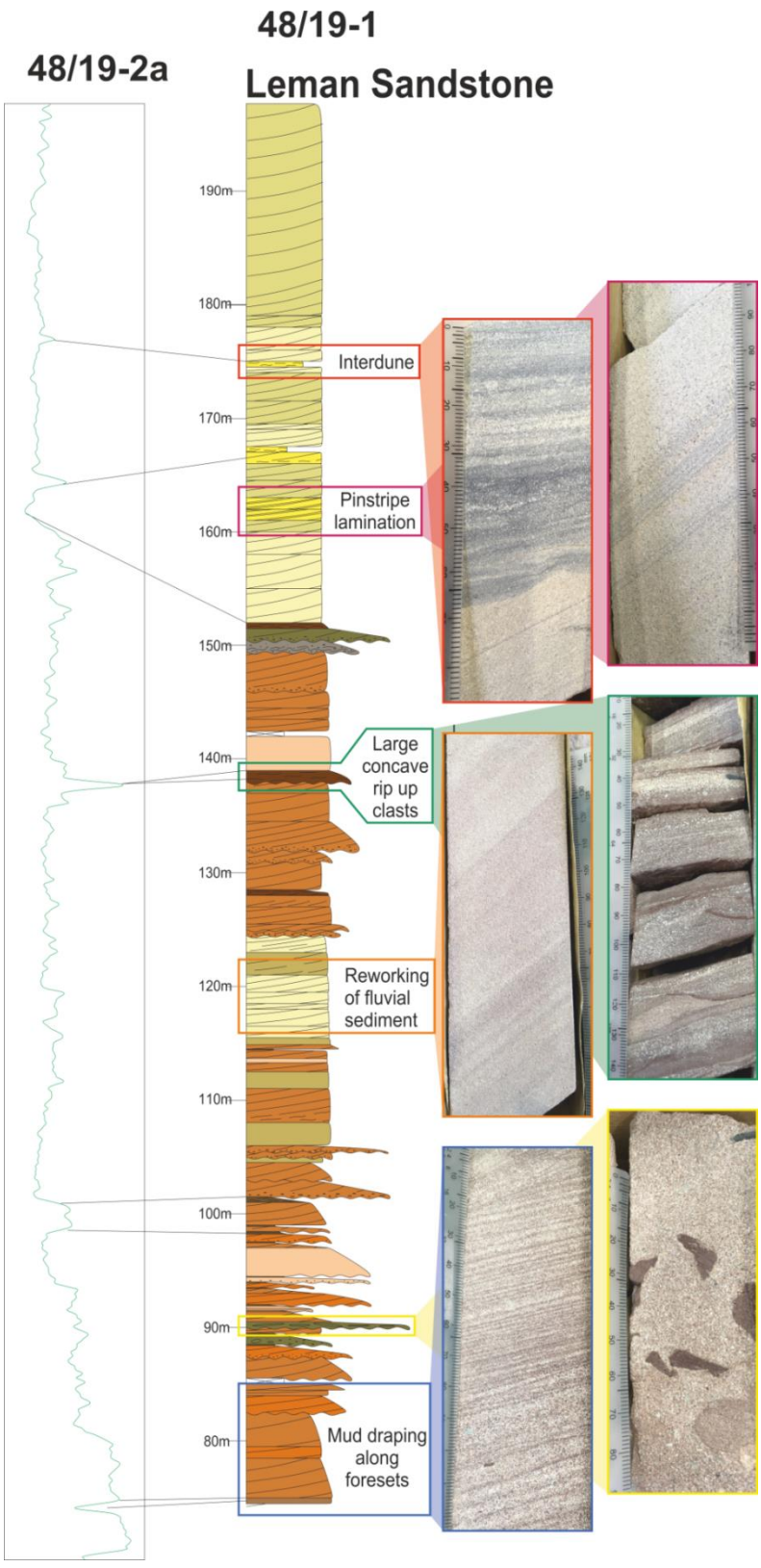

Figure 6.9 Combined core and well log from block 49 well 48/19 of the Leman Sandstone Formation. Core log is correlated to the gamma ray log, and shows the various facies and gamma ray responses to the mixed aeolian and fluvial deposits (after Priddy *et al.,* 2018).

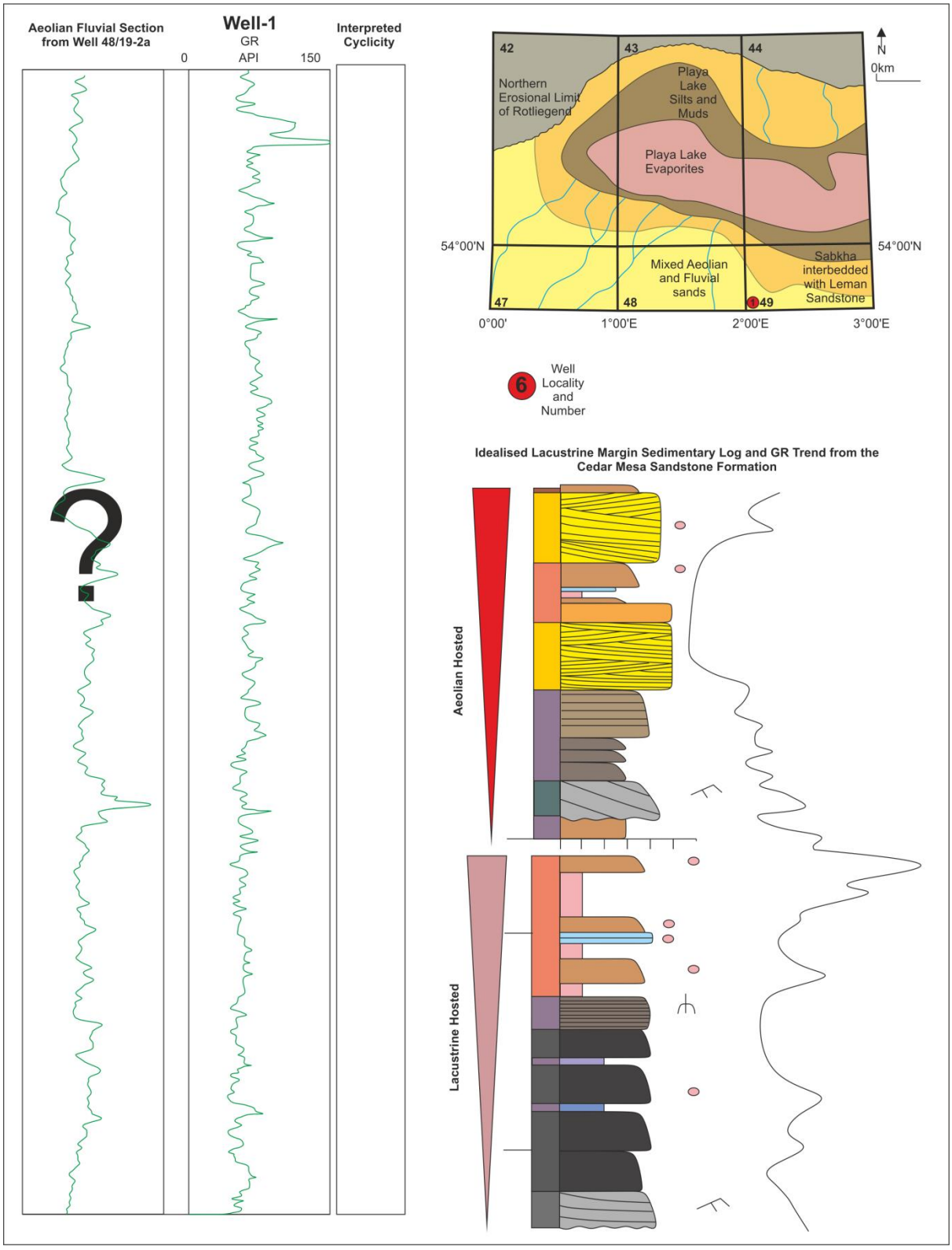

Figure 6.10 Gamma ray log of Well-2 shown in green on the right, gamma ray log from well 18/19-2a shown on left. The two gamma ray logs show similar API values and trends, so it is assumed that Well-1 is composed of the Leman Sandstone Formation and has no influence of sabkha deposits. Idealised sedimentary logs are shown in right hand side. Location of well log is shown in upper right corner over paleogeographic map.

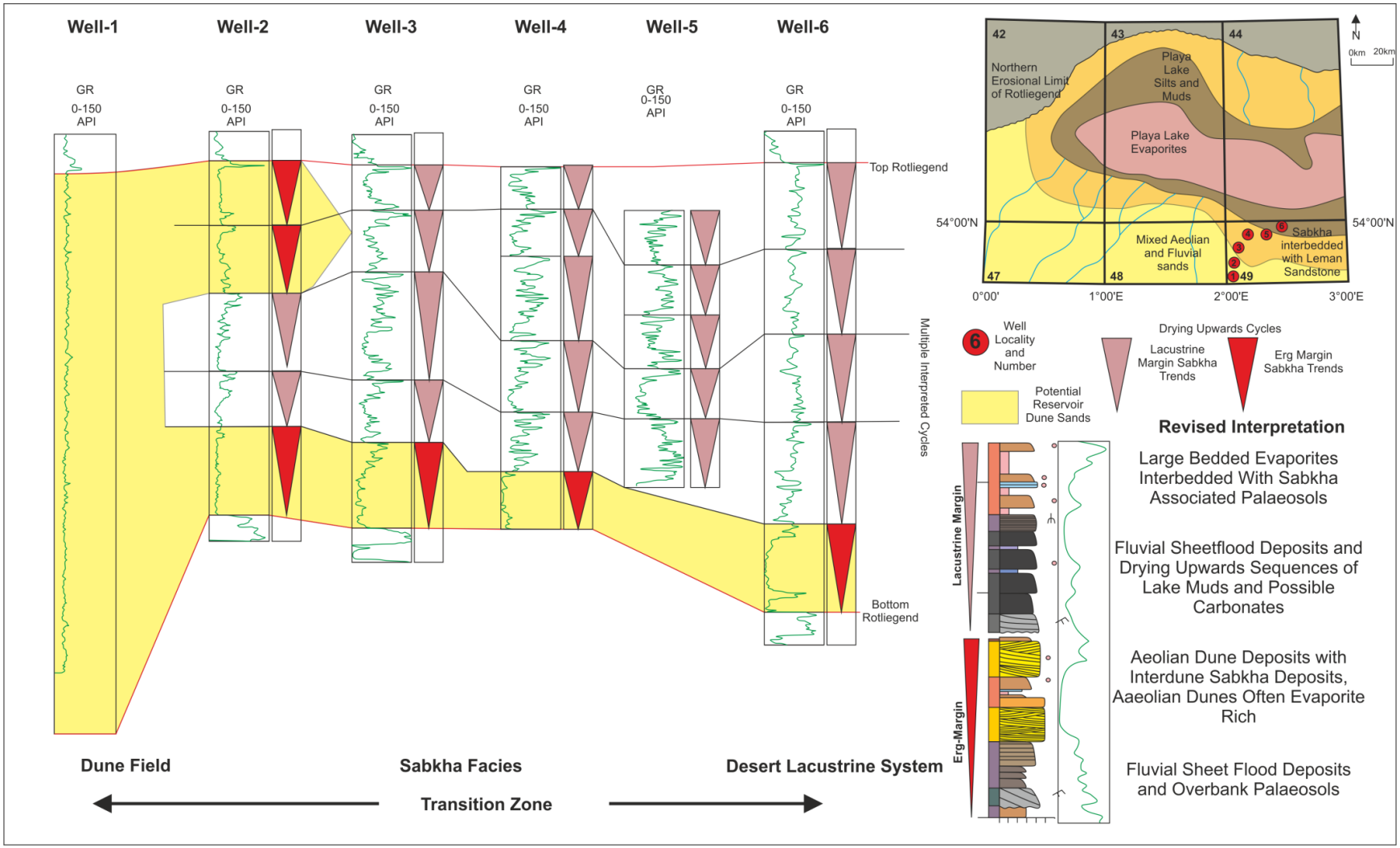

Figure 6.11 Well logs over the erg-lake transition zone, location of well logs are shown on paleogeographic map. Wells are now correlated on the basis of drying upwards cycles, lacustrine-margin trends are shown by salmon arrows, erg-margin trends are indicated by red arrows. The location of potential higher net-to-gross sand bodies are highlighted in yellow. Interpreted cyclicity and deposits of well-4 are shown on the right hand panel

6.5 Discussion/Comparison between the Cedar Mesa Sandstone Formation and the Leman Sandstone/Silverpit Formation

Using the idealised gamma ray trends derived from either the erg-margin trend or the lacustrine-margin trend from outcrop studies of the Cedar Mesa Sandstone Formation of Utah, clear comparisons can be drawn to the Silverpit Formation of the southern North Sea, UK.

6.5.1 Drying Upwards Motifs and Lack of cyclic Preservation

Previous work (Howell & Mountney, 1997) has focused mainly on interpreting cycles from wireline and core based on wetting and drying, however outcrop studies from the Cedar Mesa Sandstone, detail that cycles may only preserve drying upwards cycles, with the lower wetter half of the cycle being misinterpreted as part of a wetting trend.

The Cedar Mesa Sandstone Formation shows very regular switching of cyclic preservation between either the erg-margin or the lacustrine-margin trend. This however, is not seen within the Silverpit Formation. The reasons for this may be numerous as the drying upwards motifs themselves are generated due to a combination of sediment supply, climate and accommodation space, however the most likely cause is a combination of scale and climatic fluctuations. The Silverpit lake was a much larger lake than the Cedar Mesa Sandstone, covering 1200 km with a width of over 200 km (Glennie, 1986).

Climatic fluctuations may have been more extreme between wet and dry periods during deposition of the Cedar Mesa Sandstone Formation resulting in cyclic preservation of alternating trends. The reduced size of lacustrine deposition may

also have enabled the lake to fully dry out more readily coupled with a dune field in closer proximity than observed within the Silverpit/Leman formations.

6.5.2 Depositional Model and Implication for Hydrocarbon Exploration

The drying upwards trends show clear evidence for climatic variation and cyclicity, however higher order climatic cyclicity is also indicated by the results and regional variations of this study, with the smaller drying upwards motifs superimposed upon this larger scale allocyclic sequence.

The initial cycle of the Rotliegend, shows that all well deposits fall into the erg-margin trend derived from outcrop study of the Cedar Mesa Sandstone. This most likely represents a period of maximum climatic aridity in which dune conditions have resulted in expansion of the Leman Sandstone erg to its maximum extent (Fig. 6.12). This is followed by a period of lake expansion, as in wells 2-6 lacustrine-erg trends are present. This lake expansion is probably the result of a climatic shift to a period of maximum humidity in which increased discharge resulted in the expansion and flooding of the Silverpit palaeolake over the aeolian deposits of the Leman Sandstone and a lateral shift in the facies belt. Facies most likely represent lacustrine deposition within wells 2-6, whereas aeolian deposits are supressed in Well-1 and increased fluvial facies present (Fig. 6.12). Following this, the climate reverted to more arid conditions, as in Well-2 the top two climatic cycles show erg-margin trends, most likely representing the beginning of expansion of the Leman erg from its permanent–long-term erg centre position indicated by the deposits of Well-1. Wells 3-6 still show lacustrine-margin trends, indicating that the climate had not reached the same point of aridity as seen within the bottom most cycle, or that the effects of their proximity to the centre of the palaeolake is masking climatic changes.

However, the facies belt most likely shifted distally resulting in increased sabkha deposits in the locations of the previous Silverpit lake (Fig. 6.12).

By using these upwards drying trends, large scale regional correlations based on climatic conditions can be conducted which can help pinpoint possible reservoir sands more accurately. This has potentially large implications, firstly in terms of sediment and bulk depositional environment, as the aeolian hosted sabkha trend has larger proportions of 'good' reservoir within aeolian dune associations compared to the lacustrine hosted sabkha trend. Secondly, these trends can be used to correlate surfaces to push dry cycles with good reservoir potential further into the Silverpit lake sediments, to target marginal reserves.

The transitional facies of the Leman/Silverpit formations fall mainly into the lacustrine-margin model derived from the Cedar Mesa Sandstone Formation. From field observations, it is likely that this would not be the best settings for hydrocarbon exploration, due to the high salt content, in the form of large bedded deposits, or the frequent enterolithic and disruptive growth seen within the sediments, and the overall fine grained and muddy style of deposits, representative of a low net-gross system.

The aeolian-erg setting, with its large dune deposits would initially seem a good candidate for hydrocarbon exploration and recovery, with high net-gross. However as demonstrated by the aeolian sabkha assemblage found within the Cedar Mesa Formation there are some potential pitfalls to recovery from aeolian dune units as they are sandwiched between evaporite rich interdune units. These interactions are sub-seismic, and almost sub-wireline, scale. The Th/K plots from outcrop gamma ray logs of the Cedar Mesa Sandstone Formation (Chapter 4) fail to show the influence of evaporites on dune facies, however results from sedimentary field study show that this influence decreases upwards within the overlying aeolian dune unit,

and is proportionally linked to capillary action of the dune. Within gamma ray logs alone, this may be hard to detect and could be misconstrued as relating to the underlying bed 'bleed' effect, and therefore would require a full suite of geophysical data (resistivity, porosity, density) to be determined properly. This interaction has the potential to lower hydrocarbon recovery, by blocking or restricting potential flow paths, providing these flow paths aren't completely blocked, the permeability of the dune would be greatest towards the tops of dunes overlying evaporitic rich interdune strata. Ideal recovery would be found within dune facies stacked into multiple sets and cosets separated from evaporitic rich interdunes.

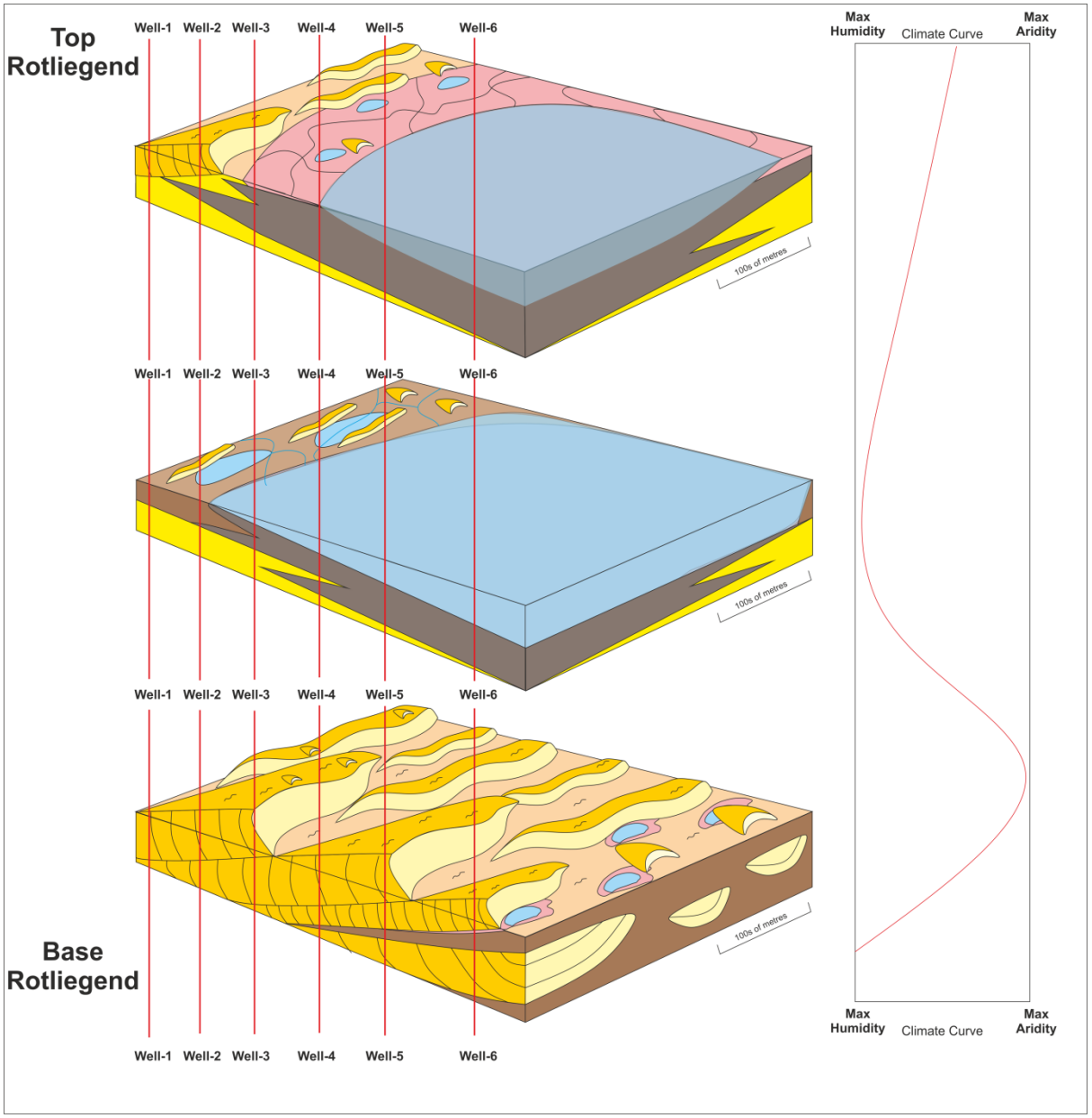

Figure 6.12 Interpreted depositional models for the location of the wells from the base Rotliegend to the top interval. The location of the wells is indicated by red lines. Interpreted climatic curve is shown on the right hand side.

6.6 Summary

By using idealised drying upwards gamma ray trends determined from outcrop study of the Cedar Mesa Sandstone Formation a revised correlation and interpretation of the Silverpit/Leman transition of the southern North Sea is presented. This shows an initial dry period in which aeolian dunes cover the full study area followed by an increase in humidity and the expansion of the Silverpit

lake. Towards the top of the formation the climate begins to revert to arid conditions and dunes once again expand from the erg centre. By using these idealised trends, correlation surfaces of dry times with high net to gross sand reservoirs can be pushed into areas further away from the erg centre to increase recovery of marginal reservoirs.

Chapter Seven: Conclusions and Future Work

Chapter eight provides conclusions based on the results of this research. Of particular importance is how detailed characterisation of the sedimentology can lead to a comprehensive understanding of the allogenic controls which influence the spatial and temporal evolution of the continental sabkhas. Broader implications regarding application to hydrocarbon exploration and potential future research are also discussed.

7.1 Introduction

This research characterises the sedimentology of an arid continental sabkha using the evaporitic deposits of the Cedar Mesa Sandstone as a case study - a facies succession that has previously received little scientific attention. This research also helps improve understanding and knowledge of the competing nature of arid continental deposits and the role evaporitic sediments play on neighbouring settings, and in doing so tests the applicability of currently published depositional models of arid continental sabkhas. Furthermore, by examining the allocyclic controls upon deposition, a thorough understanding of the complex sedimentology can be gained and can be applied to other arid continental formations.

The Cedar Mesa Sandstone Formation is a predominantly aeolian system which transitions to evaporitic sabkha deposits (Condon, 1997) at its distal margin around the town of Bluff, Utah. The style of sedimentation observed throughout the Cedar Mesa Sandstone Formation reflects the complex spatial and temporal interactions between aeolian, fluvial, sabkha and lacustrine settings at both a regional and local scale and can be considered to represent the overall processes which occur in arid continental sabkhas.

The data used in this research has been acquired through traditional sedimentological logging techniques, including ten sedimentary logs covering a cumulative sediment thickness of over seven kilometres. This data has been complemented with five high resolution outcrop gamma ray logs and microfacies analysis of over sixty five carbonate samples. The integration, description and analyses of these data have facilitated the following conclusions to be drawn.

7.2 Sedimentological Characterisation of an Arid Continental Sabkha

To fully characterise the sedimentology of an arid continental sabkha, detailed sedimentary logging was conducted. Nineteen facies were identified and combined into eleven facies associations which were, in turn, grouped into broad depositional environments: aeolian, fluvial, lacustrine or sabkha. Spatial analysis of the facies associations has enabled a framework to be developed, which demonstrates the change from a dominant aeolian erg setting through a mixed sabkha setting into a lacustrine environment. This analysis has shown unique interactions within the sabkha setting depending on the dominance of either the lacustrine or aeolian settings. These interactions preserve unique sedimentology in the form of either aeolian-sabkha assemblages or lacustrine-sabkha assemblages, which are traceable throughout the sabkha setting and have been interpreted to form in either an erg-margin sabkha or a lacustrine-margin sabkha depositional setting. Quantifiable verification of sedimentological interpretations were sought through outcrop gamma ray logging in Chapter 4 which identified unique facies comprising: palaeosol, aeolian dune, fluvio/lacustrine, sandsheet, interdune and evaporite facies, along with their associated distinctive log signatures. Microfacies analyses of carbonates identified five primary microfacies and one diagenetic microfacies. This analysis also demonstrates evidence of environmental shifts within an arid

continental sabkha, which complements and expands upon the depositional models proposed. This work also provides examples of well-preserved carbonate material from a depositional environment where preservation potential is perhaps better than previously thought.

7.3 Effect of Climatic Cyclicity on Continental Sabkha

The deposits of the Cedar Mesa Sandstone formation show cyclic temporal changes in sedimentology between either the erg-margin or the lacustrine-margin setting which have been attributed to a combination of allogenic (climate and tectonics) processes. Chapter 5 attributes these changes to climatic fluctuations between arid and humid periods, and are governed by the availability of sediment related to these climatic shifts. This interaction between climate and sediment supply results in the preservation of alternating drying upwards cycles of each trend. The preservation of drying upwards cycles only, rather than drying and wetting, resulted from the lack of accommodation space. Time series analysis of gamma ray data was conducted to help quantify the cyclicity seen within sedimentary data, results from which indicate that these cyclic changes are related to Milankovitch cycles. Integrated gamma ray signatures and sedimentary log data suggests that the erg-margin setting is primarily influenced by precession style processes compared to the lacustrine-margin trend which is influenced by obliquity. A local tectonic influence is also observed, and can help explain the facies shift from erg to sabkha style deposits, however the climatic variations were the dominant controlling factor with the influence of faulting superimposed over larger scale fluctuations.

7.4 Application

The outcrop study of the Cedar Mesa Sandstone Formation indicates that continental sabkha settings may only preserve drying upwards sequences due to

complex interactions between climatic shifts and sediment supply. Idealised gamma ray trends from both the erg-margin and lacustrine-margin depositional models were applied to the Silverpit and Leman Sandstone Formations of the southern North Sea, to test their applicability to other similar depositional settings. Application of these models has resulted in a revised correlation and interpretation of the Silverpit/Leman transition of the southern North Sea. By using these idealised trends, surfaces relating to maximum aridity with high net to gross sand reservoirs can be correlated into areas further away from the erg centre.

The demonstration of this technique in the Leman/Silverpit shows that this method has potentially wide application to many other aeolian/sabkha settings and could be used to increase hydrocarbon recovery within marginal reservoirs.

7.5 Future Work

This work presents a detailed sedimentological characterisation of arid continental sediments using a succession that has received little detailed scientific attention and places the results within a framework controlled by climatic cyclicity. Application of these results to other settings has also been demonstrated, however, there are several limitations to this work that can form the basis of future work to better refine and enhance this study.

Firstly, this work is based on the study of ancient sediments. Ancient outcrops do not preserve evaporites well, any halite that may have been in the Permian environment would have been dissolved and the gypsum/anhydrite has undergone multiple stages of hydration and dehydration. A study of modern analogues may well provide a more detailed interpretation of the primary sedimentological processes which formed the evaporites, as well as giving a clearer insight into the interactions with neighbouring coeval environments. The study of modern

analogues also allows for an indication of the preservation potential of each environment, and an assessment of potential bias that may be preferentially preserved certain environments within the rock record.

Secondly, the cyclicity presented lacks any dating constraint. This would be necessary for a more rigorous study of the cyclicity and to astronomically tune the results accurately. This may be achieved through detailed provenance, palynological, or geochemical and isotopic studies.

A detailed study of either ^{34}S or $^{87}Sr/^{86}Sr$ isotopes can also provide an interpretation of palaeoenvironment and identify whether the deposits are fully continental, whereas $\delta^{17}O/\delta^{18}O$ isotopic analyses of sulphates preserved in evaporites have the potential to record the concentrations of O_2 and CO_2, inherited from the Phanerozoic atmosphere (*cf.* Bao, 2015) to aid in the understanding of palaeoclimate.

Finally this work is applied to continental sabkhas only. There is scope to study marginal marine sabkhas that interact with coastal dune systems to investigate if any parallels can be drawn between the results of this study and that of a system with a marine influence.

7.6 Summary

The Cedar Mesa Sandstone Formation of the Paradox Basin, U.S.A provides world class exposures to study an outcrop example of an arid continental sabkha. The extensive nature of outcrop and the transition through many arid continental settings make it an ideal analogue for other, less exposed deposits or for comparison to borehole data, such as the Rotliegend Group of the southern North Sea. This research has challenged the assumption that sabkha deposits preserve both drying and wetting cycles by demonstrating the complex interaction between climate, sediment supply and accommodation space. By applying a climatic cyclicity

framework, basin-scale correlations can be conducted, which can be used to map potential reservoir units at the margins of more conventional hydrocarbon plays, and extend the life of mature basins.

References

Adams, J. A., and **Weaver, C. E.** (1958). Thorium-to-uranium ratios as indicators of sedimentary processes: example of concept of geochemical facies. *AAPG Bulletin*, ***42***, 387-430.

Ahlbrandt, T.S. and **Fryberger, S. G.** (1982) Introduction to eolian deposits. In: *Sandstone Depositional Environments* (Eds. Scholle, P. A. and Spearing, D.) *American Association of Petroleum Geologists Memoir* **31**, 11–47

Ahlbrandt, T.S. and **Fryberger, S.G**. (1981) Sedimentary features and significance of interdune deposits. In: *Recent and Ancient Nonmarine Depositional Environments: Models for Exploration* (Eds F.G. Ethridge and R.M. Flores) *SEPM Spec. Publ.,* **31**, 293-314.

Ahlbrandt, T.S., Andrews, S. and **Gwynne, D.T.,** (1978) Bioturbation in eolian deposits. *Journal of Sedimentary Research,* **48**, .839-848.

Aigner, T., Schauer, M., Junghans, W. D., and **Reinhardt, L.** (1995). Outcrop gamma-ray logging and its applications: examples from the German Triassic. *Sedimentary Geology*, **100**, 47-61.

Alderman, S.S. (1985) Geology of the Owens Lake evaporite deposit. In: *Sixth international symposium on salt* (Eds B. C. Schreiber and H. L. Harner) *Alexandria: Salt Institute.* 1, 75-83.

Alsharhan, A.S. and **Kendall, C.S.C.** (2003) Holocene coastal carbonates and evaporites of the southern Arabian Gulf and their ancient analogues. *Earth-Science Reviews*, **61**, 191-243.

Anderson, R. F., LeHuray, A. P., Fleisher, M. Q., and **Murray, J. W.** (1989). Uranium deposition in saanich inlet sediments, vancouver island. *Geochimica et Cosmochimica Acta*, ***53***(9), 2205-2213.

Anderson, R. S. (1987). A theoretical model for aeolian impact ripples. *Sedimentology*, ***34***, 943-956.

Anderson, R. S., and **P. K. Haff,** (1991) Wind modification and bed response during saltation of sand in air, *Acta Mech. Suppl*., **1**, 21–51,

Andreotti, B., Claudin, P., and **Pouliquen, O.** (2006). Aeolian sand ripples: experimental study of fully developed states. *Physical review letters*, ***96***, 028001.

Arakel, A. V. (1980). Genesis and diagenesis of Holocene evaporitic sediments in Hutt and Leeman lagoons, Western Australia. Journal of Sedimentary Research, **50**, 1305-1326.

Aubrecht, R., Szulc, J., Michalik, J., Schlögl, J., and **Wagreich, M.** (2002). Middle Jurassic stromatactis mud-mound in the Pieniny Klippen Belt (Western Carpathians). *Facies*, ***47***, 113-126.

Ayora, C., Pierre, C. and **Pueyo, J**., (1994) Refining the $\delta^{34}S$ and $\delta^{18}O$ values of sulphate in ancient oceans. *Mineralogical Magazine,* **58,** 32-33

Baars, D.L., (1962) Permian system of Colorado Plateau. *AAPG Bulletin*, **46,** 149-218.

Baars, D.L., (1975) The Permian system of Canyonlands country. In: Canyonlands Country: Four Corners Geological Society, Eighth Field Conference Guidebook (Eds J.E. Fasset and S.A. Wengerd), pp. 123–127. Four Corners Geological Society, Durango

Baars, D.L., (1979) The Permian System. In: *Permianland* (Ed. D.L. Baars). *Four Corners Geological Society*, *9th Field Conference Guidebook* pp 1-6

Baars, D.L., (1987) The Elephant Canyon Formation revisited. *Geology of Cataract Canyon and Vicinity, Tenth Field Conference*, Four Corners Geological Society, 81-90

Baars, D.L., (2000) The Colorado plateau: a geologic history. UNM Press.

Baars, D.L., and **Stevenson, G**., (1981) Tectonic evolution of the Paradox basin, Utah and Colorado. In: *Geology of the Paradox Basin* (Ed. Wiegand, D.L.) *Rocky Mountain Association of Geologists, Field Conference*, 23-31

Bábek, O., Kalvoda, J., Cossey, P., Šimíček, D., Devuyst, F. X., and **Hargreaves, S**. (2013). Facies and petrophysical signature of the Tournaisian/Viséan (Lower Carboniferous) sea-level cycle in carbonate ramp to basinal settings of the Wales-Brabant massif, British Isles. *Sedimentary Geology*, ***284***, 197-213.

Bábek, O., Přikryl, T., and **Hladil, J. (**2007). Progressive drowning of carbonate platform in the Moravo-Silesian Basin (Czech Republic) before the Frasnian/Famennian event: facies, compositional variations and gamma-ray spectrometry. *Facies*, ***53***, 293-316.

Bagnold, R. A. (1936). The movement of desert sand. Proceedings of the Royal Society of London. Series A-Mathematical and Physical Sciences, **157**, 594-620.

Bagnold, R.A. (1941) The Physics of Blown Sand and Desert Dunes Methuen, London . 265 pp.

Bailey, J. B., Arbin, P., Daffinoti, O., Gibson, P., and **Ritchie, J. S**. (1993). Permo-Carboniferous plays of the Silver Pit Basin. In *Geological Society, London, Petroleum Geology Conference series* (Ed. Parker,J.R.) *Geological Society of London,* **1**, 707-715

Bain, R. J., and **Kindler, P.** (1994). Irregular fenestrae in Bahamian eolianites; a rainstorm-induced origin. *Journal of Sedimentary Research*, *64*(1a), 140-146.

Baker, A. A. (1946). Geology of the Green River Desert-cataract Canyon Region: Emery, Wayne, and Garfield Counties, Utah (No. 950-952). *US Government Printing Office*.

Banham, S.G. and **Mountney, N.P.** (2014) Climatic versus halokinetic control on sedimentation in a dryland fluvial succession. *Sedimentology*, **61**, 570-608.

Bao, H. (2015). Sulfate: a time capsule for Earth's O2, O3, and H2O. *Chemical Geology*, ***395***, 108-118.

Barbeau, D.L. (2003) A flexural model for the Paradox Basin: implications for the tectonics of the Ancestral Rocky Mountains. *Basin Research*, **15**, 97-15.

Bathurst, R. G. (1980). Stromatactis—Origin related to submarine-cemented crusts in Paleozoic mud mounds. *Geology*, ***8***, 131-134.

Belknap, W. B., Dewan, J. T., Kirkpatrick, C. V., Mott, W. E., Pearson, A. J., and **Rabson, W. R.** (1959). API calibration facility for nuclear logs. In *Drilling and production practice **1***. American Petroleum Institute.

Benison, K.C. and **Goldstein, R.H.** (2001) Evaporites and siliciclastics of the Permian Nippewalla Group of Kansas, USA: a case for non-marine deposition in saline lakes and saline pans. *Sedimentology,* **48**, 165-188.

Berger, A., Loutre, M. F., and **Dehant, V.** (1989). Pre-quaternary Milankovitch frequencies. *Nature*, ***342***(6246), 133.

Bird, P., (1988) Formation of the rocky mountains, Western United States: a continuum computer model. *Science,* **239**, 1501-1507.

Biswas, A. (2005) Coarse aeolianites: sand sheets and zibar–interzibar facies from the Mesoproterozoic Cuddapah Basin, India. *Sedimentary Geology*, **174**, 149-160.

Blair, T. C., and **McPherson, J. G.** (1994). Alluvial fans and their natural distinction from rivers based on morphology, hydraulic processes, sedimentary processes, and facies assemblages. *Journal of sedimentary research*, **64**, 450-489.

Blakey, R. C., (1990) Stratigraphy and geologic history of Pennsylvanian and Permian rocks, Mogollon Rim region, central Arizona and vicinity. *Geological Society of America Bulletin,* **102**, 1189-1217.

Blakey, R.C., (1988) Basin tectonics and erg response. *Sedimentary Geology*, **56**, 127–151.

Blakey, R.C., (1996) Permian eolian deposits, sequences and sequence boundaries, Colorado Plateau. In: *Paleozoic Systems of the Rocky Mountain Region* (Eds M.W. Longman and S.D. Sonnenfeld), *Rocky Mountain Section SEPM*, 405–426.

Blakey, R.C., and **Ranney, W.,** (2008) Ancient landscapes of the Colorado Plateau. Grand Canyon Association.

Blakey, R.C., Peterson, F. and **Kocurek, G.** (1988) Synthesis of late Paleozoic and Mesozoic eolian deposits of the Western Interior of the United States. *Sedimentary Geology*, **56**, 3-125.

Blissenbach, E. (1954). Geology of alluvial fans in semiarid regions. *Geological Society of America Bulletin*, ***65***, 175-190.

Boehrer, B. and **Schultze, M.** (2008). Stratification of lakes. *Reviews of Geophysics*, **46**, 1-27.

Bond G.A., (1976) Evidence for continental subsidence in North America during the Late Cretaceous global submergence: *Geology* , **4**, 557–560

Bourque, P. A., and **Gignac, H.** (1983). Sponge-constructed stromatactis mud mounds, Silurian of Gaspé, Québec. *Journal of Sedimentary Research*, ***53***, 521-532

Bowler, J. M. (1986). Spatial variability and hydrologic evolution of Australian lake basins: analogue for Pleistocene hydrologic change and evaporite formation. *Palaeogeography, Palaeoclimatology, Palaeoecology*, ***54***, 21-41.

Bowler, J. M., and **Teller, J. T.** (1986). Quaternary evaporites and hydrological changes, Lake Tyrrell, north-west Victoria. *Australian Journal of Earth Sciences*, ***33***, 43-63.

Bridge, J.S. and **Best, J.L.** (1988) Flow, sediment transport and bedform dynamics over the transition from dunes to upper-stage plane beds: implications for the formation of planar laminae. *Sedimentology*, **35**, 753-763.

Bristow, C. S., and **Myers, K. J.** (1989). Detailed sedimentology and gamma-ray log characteristics of a Namurian deltaic succession I: Sedimentology and facies analysis. In: *DELTAS: Sites and Traps for Fossil Fuels* (Eds. Whateley, M. K.G., and Pickering, K.T.)*Geological Society, London, Special Publications*, ***41***, 75-80.

Bristow, C. S., and **Williamson, B. J.** (1998). Spectral gamma ray logs: core to log calibration, facies analysis and correlation problems in the Southern North Sea. In: *Core-Log Integration* (Eds. Harvey, P.A and Lovell, M.A) *Geological Society, London, Special Publications*, ***136***, 1-7.

Brooks, R. A., and **Ferrell Jr, R. E**. (1970). The lateral distribution of clay minerals in Lakes Pontchartrain and Maurepas, Louisiana. *Journal of Sedimentary Research*, **40**.

Bull, W. B. (1977). The alluvial-fan environment. *Progress in Physical geography*, **1**, 222-270.

Bullard, J. E. (1997). Vegetation and dryland geomorphology. *Arid Zone Geomorphology*, 109-131.

Burchfiel B.C. Cowan D.S. and **Davis G.A.,** (1992) Tectonic overview of the Cordilleran orogen in the western United States, In: *The Cordilleran orogen: Conterminous U.S, Boulder, Colorado.*(Ed. Burchfiel B.C), *Geological Society of America*, *Geology of North America* **G-3**, p. 407–479.

Butler, G. P. (1970). Secondary anhydrite from a sabkha, northwest Gulf of California, Mexico. In *Third symposium on salt* (Vol. **1**, pp. 153-155). Northern Ohio geol. Soc..

Butler, J. B. (1975). The West Sole Gas-Field. In Petroleum and the continental shelf of northwest Europe, (Ed. Woodland, A.W) Institute of Petroleum, London, 213-223.

Cain, S. (2009). Sedimentology and stratigraphy of a terminal fluvial fan system: the Permian Organ Rock Formation, South East Utah (Doctoral dissertation, Keele University).

Cain, S.A. and **Mountney, N.P.** (2009) Spatial and temporal evolution of a terminal fluvial fan system: the Permian Organ Rock Formation, South-east Utah, USA. *Sedimentology*, **56**, 1774-1800.

Cameron, T.D.J., Crosby, A., Balson, P.S., Jeffery, D.H., Lott, G.K., Bulat, J., and **Harrison, D.J.,** (1992*) United Kingdom offshore regional report: the geology of the southern North Sea.* (London: HMSO for the British Geological Survey)

Campbell, J.A., (1980) Lower Permian depositional systems and Wolfcampian paleogeography, Uncompahgre basin, eastern Utah and southwestern Colorado. In: *Paleozoic Paleogeography of the West-Central United States: Rocky Mountain Symposium 1*, (Eds. Fouch, T.D., Magathan, E.R.) *Rocky Mountain Section, Society of Economic Paleontologists and Mineralogists.* pp 327-340

Cant, D.J. (1978) Development of a facies model for sandy braided river sedimentation: comparison of the South Saskatchewan River and the Battery Point Formation. In: *Fluvial Sedimentology* (Ed. by A.D. Miall). *Mem. Can. Soc. Petrol. Geol*., **5**, 3-30.

Castens-Seidell, B. (1984) Morphologies of Gypsum on a Modern Sabkha: Clues to Depositional Conditions. *AAPG Bulletin*, **68**, 460-460.

Catuneanu, O. (2006). Principles of sequence stratigraphy. Elsevier.

Cecil, C.B. (1990) Paleoclimate controls on stratigraphic repetition of chemical and siliciclastic rocks. *Geology*, **18**, 533-536.

Cecil, C.B. (2003) The concept of autocyclic and allocyclic controls on sedimentation and stratigraphy, emphasizing the climatic variable. In: *Climate Controls on Stratigraphy*, (Eds C. B. Cecil, N. T. Edgar) *SEPM Spec. Publ.,* **77**, 13–20.

Cecil, C.B., (2015) Paleoclimate and the origin of Paleozoic chert: time to re-examine the origins of chert in the rock record. *The Sedimentary Record,* **13**, 4-10.

Chan, M. A., and **Archer, A. W**. (1999). Spectral analysis of eolian foreset periodicities: implications for Jurassic decadal-scale paleoclimatic oscillators. *Paleoclimates*, ***3***, 239-255.

Chan, M.A. and Huntoon, J.F., (1984) Complex Interaction of Eolian and Marine Sedimentation in Permian White Rim Sandstone, Elaterite Basin, Southeast Utah. *AAPG Bulletin,* **68,** 934-935.

Chaney, D., Lucas, S.G. and Elrick, S., (2013) New Occurrence Of An Arthropleurid Trackway From The Lower Permian Of Utah. In: The Carboniferous-Permian Transition. (Eds. Lucas, S.G., DiMichele, W. A., Barrick, J.E., Scneider, J.W., and

Spielmann, J.A.,) *New Mexico Museum of Natural History and Science, Bulletin 60.* 64-65

Claypool, G.E., Holser, W.T., Kaplan, I.R., Sakai, H. and **Zak, I.** (1980) The age curves of sulfur and oxygen isotopes in marine sulfate and their mutual interpretation. *Chemical Geology*, **28**, 199-260

Clement, A.M. and **Holland, S.M.** (2016) Sequence stratigraphic context of extensive basin-margin evaporites: Middle Jurassic Gypsum Spring Formation, Wyoming, USA. *Journal of Sedimentary Research*, **86**, 965-981.

Clemmensen, L.B. (1978) Alternating aeolian, sabkha and shallow-lake deposits from the Middle Triassic Gipsdalen Formation, Scoresby Land, east Greenland. *Palaeogeography, Palaeoclimatology, Palaeoecology,* **24**, 111-135.

Cody, R. D. (1979). Lenticular gypsum; occurrences in nature, and experimental determinations of effects of soluble green plant material on its formation. *Journal of Sedimentary Research*, ***49***, 1015-1028.

Collinson, J. (1994) Sedimentary deformational structures. In *The geological deformation of sediments.* (Ed. A.Maltman) 1st edn, pp. 95-125. Springer, Dordrecht.

Collinson, J., Mountney, N., and **Thompson, D.** (2006). Sedimentary Structures: Harpenden. *Terra*.

Condon, S.M. (1997) Geology of the Pennsylvanian and Permian Cutler Group and Permian Kaibab Limestone in the Paradox Basin, Southeastern Utah and Southwestern Colorado. *US Geol. Surv. Bull.,* **2000-P**, 46 pp

Condon, S.M. and Huffman, A.C. (1994) Northwest-southeast-oriented stratigraphic cross-sections of Jurassic through Paleozoic rocks, San Juan Basin and vicinity, Utah, Colorado, Arizona, and New Mexico. *Bull. US Geol. Surv*., 1633, 3–12.

Conway, A. M. (1986). Geology and petrophysics of the Victor field. In: *Habitat of Palaeozoic Gas in N.W. Europe* (Eds. Brooks, J., Goff, J.C., and van Hoorn, B.) *Geological Society, London, Special Publications*, ***23***, 237-249.

Cooke, R. U., and **Warren, A.** (1973). *Geomorphology in deserts*. Univ of California Press.

Court, W. M., Paul, A., and **Lokier, S. W**. (2017). The preservation potential of environmentally diagnostic sedimentary structures from a coastal sabkha. *Marine Geology*, ***386***, 1-18.

Crabaugh, M. and **Kocurek, G. (**1993) Entrada Sandstone: an example of a wet aeolian system. In *The Dynamics and Environmental Context of Aeolian Sedimentary* Systems (Ed K.Pye) *Geological Society, London, Special Publications*, **72**, 103-126.

Crampton, J. S., Meyers, S. R., Cooper, R. A., Sadler, P. M., Foote, M., and **Harte, D**. (2018). Pacing of Paleozoic macroevolutionary rates by Milankovitch grand cycles. *Proceedings of the National Academy of Sciences*, ***115***, 5686-5691.

Cripps, A. C., and **McCann, D. M.** (2000). The use of the natural gamma log in engineering geological investigations. *Engineering Geology*, ***55***, 313-324.

Davies, S. J., and **Elliott, T.** (1996). Spectral gamma ray characterization of high resolution sequence stratigraphy: examples from Upper Carboniferous fluvio-deltaic systems, County Clare, Ireland. In: *High Resolution Sequence Stratigraphy: Innovations and Applications* (Eds Howell, J.A., and Aitken, J.F.) *Geological Society, London, Special Publications*, ***104***, 25-35.

Davis, G. H. (1999). Structural geology of the Colorado Plateau region of southern Utah, with special emphasis on deformation bands (Vol. 342). Geological Society of America.

Del Valle, H. F., Rostagno, C. M., Coronato, F. R., Bouza, P. J., and **Blanco, P. D**. (2008). Sand dune activity in north-eastern Patagonia. *Journal of Arid Environments*, ***72***, 411-422.

Delecat, S., and **Reitner, J.** (2005). Sponge communities from the Lower Liassic of Adnet (Northern Calcareous Alps, Austria). *Facies*, ***51***, 385-404.

Dickinson, W.R., Soreghan, G.S. and **Giles, K.A.** (1994) Glacio-eustatic origin of Permo-Carboniferous stratigraphic cycles; evidence from the southern Cordilleran foreland region. In: *Tectonic and Eustatic Controls on Sedimentary Cycles* (Eds. J.M. Dennison & F.R. Ettensohn), *SEPM,* 25–34 pp

Doe, T.W. and **Dott, R.H.** (1980) Genetic significance of deformed cross bedding; with examples from the Navajo and Weber sandstones of Utah. *Journal of Sedimentary Research*, **50**, 793-812

Doelling, H. H. (1988). Geology of Salt Valley Anticline and Arches National Park, Grand County, Utah. In, *Salt deformation in the Paradox Region*. (Eds. H. H. Doelling, C. G. Oviatt & P. W. Huntoon)*Utah Geological and Mineral Survey Bulletin*, **122**, 7–58.

Doelling, H.H. and **Morgan, C.D.,** (2000) Geologic map of the Merrimac Butte Quadrangle, Grand County, Utah. *Utah Geological Survey.*

Dorney, L. J., Parrish, J. T., Chan, M. A., & **Hasiotis, S. T**. (2017). Petrography and Environmental Interpretation of Tufa Mounds and Carbonate Beds In the Jurassic Navajo Sandstone of Southeastern Utah, USA. Journal of Sedimentary Research, ***87***, 967-985.

Doveton, J. H. (1994). Geologic Log Analysis Using Computer Methods. Amer Assn of Petroleum Geologists **2**

Draper, J. J., and **Jensen, A. R.** (1976). The geochemistry of Lake Frome, a playa lake in South Australia. *BMR Journal of Australian Geology and Geophysics*, ***1***, 83-104.

Driese, S. G. (1985). Interdune pond carbonates, Weber Sandstone (Pennsylvanian-Permian), northern Utah and Colorado. *Journal of Sedimentary Research*, ***55***, 187-195.

Dubiel, R.F., Huntoon, J.E., Condon, S.M. and **Stanesco, J.D.** (1996) Permian deposystems, paleogeography, and paleoclimate of the Paradox basin and vicinity. In: *Paleozoic Systems of the Rocky Mountain Region* (Eds M.W. Longman and S.D. Sonnenfeld), *Rocky Mountain Section SEPM,* 405–426.

Duncan, K.A., (2006) Pond deposits examined as a stratigraphic control on migration and compartmentalization in eolian reservoirs. University of Texas at El Paso, Unpublished MSc Thesis

Dunham, R. J. (1962). Classification of carbonate rocks according to depositional textures.

Durán, M. J., Kouro, S., Wu, B., Levi, E., Barrero, F., & **Alepuz, S.** (2011). Six-phase PMSG wind energy conversion system based on medium-voltage multilevel converter. In *Proceedings of the 2011 14th European Conference on Power Electronics and Applications* (pp. 1-10). IEEE.

DzenowskI, N., Hasiotis, S.T., and **Rasmussen, D.L,** (2013) Vertebrate burrows within pedogenically modified deposits from the Lower Permian (Wolfcampian) Cedar Mesa Sandstone of southeastern Utah. *Geological Society of America National Meeting , Denver, CO*, pp 326

Eardley, A. J., and **Stringham, B. F.** (1952). Selenite crystals in the clays of Great Salt Lake [Utah]. *Journal of Sedimentary Research*, ***22***, 234-238.

Eberth, D.A. and **Miall, A.D.** (1991) Stratigraphy, sedimentology and evolution of a vertebrate-bearing, braided to anastomosed fluvial system, Cutler Formation (Permian-Pennsylvanian), north-central New Mexico. *Sedimentary Geology*, **72**, 225-252.

Ehrenberg, S. N., and **Svana, T. A.** (2001). Use of spectral gamma-ray signature to interpret stratigraphic surfaces in carbonate strata: An example from the Finnmark carbonate platform (Carboniferous-Permian), Barents Sea. *AAPG bulletin*, ***85***, 295-308.

England, P., Houseman, G., Osmaston, M. and **Ghosh, S.,** (1988) The mechanics of the Tibetan Plateau [and discussion]. *Philosophical Transactions of the Royal Society of London A: Mathematical, Physical and Engineering Sciences*, **326**, 301-320.

Escavy, J. I., and **Herrero, M. J**. (2019) Enterolithic folds in evaporites as microbially induced sedimentary structures: New model of formation and interpretation in the geological record. *Sedimentology*.

Eugster, H. P. (1980). Geochemistry of evaporitic lacustrine deposits. *Annual Review of Earth and Planetary Sciences*, ***8***, 35-63.

Eugster, H.P. (1970) Chemistry and origin of the brines of Lake Magadi, Kenya. *Mineral. Soc. Amer., Spec. Pap,* **3** ,215-235

Eugster, H.P. and **Hardie, L.A.** (1978) Saline lakes. In *Lakes, Chemistry, Geology, Physics* (Ed. A. Lerman) 1st edn, pp. 237-293. Springer, New York

Evans, R., Mory, A. J., and **Tait, A. M.** (2007). An outcrop gamma ray study of the Tumblagooda Sandstone, Western Australia. *Journal of Petroleum Science and Engineering*, ***57***, 37-59.

Fielding, C.R. (1984) Upper delta plain lacustrine and fluviolacustrine facies from the Westphalian of the Durham coalfield, NE England. *Sedimentology*, **31**, 547-567.

Flajs, G., and **Hüssner, H.** (1993). A microbial model for the Lower Devonian stromatactis mud mounds of the Montagne Noire (France). *Facies*, ***29***, 179.

Flowers, R., Wernicke, B. and **Farley, K.,** (2008). Unroofing, incision, and uplift history of the southwestern Colorado Plateau from apatite (U-Th)/He thermochronometry. *Geological Society of America Bulletin*, **120**. 571-587.

Flügel, E. (2004) Depositional Models, Facies Zones and Standard Microfacies. In: *Microfacies of Carbonate Rocks* (Ed E. Flügel) 2nd edn, pp. 657-724. Springer, Berlin.

Foos, A. (1999) Geology of the Colorado Plateau. Geology Field Trip Guides by Anabelle Foos, University of Akron. Available online at: http://www2. nature. nps. gov/geology/education.

Fourriere, A., Claudin, P., and **Andreotti, B.** (2010). Bedforms in a turbulent stream: formation of ripples by primary linear instability and of dunes by nonlinear pattern coarsening. *Journal of Fluid Mechanics*, ***649***, 287-328.

Fryberger, S. G. (1990). Role of water in eolian deposition. In *Modern and ancient eolian deposits*: *petroleum exploration and production* (Eds. Fryberger, S.G., Krystinki, L.F., Schenk, C.J) *SEPM*

Fryberger, S. G., Al-Sari, A. M., and **Clisham, T. J.** (1983). Eolian dune, interdune, sand sheet, and siliciclastic sabkha sediments of an offshore prograding sand sea, Dhahran area, Saudi Arabia. *AAPG Bulletin*, ***67***, 280-312.

Fryberger, S. G., Hesp, P., and **Hastings, K.** (1992). Aeolian granule ripple deposits, Namibia. *Sedimentology*, ***39***, 319-331.

Fryberger, S. G., Schenk, C. J., and **Krystinik, L. F.** (1988). Stokes surfaces and the effects of near-surface groundwater-table on aeolian deposition. *Sedimentology*, ***35***, 21-41.

Fryberger, S.G. and Schenk, C.J., (1988) Pin stripe lamination: a distinctive feature of modern and ancient eolian sediments. *Sedimentary Geology,* **55**, 1-15.

Gierlowski-Kordesch, E. H. (1998). Carbonate deposition in an ephemeral siliciclastic alluvial system: Jurassic Shuttle Meadow Formation, Newark Supergroup, Hartford basin, USA. *Palaeogeography, Palaeoclimatology, Palaeoecology*, ***140***, 161-184.

Gilluly, J., (1963) The tectonic evolution of the western United States Seventeenth William Smith Lecture. *Quarterly Journal of the Geological Society*, **119**, 133-174.

Glennie, K. W. (1970). Developments in Sedimentology, ***14***, 78-85.

Glennie, K. W. (1983). Early Permian (Rotliegendes) palaeowinds of the North Sea. *Sedimentary Geology*, ***34***, 245-265.

Glennie, K. W. (1986). Development of NW Europe's Southern Permian gas basin. In: *Habitat of Palaeozoic Gas in N.W. Europe* (Eds. Brooks, J., Goff, J.C., and van Hoorn, B.) *Geological Society, London, Special Publications*, ***23***(1), 3-22.

Glennie, K. W. (1987). Desert sedimentary environments, present and past—A summary. *Sedimentary Geology*, ***50***, 135-165.

Glennie, K.W. (1972) Permian Rotliegendes of northwest Europe interpreted in light of modern desert sedimentation studies. *AAPG Bulletin*, **56**, 1048-1071.

Goldhammer, R., Oswald, E. and **Dunn, P.,** (1991) Hierarchy of stratigraphic forcing: Example from Middle Pennsylvanian shelf carbonates of the Paradox Basin.

Sedimentary Modeling: Computer Simulations and Methods for Improved Parameter Definition: Kansas *Geological Survey, Bulletin*, **233**, 361-413.

Goodall, T. M., North, C. P., and **Glennie, K. W**. (2000). Surface and subsurface sedimentary structures produced by salt crusts. *Sedimentology*, ***47***, 99-118.

Goodchild, M. W., & Bryant, P. (1986). The Geology of the Rough Gas Field. In: *Habitat of Palaeozoic Gas in N.W. Europe* (Eds. Brooks, J., Goff, J.C., and van Hoorn, B.) *Geological Society, London, Special Publications*, ***23***, 223-235.

Gornitz, V. M., and **Schreiber, B. C.** (1981). Displacive halite hoppers from the Dead Sea; some implications for ancient evaporite deposits. *Journal of Sedimentary Research*, ***51***, 787-794.

Gough, A. (2015). Controls on sediment architecture and deposition in arid continental basin margin systems (*Doctoral dissertation, Keele University*).

Gradstein, F. M., Ogg, J. G., Schmitz, M., and **Ogg, G.** (2012). *The geologic time scale 2012*. elsevier.

Greeley, R., and **Iversen, J. D.** (1987). Measurements of wind friction speeds over lava surfaces and assessment of sediment transport. *Geophysical Research Letters*, ***14***, 925-928.

Gunatilaka, A. and **Mwango, S.** (1987) Continental sabkha pans and associated nebkhas in southern Kuwait, Arabian Gulf. In *Desert Sediments: Ancient and Modern* (Eds L.E. Frostick, I. Reid) *Geological Society, London, Special Publications*, **35**, 187-203.

Gündogan, I., Önal, M., and **Depçi, T.** (2005). Sedimentology, petrography and diagenesis of Eocene–Oligocene evaporites: the Tuzhisar Formation, SW Sivas Basin, Turkey. Journal of Asian Earth Sciences, **25**, 791-803.

Gwynn, J. W., and **Murphy, P. J.** (1980). Recent sediments of the Great Salt Lake basin. Great Salt Lake. A scientific, historical and economic overview. Utah Geol. Min. Surv., Bull. Salt Lake City, **116**, 83-96.

Gwynn, J.W. and **Murphy, P.J.** (1980) Recent sediments of the Great Salt Make basin. In: *Great Salt Lake: a scientific, historical and economic overview* (Ed. J.W. Gwynn), 1st edn, pp. 83-96. Utah Geologic and Mineral Survey, Salt Lake City, Utah.

Hammer, Ø. (2010). PAST v. 2.01. Reference manual. *Oslo: Natural History Museum University of Oslo*.

Hammer, Ø., Harper, D. A., and **Ryan, P. D.** (2001). PAST: paleontological statistics software package for education and data analysis. *Palaeontologia electronica*, ***4***, 9.

Hampson, G. J., Davies, W., Davies, S. J., Howell, J. A., and **Adamson, K. R.** (2005). Use of spectral gamma-ray data to refine subsurface fluvial stratigraphy: Late Cretaceous strata in the Book Cliffs, Utah, USA. *Journal of the Geological Society*, **162**, 603-621.

Handford, C. R. (1991) Marginal Marine Halite: Sabkhas and Salinas. In *Developments in sedimentology* (Vol. **50**, pp. 1-66). Elsevier.

Handford, C.R. (1981) Genetic characterization of recent and ancient sabkha systems. *AAPG Bulletin*, **65**, 1685-1685.

Handford, C.R. (1982) Sedimentology and evaporite genesis in a Holocene continental-sabkha playa basin—Bristol Dry Lake, California. *Sedimentology*, **29**, 239-253.

Hardie, L. A., and **Lowenstein, T. K**. (1978). Evaporites. *Sedimentology*, 416-426.

Hardie, L. A., Smoot, J. P., Eugster, H. P., Matter, A., and **Tucker, M. E**. (1978). Saline lakes and their deposits: a sedimentological approach. *Modern and ancient lake sediments*, ***2***, 7-41.

Hardie, L.A., (1968) The origin of the recent non-marine evaporite deposit of Saline Valley, Inyo County, California. *Geochimica et Cosmochimica Acta*, **32**, 1279-1301.

Hardie, L.A., (1984) Evaporites; marine or non-marine? *American Journal of Science*, **284**, 193-240.

Hardie, L.A., Lowenstein, T.K. and **Spencer, R.J.** (1985) The problem of distinguishing between primary and secondary features in evaporites. In *Sixth international symposium on salt* (Eds B. C. Schreiber and H. L. Harner) *Alexandria: Salt Institute.* 1, 11-39.

Harvey, A. M., Mather, A. E., and **Stokes, M.** (2005). Alluvial fans: geomorphology, sedimentology, dynamics—introduction. In: *A review of alluvial-fan research.* (Eds: Harvey, A. M., Mather, A. E., and Stokes, M) *Geological Society, London, Special Publications,* **251**, 1-7.

Hasiotis, S. T. (2007). Continental ichnology: fundamental processes and controls on trace fossil distribution. In *Trace Fossils* (pp. 268-284). Elsevier.

Hasiotis, S.T. and Rasmussen, D., (2010) Enigmatic, large-and mega-diameter burrows in the Lower Permian Cedar Mesa Sandstone, Comb Ridge and Moqui Dugway, southeastern, Utah. *Geological Society of America Rocky Mountain Section*, pp. 2.

Hays, J. D., Imbrie, J., and **Shackleton, N. J.** (1976). Variations in the Earth's orbit: pacemaker of the ice ages. *Science*, ***194***(4270), 1121-1132.

Hazel, J.E., (1994) Sedimentary response to intrabasinal salt tectonism in the Upper Triassic Chinle Formation, Paradox basin, Utah. *US Government Printing Office.*

Herczeg, A. L., and **Chapman, A**. (1991). Uranium-series dating of lake and dune deposits in southeastern Australia: a reconnaissance. *Palaeogeography, Palaeoclimatology, Palaeoecology*, *84*(1-4), 285-298.

Herron, M. M., and **Matteson, A.** (1993). Elemental composition and nuclear parameters of some common sedimentary minerals. *Nuclear Geophysics*, ***7***, 383-406.

Hesse, R. (1989). Silica diagenesis: origin of inorganic and replacement cherts. *Earth-Science Reviews*, ***26***, 253-284.

Hilgen, F. J., Krijgsman, W., Langereis, C. G., Lourens, L. J., Santarelli, A., and **Zachariasse, W. J.** (1995). Extending the astronomical (polarity) time scale into the Miocene. *Earth and Planetary Science Letters*, ***136***(3-4), 495-510.

Hilley, G. E., Mynatt, I., & **Pollard, D. D.** (2010). Structural geometry of Raplee Ridge monocline and thrust fault imaged using inverse Boundary Element Modeling and ALSM data. *Journal of Structural Geology*, ***32***, 45-58

Hladil J.I, Růžička M, and **Koptíková LE**. (2006). Stromatactis cavities in sediments and the role of coarse-grained accessories. *Bulletin of Geosciences*, ***81***, 123-146.

Hladil, J., Gersl, M., Strnad, L., Frana, J., Langrova, A., and **Spisiak, J.** (2006). Stratigraphic variation of complex impurities in platform limestones and possible significance of atmospheric dust: a study with emphasis on gamma-ray spectrometry and magnetic susceptibility outcrop logging (Eifelian-Frasnian, Moravia, Czech Republic). *International Journal of Earth Sciences*, ***95***, 703-723.

Hladil, J.I. (2005). The formation of stromatactis-type fenestral structures during the sedimentation of experimental slurries—a possible clue to a 120-year-old puzzle about stromatactis. *Bulletin of Geosciences*, ***80***, 193-211.

Hooke, R. L. (1967). Processes on arid-region alluvial fans. *The Journal of Geology*, **75**, 438-460.

Hoppie, B. W., Blum, P., and **Party, S. S.** (1994). Natural gamma-ray measurements on ODP cores: Introduction to procedures with examples from Leg 150. In *Proceedings of the Ocean Drilling Program, Initial Reports* (Vol. **150**, pp. 51-59).

Horowitz, D.H. (1982) Geometry and origin of large-scale deformation structures in some ancient wind-blown sand deposits. *Sedimentology*, **29**, 155-180.

Howell, J. and **Mountney, N.** (1997) Climatic cyclicity and accommodation space in arid to semi-arid depositional systems: an example from the Rotliegend Group of the UK southern North Sea. In: *Petroleum Geology of the Southern North Sea: Future Potential* (Eds K. Ziegler, P. Turner and S. R. Daines) *Geological Society, London, Special Publications,* **123**, 63-86.

Howell, J., and **Mountney, N.** (2001). Aeolian grain flow architecture: hard data for reservoir models and implications for red bed sequence stratigraphy. *Petroleum Geoscience*, ***7***, 51-56.

Hudson, J.D. (1977) Stable isotopes and limestone lithification. *Journal of the Geological Society,* **133**, 637-660.

Huffman, A.C. and Condon, S.M., (1993) Stratigraphy, Structure, and Paleogeography of Pennsylvanian and Permian Rocks: San Juan Basin and Adjacent Areas, Utah, Colorado, Arizona, and New Mexico. *US Government Printing Office.*

Hummel, G., and **Kocurek, G**. (1984). Interdune areas of the back-island dune field, North Padre Island, Texas. *Sedimentary Geology*, ***39***, 1-26.

Humphreys, E., Hessler, E., Dueker, K., Farmer, G.L., Erslev, E. and **Atwater, T.,** (2003) How Laramide-age hydration of North American lithosphere by the Farallon slab controlled subsequent activity in the western United States. *International Geology Review*, **45**, 575-595.

Hunter, R. E. (1977). Basic types of stratification in small eolian dunes. *Sedimentology*, ***24***, 361-387.

Hunter, R. E. (1981). Stratification Styles in Aeolian Sandstones: Some Pennsylvanian to Jurassic Examples from the Western Interior USA SEPM Special Publication, vol. **31**.

Hunter, R. E., and **Rubin, D. M**. (1983). Interpreting cyclic crossbedding, with an example from the Navajo Sandstone. In *Developments in sedimentology* (Vol. 38, pp. 429-454). Elsevier.

Hunter, R. E., and **Rubin, D. M.** (1983). Interpreting cyclic crossbedding, with an example from the Navajo Sandstone. In *Developments in sedimentology* (Vol. **38**, pp. 429-454). Elsevier.

Huntoon, J.E. and Chan, M.A., (1987) Marine origin of paleotopographic relief on eolian White Rim Sandstone (Permian), Elaterite basin, Utah. *AAPG Bulletin,* **71**, 1035-1045.

Huntoon, J.E., Dubiel, R.F., Stanesco, J.D., Mickelson, D. and **Condon, S.M.** (1996) Permian-Triassic depositional systems, paleogeography, paleoclimate, and hydrocarbon resources in Canyonlands and Monument Valley, Utah. *Geological Society of America Fieldguide*, **3**, 26 pp.

Huntoon, J.E., Stanesco, J.D., Dubiel, R.F. and **Dougan, J.** (2000) Geology of Natural Bridges National Monument, Utah. In: Geology of Utah's Parks and Monuments (Eds D.A. Sprinkel, T.C. Chidsey and P.B. Anderson), Utah Geol. Assoc. Publ., **28**, 233–249.

Huntoon, P. W. (1993). Influence of inherited Precambrian basement structure on the localization and form of Laramide monoclines, Grand Canyon, Arizona. *Geological Society of America Special Papers*, ***280***, 243-256.

Jagger, A. (2003). Sedimentology and stratigraphic evolution of the Permian Cedar Mesa Sandstone, SE Utah. *Unpublished PhD thesis, University of Keele*.

Joannin, S., Cornée, J.J., Münch, P., Fornari, M., Vasiliev, I., Krijgsman, W., Nahapetyan, S., Gabrielyan, I., Ollivier, V., Roiron, P. and Chataigner, C., (2010) Early Pleistocene climate cycles in continental deposits of the Lesser Caucasus of Armenia inferred from palynology, magnetostratigraphy, and 40Ar/39Ar dating. *Earth and Planetary Science Letters*, *291*(1-4), pp.149-158.

Jordan, D. W., Slatt, R. M., Gillespie, R. H., D'Agostino, A. E., and **Stone, C. G.** (1993). Gamma-ray logging of outcrops by a truck-mounted sonde. *AAPG Bulletin*, ***77***, 118-123.

Jordan, O.D. and **Mountney, N.P.** (2010) Styles of interaction between aeolian, fluvial and shallow marine environments in the Pennsylvanian to Permian lower Cutler beds, south-east Utah, USA. *Sedimentology*, **57**, 1357-1385.

Jordan, O.D. and **Mountney, N.P.** (2012) Sequence stratigraphic evolution and cyclicity of an ancient coastal desert system: the Pennsylvanian–Permian Lower Cutler Beds, Paradox Basin, Utah, USA. *Journal of Sedimentary Research*, **82**, 755-780.

Kelley, V. C. (1955). Monoclines of the Colorado Plateau. *Geological Society of America Bulletin*, *66*(7), 789-804.

Kelley, V.C., (1958) Tectonics of the region of the Paradox Basin.

Kendall, A.C. (1978) Facies models 11. Continental and supratidal (sabkha) evaporites. *Geoscience Canada*, **5,** 66-78.

Kendall, A.C. (1981) Continental and supratidal (sabkha) evaporates. In: *Facies Models*, (Ed. Walker, R.G.), *Geoscience Canada,* 145-157

Kendall, C.G.S.C. and **Warren, J.** (1987) A review of the origin and setting of tepees and their associated fabrics. *Sedimentology*, **34**, 1007-1027

Kirkland, D. W. (2003). An explanation for the varves of the Castile evaporites (Upper Permian), Texas and New Mexico, USA. *Sedimentology*, ***50***, 899-920.

Kocurek, G. (1988). First-order and super bounding surfaces in eolian sequences—bounding surfaces revisited. *Sedimentary Geology*, ***56***, 193-206.

Kocurek, G. (1996) Deserts Aeolian systems. In *Sedimentary environments: processes, facies and stratigraphy* (Ed. H.G. Reading) 3rd edn, pp. 125-153. Blackwell Science, Oxford

Kocurek, G., (1981) Significance of interdune deposits and bounding surfaces in aeolian dune sands. *Sedimentology*, **28**, 753-780

Kocurek, G., (1984) Origin of first-order bounding surfaces in aeolian sandstones. *Sedimentology,* **31**, 125-128.

Kocurek, G., (1991) Interpretation of ancient eolian sand dunes. *Annual Review of Earth and Planetary Sciences,* **19**, 43-75

Kocurek, G., (1999). Rather Special to Create One. *Aeolian Environments, Sediments and Landforms*, ***14***, 239.

Kocurek, G., and **Fielder, G.** (1982). Adhesion structures. *Journal of Sedimentary Research*, ***52***, 1229-1241.

Kocurek, G., and **Havholm, K. G**. (1993). Eolian Sequence Stratigraphy--A Conceptual Framework: Chapter 16: Recent Developments in Siliciclastic Sequence Stratigraphy.

Kocurek, G., and **Lancaster, N**. (1999). Aeolian system sediment state: theory and Mojave Desert Kelso dune field example. *Sedimentology*, ***46***, 505-515.

Kocurek, G., and **Nielson, J.** (1986) Conditions favourable for the formation of warm-climate aeolian sand sheets. *Sedimentology*, **33**, 795-816.

Kok, J. F., and **Renno, N. O.** (2009). A comprehensive numerical model of steady state saltation (COMSALT). *Journal of Geophysical Research: Atmospheres*, ***114*****(D17).**

Kok, J. F., Parteli, E. J., Michaels, T. I., and **Karam, D. B.** (2012). The physics of wind-blown sand and dust. *Reports on progress in Physics*, ***75***, 106901.

Kraus, M.J. (1999) Paleosols in clastic sedimentary rocks: their geologic applications. *Earth-Science Reviews*, **47**, 41-70

Kukal, Z. (1971). Open-space structures in the Devonian limestones of the Barrandian (Central Bohemia). *Cas Mineral Geol*, ***16***, 345-362.

Lanchaster, N., (1989) The Namib Sand Sea: Dune Forms, Processes and Sediments, A. A. Balkema, Brookfield, Vt.,

Langford, R.P. (1989). Fluvial-aeolian interactions: Part I, modern systems. *Sedimentology,* **36**, 1023-1035.

Langford, R.P. and **Chan, M.A.,** (1988)Flood surfaces and deflation surfaces within the Cutler Formation and Cedar Mesa Sandstone (Permian), southeastern Utah. *Geological Society of America Bulletin,* **100**, 1541-1549.

Langford, R.P. and **Chan, M.A.,** (1989) Fluvial-aeolian interactions: Part II, ancient systems. *Sedimentology,* **36**, 1037-1051

Langford, R.P. and **Chan, M.A.,** (1993) Downwind changes within an ancient dune sea, Permian Cedar Mesa Sandstone, southeast Utah. In: *Aeolian Sediments: Ancient and Modern* (Eds K. Pye and N. Lancaster), pp. 109–126. Blackwell Publishing Ltd., Oxford, UK.

Langford, R.P. and **Massad, A**. (2014) Facies geometries and climatic influence on stratigraphy in the eolian-sabkha transition in the Permian Cedar Mesa Sandstone, SE Utah In: *Geology of Utah's Far South,* (Eds J.S.MacLean, R.F. Biek, and J.E. Huntoon) *Utah Geological Association Publication*, **43**, 275-294.

Langford, R.P., Pearson, K.M., Duncan, K.A., Tatum, D.M., Adams, L. and **Depret, P.,** (2008) Eolian topography as a control on deposition incorporating lessons from modern dune seas: Permian Cedar Mesa Sandstone, SE Utah, USA. *Journal of Sedimentary Research,* **78**, 410-422.

Last, W.M. (1984) Sedimentology of playa lakes of the northern Great Plains. *Canadian Journal of Earth Sciences,* **21**, 107-125.

Lawton, T.F. and **Buck, B.J.,** (2006) Implications of diapir-derived detritus and gypsic paleosols in Lower Triassic strata near the Castle Valley salt wall, Paradox Basin, Utah. *Geology*, **34**, 885-888.

Lisiecki, L. E., and **Raymo, M. E**. (2007). Plio–Pleistocene climate evolution: trends and transitions in glacial cycle dynamics. *Quaternary Science Reviews*, ***26***, 56-69.

Liu, l. and **Gurnis, M.** (2010) Dynamic subsidence and uplift of the Colorado Plateau. *Geology,* **38**, 663-666.

Lokier, S. and **Steuber, T.** (2008) Quantification of carbonate-ramp sedimentation and progradation rates for the late Holocene Abu Dhabi shoreline. *Journal of Sedimentary Research*, **78**, 423-431.

Lokier, S. and **Steuber, T.** (2009) Large-scale intertidal polygonal features of the Abu Dhabi coastline. *Sedimentology*, **56**, 609-621.

Lokier, S. W., and **Al Junaibi, M.** (2016). The petrographic description of carbonate facies: are we all speaking the same language?. *Sedimentology*, ***63***, 1843-1885.

Lokier, S. W., Andrade, L. L., Court, W. M., Dutton, K. E., Head, I. M., van der Land, C., ... and **Sherry, A.** (2017). A new model for the formation of microbial polygons in a coastal sabkha setting. *The Depositional Record*, ***3***, 201-208

Loope, D.B. (1981) Deposition, Deflation and Diagenesis of Upper Paleozoic Eolian Sediments, Canyonlands National Park, Utah. Unpublished PhD Thesis, University of Wyoming, Laramie, 170 pp

Loope, D.B. (1984) Eolian origin of upper Paleozoic sandstones, southeastern Utah. *Journal of Sedimentary Research*, **54**, 563-580.

Loope, D.B. (1988) Rhizoliths in ancient eolianites. *Sedimentary Geology*, **56**, 301-314.

Loope, D.B., (1985) Episodic deposition and preservation of eolian sands: A late Paleozoic example from southeastern Utah. *Geology,* **13,** 73-76.

Loope, D.B., Elder, J. F., and **Sweeney, M. R**. (2012). Downslope coarsening in aeolian grainflows of the Navajo Sandstone. *Sedimentary Geology*, ***265***, 156-162.

Loope, D.B., Rowe, C. M., and **Joeckel, R. M**. (2001). Annual monsoon rains recorded by Jurassic dunes. *Nature*, ***412***, 64.

Loope, D.B., Sanderson, G.A. and **Verville, G.J.,** (1990) Abandonment of the name Elephant Canyon Formation in southeastern Utah: physical and temporal implications. *Mountain Geologist,* **27**

Løvborg, L., and **Mose, E.** (1987). Counting statistics in radioelement assaying with a portable spectrometer. *Geophysics*, ***52***, 555-563.

Lovley, D. R., Phillips, E. J., Gorby, Y. A., and **Landa, E. R**. (1991). Microbial reduction of uranium. *Nature*, ***350***(6317), 413.

Lowenstein, T.K. and **Hardie, L.A.** (1985) Criteria for the recognition of salt-pan evaporites. *Sedimentology*, **32**, 627-644.

Lüning, S., and **Kolonic, S.** (2003). Uranium spectral gamma-ray response as a proxy for organic richness in black shales: Applicability and limitations. *Journal of petroleum geology*, ***26***, 153-174.

Lüning, S., Kolonic, S., Loydell, D. K., and **Craig, J**. (2003). Reconstruction of the original organic richness in weathered Silurian shale outcrops (Murzuq and Kufra basins, southern Libya). *GeoArabia*, ***8***, 299-308.

Lüning, S., Wendt, J., Belka, Z., and **Kaufmann, B. (**2004). Temporal–spatial reconstruction of the early Frasnian (Late Devonian) anoxia in NW Africa: new field data from the Ahnet Basin (Algeria). *Sedimentary Geology*, **163**, 237-264.

Mack, G. H. (1978). The survivability of labile light-mineral grains in fluvial, aeolian and littoral marine environments: the Permian Cutler and Cedar Mesa Formations, Moab, Utah. *Sedimentology*, ***25***, 587-604.

Mack, G.H. (1977) Depositional environments of the Cutler-Cedar Mesa facies transition (Permian) near Moab, Utah. *The Mountain Geologist,* **14**, 53-68

Mack, G.H. (1979) Littoral marine depositional model for the Cedar Mesa Sandstone (Permian), Canyonlands National Park, Utah. In: Permianland (Ed. D.L. Baars). *Four Corners Geological Society, 9th Field Conference Guidebook*. pp. 33–37

Mack, G.H. and **Rasmussen, K.A.,** (1984) Alluvial-fan sedimentation of the Cutler Formation (Permo-Pennsylvanian) near Gateway, Colorado. *Geological Society of America Bulletin*, **95,** 109-116.

Mack, G.H., James, W.C. and **Monger, H.C.** (1993) Classification of paleosols. *Geological Society of America Bulletin*, **105**, 129-136.

Mainguet, M., and **Chemin, M. C.** (1983). Sand seas of the Sahara and Sahel: an explanation of their thickness and sand dune type by the sand budget principle. In *Developments in Sedimentology* (Vol. **38**, pp. 353-363). Elsevier.

Mallory, W. W. (1960) Outline of Pennsylvanian stratigraphy of Colorado. In: Guide to the Geology of Colorado, Rocky Mountain Association of Geologists, Denver, Colorado, 23-33.

Marie, J. P. P. (1975) Rotliegendes stratigraphy and diagenesis. In: *Petroleum and the Continental Shelf of North West Europe* (Ed A. Woodland), *Institute of Petroleum, London*, 205-210

Martel, A.T. and **Gibling, M.R.** (1991) Wave-dominated lacustrine facies and tectonically controlled cyclicity in the Lower Carboniferous Horton Bluff Formation, Nova Scotia, Canada. In: *Lacustrine facies analysis* (Eds. P. Anadon, L. Cabera and K. Kelts) *International Association of Sedimentologists, Special Publication* **13**, 223-243.

Martin, J.H. and **Evans, P.F.** (1988). Reservoir modeling of marginal aeolian/sabkha sequences, Southern North Sea (UK sector). Society of Petroleum Engineers, Houston, Texas, 63rd Annual Technical Conference and Exhibition, October 2–5, **SPE 18155**, p. 473–486.

Martinius, A. W., Geel, C. R., and **Arribas, J**. (2002). Lithofacies characterization of fluvial sandstones from outcrop gamma-ray logs (Loranca Basin, Spain): the influence of provenance. *Petroleum Geoscience*, ***8***, 51-62.

Massad, A., (2013). The eolian-sabkha transition in the Permian Cedar Mesa Sandstone, SE Utah. University of Texas at El Paso, Unpublished MSc Thesis

May, G., Hartley, A. J., Stuart, F. M., and **Chong, G.** (1999). Tectonic signatures in arid continental basins: an example from the Upper Miocene–Pleistocene, Calama Basin, Andean forearc, northern Chile. *Palaeogeography, Palaeoclimatology, Palaeoecology*, ***151***, 55-77.

McKay, C. P., Rask, J. C., Detweiler, A. M., Bebout, B. M., Everroad, R. C., Lee, J. Z., ... and **Al-Awar, M.** (2016). An unusual inverted saline microbial mat community in an interdune sabkha in the Rub'al Khali (the Empty Quarter), United Arab Emirates. *PloS one*, ***11***, e0150342.

McKee, E.D. (1979 Introduction to a study of global sand seas. In: *A Study of Global Sand Seas* (Ed. by E. D. McKee). *Prof. Pap. U.S. geol. Surv*. **1052**, 1–17.

McKee, E.D., Douglass, J.R. and **Rittenhouse, S.** (1971) Deformation of lee-side laminae in eolian dunes. *Geological Society of America Bulletin*, **82**, 359-378.

McKight, E.T., (1940) Geology of area between Green and Colorado rivers, Grand and San Juan counties, Utah. *US Government Printing Office*

McQuarrie, N. and **Chase, C.G**., (2000) Raising the Colorado plateau. *Geology*, **28,** 91-94.

Mertz Jr, K. A., and **Hubert, J. F.** (1990). Cycles of sand-flat sandstone and playa–lacustrine mudstone in the Triassic–Jurassic Blomidon redbeds, Fundy rift basin, Nova Scotia: implications for tectonic and climatic controls. *Canadian Journal of Earth Sciences*, ***27***, 442-451

Mettraux, M., Homewood, P. W., Kwarteng, A. Y., and **Mattner, J.** (2011). Coastal and continental sabkhas of Barr Al Hikman, Sultanate of Oman. *International Association of Sedimentology Spec. Publ*, ***43***, 183-204.

Meyers, S.R., 2019, Cyclostratigraphy and the problem of astrochronologic testing, *Earth-Science Reviews*, **190**, 190-223.

Miall, A. D. (1985). Architectural-element analysis: a new method of facies analysis applied to fluvial deposits. *Earth-Science Reviews*, ***22***, 261-308.

Miall, A. D. (2006). Reconstructing the architecture and sequence stratigraphy of the preserved fluvial record as a tool for reservoir development: A reality check. *AAPG bulletin*, ***90***, 989-1002.

Miall, A. D. (2010). *The geology of stratigraphic sequences*. Springer Science & Business Media.

Miall, A.D. (1996) The Geology of Fluvial Deposits: Sedimentary Facies, Basin Analysis and Petroleum Geology. Springer, Berlin, 582 pp.

Miall, A.D., (1990). Principles of Sedimentary Basin Analysis, 2nd edn. Springer, Berlin.

Milliken, K. L. (1979). The silicified evaporite syndrome; two aspects of silicification history of former evaporite nodules from southern Kentucky and northern Tennessee. *Journal of Sedimentary Research*, ***49***, 245-256

Mitchum Jr, R. M., and **Van Wagoner, J. C.** (1991). High-frequency sequences and their stacking patterns: sequence-stratigraphic evidence of high-frequency eustatic cycles. *Sedimentary geology*, ***70***, 131-160.

Moiola, R.J. and **Glover, E.D.** (1965) Recent anhydrite from clayton playa. Nevada. *Journal of Earth and Planetary Materials*, **50**, 2063-2069

Moucha, R., Forte, A.M., Rowley, D.B., Mitrovica, J.X., Simmons, N.A. and **Grand, S.P.,** (2009) Deep mantle forces and the uplift of the Colorado Plateau. *Geophysical Research Letters,* **36**

Mountney, N.P. (2006a) Periodic accumulation and destruction of aeolian erg sequences in the Permian Cedar Mesa Sandstone, White Canyon, southern Utah, USA. *Sedimentology*, **53**, 789-823.

Mountney, N.P. (2006b) Eolian facies models. In: *Facies Models Revisited* (Eds H. Posamentier and R.G. Walker), *Soc. Econ. Paleontol. Mineral. Mem*., **84**, 19–83.

Mountney, N.P. and **Jagger, A.** (2004) Stratigraphic evolution of an aeolian erg margin system: the Permian Cedar Mesa Sandstone, SE Utah, USA. *Sedimentology,* **51**, 713-743.

Mountney, N.P. and **Thompson, D.B.** (2002) Stratigraphic evolution and preservation of aeolian dune and damp/wet interdune strata: an example from the Triassic Helsby Sandstone Formation, Cheshire Basin, UK. *Sedimentology*, **49**, 805-833.

Mountney, N.P., and **Howell, J.** (2000). Aeolian architecture, bedform climbing and preservation space in the Cretaceous Etjo Formation, NW Namibia. *Sedimentology*, ***47***, 825-850.

Müller-Jungbluth, W. U., and **Toschek, P. H.** (1969). *Karbonatsedimentologische Arbeitsgrundlagen: Begriffe, Erläuterungen, Hinweise* (No. 4). In Kommissionsverlag der Österreichischen Kommissionsbuchhandlung.

Myers, K. J., and **Bristow, C. S.** (1989). Detailed sedimentology and gamma-ray log characteristics of a Namurian deltaic succession II: Gamma-ray logging. In: *DELTAS: Sites and Traps for Fossil Fuels* (Eds. Whateley, M. K.G., and Pickering, K.T.)*Geological Society, London, Special Publications*, ***41***(1), 81-88.

Mynatt, I., Seyum, S., and **Pollard, D. D.** (2009). Fracture initiation, development, and reactivation in folded sedimentary rocks at Raplee Ridge, UT. *Journal of Structural Geology*, ***31***, 1100-1113.

Nagtegaal, P. J. C. (1973). Adhesion-ripple and barchandune sands of the recent Namib (SW Africa) and Permian Rotliegend (NW Europe) deserts. *Madoqua*, ***2***, 5-19.

Nickling, W. G., Neuman, C. M., and **Lancaster, N.** (2002). Grainfall processes in the lee of transverse dunes, Silver Peak, Nevada. *Sedimentology*, ***49***, 191-209.

Nielson, J., and **Kocurek, G.** (1986). Climbing zibars of the Algodones. *Sedimentary Geology*, ***48***, 1-15.

North, C. P., and **Boering, M**. (1999). Spectral gamma-ray logging for facies discrimination in mixed fluvial-eolian successions: A cautionary tale. *AAPG bulletin*, ***83***, 155-169.

North, C. P., and **Taylor, K. S.** (1996). Ephemeral-fluvial deposits: integrated outcrop and simulation studies reveal complexity. *AAPG bulletin*, ***80***, 811-830.

Nuccio, V.F. and **Condon, S.M.,** (1996) Burial and thermal history of the Paradox Basin, Utah and Colorado, and petroleum potential of the Middle Pennsylvanian Paradox Basin. *US Geol. Surv. Bull.,* **2000-O**, 20 pp

Olsen, H., Due, P.H. and **Clemmensen, L.B.,** (1989) Morphology and genesis of asymmetric adhesion warts—a new adhesion surface structure. *Sedimentary Geology,* **61**, 277-285.

O'Sullivan, R. B. (1965) Geology of the Cedar Mesa-Boundary Butte area, San Juan County, Utah (Vol. 1186). *US Government Printing Office.*

Owen, A., Nichols, G. J., Hartley, A. J., Weissmann, G. S., and **Scuderi, L. A.** (2015) Quantification of a distributive fluvial system: the Salt Wash DFS of the Morrison Formation, SW USA. *Journal of Sedimentary Research*, **85**, 544-561.

Owen, P. R. (1964). Saltation of uniform grains in air. *Journal of Fluid Mechanics*, ***20***, 225-242.

Owen, R.A., Owen, R.B., Renaut, R.W., Scott, J.J., Jones, B. and **Ashley, G.M.** (2008) Mineralogy and origin of rhizoliths on the margins of saline, alkaline Lake Bogoria, Kenya Rift Valley. *Sedimentary Geology*, **203**, 143-163.

Pandita, S. K., Bhat, S. K., and **Kotwal, S. S**. (2011). Facies evaluation of boulder conglomerate formation, Upper Siwalik, Jammu Himalaya. *Himalayan Geology*, ***32***, 63-69.

Parrish, J. T., Hasiotis, S. T., & **Chan, M. A.** (2017). Carbonate Deposits In the Lower Jurassic Navajo Sandstone, Southern Utah and Northern Arizona, USA. *Journal of Sedimentary Research*, ***87***, 740-762.

Parsons, A. J., and **Abrahams, A. D.** (2009). Geomorphology of desert environments. In Geomorphology of Desert Environments (pp. 3-7). Springer, Dordrecht.

Parsons, T., Thompson, G.A. and **Sleep, N.H.,** (1994) Mantle plume influence on the Neogene uplift and extension of the US western Cordillera? *Geology*, **22**, 83-86.

Parteli, E. J., Duran, O., and **Herrmann, H. J.** (2007). Minimal size of a barchan dune. *Physical Review E*, ***75***, 011301.

Peterson, F., (1988) Stratigraphy and nomenclature of middle and upper Jurassic rocks, Western Colorado Plateau, Utah and Arizona. *US Geological Survey, Bulletin*, 13-56.

Pettigrew, R., Clarke, S., Richards, P., and **Milodowski, A.** (2018). Clastic/Evaporitic Interactions in Arid Continental Settings: Implications for Reservoir Characterization and Modelling. In *AAPG ACE 2018*.

Platt, N. H. (1989). Lacustrine carbonates and pedogenesis: sedimentology and origin of palustrine deposits from the Early Cretaceous Rupelo Formation, W Cameros Basin, N Spain. Sedimentology, ***36***, 665-684.

Platt, N.H. and **Wright, V.P.** (1991) Lacustrine carbonates: facies models, facies distributions and hydrocarbon aspects. In: *Lacustrine facies analysis*. (Eds P. Anadon, L. Cabrera and K. Kelts) *Special Publication of the International Association of Sedimentologists*. 13, 57-74

Postma, G., and **Ten Veen, J. H**. (1999). Astronomically and tectonically linked variations in gamma-ray intensity in Late Miocene hemipelagic successions of the Eastern Mediterranean Basin. *Sedimentary Geology*, **128**, 1-12.

Priddy, C., Clarke, S., Richards, P., and **Randles, T**. (2018) Fluvial-Aeolian Interactions Within Arid Continental Basins: Implications for Reservoir Characterisation and Basin Modelling. In *AAPG ACE 2018*.

Pulvertaft, T. C. R. (1985). Aeolian dune and wet interdune sedimentation in the Middle Proterozoic Dala Sandstone, Sweden. *Sedimentary Geology*, ***44***, 93-111.

Purvis, K. (1991) Stoss-side mud-drapes: deposits of interdune pond margins. *Sedimentology,* **38**, 153-156

Quigley, M. C., Sandiford, M., and **Cupper, M. L**. (2007). Distinguishing tectonic from climatic controls on range-front sedimentation. *Basin Research*, ***19***, 491-505.

Raine, R.J. and **Smith, M.P.** (2017) Sabkha facies and the preservation of a falling-stage systems tract at the Sauk II–III supersequence boundary In the Late Cambrian Eilean Dubh Formation, NW Scotland. *Journal of Sedimentary Research*, **87**, 41-65.

Rankey, E.C., (1997) Relations between relative changes in sea level and climate shifts: Pennsylvanian–Permian mixed carbonate-siliciclastic strata, western United States. *Geological Society of America Bulletin,* **109,** 1089-1100.

Reeves Jr, C. C. (2009). Economic significance of playa lake deposits. *Lake Sediments*, ***104***, 279.

Retallack, G.J. (1994) The environmental factor approach to the interpretation of paleosols. In: *Factors of Soil Formation: a Fiftieth Anniversary Retrospective* (Ed. R. Amundsen), *SSSA Special Publication*, 33, 31-31.

Rhys, G. H. (1975). A proposed standard lithostratigraphic nomenclature for the southern North Sea. *Petroleum and the Continental Shelf of North West Europe*, ***1***, 151-163.

Rider M.H. (1999) The Geological Interpretation of Well Logs. *Whittles Publishing Services, Dunbeath*

Rider, M. H. (1990). Gamma-ray log shape used as a facies indicator: critical analysis of an oversimplified methodology. In: *Geological Application of Wireline Logs* (Eds. Hurst, A., Lovell, M.A., and Morton, A.C.) *Geological Society, London, Special Publications*, ***48***(1), 27-37.

Riding, R. (2000). Microbial carbonates: the geological record of calcified bacterial–algal mats and biofilms. *Sedimentology*, ***47***, 179-214

Rogers, S. L. (2018). A novel population of composite mounds: their initiation, growth and demise. San Emiliano Formation, Cantabrian Mountains, Spain. *Journal of Iberian Geology*, 1-17.

Roy, M., Kelley, S., Pazzaglia, F., Cather, S. and **House, M.,** (2004) Middle Tertiary buoyancy modification and its relationship to rock exhumation, cooling, and subsequent extension at the eastern margin of the Colorado Plateau. *Geology,* **32**, 925-928.

Rubin, D. M. (1987). Formation of scalloped cross-bedding without unsteady flows. *Journal of Sedimentary Research*, ***57***, 39-45.

Rubin, D. M., and **Carter, C. L**. (2006). *Bedforms and cross-bedding in animation* SEPM, Atlas Series, 2, DVD.

Rubin, D.M. and **Hunter, R.E.** (1982) Bedform climbing in theory and nature. *Sedimentology*, **29**, 121-138.

Sahagian, D., Proussevitch, A. and **Carlson, W.,** (2002) Timing of Colorado Plateau uplift: Initial constraints from vesicular basalt-derived paleoelevations. *Geology*, **30**. 807-810.

Sanz, M. E., Zarza, A. A., and **Calvo, J. P.** (1995). Carbonate pond deposits related to semi-arid alluvial systems: examples from the Tertiary Madrid Basin, Spain. Sedimentology, **42**, 437-452.

Scholle, P. A., and **Ulmer-Scholle, D. S.** (2003). A Color Guide to the Petrography of Carbonate Rocks: Grains, Textures, Porosity, Diagenesis, AAPG Memoir **77** (Vol. 77). AAPG.

Schreiber, B.C. and **Kinsman, D.J.** (1975) New observations on the Pleistocene evaporites of Montallegro, Sicily and a modern analog. *Journal of Sedimentary Research*, **45**, 469-479.

Seard, C., Camoin, G., Rouchy, J. M., and **Virgone, A.** (2013). Composition, structure and evolution of a lacustrine carbonate margin dominated by microbialites: Case study from the Green River formation (Eocene; Wyoming, USA). Palaeogeography, Palaeoclimatology, Palaeoecology, ***381***, 128-144

Sears, J.D., (1956) Geology of Comb Ridge and vicinity north of San Juan River, San Juan County, Utah (No. 1021-E). US Geological Survey.

Seppälä, M., and **Lindé, K.** (1978). Wind tunnel studies of ripple formation. *Geografiska Annaler: Series A, Physical Geography*, ***60***, 29-42.

Serra, O. (1984). Fundamentals of well-log interpretation. 1: the acquisition of data. *Developments in Petroleum Science A*, *15*.

Shackleton, N. J. (2000). The 100,000-year ice-age cycle identified and found to lag temperature, carbon dioxide, and orbital eccentricity. *Science*, ***289***(5486), 1897-1902.

Shanley, K. W., and **McCabe, P. J.** (1994). Perspectives on the sequence stratigraphy of continental strata. *AAPG bulletin*, ***78***, 544-568.

Shao, Y. (2008). *Physics and modelling of wind erosion* (**Vol. 37**). Springer Science & Business Media.

Sharp, R. P. (1963). Wind ripples. *The Journal of Geology*, ***71***, 617-636.

Shearman, D. J. (1978). Evaporites of coastal sabkhas. *Marine evaporites*, ***4***, 6-42.

Shi, J., Jin, Z., Liu, Q., Zhang, R., and **Huang, Z.** (2019). Cyclostratigraphy and astronomical tuning of the middle eocene terrestrial successions in the Bohai Bay Basin, Eastern China. *Global and Planetary Change*, ***174***, 115-126.

Shinn, E. A. (1968). Practical significance of birdseye structures in carbonate rocks. *Journal of Sedimentary Research*, ***38***, 215-223.

Sierro, F. J., Ledesma, S., Flores, J. A., Torrescusa, S., and **del Olmo,** W. M. (2000). Sonic and gamma-ray astrochronology: Cycle to cycle calibration of Atlantic climatic records to Mediterranean sapropels and astronomical oscillations. *Geology*, ***28***, 695-698.

Šimíček, D., and **Bábek, O.** (2015). Spectral gamma-ray logging of the Gres d'Annot, SE France: An outcrop analogue to geophysical facies mapping and well-log correlation of sand-rich turbidite reservoirs. Marine and Petroleum Geology, **60**, 1-17.

Slatt, R. M., Jordan, D. W., D'Agostino, A. E., and **Gillespie, R. H.** (1992) Outcrop gamma-ray logging to improve understanding of subsurface well log correlations. In: *Geological Applications of Wireline Logs II* (Eds. Hurst, A., Griffiths, C.M., and Worthington, P.F.) *Geological Society, London, Special Publications*, **65**, 3-19.

Smoot, J.P. and **Lowenstein, T.K.** (1991) Depositional environments of non-marine evaporites. In *Evaporites, Petroleum and Mineral Resources* (Ed J. L. Melvin) *Developments in sedimentology,* 50, 189-347).

Sneh, A. (1983) Desert stream sequences in the Sinai Peninsula. *Journal of Sedimentary Research*, **53**, 1271-1279.

Sonnenfeld, P., and **Hudec, P. P.** (1985). Origin of clay films in rock salt. *Sedimentary geology*, ***44***, 113-120.

Soreghan, G.L., Elmore, R.D. and **Lewchuk, M.T.,** (2002) Sedimentologic-magnetic record of western Pangean climate in upper Paleozoic loessite (lower Cutler beds, Utah). *Geological Society of America Bulletin,* **114,** 1019-1035.

Spencer, J.E., (1996) Uplift of the Colorado Plateau due to lithosphere attenuation during Laramide low-angle subduction. *Journal of Geophysical Research: Solid Earth*, **101(B6),** 13595-13609.

Spencer, R. J., Baedecker, M. J., Eugster, H. P., Forester, R. M., Goldhaber, M. B., Jones, B. F., and **Rubin, M**. (1984). Great Salt Lake, and precursors, Utah: the last 30,000 years. *Contributions to Mineralogy and Petrology*, ***86***, 321-334.

Spötl, C., and **Wright, V. P.** (1992). Groundwater dolocretes from the Upper Triassic of the Paris Basin, France: a case study of an arid, continental diagenetic facies. Sedimentology, ***39***, 1119-1136

Stanesco, J. D. (1991). Sedimentology and cyclicity in the Lower Permian De Chelly Sandstone on the Defiance Plateau: Eastern Arizona. *The Mountain Geologist*.

Stanesco, J.D. and **Campbell, J.A**. (1989) Eolian and noneolian facies of the lower Permian Cedar Mesa Sandstone Member of the Cutler Formation, southeastern Utah. *US Geol. survey bull.*; **1808, Chap. F.** Evolution of sedimentary basins-San Juan basin

Stanesco, J.D., Dubiel, R.F. and **Huntoon, J.E.** (2000) Depositional environments and paleotectonics of the Organ Rock Formation of the Permian Cutler Group,

southeastern Utah. In*: Geology of Utah's Parks and Monuments* (Eds D.A. Sprinkel, T.C. Chidsey, Jr and P.B. Anderson), *Utah Geol. Assoc. Publ.,* 28, 591–605.

Stear, W.M. (1985) Comparison of the bedform distribution and dynamics of modern and ancient sandy ephemeral flood deposits in the southwestern Karoo region, South Africa. *Sedimentary Geology*, **45**, 209-230.

Steele-Mallory, B.A., (1982) The depositional environment and petrology of the White Rim sandstone member of the Permian Cutler Formation, Canyonlands National Park, Utah, (No. 82-204). *US Geological Survey*

Steenbrink, J., Kloosterboer-van Hoeve, M. L., and **Hilgen, F. J.** (2003). Millennial-scale climate variations recorded in Early Pliocene colour reflectance time series from the lacustrine Ptolemais Basin (NW Greece). *Global and Planetary Change*, ***36***, 47-75.

Stenzel, S. R., and **James, N. P.** (1995). Shallow-Water Stromatactis Mud-Mounds on a Middle Ordovician Foreland Basin Platform, Western Newfoundland. *Carbonate Mud-Mounds: Their Origin and Evolution*, 125-149.

Stewart, J.H., Poole, F.G. and **Wilson, R.F.,** (1972) Stratigraphy and origin of the Triassic Moenkopi Formation and related strata in the Colorado Plateau region. *US Government Printing Office.*

Stoertz, G. E., and **G. E. Ericksen** (1974) Geology of salars in northern Chile, *U.S. Geol. Surv. Prof. Pap*., **811**, 65

Stoffers, P., and **Hecky, R. E.** (1978). Late Pleistocene–; Holocene Evolution of the Kivu–Tanganyika Basin. *Modern and Ancient Lake Sediments*, 43-55.

Stokes, W.L., (1952) Lower Cretaceous in Colorado Plateau. *AAPG Bulletin*, **36**, 1766-1776.

Stokes, W.L., (1968) Multiple parallel-truncation bedding planes--a feature of wind-deposited sandstone formations. *Journal of Sedimentary Research,* **38**, 510-515

Svendsen, J. B., and **Hartley, N. R**. (2001). Comparison between outcrop-spectral gamma ray logging and whole rock geochemistry: implications for quantitative reservoir characterisation in continental sequences. *Marine and Petroleum Geology*, ***18***, 657-670.

Taberner, C., Cendón, D., Pueyo, J. and **Ayora, C.,** (2000) The use of environmental markers to distinguish marine vs. continental deposition and to quantify the significance of recycling in evaporite basins. *Sedimentary Geology,* **137**, 213-240.

Talbot, M. R. (1985). Major bounding surfaces in aeolian sandstones—a climatic model. *Sedimentology*, ***32***, 257-265.

Tanner, L.H. and **Lucas, S.G.** (2007). The Moenave Formation: Sedimentologic and stratigraphic context of the Triassic–Jurassic boundary in the Four Corners area, southwestern USA. *Palaeogeography, Palaeoclimatology, Palaeoecology*, **244,** 111-125.

Taylor, A.M. and **Goldring, R.** (1993) Description and analysis of bioturbation and ichnofabric. *Journal of the Geological Society, London*, **150**, 141-148.

Tebbutt, G. E., Conley, C. D., and **Boyd, D. W**. (1965). Lithogenesis of a distinctive carbonate rock fabric. *Rocky Mountain Geology*, ***4***, 1-13.

Terrell, F.M., (1972) Lateral facies and paleoecology of Permian Elephant Canyon Formation, Grand County, Utah. *Brigham Young University Geological Studies* **(19),** 3-44.

Thompson, D.B., (1969) Dome-shaped aeolian dunes in the frodsham member of the so-called "keuper" sandstone formation (scythian-anisian: triassic) at Frodsham, Cheshire (England). *Sedimentary Geology,* **3**, 263-289.

Todd, S.P. (1996) Sedimentary structures. In: *Advances in Fluvial Dynamics and Stratigraphy* (Eds P. A . Carling and M. R. Dawson) 1st edn, pp. 299-350. Wiley, Oxford.

Tooth, S. (2005) Splay formation along the lower reaches of ephemeral rivers on the Northern Plains of arid central Australia. *Journal of Sedimentary Research*, ***75***, 636-649.

Trudgill, B., (2011) Evolution of salt structures in the northern Paradox Basin: Controls on evaporite deposition, salt wall growth and supra-salt stratigraphic architecture. *Basin Research,* **23,** 208-238.

Trudgill, B., Banbury, N. and Underhill, J., (2004) Salt evolution as a control on structural and stratigraphic systems: Northern Paradox foreland basin, southeast Utah, USA, *Salt-Sediment Interactions and Hydrocarbon Prospectivity: Proceedings, Gulf Coast Section SEPM Foundation (Society for Sedimentary Geology), Annual Bob F. Perkins Research Conference* 2004, SEPM, pp. 669-700.

Tsien, H. H. (1985). Origin of stromatactis—a replacement of colonial microbial accretions. In *Paleoalgology* (pp. 274-289). Springer, Berlin, Heidelberg.

Tucker, M.E. (1978) Triassic Lacustrine Sediments from South Wales: Shore-Zone, Evaporites and Carbonates. In: *Modern and ancient lake sediments* (Eds A. Matter and M.E. Tucker), *International Association of Sedimentologists, Special Publication* 2, 205-224.

Tunbridge, I.P. (1981) Sandy high-energy flood sedimentation—some criteria for recognition, with an example from the Devonian of SW England. *Sedimentary Geology*, **28**, 79-95

Ungar, J. E., and **Haff, P. K.** (1987). Steady state saltation in air. *Sedimentology*, ***34***, 289-299.

Vail, P.R., Audemard, F., Bowman, S.A., Eisner, P.N., and **Perez-Crus, C.** (1991) The stratigraphic signatures of tectonics, eustasy and sedimentology—an overview. In: *Cycles and Events in Stratigraphy* (Eds Einsele, G., Ricken, W., Seilacher A.), *Springer-Verlag, Berlin*. 617-659

Van Dam, J.A., Aziz, H.A., Sierra, M.Á.Á., Hilgen, F.J., van den Hoek Ostende, L.W., Lourens, L.J., Mein, P., van Der Meulen, A.J. and Pelaez-Campomanes, P., (2006) Long-period astronomical forcing of mammal turnover. *Nature*, *443*(7112), p.687.

Van Gemerden, H. (1993). Microbial mats: a joint venture. *Marine Geology*, ***113***, 3-25.

Van Veen, F. R. (1975). Geology of Leman Gas-Field. Geology, **1,** 223-231.

Van Wagoner, J. C., Mitchum Jr, R. M., Posamentier, H. W., and **Vail, P. R**. (1987). Seismic stratigraphy interpretation using sequence stratigraphy: Part 2: Key definitions of sequence stratigraphy. In: *Atlas of Seismic Stratigraphy*, (ED. Bally, A. W.) *AAPG Studies in Geology **27**,* 11-14

Van Wagoner, J. C., Mitchum, R. M., Campion, K. M., and **Rahmanian, V. D.** (1990). Siliciclastic sequence stratigraphy in well logs, cores, and outcrops: concepts for high-resolution correlation of time and facies. *AAPG Methods in Exploration* **7**

Von der Borch, C. C. (1976). Stratigraphy and formation of Holocene dolomitic carbonate deposits of the Coorong area, South Australia. *Journal of Sedimentary Research*, ***46***, 952-966.

Wallace, M. W. (1987). The role of internal erosion and sedimentation in the formation of stromatactis mudstones and associated lithologies. *Journal of Sedimentary Research*, ***57***, 695-700

Waltham, D. (2015). Milankovitch period uncertainties and their impact on cyclostratigraphy. *Journal of Sedimentary Research*, ***85***, 990-998.

Wang, Y., Straub, K. M., and **Hajek, E. A**. (2011). Scale-dependent compensational stacking: an estimate of autogenic time scales in channelized sedimentary deposits. *Geology*, ***39***(9), 811-814.

Warren, J. K. (1991). Sulfate Dominated Sea-Marginal and Platform Evaporative Settings:: Sabkhas and Salinas, Mudflats and Salterns. In *Developments in Sedimentology* (Vol. **50**, pp. 69-187). Elsevier.

Warren, J.K. (1983) Tepees, modern (southern Australia) and ancient (Permian—Texas and New Mexico)—a comparison. *Sedimentary Geology*, **34**, 1-19.

Warren, J.K. (1989) Evaporite Sedimentology: Its importance in hydrocarbon accumulations. Englewood Cliffs, Prentice-Hall, 285 pp.

Warren, J.K. (2016) Evaporites: A geological compendium. 2nd edn. Springer, Switzerland. 1783 pp.

Warren, J.K. and **Kendall, C.G.S.C.** (1985) Comparison of sequences formed in marine sabkha (subaerial) and salina (subaqueous) settings--modern and ancient. *AAPG Bulletin*, **69**, 1013-1023.

Warrener, H. (2016) The sedimentology of wet aeolian systems and their implications on hydrocarbon reservoirs: an example from the Navajo Formation, Western U.S.A. Unpublished MSc Thesis. *Keele University*

Wasson, R. J., and **Hyde, R.** (1983). Factors determining desert dune type. *Nature*, ***304***, 337.

Weedon, G.P. (2003) Time Series Analysis and Cyclostratigraphy: Examining Stratigraphic Records of Environmental Cycles. Cambridge University Press, Cambridge

Weiler, Y., Sass, E. and **Zak, I.** (1974) Halite oolites and ripples in the Dead Sea, Israel. *Sedimentology*, **21**, 623-632.

Williams, M.R., (2009) Stratigraphy of Upper Pennsylvanian cyclic carbonate and siliciclastic rocks, western Paradox Basin, Utah. In: *The Paradox Basin Revisited – New Developments in Petroleum Systems and Basin Analysis.* (Eds Houston, W. S., Wray, L. L., Moreland, P. G.) *The Rocky Mountain Association of Geologist.*

Wilson, I. G. (1972). Aeolian bedforms—their development and origins. *Sedimentology*, ***19***, 173-210.

Wilson, I.G. (1971) Desert sandflow basins and a model for the development of ergs. *Geogr. J.* **137**, 180–199.

Wolfe, J.A., Forest, C.E. and **Molnar, P**., (1998) Paleobotanical evidence of Eocene and Oligocene paleoaltitudes in midlatitude western North America. *Geological Society of America Bulletin*, **110**, 664-678.

Yang, C. S., and **Baumfalk, Y. A.** (1997). Application of high-frequency cycle analysis in high-resolution sequence stratigraphy. In: Petroleum Geology of the Southern

North Sea: Future Potential (Eds K. Ziegler, P. Turner and S. R. Daines) Geological Society, London, Special Publications, **123**, 181-203.

Zanzonico, P. (2012). Principles of nuclear medicine imaging: planar, SPECT, PET, multi-modality, and autoradiography systems. *Radiation research*, ***177***, 349-364.

Zuchuat, V., Sleveland, A.R., Pettigrew, R.P., Dodd, T.J., Clarke, S.M., Rabbel, O., Braathen, A. and **Midtkandal, I.**, (2019) Overprinted allocyclic processes by tidal resonance in an epicontinental basin: the upper jurassic curtis formation, east-central Utah, USA. *The Depositional Record*.